Characterization of the PAO/phyllobilin Pathway of Chlorophyll Breakdown in Grasses

Dissertation

zur

Erlangung der naturwissenschaftlichen Doktorwürde

(Dr. sc. nat.)

vorgelegt der

Mathematisch-naturwissenschaftlichen Fakultät

der

Universität Zürich

von

Aditi Das

aus

Indien

Promotionskomitee

Prof. Dr. Stefan Hörtensteiner (Vorsitz und Leitung der Dissertation)

Prof. Dr. Enrico Martinoia

Prof. Dr. Karin Krupinska

Zürich, 2016

আমি আমার মাম্মা ও বাবা কে এই প্রবন্ধ উৎসর্গ করতে চাই, যারা আমাকে সেরা সম্ভাবনা প্রদান করার সব প্রচেষ্টা করেছেন।

I would like to dedicate this thesis to my *Mamma* and *Baba*, who made every effort to provide me with the best of possibilities.

Acknowledgments

I would like to express my sincere gratitude to my supervisor Prof. Stefan Hörtensteiner for having given me this opportunity to work with him and for believing in me. I cannot thank enough for his impeccable support in every possible way during my PhD tenure. His guidance was pivotal during my research and writing of this thesis. I couldn't imagine having a better advisor and mentor for my research study.

I am thankful to my supervisory committee members, Prof. Enrico Martinoia and Prof. Karin Krupinska, for their steadfast support and encouragement.

I would like to thank all the Chl degraders: Bastien, Luzia, Kathrin, Lukas, Noemi, Song and Mareike who have been such wonderful colleagues and friends. In particular, I am very grateful to Bastien and Luzia for their constant significant support with my experiments. I would like to thank Kathrin, to whom I could look forward to both as a friend and guide. Nevertheless, I would like to thank the "Zivis": Sergeui, Damian, and Remo for their technical support which definitely aided to progress faster. In short, my experience with my group inside and outside the lab is priceless.

I would also like to thank all the members of P1 who made the lab environment a joyous place to work. My extended thanks goes to Joelle, Chris, Lorenzo, Guowei and Barbara.

I would like to thank Kari and Christian, the gardeners who have helped and taken care of my research plants which made my experiments a lot easier. I would also like to thank Bea for taking care of the seed generation in the Reckenholz fields.

I would also like to thank the members of the Keller group like Saverine, Geri and Justine for providing me with the required wheat seeds and letting me use their growth chambers when needed.

I would like to thank all the Crop Life members for their great input, support and providing an amazing work experience during our meetings.

I would also like to acknowledge Dr. Karin Krupinska and her lab members (especially Weronika, Andrea and Sussan) for their support and allowing me to use their laboratories to conduct the localization and field trails needed for this research.

I would like to thank my two great friends Jyoti and Sanae for being there with me to share the sweet and bitter aspects of this journey.

Last but not the least, I thank my family (mamma, baba and jo-chu) from the bottom of my heart who have infinitely been with me through thick and thin. Everything would be incomplete, if my family would not have stood beside me in every aspect of my life. I also want to immensely thank my dearest companion, Parth for sailing with me through all the low and high tides since I have known him.

I thank everyone whose contribution either helped me or made me happy throughout.

Table of Contents

List of Abbreviations

AAO	Ascorbic acid oxidase
ABA	Abscisic acid
ABC	ATP binding cassette
ACC	Amino cyclopropane carboxylate
ACO	ACC oxidase
Acd	Accelerated cell death
ACS	ACC synthetase
ACT	Actin
ADP	Adenosine diphosphate
ALA	5-aminolevulinic acid
AOA	Amino-oxyacetic acid
Ap	*Acer platanoides*
Arabidopsis, At	*Arabidopsis thaliana*
ARF	Auxin response factor
ATAF	Arabidopsis transcription activation factor
ATG	Autophagy related genes
AVG	Aminoethoxyvinylglycine
Bn	*Brassica napus*
bp	base pairs
Bpy	2,2'-Bipyridyl
BSA	Bovine serum albumin
CaMV	Cauliflower mosaic virus
CAO	Chl *a* oxygenase
CAT	Catalase
CAU	Christian-Albrechts-Universität
CBR	Chl *b* reductase
CCE	Chlorophyll catabolic enzyme
cDNA	Copy DNA
Chl	Chlorophyll
Chlide	Chlorophyllide
Cj	*Cercidiphyllum japonicum*
CLH	Chlorophyllase
CLSM	Confocal laser scanning microscopy
CO	Carbon monoxide
coi1	coronatine-insensitive 1
Col-0	Columbia-0 ecotype
CS	Chlorophyll synthase
CUC	cup shaped cotyledon
CYP	Cytochrome P450
DDI	Days of dark incubation
DFCC	1,19-dioxobilin-type fluorescent chl catabolite
DNA	Deoxyribonucleic acid
DNCC	Dioxobilin-type nonfluorescent Chl catabolite
dT	Deoxy thymidine

E. *coli*	*Escherichia coli*
EDTA	Ethylenediaminetetraacetic acid
EST	Expressed sequence tag
EtOH	Ethanol
ETR1	Ethylene receptor 1
FCC	Fluorescent Chl catabolite
Fd	Ferredoxin
FDCC	Fluorescent dioxobilin-type Chl catabolite
FRK1	FLG22-induced receptor-like kinase 1
FW	Fresh weight
GAB	Gabaculine
GFP	Green fluorescent protein
HCAR	7-hydroxymethyl Chl *a* reductase
HEPES	4-(2-Hydroxyethyl) piperazine-1-ethanesulfonic acid
hmFCC	Hypermodified FCC
HPLC	High performance liquid chromatography
Hv	*Hordeum vulgare*
IAA	Indole-3- acetic acid
IPK	Institut für Pflanzengenetik und Kulturpflanzenforschung
IPT	Isopentyl transferase
IPTG	Isopropyl β-D-1-thiogalactopyranoside
JA	Jasmonic acid
JUB	Jungbrunnen
kb	kilo base
kD	kilo dalton
LHC	Light harvesting complex
Lls	Lethal leaf spot
Lo	*Liquidambar orientalis*
LP	Left primer
Ls	*Liquidambar styraciflua*
Ma	*Muca acuminata*
Mbp	Mega base pairs
Mc	*Musa Cavendish*
MBP	Maltose binding protein
MCS	Metal chelating substance
MeJA	Methyl jasmonate
MeOH	Methanol
MES	Methyl esterase
MeSA	Methyl-SA
MgCH	Magnesium chelatase
MRP	Metal-releasing protein

Ms	*Malus sylvestris*
MS	Mass spectrometry
NAC	Acronym of NAM, ATAF1/2, CUC
NAM	No apical meristem
NEB	New England Biolabs
NCC	Non fluorescent Chl catabolite
NCED	Nine-cis-epoxycaratenoid dioxygenase
n.d.	not detected
NOL	NYC-1 like
NPR1	Non-expressor of pathogenesis related gene1
Nr	*Nicotiana rustica*
NYC1	Non-yellow coloring 1
OCS	Octopine synthase
ODS	Octadecysilyl
ORE	Oresara ; long-living in Korean
PAD	Phytoalexin deficient
PAGE	Polyacrylamide gel electrophoresis
PAO	Pheide *a* oxygenase
PCD	Programmed cell death
PCR	Polymerase chain reaction
Pheide	Pheophorbide
Phein	Pheophytin
pFCC	Primary FCC
PG	Plastoglobule
POR	Protochlorophyllide oxidoreductase
PPD	Pheophorbidase
PPH	Phein Pheide hydrolase
PS	Photosystem
PVPP	Polyvinylpolypyrrolidone
qPCR	quantitative PCR or real-time PCR
RCB	Rubisco-containing body
RCC	Red Chl catabolite
RCCR	RCC reductase
RFF	RCC forming factor
RNA	Ribonucleic acid
ROS	Reactive oxygen species
RP	Right primer
SA	Salicylic acid
SAG	Senescence associated gene

SAV	Senescence-associated vesicle
SDS	Sodium dodecyl suphate
SGR	Stay-green
SIRK	Senescence-induced receptor-like serine/threonine-protein kinase
So	*Spinacia oleracea*
Sw	*Spathiphyllum wallisii*
TBS	Tris-buffered saline
Tc	*Tilia cordata*
T-DNA	Transfer DNA
TEMED	*N*, *N*, *N*′, *N*′-Tetramethylethylenediamine
TIC	Translocon of the inner envelope membrane of chloroplast
Tris	Tris(hydroxymethyl)aminomethane
TTBS	Tween 20 TBS
UCC	Urobilinogenoidic Chl catabolite
UGTs	UDP-glucosyltransferases
UHPLC	Ultra-high performance liquid chromatography
UV	Ultraviolet
UZH	University of Zurich
VNI	VND – interacting
VND	Vascular-related NAC domain
WT	Wild-type
Xv	*Xeropyhta viscosa*
YCC	Yellow Chl catabolite
Zm	*Zea mays*

Abstract/Summary

The phenomenal yellowing of a fully developed leaf is an intricate multifactorial process called senescence which is beneficially tailored in different groups of plants. Specifically, in monocarpic species, leaf senescence is an effective mechanism for remobilizing nutrients from leaves to sink organs like seeds. Most important in this respect is the dismantling of chloroplasts that contain 70% of the total cellular nitrogen whose availability is generally limited in plants. The green pigment chlorophyll, which is essential for light absorption during photosynthesis, is naturally broken down to colorless catabolites to prevent its cytotoxic effects upon photosensitization during senescence-related photosystem degradation. Therefore, the activity of the chlorophyll breakdown machinery is crucial for a plant to allow simultaneous degradation of soluble and membrane-bound photosynthetic protein constituents. The chlorophyll breakdown pathway has been well characterized in the dicot model species *Arabidopsis thaliana* but there is a need to transfer the knowledge to important model crop plants like barley and rice. In the future, this would potentially benefit breeders to have an improved grain yield if the controlling factors, such as onset of leaf senescence, could be engineered in cereals.

Chlorophyll is degraded to two groups of colorless linear tetrapyrroles termed phyllobilins, i.e. DNCCs and NCCs, *via* the so-called PAO/phyllobilin pathway. PAO (pheophorbide *a* oxygenase) is the key committed step in the pathway that ultimately leads to phyllobilin formation. The pathway is divided into two parts, a common first part that leads to the formation of a common intermediate, *p*FCC, and a second part where peripheral modifications are introduced into *p*FCC in a species-specific manner. Despite the vital importance of chlorophyll breakdown during leaf senescence, almost nothing is known about the underlying molecular mechanisms in grasses.

From the investigation of chlorophyll breakdown (largely) in dicot species, most proteins termed chlorophyll catabolic proteins (CCEs) that catalyze the reaction of the first part of breakdown, i.e. SGR, NYC1, NOL, PPH, PAO and RCCR, are molecularly identified. In the work documented in this thesis, I identified potential barley orthologues of these CCE-encoding genes. Using green fluorescence protein fusion constructs, I could demonstrate that, like their *Arabidopsis* counterparts, the barley proteins localize to the chloroplast. Gene and protein expression pattern analysis showed that genes encoding the *Hv*CCEs are upregulated

during senescence. Additionally, I investigated the impact of PAO in chlorophyll breakdown in barley by chemical blocking its activity using a metal chelating substance and confirmed by complementation tests in *Arabidopsis pao1* and *pph-1* mutants that *Hv*PAO and *Hv*PPH are the respective true orthologs in barley. Together these data clearly demonstrate the PAO/phyllobilin pathway to be active in barley (and other cereals), like in dicots such as *Arabidopsis*.

To correlate this with the occurrence of phyllobilins, the proposed end products of breakdown, I investigated their formation by liquid chromatography-mass spectrometry (LC-MS). In the investigated grass species, i.e. barley, wheat, ryegrass, sorghum and rice, I was able to identify a total of 13 phyllobilins, among them four novel, not yet described, DNCCs and three new NCCs. In addition to studying the diversity of phyllobilin formation in grasses, I attempted to examine the nature of some enzymes catalyzing *p*FCC-modifying reactions (second part of the PAO/phyllobilin pathway) that form the diversity of DNCCs and NCCs in grasses using CO and $^{18}O_2$ labelling. Altogether, my data imply that the activities of *p*FCC-modifying enzymes are highly variable between the analyzed monocot species, and their molecular nature remains elusive.

Furthermore, I studied the abundance of phyllobilins in various modern and ancestral varieties of the monocot species to correlate phyllobilin formation with degradation of chlorophyll in leaves. My data show that overall only about 40% to 70% of the degraded chlorophyll is found in the accumulated phyllobilins. More dramatically, in several species such as sorghum, rice and field-grown barley, only traces of phyllobilins were present; i.e. by far not matching the amounts of degraded chlorophyll. Since I could show that the PAO/phyllobilin pathway is active, these data imply that a high proportion of phyllobilins might get further degraded in grasses. For a deeper understanding and identification of such potential further chlorophyll-derived degradation products, ^{13}C-amino levulinic acid-labeling was tested, which would allow following labeled chlorophyll degradation products by LC-MS. However, the preliminary results were too inconclusive and additional research is needed for further dissection of the fate of chlorophyll during degradation in grasses.

Zusammenfassung

Das phenomenologische Vergilben von Blättern erfolgt durch einen komplexen Vorgang, der als Seneszenz bezeichnet wird, und der auf die unterschiedlichen Bedingungen verschiedener Pflanzengruppen optimal zugeschnitten ist. Besonders in einjährigen Pflanzen dient die Blattseneszenz der Remobilisierung von Nährstoffen aus den Blättern in Speicherorgane wie z.B. Samen. In diesem Zusammenhang besonders wichtig ist der Abbau von Chloroplasten, die bis zu 70% des gesamten zellulären Stickstoffs enthalten, dessen Verfügbarkeit für Pflanzen generell limitierend ist. Chlorophyll, das essentiell für die Lichtabsorption während der Photosynthese ist, wird während der Senszenz zu farblosen Abbauprodukten abgebaut, um potentielle phototoxische Effekte zu verhindern, die während des Abbaus der Photosystemkomplexe auftreten könnten. In diesem Sinne ist die Aktivität der chloropyll-abbauenden Maschinerie entscheidend, um der Pflanze den Abbau sowohl löslicher wie auch membrangebundener Proteine der Photosynthese zu ermöglichen. Der Abbauweg des Chlorophylls wurde zwar eingehend in der zweikeimblättrigen Modellpflanze *Arabidopsis thaliana* untersucht, jedoch fehlen bis jetzt weitestgehend entsprechende Untersuchungen in wichtigen Getreidepflanzen, wie der Gerste oder dem Reis. Solche Untersuchungen könnten Züchtern in der Zukunft helfen, neue Sorten mit höherem Ertrag herzustellen, z.B. durch eine verbesserte Kontrolle des Starts der Seneszenz.

Chlorophyll wird zu sogennanten Phyllobilinen, linearen farblosen Tetrapyrrolen, abgebaut, die in zwei Gruppen, sogenannten DNCCs und NCCs, vorkommen. Der Abbauweg wird als PAO/Phyllobilin Weg bezeichnet, da PAO (Pheophorbid *a* Oxygenase) das Schlüsselenzym des Abbauwegs ist, dessen Aktiviät schlussendlich zur Bildung der Phyllobilline führt. Der Abbauweg kann in zwei Phasen eingeteilt werden, einer ersten Phase, die in allen Pflanzen vorkommt und zur Bildung eines gemeinsammen Intermediates, *p*FCC genannt, führt; und einer zweiten Phase, während der pflanzenspezifisch periphere Modifikationen in *p*FCC eingefügt werden. Trotz der Wichtigkeit des Chlorophyllabbaus während der Seneszenz ist beinahe nichts über die zugrunde liegenden molekularen Mechanismen in Gräsern bekannt.

Von Untersuchungen des Chlorophyllabbaus, vor allem in zweikeimblättrigen Pflanzen, sind die meisten Enzyme des Abbaus (sogennante CCEs), die die Reaktionen der ersten Phase katalysieren, wie SGR, NYC1, NOL, PPH, PAO und RCCR, bekannt. In meiner

Doktorarbeit habe ich die potentiellen orthologen CCEs der Gerste identifiziert und mit Hilfe von „green fluoescence protein"-Fusionen zeigen können, dass alle untersuchten Gerste CCEs in Chloroplasten lokalisiert sind, wie es bereits für die entsprechenden *Arabidopsis* CCEs gezeigt wurde. Genexpressionsanalysen zeigten, dass alle Gerste CCEs während der Seneszenz transkriptionell hoch reguliert sind. Zusätzlich konnte ich Bedeutung der PAO für den Chlorophyllabbau in der Gerste durch eine Hemmbarkeit ihrer Aktivität mit einem Chelator zeigen. Durch erfolgreiche Komplementation von *Arabidopsis* Mutanten, die entweder einen Defekt in der PAO oder der PPH haben, konnte ich zeigen, dass die untersuchten Gerste PAO und PPH Proteine tatsächlich ortholog zu den entsprechenden *Arabidopsis* CCEs sind. Zusammenfassend lässt sich also sagen, dass der PAO/Phyllobilin Weg in Gerste (und anderen Gräsern) aktiv ist, so wie in dikotylen Pflanzen wie *Arabidopsis*.

Um einen Bezug zwischen der Aktivität der Enzyme des Chlorophyllabbaus (siehe oben) und der Bildung von Phyllobilinen, den Endprokuten des Abbaus, herzustellen, habe ich deren Auftreten mit Hilfe von Flüssigchromatographie gekoppelt an Massenspektrometrie (LC-MS) untersucht. Ich konnte in den untersuchten einkeimblättrigen Pflanzenarten, d.h. in Gerste, Weizen, Hirse, Raygras und Reis, insgesamt 13 verschiedene Phyllobiline identifizieren, darunter vier bisher nicht beschriebene neue DNCCs und drei neue NCCs. Zusätzlich zur Analyse der Diversität ihres Auftretens in den untersuchten Gräserarten, habe ich Untersuchungen mit Kohlenmonoxid und $^{18}O_2$ Markierungsstudien durchgeführt, um die Aktivität einiger *p*FCC-modifizierender CCEs (also Enzyme der zweiten Phase des PAO/Phyllobilin Abbauwegs), die schlussendlich für die Phyllobilindiversität verantwortlich sind, zu charakterisieren. Zusammengefasst zeigen diese Arbeiten, dass die Aktivität *p*FCC-modifizierender Enzyme innerhalb der untersuchten Gräserarten höchst unterschiedlich ist; ihre molekulare Identität jedoch unbekannt bleibt.

Des weiteren habe ich die Menge der Phyllobiline in verschiedenen modernen und ursprünglichen Gräsersorten untersucht, um einen Bezug zwischen der gebildeten Phyllobilinmenge und der Menge des abgebauten Chlorophylls herzustellen. Meine Daten zeigen, dass durchschnittlich nur gegen 40%-70% des abgebauten Chlorophylls in Phyllobilinen wiederzufinden sind. In einigen Extremfällen, wie Hirse, Reis und auf dem Feld gewachsener Gerste, akkumulierten nur Spuren von Phyllobilinen, d.h. viel zu wenig verglichen mit der Menge abgebauten Chlorophylls. Da ich zeigen konnte, dass der PAO/Phyllobilinweg aktiv ist, legen diese Daten nahe, dass ein grosser Anteil der Phyllobiline

noch weiter abgebaut werden könnte. Um diese Möglichkeit zu untersuchen und entsprechende weitere mögliche Abbauprodukte zu identifizieren, habe ich begonnen eine Methode zu entwickeln, um Chlorophyll mit ^{13}C-Aminolävulinsäure zu markieren und die Markierung der Abbauprodukte anschliessend mit LC-MS zu verfolgen. Die durchgeführten vorläufigen Experimente waren jedoch zu unschlüssig und es braucht in der Zukunft mehr Forschung, um den Mechanismus des Chlorophyllabbaus in Gräsern vollständig zu entschlüsseln.

INTRODUCTION

1. Leaf Senescence

1.1. Brief introduction to leaf senescence

In layman's term, the process behind the magnificent display of autumnal color changes in the leaves of various trees across the globe is known as leaf senescence. Scientifically, it is better described as the orchestrated event which is tightly regulated by series of biochemical and physiological processes encompassing the final stage of plant tissue, organ or whole plant development (Parrott et al., 2005; Lim et al., 2007). It is not a fully understood process but a lot is unveiled over the past century to a great extent by using *Arabidopsis* as a model plant. Senescence takes place differently in various parts of the plant. This evolutionarily selected developmental process can be broadly classified into two types of senescence: mitotic (replicative/proliferative) senescence and post-mitotic senescence (Gan, 2007). Mitotic senescence refers to the stage that ends the mitotic cell division of a cell. For example, the apical meristem in plants is a collection of non-differentiated germ-like cells which when losing the capacity to produce cells for formation of new organs (leaves or flowers etc.) undergoes replicative senescence. On the other hand, plant organs such as leaves where cell expansion takes place more than cell division and its inability to divide is not the primary factor behind leaf senescence. In other terms, leaves exhibit post-mitotic senescence which is a degenerative process that takes place when the cell is fully matured or differentiated (Gan, 2007).

Leaf development starts with the formation of a leaf primordium followed by its expansion, maturation until it is withered and separated from the plant. The deterioration process starts after reaching leaf maturity or in other words leaf senescence is basically governed by the developmental age. The classic example to this can be set by a monocarpic plant (like *Arabidopsis*) that has a single reproductive phase after which it senesces and finally dies (Hensel et al., 1993; Noodén and Penney, 2001). Although it is not vividly clear how developmental age regulates the onset of senescence it has been reported that leaf senescence can be correlated to leaf longevity. For example, in *Arabidopsis*, late flowering and male/female sterile mutants that have delayed or impaired reproductive growth, respectively, showed leaf lifespan like a wild-type (Hensel et al., 1993; Noodén and Penney, 2001). In a

plant's life, developmental age is an important factor along with many other players such as hormones, genes, transcription factors, epigenetics, enzymatic reactions, proteins etc. which constitutively play a crucial role in driving the plant's physiology.

1.2. Regulatory overview

The regulation of leaf senescence is governed by a lot of metabolic and genetic factors. The complexity of metabolic regulation of senescence has been studied over the past decades but a clear picture could yet not be drawn. The metabolic profile in a plant is liable to changes occurring in the system and hence metabolites like sugars play a key role in the regulation of plant metabolism and development (Wingler and Roitsch, 2008). Senescence is also influenced by various external and internal factors. These external or environmental factors can be divided into abiotic and biotic ones. Drought, nutrient limitation, extreme temperature, and oxidative stress by UV-B irradiation and ozone contribute as abiotic factors. The biotic factors affecting leaf senescence include phytohormones, pathogen infection and shading by other plants (Lim et al., 2007). These environmental conditions very often become unfavorable for plants; thus, to combat plants have evolved rapid response mechanisms (like senescence of a diseased part etc.) surpassing their immobility. Thus, during senescence plants possess a complex regulatory interaction of sugars and plant hormones modulated by abiotic factors and developmental age as outlined in **Figure 1**.

The effect of intercellular sugars on the onset of senescence has long been debated. There were several studies in the past which show that increase or decrease in sugar levels affect leaf senescence. But accumulation of sugars during senescence has also been questioned with a thought that it could be the result of senescence rather being the causal signal. Various studies carried out favor one or the other hypothesis about sugar levels triggering senescence (Van Doorn, 2008). However, sugar signaling intensively interacts with plant hormone signaling which leaves scientists more intrigued about the underlying regulatory mechanisms. Major plant hormones or phytohormones such as auxins, cytokinins, ethylene, abscisic acid and gibberellins play a crucial role in plant development and regulation of leaf senescence but again the precise mechanisms of action are not exactly known yet (Lim et al., 2003; Gan, 2007; Lim et al., 2007; Abreu and Munné-Bosch, 2008). There are also other plant growth regulators like salicylates, jasmonates, brassinosteroids and polyamines which are known to influence

leaf senescence (Abreu and Munné-Bosch, 2008). The regulatory role of some of the hormones on leaf senescence are discussed further in this section.

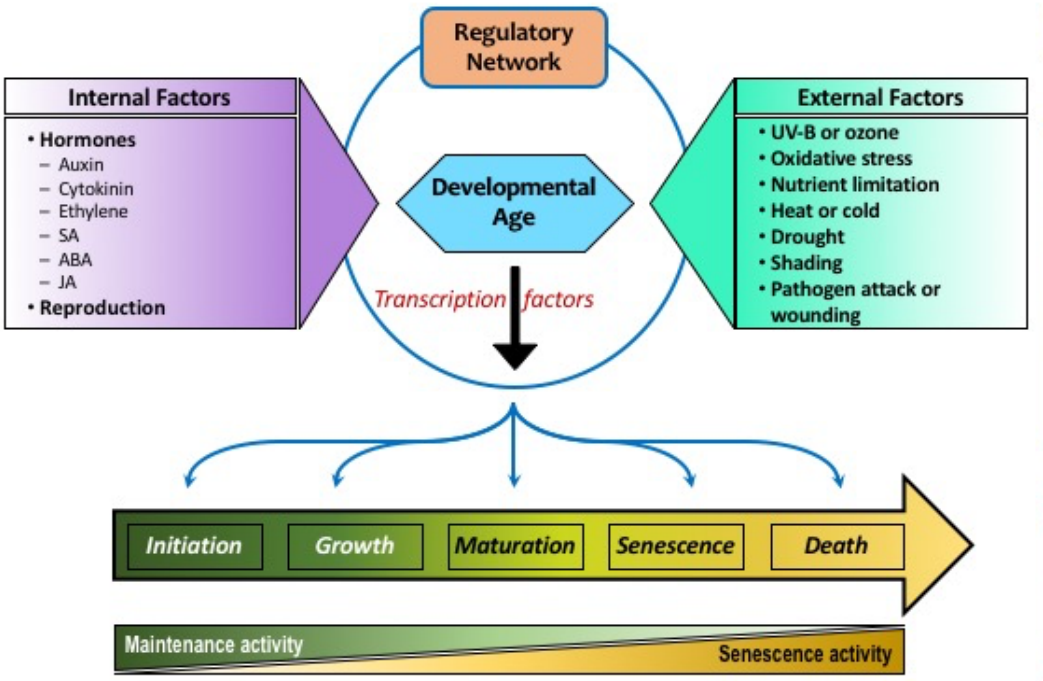

Figure 1: A model for regulatory network pathways in leaf senescence. Leaf senescence is a complicated process involving trigger factors such as internal and external signals along with various transcription factors that integrate into the developmental age-dependent senescence pathways. The figure is adapted and modified from Lim et al., 2007.

1.3. Role of auxins

Several studies suggest the involvement of auxin in the senescence process and abscission but questions exist about its mode of action. Auxins are one of the most important plant growth hormones. It was observed in *Arabidopsis* that increase of production of the commonly known endogenous auxin, IAA (indole-3-acetic acid) leads to a delay in plant senescence (Ellis et al., 2005; Okushima et al., 2005). The expression of the transcription factor Auxin Response Factor 2 (ARF2) has been shown to increase in response to senescence but also said that targets of ARFs may vary which would bring about variation of different aspects of senescence (Ellis et al., 2005). Numerous more studies are required to understand auxin-regulated senescence or whether senescence affects auxin.

1.4. Role of cytokinins

Among the major plant hormones, cytokinins and ethylene are known to have definite roles in the regulation of senescence (Smart, 1994). The first experiments were performed in excised leaves of *Xanthium pennsylvanicum* that showed a negative correlation between cytokinin treatment and chlorophyll content (Richmond and Lang, 1956). Further experimentation showed that cytokinins were responsible for delaying senescence (Zwack and Rashotte, 2013). Cytokinins are plant hormones that are synthesized mainly in the roots and transported by the xylem to other parts of the plant where they are responsible for cell division, growth and developmental processes. Rapid decrease in xylem cytokinin levels have been observed at the onset of senescence in *Glycine max* (Noodén et al., 1990). Likewise, the xylem sap of a normal senescing *Sorghum* cultivar carried less cytokinin compared to a cultivar exhibiting delayed leaf senescence (Zwack and Rashotte, 2013). The enzyme isopentenyl transferase (IPT) catalyzes the rate-limiting step in cytokinin biosynthesis. Transgenic plants containing the *IPT* gene under the regulation of the promoter of the senescence associated gene (SAG) *SAG12* showed significant suppression of leaf senescence along with high photosynthetic activity and flower production (Gan and Amasino, 1995). This proSAG:*IPT* system has been used in many crop plants like rice, wheat, ryegrass, cassava etc. In addition to this, transcriptomic studies have also shown that expression of cytokinin biosynthetic genes is indirectly proportional to the expression of cytokinin degrading genes in *Arabidopsis* leaves (Buchanan-Wollaston et al., 2005; Breeze et al., 2011). These observations suggest that delay in leaf senescence by cytokinins is part of a endogenous developmental process and not a mere result of exogenous treatment (Zwack and Rashotte, 2013).

1.5. Role of ethylene

Ethylene is one of the commonly known phytohormones famous for its regulatory role in seed germination, fruit ripening and flower senescence. It also acts as a hormonal response to external signals such as wounding, pathogens and stress caused by ozone (Zarembinski and Theologis, 1994). Earlier studies in climacteric fruits and certain flowers have shown that ethylene regulates the expression of transcripts of the enzymes involved in fruit and flower senescence, respectively (Theologis, 1992). The two key enzymes 1-amino-cyclopropane-1-carboxylic acid (ACC) synthase (ACS) and ACC oxidase (ACO) are involved in the

biosynthesis of ethylene from S-adenosyl methionine. There are many studies that detected increased expression of the genes encoding these enzymes in senescing fruit and petals (Hamilton et al., 1990; Park et al., 1992). In transgenic tomato plants where expression of the *ACO* gene was repressed, significant decrease in the rate of fruit ripening was observed when the gene and ethylene production was reduced (Picton et al., 1993). Comparatively, its effect on leaf senescence was smaller i.e. although leaf senescence was delayed by about 10-14 days and leaves remained photosynthetically active, it progressed with the same speed as in wild-type leaves after the onset of senescence (John et al., 1995).

Similarly, an involvement of ethylene in the regulation of leaf senescence of detached rice leaves has been demonstrated by the external application of ACC and some inhibitors. Exogenous supply of ACC to detached rice leaves showed significant increase in ethylene production which in turn accelerated senescence of the leaves under both dark and light conditions. The opposite effect was observed in the presence of inhibitors of ethylene production such as aminoethoxyvinylglycine (AVG) and aminooxyacetic acid (AOA) (Bradford et al., 1982). Senescence was retarded in the detached rice leaves when they were subjected to Co^{2+}or Ni^{2+} (inhibitors of ethylene production) (Kao and Yang, 1983).

The ethylene-insensitive *Arabidopsis* mutant *etr1-1 (ethylene-resistant)* showed delayed senescence but once started no significant changes in the level of expression of SAGs was noticed compared to the wild-type plants. The SAGs expression was age-related even when wild-type plants were externally treated with ethylene. This effect is similar to the fact that tomatoes have to be of certain age before they can be ripened by ethylene induction. These studies suggest that ethylene can only activate senescence-related genes when age-related factors are expressed. Therefore, it can be said that ethylene does not directly modulate leaf senescence (Buchanan-Wollaston, 1997).

1.6. Role of abscisic acid

Abscisic acid (ABA) is a vital plant hormone that regulates plant growth, developmental processes like seed and bud dormancy, seed germination etc. and also mediates stress responses to abiotic factors such as drought, cold and high salinity (Lim et al., 2007; Yamburenko et al., 2013; Zhao et al., 2016). ABA is known to induce stomatal closure as a quick and short response to extreme drought which blocks most water loss and enables the

plant to prepare for long-term responses such as induction of a dormant phase mainly in seeds and buds. This defensive act of plants involves leaf senescence and/or abscission of old organs. It has been documented through various experiments that plants such as rice, maize, *Arabidopsis* and tobacco show high endogenous ABA levels in senescing leaves promoted by environmental stress conditions (Lim et al., 2007; Lee et al., 2011). In addition to this, genes associated with ABA signaling are up-regulated and exogenous application of ABA induces many SAGs which eventually accelerate leaf senescence indicating interplay between ABA signaling and leaf senescence (Quiles et al., 1995; Tan et al., 2003). Senescing leaves show increased levels of genes involved in ABA biosynthesis encoding 9-*cis*-epoxycarotenoid dioxygenase (NCED) and abscisic aldehyde oxidases AAO1 and AAO3 along with increased ABA levels (Lim et al., 2007; Finkelstein, 2013). These studies suggest ABA as an important regulator of plant senescence. Furthermore, several studies focused on using ABA-defective and ABA-insensitive mutants but the underlying molecular mechanism is still limited (Lee et al., 2011). Recent studies using transgenic *Arabidopsis* have shown that concurrent regulation of ABA-induced dormancy-related genes and ABA-induced senescence-related genes takes place such that source tissues undergo senescence and sink tissues turn dormant to sustain stressful environmental conditions (Zhao et al., 2016).

1.7. Role of salicylic acid

Plants have many signaling components in response to exogenous stresses like pathogen invasion, ozone and UV-B exposure (Morris et al., 2000). One of the key phytohormones that plays a crucial role in plant defense and stress responses is salicylic acid (SA) which is a phenolic compound by nature (Zhang et al., 2013). Salicylic acid has been reported to promote resistance of plants against biotrophic pathogens (Wingler and Roitsch, 2008). Apart from its primary roles, many studies in *Arabidopsis* suggest that SA participates either directly or indirectly in the regulation of SAGs during leaf senescence. Senescing leaves of *Arabidopsis* contain four times higher amounts of endogenous SA which seems to play a role in upregulating several SAGs (Jirage et al., 1999).

Mutants such as *npr1* (*non-expressor of pathogenesis related gene1*; which lacks NPR1-dependent SA signaling), *pad4* (*phytoalexin deficient 4*; which exhibits defects in defense responses like SA signaling) and *NahG* transgenic plants encoding a protein that

degrades SA show substantial decrease in the expression of the cysteine protease gene *SAG12* pointing towards its involvement of gene expression during developmental leaf senescence (Jirage et al., 1999; Morris et al., 2000; Lim et al., 2007; Jayakannan et al., 2015). Transcriptomic analysis of transgenic plants positively supports the aforementioned finding of the role of SA (Buchanan-Wollaston et al., 2005). However, it has been found that SA also participates in the regulation of drought-induced leaf senescence of the perennial plant *Salvia officinalis* although molecular mechanisms of its regulation needs further investigation (Abreu and Munné-Bosch, 2008).

1.8. Role of jasmonic acid

It has been long since it is known that methyl jasmonate (MeJA) and its precursor jasmonic acid (JA) are powerful promoters of leaf senescence which was first shown in detached oat leaves (Rudell et al., 2002). Several studies have shown acceleration of senescence and SAG expression in attached and detached leaves of wild-type *Arabidopsis* when subjected to exogenous JA although *Arabidopsis* mutants in JA synthesis or signal transduction do not show a delayed leaf senescence phenotype (Rudell et al., 2002) . On the other hand, JA-insensitive *coronatine insensitive 1* (*coi1*) mutants have been shown to be defective in JA-dependent senescence. The role of JA in leaf senescence is yet not clear. Similar studies in barley have also demonstrated that external application of MeJA and JA decreased the expression of the gene encoding for the small subunit of Rubisco and increased the degradation of Rubisco and chlorophyll (Parthier, 1983; Weidhase et al., 1987). Furthermore, a nuclear-localized CCCH-type zinc finger protein *Os*DOS (*Oryza sativa* Delay of the Onset of Senescence) in rice was shown to be involved as a negative regulator of leaf senescence integrating the JA pathway (Kong et al., 2006).

1.9. Transcriptional and genetic regulation

Like many other biological processes, leaf senescence is a genetically active program that involves differential expression of hundreds of genes during the process. Genes whose corresponding messenger RNAs are upregulated during senescence are collectively known as senescence-associated genes (SAGs) (Buchanan-Wollaston, 1997). In the past years such genes

have been used as tools to study biochemical, regulatory and cellular pathways associated with senescence (Gepstein et al., 2003). Some of the prominent SAGs to mention are those encoding for degenerative enzymes such as proteases, lipases, nucleases, glutamate synthase etc., but recently numerous SAGs have been identified that encode transcription factors that presumably act as central elements of the regulatory network (Woo et al., 2013). Genetic regulation by transcription factors and the genes encoding them is a vast and complex process which is very briefly discussed below. It has been reported that in *Arabidopsis* alone, genes for 96 transcription factors have identified that are upregulated at least threefold in senescing leaves. These belong to 20 different transcription factor families, the largest groups being NAC, WRKY, C2H2-type zinc finger, AP2/EREBP, Aux/IAA, and MYB proteins (Lim et al., 2007).

It has been about twenty years that NAC (NAM, ATAF1 AND CUC2) transcription factors have been identified, which are one of the largest families of plant-specific transcription factors. *NAC* genes are highly abundant and very specific to plants (Olsen et al., 2005). There are more than 100 known *NAC* genes in *Arabidopsis* (Buchanan-Wollaston et al., 2005). Various studies have shown that *NAC* family genes have substantial function in developmental processes like embryo and shoot meristem development, flower and lateral root formation, hormone signaling, and defense response to biotic and abiotic stress and senescence (Hoth et al., 2002; Seki et al., 2002; Rabbani et al., 2003; Hennig, 2004; Lin and Wu, 2004).

The significant role of *NAC* genes and proteins during *Arabidopsis* senescence has been demonstrated over the past years. *At*NAP, ORE1, ORS1, ANAC016 and ATAF1 are some of the known positive NAC regulators of senescence in *Arabidopsis* and their functional blockage causes delayed senescence (Podzimska-Sroka et al., 2015). On the contrary, JUB1 and VNI2 are negative regulators of leaf senescence. In barley, the putative *NAC* genes have been classified into three groups based on gene expression data (Christiansen and Gregersen, 2014). *HvNAC026* represents the first group which is highly up-regulated in senescing flag leaves. The second group consists of 5 genes, *HvNAC005*, *HvNAC023*, *HvNAC027*, *HvNAC029* and *HvNAC030* which are initially up-regulated but gradually are down-regulated at later stages of flag leaf senescence. *HvNAC013*, *HvNAC022* and *HvNAC025* make up the third group which show strong up-regulation in the final stages of flag leaf senescence (Christiansen and Gregersen, 2014). There are several other studies in rice, cotton, wheat etc. where a role of *NAC* genes in leaf senescence has been studied and their active participation has been demonstrated (Liu et al., 2008; Meng et al., 2009).

The other plant-specific transcription factors are the WRKY proteins encoded by a multigene family. The most characterized among these in relation to leaf senescence are *At*WRKY6 and WRKY53. Expression studies have shown that *AtWRKY6* is strongly upregulated during leaf senescence (Robatzek and Somssich, 2001). *SIRK*, a gene encoding a receptor-like protein kinase now known as *FLG22*-induced receptor like kinase 1 (*FRK1*), whose developmental expression is strongly induced specifically during leaf senescence, is dependent on WRKY6 function (Rinerson et al., 2015). Reduced formation of *FRK1* transcripts was observed in senescing leaves of *wrky6* knockout mutants while green leaves of WRKY6 overexpression lines showed elevated *FRK1* transcript levels. *In vivo* studies have also demonstrated the specific activation of the *FRK1* promoter by WRKY6 (Robatzek and Somssich, 2002).

*At*WRKY53 plays a crucial role in both leaf senescence and pathogen responses. WRKY53 knockout lines exhibited delayed leaf senescence whereas when overexpressed, it led to premature leaf senescence (Miao et al., 2004). It has recently been found that there are other *At*WRKY factors that influence leaf senescence such as *At*WRKY18, which acts as a positive regulator of leaf senescence by repressing *At*WRKY53 activity and *At*WRKY22 having a regulatory role in dark-induced leaf senescence (Potschin et al., 2014; Rinerson et al., 2015). Perhaps, there is cross regulation between *At*WRKY22, *At*WRKY6, *At*WRKY53 and *At*WRKY70 (Zhou et al., 2011b). Apart from *Arabidopsis*, WRKY factors from rice such as *Os*WRKY42, *Os*WRKY80 and *Os*WRKY23 have also been demonstrated to play an important role in regulating senescence of leaves (Han et al., 2014).

Evidently, from past findings and recent observations it can be said that a lot has been understood in the field of hormonal and genetic regulation of leaf senescence. But considering the complexity of leaf senescence more effort is required to investigate further its molecular mechanisms. Nevertheless, substantial knowledge has also been acquired in the structural and biochemical aspects of leaves during senescence some of which is discussed in part 3 of this Introduction section. But before, I will present various possibilities of translating the aforementioned physiological information of leaf senescence to the field and the importance behind this.

2. Importance and Impact of Leaf Senescence on Crop Improvement

One of the major global concerns today is feeding the growing world's population both at present and in the future. With each passing day, the world population is increasing at an alarming rate which is proportional to the rate of the diminishing of arable land. Other factors such as drastic changes in climate patterns, excessive food waste in developed countries, water scarcity and lack of efficient post-harvest management in developing nations have resulted in tremendous amount of pressure on utilizable resources (Wu et al., 2012). Combined together, these factors contribute to global food insecurity which is comprised of plant species that have been cultivated for food and feed since time immemorial, known as food crops. Food crops are the commonly grown grains, fruits and vegetables for human consumption. The major known grain crops include rice (*Oryza sativa*), wheat (*Triticum aestivum*) and maize (*Zea mays*) (Ji et al., 2013). There are other grain crops such as barley which is mainly used for feed and malt. Orphan grain crops or underutilized crops such as *Sorghum*, soybean, millet, quinoa, etc. are produced as staple crops in the developing nations. These orphan crops are occasionally considered major in their regional preference. Most of these grain crops are annual monocarpic cereal plants (Ji et al., 2013). One of the current major limitation in crop production posed by scientists and breeders are the individual or combined effects of biotic and abiotic stresses leading to about 30-60% global yield loss per annum.

Scientists and breeders from all over the world are actively looking for different traits, markers and other possible mechanisms that can be manipulated for improving crop yield and quality, both pre- and post-harvest (Gan and Amasino, 1997). By now we know that senescence is an integral and essential physiological process in plants which is well coordinated at the molecular, genetic, cellular and subcellular levels. It is an interactive play of different metabolic pathways in a highly organized manner. It occurs in leaves, flowers, fruits, roots etc. among these one of the agronomically important subject is leaf senescence which encompasses sequential regulation at various levels within the leaf finally leading to death in monocarps. In agriculture, leaf senescence is under the limelight of scientific research for a deeper understanding of regulatory mechanisms which can be targeted for crop improvement.

There are primarily four main benefits of studying leaf senescence as a potential agronomic trait. It has been associated with increase in crop yield, biomass, postharvest longevity and quality (Gan, 2014). Taking the amount of journal publications into consideration it is obvious that intensive research in leaf senescence has been carried out in the

dicot model plant *Arabidopsis* due to innate reasons like short generation time (8 weeks from seed to seed), small height and genome size (140 Mb), easy growth at high density in greenhouses, self-pollination, ability to produce thousands of seeds. In addition to these natural benefits, availability of vast genetic resources (includes various natural variants, mutant and transgenic lines, genetic map etc.), efficient stable transformation techniques and completely sequenced genome aids in ease of *Arabidopsis* research (Meinke, 1998). Nevertheless, there are also several other dicot species being studied like tomato, pea, petunia etc. which are commercially more demanding.

Table 1: Table showing some of the advantages and disadvantages of four of the world's major crops in comparison with the dicot model *Arabidopsis*. Table compiled from multiple sources.

Characteristic	*Arabidopsis*	Rice	Wheat	Maize	Barley
Dicot / Monocot	Dicot	Monocot	Monocot	Monocot	Monocot
Number of chromosomes	2n=10	2n=24	2n=42	2n=20	2n=14
Genome size (Mbp)	125	430	17000	2300	5100
Genetic transformation	Possible	Possible	Possible	Possible	Possible
Pollination	Self	Self	Self	Self	Self
Naturally stress tolerant (drought)	Yes	No	No	Yes	Yes
Limitation	Not a cereal crop	Demanding growth conditions	Complex genome	Large plant size	Diseases and pests

In the course of their studies, scientists have eventually realized the importance to transfer the knowledge from *Arabidopsis* to plant species responsible for feeding the world i.e. crop grain plants or cereals. A lot has been studied in understanding different aspects of the

two major cereals i.e. wheat and rice. Extensive research is being carried out to find targets for crop improvement. Rice being a major crop that has been cultivated for more than 7000 years and feeding more than half the world population. The major cereal crops like rice, wheat, barley, maize vary to a large extent in their genome complexity, anatomy and physiology. Each of these species offer certain advantages and limitations as briefly listed in **Table 1** (Biswas and Choudhuri, 1980; Boote et al., 1996; Shimamoto and Kyozuka, 2002; Gan, 2007; Burger et al., 2008; Strable and Scanlon, 2009; Koornneef and Meinke, 2010; Gregersen et al., 2013; Michael and Jackson, 2013). Small genome, rapid life cycle, easy transformability, diploid genetics with few chromosomes, being well positioned in plant phylogeny, small stature (for growth in small space), production of large numbers of seeds, convenience for discovery of gene-trait linkages at low cost and high speed are some of the key attributes of a model crop species. However, none of the monocot crops fulfills all of these criteria. Furthermore, the evolutionary distance between *Arabidopsis* and monocots (**Figure 2**) always limits the use of knowledge from one species to another after a certain point. Thus scientifically, monocot research had to co-evolve and currently various cereal crops such as wheat, rice, barley and maize are intensely investigated. Also, the economic value adds to the demand of studying these crops in details.

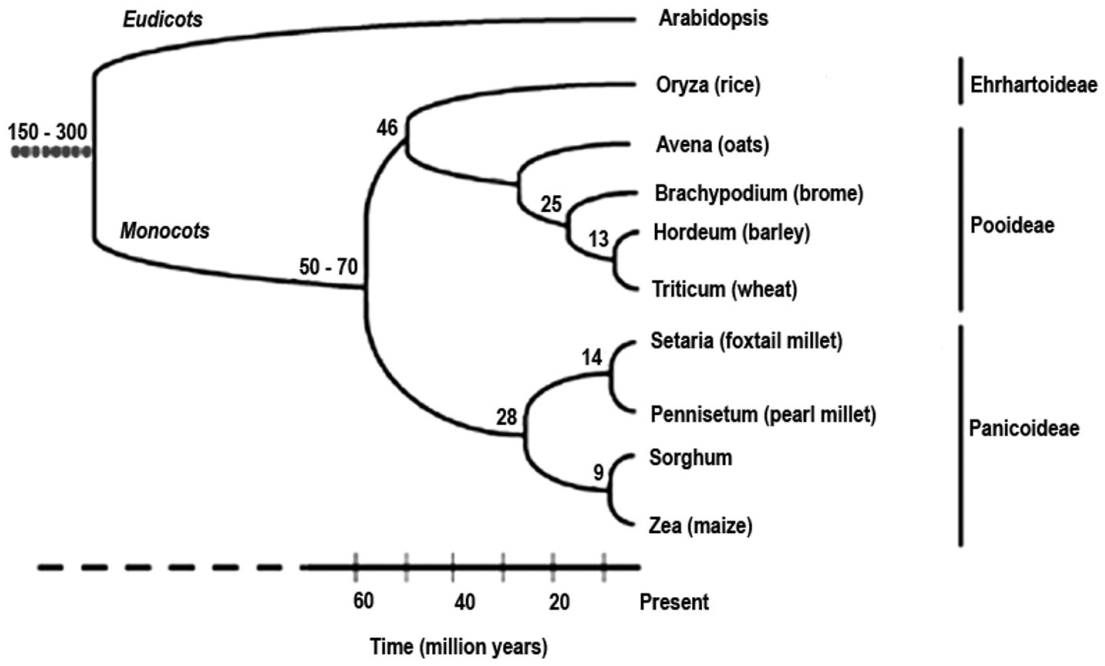

Figure 2: Evolutionary and phylogenetic relationship of *Arabidopsis* to other cereal crops (Strable and Scanlon, 2009).

Most of the crop plants being discussed in this thesis and in the world undergo monocarpic senescence which involves remobilization and translocation of mineral nutrients from vegetative parts to sink organs (maturing fruit) in the final stage of plant development. Thus, many scientists have studied the association between senescence and crop plant productivity.

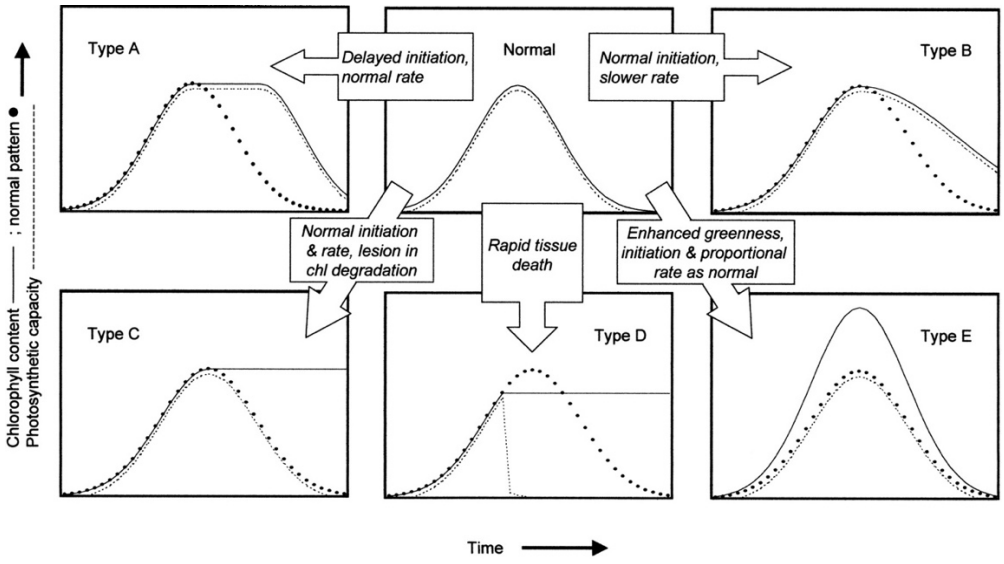

Figure 3: Diagram depicting the five suggested ways to attain a stay-green phenotype. The curves depict the nature of chlorophyll content and photosynthetic capacity (arbitrary scale) for a representative leaf, whole plant or canopy (Thomas and Howarth, 2000).

Basically it has always been assumed that delayed senescence leads to higher yields considering that an extended period in the field allows the plant to have maximal photosynthetic activity. Indeed, there are numerous reports that demonstrate in various cultivars, mutants and transgenic plants a correlation between delayed senescence phenotypes and increased amounts of biomass or grain/seed yield. Delayed senescence is visible to the eye as retention of chlorophyll when compared to standard reference senescing leaves. In other words, plant variants which show delayed loss of chlorophyll or retention of chlorophyll are generally termed as stay-green and have fundamentally been classified into five types (Thomas and Howarth, 2000).

Type A stay-greens are delayed in the onset of senescence but follow normal rates of senescence progression whereas type B stay-greens are opposite in action. Type-C stay-greens

are also known as cosmetic stay-greens because they carry out senescence kinetics normally but phenotypically retain chlorophyll more or less indefinitely. Type D stay-greens retain their green pigments due to sudden death of the tissue from shock treatments such as freezing, boiling etc. Type E stay-greens display intense chlorophyll content with a normal pace of senescence kinetics. The five ways to stay-green are illustrated in **Figure 3** (Thomas and Howarth, 2000). Over the years, it has been demonstrated that delayed senescence in plants can be achieved through (i) alteration of endogenous hormone level in transgenic plants which can manipulate plant senescence; (ii) manipulation of SAGs and other key regulatory transcription factors which could bring about changes in chlorophyll content, photosynthesis etc.; (iii) manipulation of translation initiation factors involved during plant senescence (Guo and Gan, 2014).

One such revolutionary change leading to a stay-green phenotype is the hormone approach. As mentioned earlier, cytokinins are one of the key hormones known to retard senescence. As mentioned above, in 1995 a group of scientists first exploited this hormonal system by altering the *IPT* gene which encodes for the enzyme (isopentenyl transferase) catalyzing the rate-limiting step in cytokinin biosynthesis (Gan and Amasino, 1995). Later on, many transgenic plants were produced by employing the *IPT* gene from *Agrobacterium tumefaciens* with a senescence-inducible promoter. Such plants have shown correlation between delayed leaf senescence and enhanced productivity. A few examples are listed in **Table 2**. Additionally, it has been reported in *Arabidopsis* that altered expression of genes encoding transcription factors such as WRKY and NAC can be potential targets for senescence manipulation leading to crop enhancement. For example, a NAC transcription factor NAM-B1 encoded by an allele of ancestral wild emmer wheat have been found to accelerate senescence and increases nutrient reallocation from leaves to developing grains. An opposite effect has been observed in the modern wheat varieties carrying the nonfunctional *NAM-B1* allele (Uauy et al., 2006). Enhancement of crop productivity relates to the two most important factors, i.e. biomass and seed yield. To reach this goal, further extensive research is needed to understand the coordinated processes of plants between the vegetative and reproductive phase of development because the length of the reproductive period of a plant is often related to the time of anthesis and to photosynthetic activity. Stay-green variants with delayed onset of senescence can prove beneficial for biomass production through their "green" growth phase. On the other hand, slow kinetics of senescence enhances seed yield owing to a longer grain filling period (Gregersen et al., 2013). Many such studies strongly support the importance of studying

senescence for crop improvement and productivity although it's a very complex relationship. However, multidisciplinary studies on this subject shall aid in achieving this goal.

Table 2: Table showing some of the transgenic crop plants with autoregulated expression of the *IPT* gene during leaf senescence (n.d. = not determined) (modified from Gregersen et al., 2013).

Plant species	Promoter	Chlorophyll	Other phenotypic characteristics	Biomass/Yield
Tobacco	*SAG12*	Stay-green	Prolonged photosynthetic life-span	50 % more biomass (dry weight)
	SAG12	250 % compared to wild-type	Delay in decline of photosynthesis related enzymes	n.d.
	SAG12	No decline	Delay in decline of photosynthesis	Higher dry weight of basal leaves
	SARK	–	Drought tolerance	Increase in biomass
Rice	*SAG12*	Stay-green	n.d.	Higher number of seeds and panicles
	SAG39	Stay-green	Altered source-sink relations	Higher number of panicles
Maize	*SAG12*	Normal leaf yellowing	–	More florets
	SEE1	No leaf yellowing, sudden cell death	Extension of photosynthesis in old leaves	n.d
Ryegrass	*SEE1*	Stay-green	Spontaneous lesions	n.d.
Wheat	*SAG12*	+32 %, Flag leaves 10 daf	n.d	No effect on grain yield

3. Chlorophyll Breakdown Pathway

3.1. Brief introduction to degradation of chlorophyll

After the onset of senescence, a series of metabolic reactions takes place in the leaf, but the most visible symptom of the process is the loss of chlorophyll. During this process, apart from biochemical changes, there are also some structural changes that take place such as dismantling of various organelles, although not at the same time. The first structural change is the conversion of chloroplasts into senescing chloroplasts, called gerontoplasts, while the mitochondria and nucleus remain more or less intact until the last stages of leaf senescence. The term gerontoplasts was first coined by Sitte in 1977 (Matile et al., 1999). Gerontoplasts are known by their small size, decreased amounts of stromal and thylakoid components and presence of vesicular bodies called plastoglobules. Senescence is also accompanied by thylakoid galactolipid degradation forming free fatty acids which in turn provide energy for the senescence process (Matile et al., 1999).

Chlorophyll (Chl) is broken down via the PAO/phyllobilin pathway. This pathway has been well elucidated in the dicot model plant *Arabidopsis*. The name of the pathway accounts to the structural similarity of the degradation products to bilins, degradation products of heme, and to pheophorbide *a* oxygenase (PAO) for being the key enzyme of the pathway (Christ and Hörtensteiner, 2014). The PAO/phyllobilin pathway comprises sequential enzymatic reactions that can be broadly divided into an early and a late phase. These reactions are catalyzed by different enzymes collectively known as chlorophyll catabolic enzymes (CCEs). It has been recently hypothesized that the chloroplast-localized stay-green (SGR) protein might play the essential role of recruiting these CCEs at the thylakoid membrane for the catabolism to take place (Sakuraba et al., 2012). Although the precise role of SGR is still unclear, it seems crucial considering the findings that *sgr* mutants have a type-C stay-green phenotype and partially retain LHCs along with the core subunits of photosystem (PS) I and II. Additionally, SGR has been shown to interact with LHC proteins of PSII which cumulatively suggests that SGR might be involved in the destabilization of Chl-apoprotein complexes of PSII during senescence. However, there are other studies that show SGR participating in root nodule senescence in *Medicago truncatula* (Zhou et al., 2011a) or in carotenoid biosynthesis during tomato fruit ripening (Luo et al., 2013). Perhaps, the role of SGR is not limited to the chlorophyll breakdown process (Christ and Hörtensteiner, 2014).

3.2. Early phase

The early phase of the pathway takes place in gerontoplasts. It starts with the conversion of Chl *b* to *a* and is followed by the formation of various intermediates until *p*FCC.

3.2.1. Conversion of Chl b to Chl a

The PAO/phyllobilin pathway commences with the conversion of Chl *b* to Chl *a* as a prerequisite of the downstream enzyme PAO, which only accepts pheophorbide (pheide) *a* as the substrate (Hörtensteiner et al., 1995; Ito et al., 1996). It has been shown that all phyllobilins (except one) are derived from Chl *a* and not from Chl *b* as indicated by the presence of a methyl group at the C^2 position found in all chlorophyll catabolites (Kräutler and Matile, 1999). An exception to this finding is the existence of one catabolite in *Arabidopsis* which has a hydroxymethyl group at the C^2 position (see **Figure 5A** for atom numbering of phyllobilins) which was thought to be derived from incompletely reduced Chl *b* (Müller et al., 2006). The conversion of Chl *b* to Chl *a* is catalyzed by two enzymes, chl *b* reductase (CBR) and 7-hydroxymethyl chlorophyll *a* reductase HCAR (Tanaka and Tanaka, 2011). Chl *b* reductase is a NADPH-dependent enzyme encoded by *non-yellow coloring 1 (NYC1*) and *NYC-like (NOL)* in plants (Kusaba et al., 2007; Sato et al., 2007; Sato et al., 2009). *NYC1* and *NOL* were first isolated from rice and it was experimentally shown that the proteins co-localize in the thylakoid membrane possibly forming heterodimers (Kusaba et al., 2007). From *in silico* hydrophobicity analysis of their protein sequences, NYC1 and NOL were suggested to be a membrane and soluble protein, respectively (Kusaba et al., 2007). Supression of either rice ortholog, NYC1 or NOL, causes a cosmetic stay-green phenotype with high Chl *b* retention in the mutants without signs of lesions.

3.2.2. Demetalation

The literature describes two possible kinds of metal chelating activities. One of them are metal chelating substances (MCS) which are heat stable, low molecular weight compounds isolated from *Chenopodium album* (Shioi et al., 1996) and strawberries (Costa et al., 2002). The other are Mg-releasing proteins (MRP) (Suzuki and Shioi, 2002). The difference between the two activities lies in their substrate specificity. It was shown that MCS was active with both chlorophyllide (native substrate) and chlorophyllin (artificial substrate) whereas MRP resulted in activity only in the presence of chlorophyllin which suggested that the low molecular weight compounds could be responsible for the loss of Mg (Suzuki and Shioi, 2002; Suzuki et al.,

2005). There are other evidences that indicate that Mg-dechelation is not an enzymatic reaction but rather may be sensitive to pH changes (Hirai et al., 2009; Saga and Tamiaki, 2012). But the molecular mechanism underlying Mg removal is still not yet clear and needs more scientific investigation. Thus, this step of the pathway has made researchers ponder over its sequential positioning for years. For a long time, Chl dephytylation was thought to precede demetalation until recent demonstration of the dephytylation activity by the hydrolase pheophytinase (PPH) following demetalation as the first step of Chl *a* breakdown (Schelbert et al., 2009).

3.2.3. Phytol chain cleavage

Dephytylation i.e. removal of the phytol chain, is of great significance because the cleavage of the hydrophobic ester bond increases the water solubility of further breakdown products. In 1913, Willstätter and Stoll first discovered an enzyme called chorophyllase (CLH) which could hydrolyze the phytol tail of Chl. Later, chlorophyllase was purified and characterized *in vitro* from many different species like barley leaves, *Citrus* fruits and leaves as well as *Ginkgo* leaves (Garcia and Galindo 1991; Trebitsh et al., 1993, Matile et al., 1997, Okazawa et al 2006). In *Arabidopsis* Benedetti et al., (1998) first identified *ATHCOR1,* or currently known as *AtCLH1,* as a gene that is induced by a chlorosis-inducing phytotoxin called coronatine produced by many plant pathogenic bacteria. *At*CLH1was found to be upregulated upon wounding and application of methyl jasmonate. In *Arabidopsis* two chlorophyllase genes are present, but respective mutants do not exhibit a stay-green phenotype during senescence. Additionally, the different views on CLH localization made researchers ponder over its enzymatic function (Schenk et al., 2007). Recently, pheophytinase pheophorbide hydrolase (PPH) from *Arabidopsis* has been shown to catalyze the removal of the phytol chain, strictly accepting pheophytin as its substrate but not chlorophyll (Schelbert et al., 2009). *At*PPH is structurally distinct from CLH but like it is a α/β-hydrolase with an active center containing a serine residue, hydrolytically cleaving the phytol ester. PPH has been shown to be highly specific for the tetrapyrrole ring structure. Localization studies have found *At*PPH in the stroma of the chloroplast and to be transcriptionally highly upregulated in senescing leaves. During senescence, *pph* mutants display a stay-green phenotype (type-C) rendering them as non-functional cosmetic mutants. They accumulate pheophytin *a* but unlike *pao* mutants (see below) do not result in a lesion-mimic phenotype which might be due to pheophytin binding to LHCs. To date, PPH has been identified in several other species performing the same function

of dephytylation during leaf senescence. Perhaps, in fruits PPH alone may not be serving the same task but may be accompanied by other hydrolases or chlorophyllase (Guyer et al., 2014).

3.2.4. Porphyrin ring opening and reduction of RCC

After the cleavage of the phytol chain, PAO oxygenolytically opens the tetrapyrrole ring of pheide *a* and adds oxygen across the methine bridge between rings D and A forming red chlorophyll catabolite (RCC) (Hörtensteiner et al., 1995; Pruzinská et al., 2003). RCC is a photoactive linear tetrapyrrole that rapidly gets channelized to go through a reduction reaction catalyzed by a soluble enzyme named red chlorophyll catabolite reductase (RCCR) which destroys the residual conjugated bond system (C15/C16 double bond) yielding a colorless product, *p*FCC (Rodoni et al., 1997; Hörtensteiner et al., 2000; Hörtensteiner, 2006; Hörtensteiner, 2012). This irreversible two-step reaction aids in removing the risk of photodamage with the loss of pigment color and, thus, is considered a key step in chlorophyll catabolism (Hörtensteiner, 2012). Moreover, PAO is considered as the key regulator of the Chl breakdown pathway, which specifically accepts only pheide *a* and molecular oxygen as its substrates, with pheide *b* being a competitive inhibitor (Hörtensteiner et al., 1995). Therefore, the re-conversion of Chl *b* to Chl *a* takes place and most of the chlorophyll catabolites identified up to date are derived from Chl *a* (Hörtensteiner, 2012).

It has been observed in many plant species like *Arabidopsis*, rice, maize and tomato that PAO is highly upregulated during senescence (Spassieva and Hille, 2002; Pruzinská et al., 2003; Tanaka et al., 2003; Tang et al., 2011). *Arabidopsis* PAO mutant lines such as *accelerated cell death 1* (*acd1*), similar to that of *lethal leaf spot 1* (*lls1*) in maize, accumulate pheide *a* resulting in a stay-green phenotype and premature cell death (Gray et al., 1997). PAO is localized in the thylakoid membrane of the chloroplast (Sakuraba et al., 2012). Similarly, when RCCR is suppressed, it leads to cell death as observed in *acd2* (Greenberg et al., 1994). RCCR was first purified and partially cloned from barley. It was highly expressed in senescing barley leaves (Wüthrich et al., 2000). In *Arabidopsis*, it was shown to localize to the chloroplast with partial association with mitochondria upon stress pointing towards other roles of RCCR besides reduction of RCC to *p*FCC (Mach et al., 2001). The stereospecific manner of activity is a characteristic feature of RCCR and depends on the source of RCCR, based on which one of two C16 isomers of *p*FCC is formed (Hörtensteiner, 2012). *p*FCC-1 is formed in *Arabidopsis* while *p*FCC-2 (also named epi-*p*FCC) is produced in tomato. After numerous screening studies, it has been found to be a family-specific feature (Hörtensteiner, 2012). The formation

of *p*FCC by these two enzymes represents the last stage of the first phase of chlorophyll breakdown. The sequential and orderly conversion of Chl *a* to *p*FCC in a multi-enzymatic pathway indicates the significance of chlorophyll catabolism during senescence.

3.3. Late phase

The late phase of the pathway comprises the transport of *p*FCCs across the envelope followed by different side chain modifications and further transport to the vacuole for the final storage of phyllobilins. The idea of transport arouse when the first NCC from barley was identified in the vacuole (Matile et al., 1988). However, the exact transport machineries and mechanisms still remain a puzzle. The different side chain modifications of *p*FCC helps in increasing the polarity of the catabolites which aids in easy storage in the vacuole. The mechanisms behind the modifications identified until now are discussed below and the various resulting phyllobilins i.e. NCCs and DNCCs, formed in different plant species are listed in **Table 3.**

3.3.1. Hydroxylation

The only common side chain modification found in all investigated higher plants is the $C3^2$-hydroxylation of colorless chlorophyll catabolites (Christ and Hörtensteiner, 2014). Experiments on isolated barley gerontoplasts have revealed two FCCs, of which one was more polar than *p*FCC and was thought to be $C3^2$-OH-*p*FCC but its chemical structure or subcellular localization still remained unknown (Matile et al., 1992). Recently, a more polar FCC i.e. $C3^2$-OH-*p*FCC has been found inside isolated gerontoplasts of *Arabidopsis* from subcellular localization studies. In addition to it, the nature of the enzyme responsible for the $C3^2$ hydroxylation was characterized to be a membrane-bound enzyme with an active site towards the stroma which required ferredoxin (Fd) and a Fd-reducing system as cofactors. Taken together, *in vivo* studies demonstrated TIC55 which belongs to a family of Fd-dependent Rieske-type monoxygenases as the responsible $C3^2$ hydroxylating enzyme (Hauenstein et al.; a manuscript submitted for publication, see **Chapter 5**).

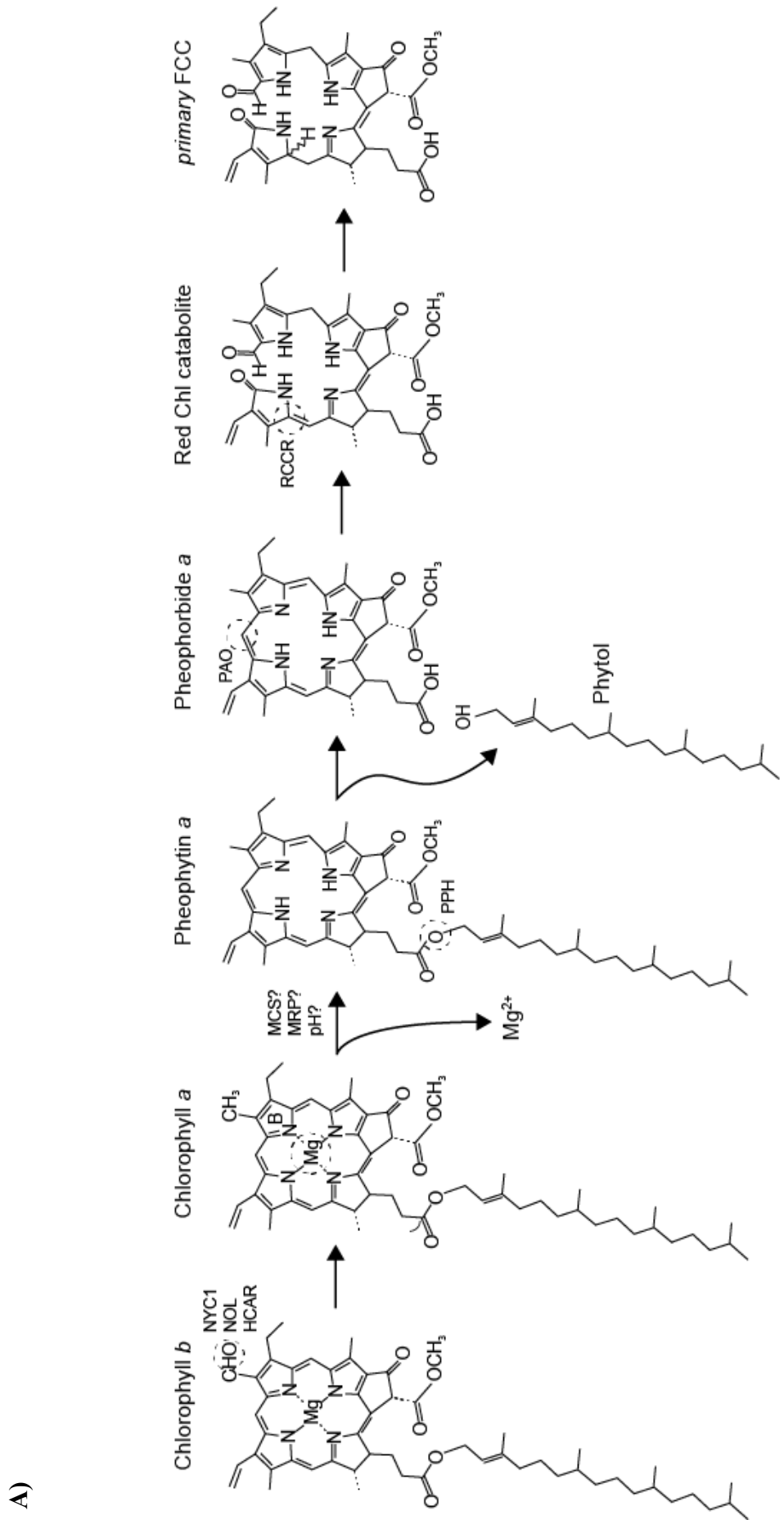
A)
Chlorophyll b
NYC1
NOL
HCAR
Chlorophyll a
MCS?
MRP?
pH?
Mg^{2+}
Pheophytin a
PPH
Pheophorbide a
PAO
Red Chl catabolite
RCCR
primary FCC
Phytol
OH

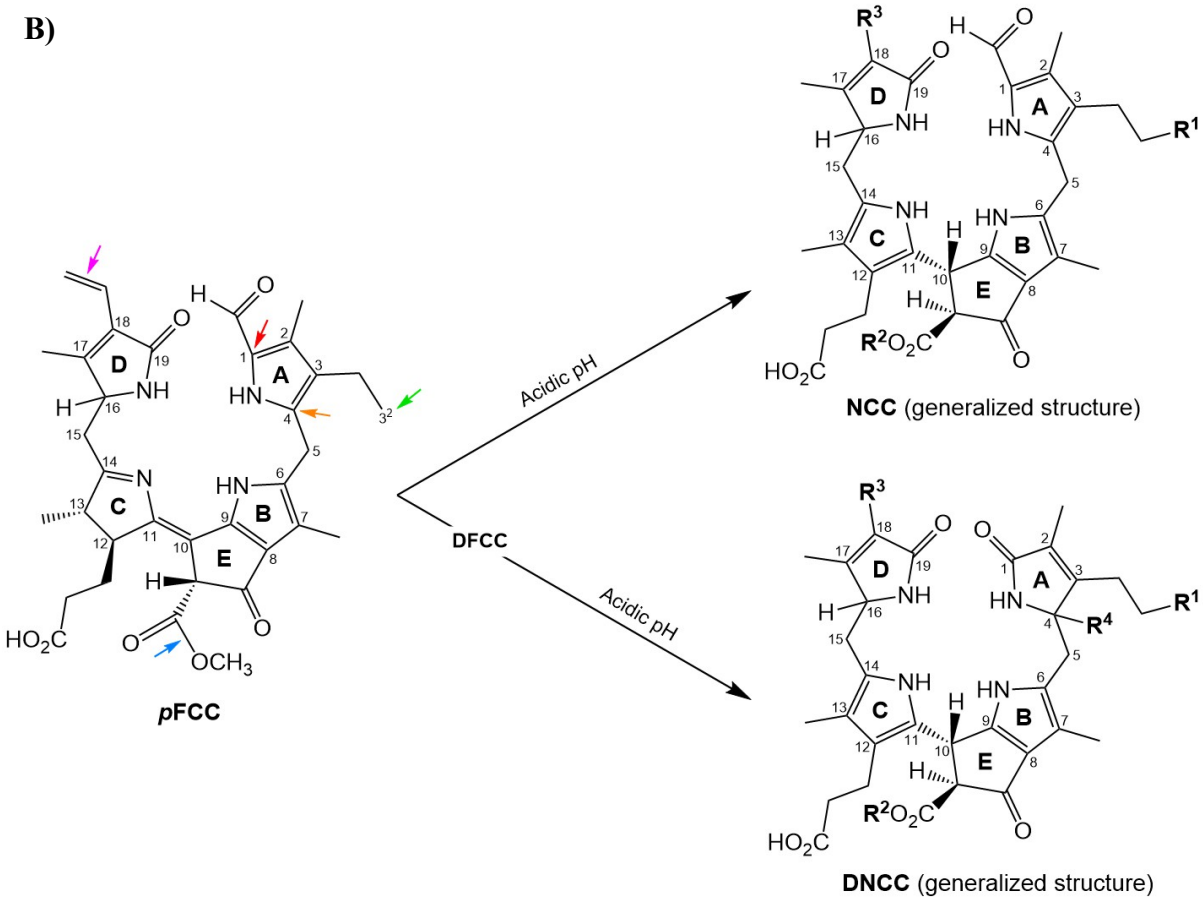

Figure 4: A) The top part of the figure represents the early phase of the PAO/phyllobilin pathway. It begins with the conversion of Chl *b* to Chl *a* and continues until the formation of *p*FCC. The action site of the different enzymes is indicated by dotted circles. **B**) The bottom part of the figure shows the different possible modifications of *p*FCC and the formation of the classes of final catabolites, NCCs and DNCCs. The colored arrows indicate the site of action of various modification; red for oxidative deformylation leading to the formation of DFCCs, green for hydroxylation and glucosylation, orange for hydroxymethylation, blue for demethylation and pink for dihydroxylation.

3.3.2. Deformylation

NCCs were thought to be the major colorless catabolites formed in *Arabidopsis* during chlorophyll degradation until recently, when DNCCs were found to represent almost 90% of the total chlorophyll catabolites or phyllobilins rendering NCCs as minor products of the chlorophyll breakdown pathway (Hörtensteiner, 2012; Christ and Hörtensteiner, 2014). DNCCs are dioxobilin-type NCCs without the C5-carbon of Chl which is removed by oxidative deformylation of FCCs through the cytochrome P450 monooxygenase CYP89A9 forming DFCCs that subsequently isomerize into DNCCs under acidic pH conditions (see below)

(Christ et al., 2013). Furthermore, *cyp89a9* mutants accumulated NCCs in large quantities but not DNCCs which strongly support the role of CYP89A9 and indicate that NCCs and DNCCs share a common precursor. CYP89A9 has been found to be present in the cytosol in association with the endoplasmic reticulum. Despite these findings, neither any obvious visible phenotype has been noticed in *cyp89a9* mutants nor its biological function has been elucidated (Christ et al., 2013). Also, it will be interesting to find out which other species apart from *Arabidopsis* form DNCCs as the major chlorophyll catabolites although structurally similar DNCCs have been reported earlier in barley and Norway maple (Christ and Hörtensteiner, 2014).

3.3.3. Demethylation

Methyl esterase 16 (MES16) has been recently discovered as the responsible enzyme for the demethylation of the $C8^2$-carboxymethyl group at the isocyclic ring (Christ et al., 2012). In *Arabidopsis*, MES16 is the closest homolog to *Rs*PPD (*Raphanus sativus* pheophorbidase) which has been earlier shown to catalyze the demethylation step with pheide as substrate (Suzuki et al., 2006). Both proteins structurally belong to the *α/β*-hydrolase protein "superfamily". It has been recently demonstrated that *MES16* is upregulated during senescence and the protein localized in the cytosol. *mes16* mutants were shown to largely accumulate FCCs and only partially NCCs with an intact $C8^2$-carboxymethyl group, which causes the lack of efficient (D)FCC-to-(D)NCC isomerization leading to high UV-fluorescence in senescing leaves (Christ et al., 2012). *In vivo* experiments also ruled out the earlier suggested pheide as a substrate for MES16, rather it acts only on FCCs. However, no obvious phenotype has been reported for *mes16* mutants until now and the physiological function of demethylation is yet not clear. Nevertheless, it has been shown that demethylation mostly takes place after deformylation despite having the responsible enzymes for both reactions seated in the cytosol. Thus, CYP89A9 was found inactive on demethylated FCCs. The *Arabidopsis* ecotype Landsberg *erecta* (Ler) is a naturally occurring *mes16* mutant which might provide some insight behind the importance of this modification (Christ et al., 2012).

3.3.4. Glycosylation and Malonylation

There are former reports in certain species like tobacco, *Arabidopsis* and oilseed rape of NCCs whose $C3^2$ hydroxyl group is either glucosylated or malonylated. Malonyltransferase activity has been purified from oilseed rape in the past. UDP-dependent glycosyltransferases (UGTs) from *Arabidopsis* may be involved in the glycosylation activity (Christ and

Hörtensteiner, 2014). Not much is still known about the molecular mechanism behind these activities.

3.3.5. Other modifications

Apart from the major known side chain modifications of FCCs, there are hypermodified FCCs (*h*FCCs) derived from *p*FCCs in which the C12 propionic acid chain may be substituted with digalactosylglyceryl or daucic acid (Christ and Hörtensteiner, 2014). *h*FCCs have been found in senescing leaves and fruits of some plant species such as *Musa acuminata*, *Musa Cavendish* and *Spathiphyllum wallisii.* Interestingly, *h*FCCs fluoresce under UV light due to their inability to isomerize into NCC because of the presence of the C17^{3}ester. In few species like barley, maize and spinach NCCs contain a dihydroxyethyl group at C18. The species-specific dihydroxylation of the vinyl group at C18 could be catalyzed by P450 enzymes (Christ et al., 2013). The less known yellow chlorophyll catabolites (YCCs) have been observed in *Cercidiphyllum japonicum* and *Tilia cordata* and may represent products of NCC oxidation (Christ and Hörtensteiner, 2014). Recently, three new dioxobilin-type Chl catabolites that carried stereospecific hydroxymethyl groups were observed in *Arabidopsis* (Süssenbacher et al., 2014).

3.4. Transport of catabolites

The fact, that chlorophyll catabolites have to be first translocated across the chloroplast envelope to the cytosol and subsequently into the vacuole indicates the presence of two translocation systems in the later phase of the chlorophyll breakdown pathway (Hörtensteiner, 2006; Hörtensteiner, 2012). It has been hypothesized that ABC (ATP binding cassette) transporters may be involved in the transport of FCCs across the chloroplast envelope based on studies carried out in isolated barley gerontoplasts (Matile et al., 1992). On the other hand, *in vitro* studies in yeast revealed the ability of *At*MRP2 and *At*MRP3 to import oilseed rape NCCs which lead to further speculation that such type of transporters may be responsible for transport of chlorophyll catabolites across the tonoplast (Hörtensteiner, 2012). Further *in vivo* experiments are required to prove these hypotheses, taking its high functional redundancy into consideration, which is a major hindrance (Hörtensteiner, 2006; Hörtensteiner, 2012).

Table 3: List of NCCs and DNCCs identified from higher plants. Adapted from (Christ and Hörtensteiner, 2014).

Name	R[1c]	R[2c]	R[3c]	R[4c]	C16-epimer[d]	Source[e]	Reference
NCCs							
At-NCC-1[a]	*O*-glucosyl	H	Vinyl	H	1	L	Pružinská *et al.* (2005)
At-NCC-2[a]	OH	H	Vinyl	H	1	L	Pružinská *et al.* (2005)
At-NCC-3[a]	OH[f]	H	Vinyl	H	1	L	Pružinská *et al.* (2005)
At-NCC-4[a]	*O*-glucosyl	CH_3	Vinyl	H	1	L	Pružinská *et al.* (2005)
At-NCC-5[a]	H	H	Vinyl	H	1	L	Pružinská *et al.* (2005)
Bn-NCC-1[a]	*O*-malonyl	H	Vinyl	H	1	L	Mühlecker and Kräutler (1996)
Bn-NCC-2[a]	*O*-glucosyl	H	Vinyl	H	1	L	Mühlecker and Kräutler (1996)
Bn-NCC-3[a]	OH	H	Vinyl	H	1	L	Mühlecker and Kräutler (1996)
Bn-NCC-4[a]	H	H	Vinyl	H	1	L	Pružinská *et al.* (2005)
Cj-NCC-1[a]	OH	CH_3	Vinyl	H	*epi*	L	Curty and Engel (1996)
Cj-NCC-2[a]	H	CH_3	Vinyl	H	*epi*	L	Oberhuber *et al.* (2003)
Hv-NCC-1[a]	OH	CH_3	Dihydroxy-ethyl	H	1	L	Kräutler *et al.* (1991)
Lo-NCC-1[a]	OH	CH_3	Vinyl	H	nd	L	Iturraspe *et al.* (1995)
Ls-NCC-1[a]	OH	CH_3	Vinyl	H	nd	L	Iturraspe *et al.* (1995)
Ms-NCC-2[a]	OH	CH_3	Vinyl	H	*epi*	F	Müller *et al.* (2007)
Nr-NCC-1[a]	*O*-glucosylmalonyl	CH_3	Vinyl	H	*epi*	L	Berghold *et al.* (2004)
Nr-NCC-2[a]	*O*-glucosyl	CH_3	Vinyl	H	*epi*	L	Berghold *et al.* (2004)
Pc-NCC-1[a]	*O*-glucosyl	CH_3	Vinyl	H	*epi*	F	Müller *et al.* (2007)
Pc-NCC-2[a]	OH	CH_3	Vinyl	H	*epi*	F	Müller *et al.* (2007)
So-NCC-1[a]	OH	H	Dihydroxy-ethyl	H	*epi*	L	Berghold *et al.* (2002)
So-NCC-2[a]	OH	CH_3	Dihydroxy-ethyl	H	*epi*	L	Oberhuber *et al.* (2001)
So-NCC-3[a]	OH	H	Vinyl	H	*epi*	L	Berghold *et al.* (2002)
So-NCC-4[a]	OH	CH_3	Vinyl	H	*epi*	L	Berghold *et al.* (2002)
So-NCC-5[a]	H	CH_3	Vinyl	H	*epi*	L	Berghold *et al.* (2002)
Sw-NCC-58[b]	OH	CH_3	Vinyl	H	1	L	Kräutler *et al.* (2010)
Tc-NCC-1[a]	*O*-glucosyl	CH_3	Dihydroxy-ethyl	H	*epi*	L	Scherl *et al.* (2012)
Tc-NCC-2[a]	*O*-glucosyl	CH_3	Vinyl	H	*epi*	L	Scherl *et al.* (2012)
Xv-NCC-1[a]	*O*-glucosyl	CH_3	Vinyl	H	*epi*	L	Christ *et al.* (2013)
Zm-NCC-1[a]	*O*-glucosyl	CH_3	Dihydroxy-ethyl	H	*epi*	L	Berghold *et al.* (2006)
Zm-NCC-2[a]	*O*-glucosyl	CH_3	Vinyl	H	*epi*	L	Berghold *et al.* (2006)
DNCCs							
Hv-UCC-1[a,g]	OH	CH_3	Dihydroxy-ethyl	H	1	L	Losey and Engel (2001)
Ap-UCC-1[a,g]	OH	CH_3	Dihydroxy-ethyl	H	*epi*	L	Müller *et al.* (2011)
At-NDCC-1[a]	OH	H	Vinyl	H	1	L	Christ *et al.* (2013)

[a] A nomenclature for NCCs (and FCCs) has been defined by Ginsburg and Matile (1993) in which a prefix indicates the plant species and a suffix number indicates decreasing polarity in reversed-phase HPLC.

[b] These catabolites are indexed according to their retention time in HPLC analysis. *Ap Acer platanoides*, *At Arabidopsis thaliana*, *Bn Brassica napus*, *Cj Cercidiphyllum japonicum*, *Hv Hordeum vulgare*, *Lo Liquidambar orientalis*, *Ls Liquidambar styraciflua*, *Ma Muca acuminate*, *Mc Musa cavendish*, *Ms Malus sylvestris*, *Nr Nicotiana rustica*, *So Spinacia oleracea*, *Sw Spathiphyllum wallisii*, *Tc Tilia cordata*, *Xv Xeropyhta viscosa*, *Zm Zea mays*.

[c] R^1–R^4 indicate residues at $C3^2$, $C8^2$, $C18^1$ and C4 side positions, respectively, of NCCs and DNCCs. Note that R^4 can also be placed at C2.

[d] C16 stereochemistry refers to the type of *p*FCC, i.e. *p*FCC (1) or *epi*-*p*FCC (*epi*), formed in the respective species or genus; nd, not determined.

[e] Source of material used for catabolite isolation: F, fruits; L, leaves.

[f] In *At*-NCC-3, the site of hydroxylation is indicated to be C2 (rather than $C3^2$) (Müller *et al.*, 2006).

[g] *Hv*-UCC-1 and *Ap*-UCC-1 are indicated to be pseudo-enantiomers (Müller *et al.*, 2011).

4. Importance of Chlorophyll Breakdown

Over the years, scientists have suggested various significant roles of chlorophyll breakdown in a plant's life. Earlier, chlorophyll derived nitrogen remobilization was considered as the prime reason behind degrading chlorophyll. Chloroplasts contain more than 70% of the nitrogen of a mesophyll cell among which Rubisco holds the major share. About 20% cellular nitrogen is contained in chlorophyll apoproteins and chlorophyll is important for stabilization of Chl-binding proteins, so, in a way, removal of chlorophyll is a prerequisite to release the nitrogen from the apoprotein complex. The actual nitrogen within a chlorophyll molecule accounts to only about 2% which is not recycled due to its retention within the chlorophyll catabolites stored in the vacuole (Hörtensteiner and Kräutler, 2000; Hörtensteiner et al., 2008; Hörtensteiner, 2012; Christ and Hörtensteiner, 2014).

Chlorophyll breakdown can rather be considered as a detoxification process. When leaves accumulate free chlorophyll or porphyrin, this can lead to cell death due to light-dependent oxidative stress. The light absorbing capacity of the conjugated electron system of the chlorophyll molecule in particular when uncoupled from the photosystem machinery can produce considerable amounts of singlet oxygen resulting in cell death (Hörtensteiner and Feller, 2002). This can be observed in *Arabidopsis* PAO *and* RCCR mutant plants that accumulate phototoxic Chl degradation intermediates causing cell death. It is also notable that the early phase of chlorophyll degradation produces photoactive products that are step-wise detoxified by producing non-photoreactive linear tetrapyrroles in the later phase. This shows that plants aim in minimizing the rise of photodamage through free Chl. It has been recently shown that NCCs could be potent antioxidants and may be involved in the viability of ripe fruits like apples or pears (Müller et al., 2007) although experimental proof of biological roles of chlorophyll catabolites is still missing (Christ et al., 2013; Christ and Hörtensteiner, 2014).

Through the process of chlorophyll catabolism, not only about 70-80% of nitrogen is recycled but it also aids in significant re-allocation of carbon, phosphate, potassium, sulphur and other micronutrients to sink organs such as grains in crops. An effective transfer of nutrients and the ability to synthesize new compounds can affect the yield in crop plants. The leaf is an important organ of the plant system that harbors both anabolic and catabolic processes for its own good.

The last leaf before producing spikes, i.e. the flag leaf of monocarpic crop plants, is a major crucial determinants of crop yield and biomass production. There are many examples in which it has been seen that premature senescence has imparted huge losses in yield and on the other hand late onset of leaf senescence, in hybrid maize for example, results in a significant rise in yield. Since chlorophyll breakdown is a crucial part of leaf senescence and one of the last stages of the whole plant development, it has an impact on crop yield and quality. To understand the chlorophyll breakdown pathway in crop plants is, thus, an important aspect for crop improvement by targeting leaf senescence (Gan, 2014).

5. Aim of the Thesis

This thesis primarily focused on the analysis of chlorophyll breakdown during the lifespan of monocot leaves. For this the two main points were addressed:

- To characterize phyllobilin formation in different grass species, which includes their identification followed by analysis of diversity and abundance.

- To characterize the PAO/phyllobilin pathway in barley by identifying barley CCEs (*NYC1, NOL, PPH, PAO* and *SGR)*, to study their subcellular localization in barley protoplasts and analyse their gene expression and protein abundance. Additionally, to confirm the functionality of *Hv*PPH and *Hv*PAO by complementation of *At pph-1* and *pao*1 KO mutants, respectively.

MATERIALS AND METHODS

1. Plant materials

This study primarily focused on using monocot crops like barley (*Hordeum vulgare*), wheat (*Triticum aestivum*), ryegrass (*Lolium perenne*), rice (*Oryza sativa*), *Sorghum* (*Sorghum bicolor*). The wild and domesticated varieties of the aforementioned plant species used during this study are listed in **Tables 4 and 5**, respectively.

Table 4: The wild varieties of different crop species used in this work.

Crop	Accession ID	Wild variety	Country of origin	Source of seeds
Barley	HOR 8502	*Hordeum spontaneum* K.Koch var. *spontaneum*	Israel	IPK Gatersleben
	HOR 13981	*Hordeum spontaneum* K.Koch var. *ischnatherum*	Union of Soviet Socialist Republics	IPK Gatersleben
Wheat	TRI 612	*Triticum monococcum* L. var. *sofianum Stranski*	Albania	IPK Gatersleben
	TRI 618	*Triticum monococcum* L. var. *vulgare Körn.*	Albania	IPK Gatersleben
	TRI 18446	*Triticum baeoticum* Boiss. subsp. *baeoticum* var. *viridiboeoticum*	Turkey	IPK Gatersleben

Table 5: The domesticated varieties of different crop species used in this work.

Crop	Domesticated variety	Ploidy	Source of seeds
Barley (*H. vulgare*)	Baraka	Diploid	Prof. Dr. Enrico Martinoia, UZH
	Golden Promise	Diploid	Prof. Dr. Enrico Martinoia, UZH
Wheat (*T. aestivum*)	Chinese Spring	Hexaploid	Prof. Dr. Beat Keller, UZH
	Chancellor	Hexaploid	Prof. Dr. Beat Keller, UZH
	Kanzler	Hexaploid	Prof. Dr. Beat Keller, UZH
	Bob White	Hexaploid	Prof. Dr. Beat Keller, UZH
Ryegrass (*L. perenne*)	Ceres	Diploid	Prof. Dr. Karin Krupinska, CAU
Sorghum (*S. bicolor*)	E-Tian	Diploid	Professor Hai-Chun Jing, CAS
Rice (*O. sativa*)	Nipponbare	Diploid	Prof. Dr. Beat Keller, UZH

The wild-type ecotype of *Arabidopsis thaliana*, named Columbia-0 (Col-0), was also investigated in some of the experiments. SALK_111333 (*pao1*) and SALK_000095 (*pph-1*), mutant lines with T-DNA insertions within the *PAO* (At3g44880) and the *PPH* gene (At5g13800), respectively, originally obtained from the European Arabidopsis Stock Centre (Nottingham, UK), were available in the lab.

2. Plant growth conditions

The monocot crop plants were grown on vermiculite in Conviron® growth chambers equipped with 400 Watt pulse start lamps (*Conviron*, Winnipeg, Canada). The optimum growth conditions used for these different species are listed in **Table 6.** *Arabidopsis* plants were usually grown in 12 h light/12 h dark (12/12) or 8 h light/16 h dark (short-day) growth chambers equipped with fluorescent light of an intensity of 60-120 µmol photons m^{-2} s^{-1} at 22°C and 60% relative humidity. However, for seed production, they were grown under greenhouse conditions (25°C, 60% relative humidity and a light intensity of 100-200 µmol photons m^{-2} s^{-1}) for 4-5 weeks.

Table 6: The optimum growth conditions of the different monocot species used in this thesis according to recommendations by Parrott et al., 2007; Rong et al., 2013; Johnson et al., 2015.

Crop	Temperature (°C)	Light intensity (µmol photons $m^{-2}s^{-1}$)	Humidity (%)	Light/dark periods (h)
Barley	22 (d); 16 (n)	500	60	16/8
Wheat	22 (d); 16 (n)	500	60	16/8
Ryegrass	22 (d & n)	60-120	60	12/12
Sorghum	28 (d); 22 (n)	500	50	16/8
Rice	28 (d); 24 (n)	600	75	16/8

3. Senescence induction

To induce senescence, detached leaves of 1-week-old (monocots) or 5-weeks-old (12/12 h *Arabidopsis*) plants were incubated on wet filter paper in dark cabinets at ambient temperature for 7-10 days depending on the species.

Short-day *Arabidopsis* leaves were excised for dark incubation (7-10 days) in desiccators containing carbon monoxide (CO) (*PanGas AG*, Dagmersellen, Switzerland) mixed with ambient air [0% or 50% (v/v)] or oxygen-18 (^{18}O) [97% (v/v)] (*Campro Scientific*, Berlin, Germany) each.

4. 2,2′-Bipyridyl treatment

For treatments with 2,2′-Bipyridyl (Bpy) two sets of 10-days-old barley var. Golden Promise primary leaves were cut and initially placed on wet filter paper soaked with distilled water. After 3 days in darkness at ambient temperature, one set of leaves was transferred to wet filter paper soaked in 0.1 mM Bpy (*Sigma-Aldrich*, Buchs, Switzerland). The other set of leaves (control) was transferred to water-soaked filter papers as before. After 5 more days in darkness, the leaves were processed for chlorin determination (see below).

5. cDNA clones

Barley cDNA clones for different chlorophyll catabolic genes were identified and selected on the basis of their high sequence similarity on the protein level with respective *A. thaliana* genes. The locus IDs of the *A. thaliana* genes and the GenBank IDs of their corresponding barley homologs are listed in **Table 7**. Full-length cDNA clones derived from the *Hordeum vulgare* ssp. *vulgare* strain. *'Haruna nijo'*. were obtained from the National Institute of Agrobiological Sciences (Ibaraki, Japan) (Matsumoto *et al*., 2011) and were transformed into DH10-β competent *E. coli* cells.

Table 7: The barley homologs showing high sequence similarity with corresponding *Arabidopsis* gene products.

Gene name	TAIR locus ID *(Arabidopsis)*	GenBank ID *(H. vulgare)*	Sequence similarity (%)	Locus definition *(H. vulgare)*
NYC	AT4G13250.1	AK356173.1	76	*Hordeum vulgare* subsp. *vulgare* mRNA for predicted protein, complete cds, clone: NIASHv1030P11
NOL	AT5G04900.1	AK369003.1	81	*Hordeum vulgare* subsp. *vulgare* mRNA for predicted protein, complete cds, clone: NIASHv2083K11
PPH	AT5G13800.2	AK364879.1	68	*Hordeum vulgare* subsp. *vulgare* mRNA for predicted protein, complete cds, clone: NIASHv2029B03
PAO	AT3G44880.1	AK353593.1	73	*Hordeum vulgare* subsp. *vulgare* mRNA for predicted protein, complete cds, clone: NIASHv1001F03
SGR	AT4G22920.1	AK356089.1	61	*Hordeum vulgare* subsp. *vulgare* mRNA for predicted protein, complete cds, clone: NIASHv1029O23

6. GFP fusion protein production

The genes encoding barley chlorophyll catabolic enzymes (CCEs) were amplified by PCR with KAPA HiFi HotStart DNA polymerase (*Kapa Biosystems*, Baden, Switzerland) using primers carrying additional restriction sites at the ends. These primers are listed in **Table 8**. The PCR fragments were cloned into pGEM®-T Easy (*Promega*, Dübendorf, Switzerland) and after respective restriction digestions, subcloned into pUC18-spGFP6 (Meyer *et al*., 2006), thereby producing gene fusions with C-terminally located GFP. During the process of cloning, the PCR products were purified using Wizard® SV Gel and PCR Clean-Up System (*Promega*, Dübendorf, Switzerland) and ligated using T4 polymerase (*New England Biolabs*, Allschwil, Switzerland). Plasmid purification was carried out using Wizard® *Plus* SV Minipreps DNA Purification System (*Promega*, Dübendorf, Switzerland).

Table 8: Primers with additional restrictions sites used for the PCR amplification of different barely CCEs.

Gene name	Primer name	Primer sequence (5' → 3')	Restriction site
NYC	NYC_F	CAT GTA ACT AGT ATG GCC GCC GC	*Spe*I
	NYC_R	ATC TGC ACT AGT TGT GCC AGG GAA AGG	*Spe*I
NOL	NOL_F	GAT CAT ACT AGT ATG GCC ACC GTC GC	*Spe*I
	NOL_R	TAG ACA AGA TCT GCA TCC TCG GCA AC	*Bgl*II
CLH	CLH_F	CAT GTA ACT AGT ATG GCG TCT GCA GGC G	*Spe*I
	CLH_R	GCC TGC AGA TCT ATT TCA TCG CGG AAC TC	*Bgl*II
PPH	PPH_F	GTA TTC ACT AGT ATG GAA GTG GTT TCT TC AGC	*Spe*I
	PPH_R	ATC TGC ACT AGT TCT GGA CAC TAC CCG TAG	*Spe*I
PAO	PAO_F	CAT GTA ACT AGT ATG CCT ACC GCC TCC	*Spe*I
	PAO_R	GAA TAC AGA TCT ATA TCA ATG TCA GCG TG	*Bgl*II
SGR	SGR_F	CAT GTA ACT AGT ATG GCC ATC GCC GCT GC	*Spe*I
	SGR_R	GAA TAC AGA TCT ATC TGC GGC GGC GCC TG	*Bgl*II

7. Isolation and transformation of barley protoplasts and confocal microscopy

The front face of a barley leaf (~10 days old) was carved ~1 cm beneath the tip without cutting through the lower epidermis. The tip was then folded backwards and the lower epidermis was carefully peeled off. The cell wall was digested by soaking the open side of the leaf in the digestion buffer, [1% (w/v) Cellulase R-10, 0.3% (w/v) Macerozym R-10, 20 mM succinate in mother buffer containing 0.5 M sorbitol, 0.5 mM KH_2PO_4, 1 mM KNO_3, 1 mM $MgSO_4 \cdot 7H_2O$, 1 mM $EDTA \cdot 2H_2O \cdot 2Na^+$, 0.025% (w/v) BSA; pH=5.7] and gently shaking for 1 h at RT under low light condition. The digestion buffer, now containing isolated protoplasts, was filtered through a 90 µm nylon gauze and more protoplasts were recovered by squeezing the digested leaves residues. The filtration and squeezing steps were repeated in W5 solution [154 mM NaCl, 125 mM $CaCl_2 \cdot 2H_2O$, 5 mM KCl, 5 mM glucose; pH=5.8] to maximize protoplast recovery.

The filtrate was subjected to centrifugation at 63×*g* for 5 min at RT and the pellet was re-suspended in a small quantity of suspension buffer. The protoplast suspension was sandwiched between 10 mL of floatation buffer [1 mM $CaCl_2$, 1 mM sucrose, 100 mM sorbitol, 25 mM MES, pH=5.8], carefully added at the very bottom, and 2 mL of W5 solution, added on top of the suspension. This layered arrangement was spun down at 80×*g* for 10 min at RT. The intact protoplasts were retrieved, from the interface between the floatation buffer and W5 solution, using a wide-bore pipette tip. The protoplasts were suspended in 8 mL of W5 solution and their density was quantified with the help of the Fuchs-Rosenthal chamber.

For transformation, 4.0×10^6 protoplasts were settled down by centrifugation at 70×*g* for 5 min at RT. The pellet was re-suspended in 500 µL MaMg solution [0.4 M mannitol, 15 mM $MgCl_2\cdot2H_2O$, 0.1% (w/v) MES; pH = 6.5] and incubated with 20-50 µg plasmid DNA and 500 µL PEG solution [40% (w/v) PEG 1500 in MaMg-Lösung; pH=5.6–7.0] for 20 min at RT with occasional mixing. W5 solution was added intermittently with continuous and gentle mixing, up to a total volume of 5 mL. The mixture was spun down at 70×*g* for 10 min at RT and the sedimented protoplasts were re-suspended in 1 mL of W5 solution at a density of 4.0×10^6 cells/mL. They were finally incubated overnight in darkness at 22°C. Protoplasts were transformed with plasmid carrying GFP constructs using 20% polyethylene glycol (Meyer *et al*., 2006). Transformed cells were incubated in the dark for 48 h at room temperature before analyzing them with laser scanning confocal microscope DM IRE2 (*Leica Microsystems*, Heerbrugg, Switzerland). GFP fluorescence was imaged at an excitation wavelength of 488 nm and the emission signal was recovered between 495 and 530 nm. Free GFP expressed from empty pUC18-spGFP6 was used as a control for cytosolic localization**.** Detection of Chl autofluorescence was at 730 nm.

8. RNA isolation and real-time quantitative PCR (qPCR)

RNA was isolated using the RNeasy Plant Mini Kit (*Qiagen*, Hombrechtikon, Switzerland). Two additional steps were incorporated into the protocol. 250 µL each of water-saturated phenol and a 24:1 (v/v) mixture of chloroform:isoamylalcohol were added to the supernatant obtained after transferring the plant material to lilac shredder. This step helped to denature proteins which gets collected at the organic phase leaving the nucleic acids in the aqueous phase. After vigorous vortexing, the mixture was centrifuged at 16,000×*g* for 5 min

at 4°C. To the upper aqueous phase, double the volume of chloroform:isoamylalcohol mixture was added followed by vortexing and centrifugation as before. The upper aqueous phase was mixed with an equal volume of ethanol and immediately transferred to the pink shredder from the kit. Thereafter, the provided protocol of the kit was followed. RNA was quantified using a Nanodrop 1000 spectrophotometer (*Thermo Fischer Scientific*™, Dietikon, Switzerland).

1 µg of RNA was used for the synthesis of first strand cDNA using Moloney murine leukemia virus reverse transcriptase and oligo $(dT)_{15}$ primers after DNAse treatment (*Promega*, Dübendorf, Switzerland). For qPCR studies, three biological and technical replicates of each samples were analyzed. For quantification, SYBR™ Green master mix (*Thermo Fischer Scientific*™, Dietikon, Switzerland) was used to run qPCR on a 7500 Fast Real-time PCR system (*Life Technologies*, Zug, Switzerland). The gene-specific primers used for qPCR analysis are listed in **Table 9**. The *HvS40* gene and the *ADP* gene were used as senescence control and housekeeping control genes respectively.

Table 9: The primers used for real-time PCR analyses.

Barley gene name	Primers	Primer sequence (5' → 3')
HvADP	ADP_RF_F	TCT CAT GGT TGG TCT CGA TG
	ADP_RF_R	GGA TGG TGG TGA CGA TCT CT
HvNYC	NYC_F_RT	GGA GTC GCC AAA CCA GAC A
	NYC_R_RT	CTT TGC CCC CTT CAC AAC AT
HvNOL	NOL_F_RT	CGC TCG CTC GCT CCA G
	NOL_R_RT	CGG GAA GAA GGC TGC GT
HvCLH	CLH1_RT_F	CCT CCC ATG GCT TCA TCG TT
	CLH1_RT_R1	GTG CGA GCT TGG AAG AGA GG
HvPPH	PPH_F_RT	AAG TGG CGA TTC CTG GTC TG
	PPH_R_RT	CGC CTT GCT ATT CTT GGT GC
HvPAO	PAO_F_RT	TAC GAC CGC CAG AAG CAT TT
	PAO_R_RT	CAC CAC ACC ACA TCC TCA CA
HvSGR	SGR_RT_F	CGC GCC ATA CGA TGA CGA A
	SGR_RT_R	CCG GCG GGA AGC AGC
HvS40	HvS40_RT_F	CGA CGG CGA CGT CCG ATG TA
	HvS40_RT_R	CGA CGG CGA CGT CCG ATG TA
ADP	ADP_RT_F	TCT CAT GGT TGG TCT CGA TG
	ADP_RT_R	GGA TGG TGG TGA CGA TCT CT

9. Complementation tests

Full-length cDNA sequences of *HvPPH* and *HvPAO* were amplified using KAPA HiFi HotStart DNA polymerase (*Kapa Biosystems*, Baden, Switzerland) and the primers listed in **Table 10**. Using *Xho*I and *BamH*I restriction sites, the amplicons were first cloned into pHannibal (Wesley et al., 2001) containing a CaMV 35S double enhancer promoter and an OCS terminator. Constructs were then subcloned into pGreen 0029 (Hellens et al., 2000) via *Not*I sites. The inserts were verified by sequencing and the constructs were further transformed into *Agrobacterium* strain GV3101 along with pSOUP (Hellens et al., 2000). *Arabidopsis pph-1* and *pao1* mutant plants were transformed with the floral dip method (Clough and Bent, 1998). The transformants, named *pph-1*/35S:*Hv*PPH and *pao1*/35S:*Hv*PAO, respectively, were selected on ½ MS plates containing kanamycin. Homozygosity for the original T-DNA insertion of *pph-1* and *pao1* was verified on T2 plants using the gene-specific RP and LP primers and the T DNA-specific primer, LBb1.3 as listed in **Table 10**.

For this, DNA was extracted from a small piece of a young *Arabidopsis* leaf by adding 100 µL of extraction buffer [200 mm Tris, 250 mM NaCl, 25 mM EDTA and 0.5% (w/v) SDS; pH=7.5] and grinding with a pellet pestle. 200 µL of absolute ethanol was added to the homogenate and vortexed for 2 min followed by centrifugation at 16,000×*g* for 10 min at room temperature. The supernatant was discarded, the pellet dissolved in Milli-Q water and used for PCR.

Table 10: The primers used in PCR analyses of complementation test.

Gene/Mutant Name	Primer name	Primer sequence (5' → 3')
PPH	PPH_F_BPHAN	CAT GTA CTC GAG ATG GAA GTG GTT TCT TCC
	PPH_R_BPHAN	ATC TGC GGA TCC TCA TCT GGA CAC TAC
PAO	PAO_HAN_FOR	CTC GAG ATG CCT ACC GCC TCC CTC
	PAO_HAN_REV	AAG CTT TCA ATC AAT GTC AGC GTG CAC
pao-1	N14-RP	GGCTCACCTGACGCTTGGTTA
	N14-LP	CGACGGTGACAATTCAAAGGG
pph-1	95-RP	TGTACAGGTTATCGGTGAGCC
	95-LP	CTACCAATCCTGGACTCCTCC
SALK T-DNA	LBb1.3	ATTTTGCCGATTTCGGAAC

10. Extraction and analysis of chlorins

For extraction of chlorins, leaf tissue was homogenized in liquid nitrogen and 3-fold (v/w) extraction buffer [90% acetone, 10% (v/v) Tris-HCl; pH = 8.0, pre-cooled to -20°C] added. Following this step, the samples were sonicated in the dark at 4°C. The sonication time depended on the senescence stage of the leaves and the species used. For example, the senescent leaves from any of the used species required less time (approx. 15 min) than the green leaves of rice, which needed an hour of incubation. A detailed description can be found in Das and Guyer *et al.* (a manuscript submitted for publication, see **Chapter 6**). After appropriate incubation the samples were centrifuged twice at 16,000×*g* for 2 min and the supernatant was divided into two fractions for spectrophotometric determination and analysis of chlorophyll concentrations (Strain *et al*., 1971) on a Beckman Coulter DU-800 UV/Vis spectrophotometer (*Beckman Coulter*, Nyon, Switzerland) and HPLC analysis for the analysis of Pheide *a* respectively.

Reversed-phase HPLC was performed according to a published procedure (Langmaier *et al*., 1993) and was comprised of a C18 Hypersil ODS column (125 x 4 mm; 5 µm; *Thermo Fisher Scientific*, Dreieich, Germany) and a diode array detector (Linear 206 PHD-365-700 nm) with a flow rate of 1 mL min^{-1}. The solvents used were: solvent A [20:80 (v/v) 1 M ammonium acetate:methanol] and solvent B [20:80 (v/v) acetone:methanol], and the column developed with the following program: from 100% solvent A to 100% solvent B in 15 min, 100% solvent B for 10 min, back to 100% solvent A in 3 min and 100% solvent A for 4 min. Pheide *a* was identified according to its absorption spectra (Pheide *a* at 665 nm) and quantified using authentic standards. Peaks were analyzed using the software Chromeleon Client (version 6.80, build 2212; *Dionex*, *Thermo Fisher Scientific*, Dreieich, Germany). Peak areas of the desired chlorins were quantified as described in **Chapter 6**.

11. Extraction and analysis of colorless catabolites (phyllobilins)

Leaves were subjected to shock-freeze in liquid nitrogen and then phyllobilins were extracted following the procedure demonstrated recently (Christ et al., 2016). The sample supernatant was used for analysis on an ultrahigh performance liquid chromatography (UHPLC) mass spectrometry (MS) system with an electrospray ionization (ESI)- quadrupole-time of flight (qTOF) mass spectrometer (*Bruker Daltonics*, Bremen, Germany).

12. Extraction of soluble and membrane plant proteins

For protein extraction, leaf material was homogenized in liquid nitrogen followed by the addition of extraction buffer [20 mM NaH_2PO_4, 0.1% (v/v) β-mercaptoethanol; pH = 7.5] containing 1% (w/v) polyvinylpolypyrrolidone (PVPP) and protease inhibitor cocktail. The homogenate was then filtered through two layers of miracloth in an Eppendorf tube and centrifuged for 10 min at 16,000×*g* at 4°C. After centrifugation, the supernatant (soluble fraction) was transferred to another Eppendorf tube. The tube containing the pellet (membrane fraction) was re-suspended with the same volume of extraction buffer without PVPP. All steps were carried out on ice and as quickly as possible.

13. Expression of recombinant *Hv*PPH

MBP-Δ*At*PPH was obtained from Dr. Luzia Guyer (University of Zurich). MBP-Δ*Hv*PPH_1 and MBP-Δ*Hv*PPH_2 were cloned from a truncated PPH fragment which didn't contain the base pairs encoding the chloroplast transit peptide. MBP-Δ*Hv*PPH_1 and MBP-Δ*Hv*PPH_2 were amplified by KAPA HiFi HotStart DNA polymerase (*Kapa Biosystems*, Baden, Switzerland) using the primers listed in **Table 11.** *Hv* PPH_BamHI_f and *Hv* PPH_R, *Hv* PPH_F and *Hv* PPH_SalI_r primer pairs amplified the full length coding region of PPH. The other two primers, PPH_F_inner and *Hv* PPH_R_inner, were used in a two-step PCR to amplify the MBP-Δ*Hv*PPH_2 sequence which contained the single nucleotide change that differed between MBP-Δ*Hv*PPH_1 and MBP-Δ*Hv*PPH_2 (as discussed in **Part 2** of the RESULTS). The amplicons were digested (with *BamH*I and *Sal*I) and ligated to the linearized pMal™-c2 vector (*New England Biolabs*, Allschwil, Switzerland) using T4 ligase. The construct was then transformed into NEB 10-β high-efficiency competent *E. coli* cells (*New England Biolabs*, Allschwil, Switzerland). The construct was verified by sequencing and finally transformed into *E. coli* BL21 (DE3) (*New England Biolabs*, Allschwil, Switzerland).

Table 11: The primers used for PCR amplification of fusion proteins.

Gene Name	Primer name	Primer sequence (5' → 3')
PPH	*Hv* PPH_R	GGT GCC AGA CTT CTC GTA GTA TAC CGT CAG C
	Hv PPH_F	CCT TCC TAA TCC TGC AAG ATC TCC TCG
	Hv PPH_F_inner	CGA GAA GTC TGG CAC CAA GAA TAG CAA GGC
	Hv PPH_R_inner	GCA GGA TTA GGA AGG AAA CCC CAA AAT GGC
	Hv PPH_BamHI_f	GGGATCCGTGCTCTGTGTTGGGAGAGCTTC
	Hv PPH_SalI_r	CCCGTCGACTCATCTGGACACTACCCG

For protein expression, bacterial pre-cultures incubated overnight at 37°C, with ampicillin (100 µg/mL), were used the following day to set up cell suspensions of 100 mL. These cultures were grown at 37°C until they reached an OD_{600} value of 0.5~0.6. Recombinant protein expression was induced by adding isopropyl-β-D-1-thiogalactopyranoside (IPTG) at a concentration of 1.0 mM. pMal-c2-Δ*At*PPH (MBP-Δ*At*PPH) and pMal-c2-Δ*Hv*PPH (MBP-Δ*Hv*PPH) were expressed at 37°C for 3 h after which the bacterial cells were centrifuged at 16,000×*g* for 15 min at 4°C. The cell pellets were re-suspended in disruption buffer (20 mM Tris-HCl and 200 mM NaCl at pH 8.0) and lysed using a French press (Constant Cell Disruption System; *Constant Systems*, Northamptonshire, UK) at 150 MPa. The cell lysates were then centrifuged at 16,000×*g* for 30 min at 4°C to separate soluble and membrane fractions. In my study, the soluble fractions were used for further experiments.

14. Activity assays

For PPH assays, recombinant proteins (0.4 µg μL^{-1}) were incubated for 30 min at 34°C with pheophytin *a* (~1 µg μL^{-1} dissolved in acetone) in assay buffer [0.1 M Hepes-KOH, 1 mM EDTA; pH=8.0]. The total volume of each assay was 70 µL. Reactions were stopped by adding 2 volumes of acetone. The mixture was then centrifuged and formation of Pheide *a* analyzed by HPLC as described above and in **Chapter 6**. Pheophytin was produced as described (Guyer et al., 2014).

15. Protein quantification

Protein was quantified by the Bradford dye-binding method (Bradford, 1976) using Coomassie brilliant blue G-250 (*Bio-Rad Laboratories*, Cressier, Switzerland) and varying concentrations of BSA as standard. OD_{595} values of protein samples were recorded on a Synergy H1 Hybrid microplate reader (*BioTek Instruments*, Luzern, Switzerland) using the inbuilt Bradford program in the Gen5 Data Analysis Software provided by the same company.

16. SDS-PAGE

Proteins were separated under denaturing conditions using polyacrylamide gel electrophoresis (PAGE). For each casted gel (18×16 mm), 12.5% separating gel was prepared using 3.33 mL of 30% acrylamide/bis-acrylamide (37.5:1) solution, 2 mL of 1.5 M Tris-HCl (pH=8.8), 80 µL of 10% (w/v) sodium dodecyl sulfate (SDS), 8 µL tetramethylethylenediamine (TEMED), 80 µL of 10% (w/v) ammonium persulfate (APS) and 2.5 mL distilled water. 4% stacking gel, containing 667 µL of 30% acrylamide/bis-acrylamide (37.5:1) solution, 1.25 ml of 0.5 M Tris-HCl (pH=6.8), 50 µL of 10% (w/v) SDS, 5 µL TEMED, 50 µL of 10% (w/v) APS and 3 mL distilled water, was polymerized on top of the separating gel layer. For loading, 1 part of each protein sample was mixed with 4 parts of 5X Laemmli buffer [250 mM Tris-HCl, 10% (w/v) SDS, 30% (w/v) glycerol, 0.02% (w/v) bromophenol blue and 5% (v/v) β-mercaptoethanol; pH=6.8] and boiled for 5 min at 95°C. The samples were then run at 150 V for ~90 min using 1X running buffer [25 mM Tris-HCl, 192 mM glycine and 0.1% (w/v) SDS; pH=8.5].

17. Immunoblot analysis

After separating the proteins by SDS-PAGE, the gels were equilibrated in TTBS containing 50 mM Tris (pH=7.5), 200 mM NaCl and 0.05% (v/v) Tween® 20 for about 30 min. The proteins were transferred to Whatman® Protran® nitrocellulose membranes (*Sigma-Aldrich*, Buchs, Switzerland) according to standard procedures. After the transfer, the membranes were blocked with TTBS containing 5% (w/v) nonfat dry milk for 1 h at room temperature. The membranes were washed three times with TTBS for 10 min each. Proteins

were labelled with anti-PAO (mouse-monoclonal, 1:500 Gray *et al.*, 2004) or mouse anti-MBP monoclonal (1:10,000; *New England Biolabs*, Allschwil, Switzerland) antibodies. Following overnight incubation at 4°C, the membranes were thoroughly washed with TTBS for three times, 10 min each, and incubated in HRP-conjugated secondary antibodies (goat anti-rabbit IgG or rabbit anti-mouse IgG, 1:100,000; *Sigma-Aldrich*, Buchs, Switzerland) for 1.5 h at room temperature. The blots were then developed by chemiluminiscence technique using Immun-Star WesternC kit (*Bio-Rad Laboratories*, Cressier, Switzerland) and visualized by Chemidoc XRS gel-documentation system (*Bio-Rad Laboratories*, Cressier, Switzerland).

RESULTS

———(Part 1)———

Characterization of phyllobilins in grasses

1. Diversity and the nature of phyllobilin formation in grasses

1.1. Identification of phyllobilins

It was of interest to investigate the diversity of phyllobilins formed across various species of grasses like barley, wheat, ryegrass, sorghum and rice under artificially induced senescence conditions. For this study, the conventional approaches of HPLC and UV/Vis spectroscopy-based peak integration as initially taken. This yielded preliminary data of phyllobilins present based on previously established spectra of NCCs and DNCCs. To overcome the limitations associated with spectra-based detection, such as technical barriers or inability to detect catabolites that are present in trace amounts, we moved to LC-ESI-MS that was recently established in our lab (Christ et al., 2016) for detailed analysis of the types of phyllobilins that occur in the species of interest. We also assigned provisional names for all the identified catabolites that is based on the monoisotopic molecular mass. This nomenclature is used in the following along with names for those catabolites, which were already known. Information about all phyllobilins identified in this work are summarized in **Table 12** and their chemical structures are shown in **Figure 5**.

While *Arabidopsis* is characterized by the exclusive presence of a vinyl group at the C18 position, all monocot varieties used in this study have phyllobilins (see **Figure 5A** for atom numbering) that are dihydroxylated at this position. Besides already known phyllobilins, four novel DNCCs, named DNCC_650, 794, 828 and 880, were discovered here. From these, DNCC_794 and 880 are extensively found in ryegrass and the remaining two are only seen in

barley. DNCC_666 (aka. *Hv*-UCC-1) is present in all investigated species. DNCC_632-3 (aka. *At-mes16*-DNCC-38) is found to exist in certain varieties of barley, wheat and ryegrass. Among the NCCs, three novel ones namely NCC_662, 840 and 926, were discovered in this study. NCC_662 is found in certain varieties of barley and wheat. While NCC_840 and 926 are detected in all varieties of barley, wheat and sorghum, they are absent in ryegrass and rice. NCC_678, the first ever known chlorophyll catabolite (aka. *Hv*-NCC-1), is found in all varieties of each species except ryegrass. Among the other known NCCs, NCC_644 (aka. *Cj*-NCC-1) is seen only in certain varieties of wheat, NCC_806 (aka. *Nr*-NCC-2) is found in barley, sorghum, rice and certain varieties of wheat and NCC_892 (aka. *Nr*-NCC-1) is detected in certain varieties of barley, wheat and ryegrass.

The identity of the detected phyllobilins was validated by data-dependent MS/MS experiments on individual precursor ions (see **Figure 6** for the MS and MS/MS data of all phyllobilins identified in this work). Tandem MS (MS/MS) experiments produced collision-induced dissociation (CID) MS/MS fragmentation patterns which exhibited main fragments corresponding to the loss of pyrrole rings D and/or A. This analysis helped to understand the fragmentation patterns of each phyllobilin found in grasses and how different they are from the previously known Arabidopsis phyllobilin fragmentation patterns (Christ et al., 2016).

Figure 5

A)

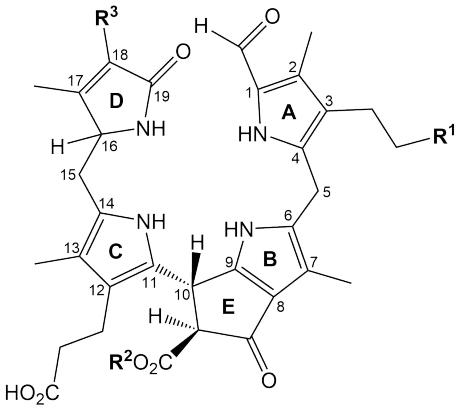

NCC (generalized structure)

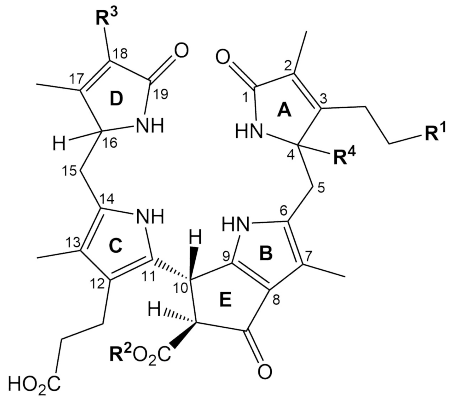

DNCC (generalized structure)

Figure 5 (continued)

B)

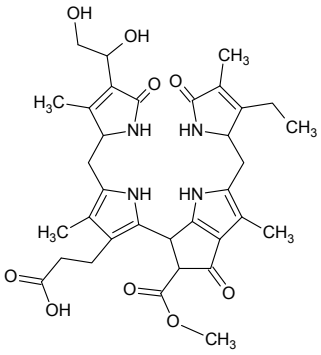

DNCC_650

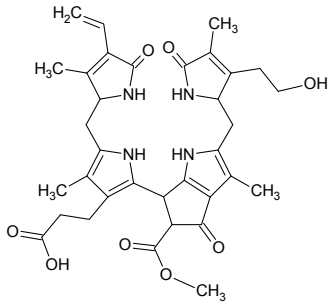

DNCC_632_3

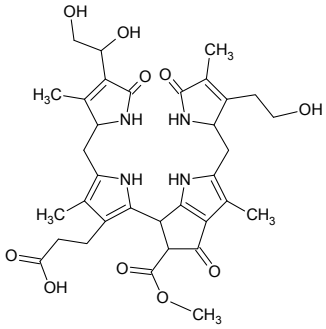

DNCC_666

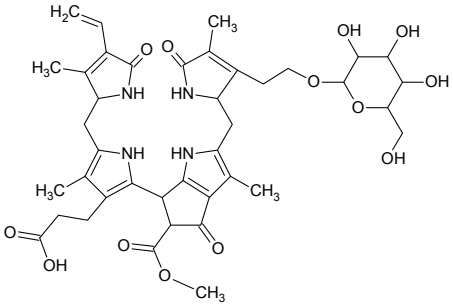

DNCC_794

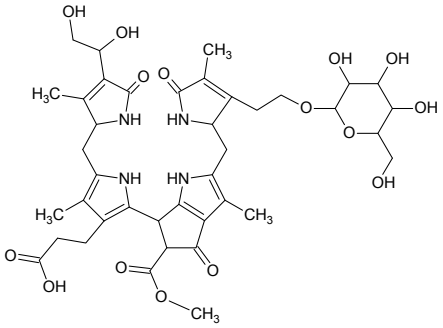

DNCC_828

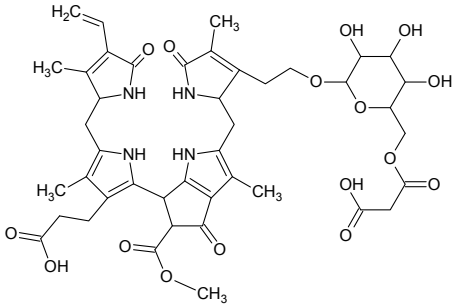

DNCC_880

Figure 5 (continued)

C)

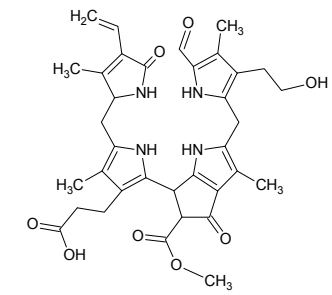

NCC_644

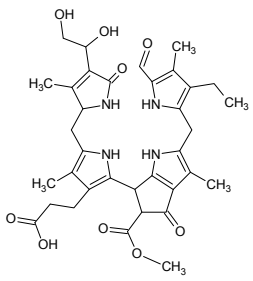

NCC_662

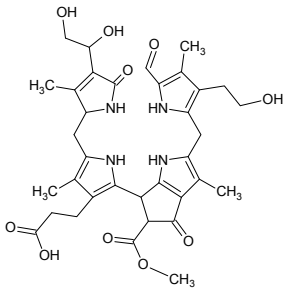

NCC_678

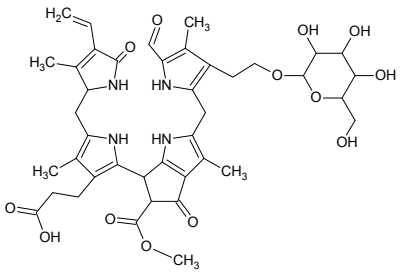

NCC_806

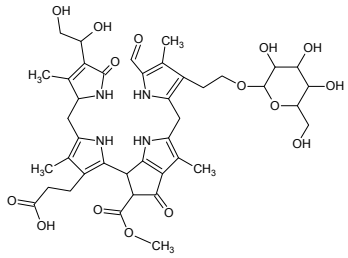

NCC_840

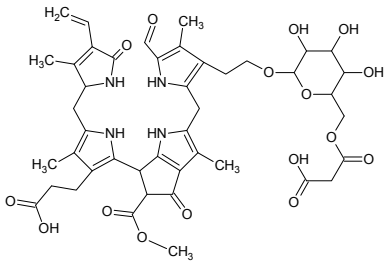

NCC_892

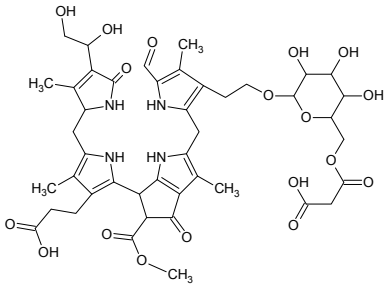

NCC_926

Figure 5: Chemical structures of various Chl catabolites. **A)** General structures of nonfluorescent Chl catabolite (NCC) and dioxobilane-type nonfluorescent Chl catabolite (DNCC). Chemical structures of various DNCCs **(B)** and NCCs **(C)** found in modern varieties of barely, wheat, ryegrass, sorghum and rice analyzed in this work. For specific side-chain modification in each structure, refer to **Table 12**.

Table 12: List of various NCCs and DNCCs found in investigated plant species. The table summarizes information, such as chemical formulae, molecular weight and characteristic side-chain functional groups of various NCCs and DNCCs found in the modern varieties of barley, wheat, ryegrass, sorghum and rice, investigated is this study.

Assigned Name	m/z $[M+H]^+$ measured[1]	m/z $[M+H]^+$ calculated	Formula (M)	Side chain modifications[2]			Retention time[3]	Other names[4]	Presence[5]									Reference[4]
				R^1 ($C3^2$)	R^2 ($O8^4$)	R^3 (C18)			BA	GP	KA	BW	CS	CH	CE	ET	NB	
DNCC_632-3	633.2931^{CE}	633.2919	$C_{34}H_{40}N_4O_8$	OH	CH_3	vinyl	7.5	*At-mes16*-DNCC-38	-	x	x	x	-	-	x	-	-	Süssenbacher *et al.* 2014
DNCC_650	651.3034^{GP}	651.3030	$C_{34}H_{42}N_4O_9$	H	CH_3	DHethyl	7.0	-	x	x	-	x	-	-	-	-	-	This work
DNCC_666	667.2983^{GP}	667.2979	$C_{34}H_{42}N_4O_{10}$	OH	CH_3	DHethyl	6.0	*Hv*-UCC-1	x	x	x	x	x	x	x	x	x	Losey and Engel 2001
DNCC_794	795.3471^{CE}	795.3453	$C_{40}H_{50}N_4O_{13}$	OGlc	CH_3	vinyl	6.8	-	-	-	-	-	-	-	x	-	-	This work
DNCC_828	829.3520^{GP}	829.3507	$C_{40}H_{52}N_4O_{15}$	OGlc	CH_3	DHethyl	5.6	-	x	x	-	-	-	-	-	-	-	This work
DNCC_880	881.3474^{CE}	881.3457	$C_{43}H_{52}N_4O_{16}$	OGlcMal	CH_3	vinyl	7.0	-	-	-	-	-	-	-	x	-	-	This work
NCC_644	645.2968^{KA}	645.2924	$C_{35}H_{40}N_4O_8$	OH	CH_3	vinyl	7.8	*Cj*-NCC-1	-	-	x	x	-	-	-	-	-	Curty and Engel 1996
NCC_662	663.3046^{BW}	663.3030	$C_{35}H_{42}N_4O_9$	H	CH_3	DHethyl	7.8	-	x	-	x	x	-	-	-	-	-	This work
NCC_678	679.2989^{BA}	679.2979	$C_{35}H_{42}N_4O_{10}$	OH	CH_3	DHethyl	6.5	*Hv*-NCC-1	x	x	x	x	x	x	-	x	x	Kräutler *et al.* 1991
NCC_806	807.3466^{BW}	807.3453	$C_{41}H_{50}N_4O_{13}$	OGlc	CH_3	vinyl	7.0	*Nr*-NCC-2	x	x	x	x	-	-	-	x	x	Berghold *et al.* 2004
NCC_840	841.3502^{BW}	841.3507	$C_{41}H_{52}N_4O_{15}$	OGlc	CH_3	DHethyl	5.9	-	x	x	x	x	x	x	-	x	-	This work
NCC_892	893.3472^{KA}	893.3457	$C_{44}H_{52}N_4O_{16}$	OGlcMal	CH_3	vinyl	7.5	*Nr*-NCC-1	-	x	x	x	-	-	x	-	-	Berghold *et al.* 2004
NCC_926	927.3534^{KA}	927.3511	$C_{44}H_{54}N_4O_{18}$	OGlcMal	CH_3	DHethyl	6.1	-	x	x	x	x	x	x	-	x	-	This work

[1]measured masses obtained from the analyses of the varieties named in superscript; for list of varieties, see footnote [5]; [2]positions of modifications as depicted in Figure 1; DHethyl, dihydroxyethyl; Glc, glucosyl; Mal, malonyl; [3]only retention time [min] of the major isomer of each phyllobilin is shown; [4]the names and references describing the first identification are given; [5]BA, Baraka (barley); GP, Golden promise (barley); KA, Kanzler (wheat); BW, Bobwhite (wheat); CS, Chinese Spring (wheat); CH, Chancellor (wheat); CE, Ceres (ryegrass); ET, E-Tian (sorghum); NB, Nippon Bare (rice) var.

Figure 6

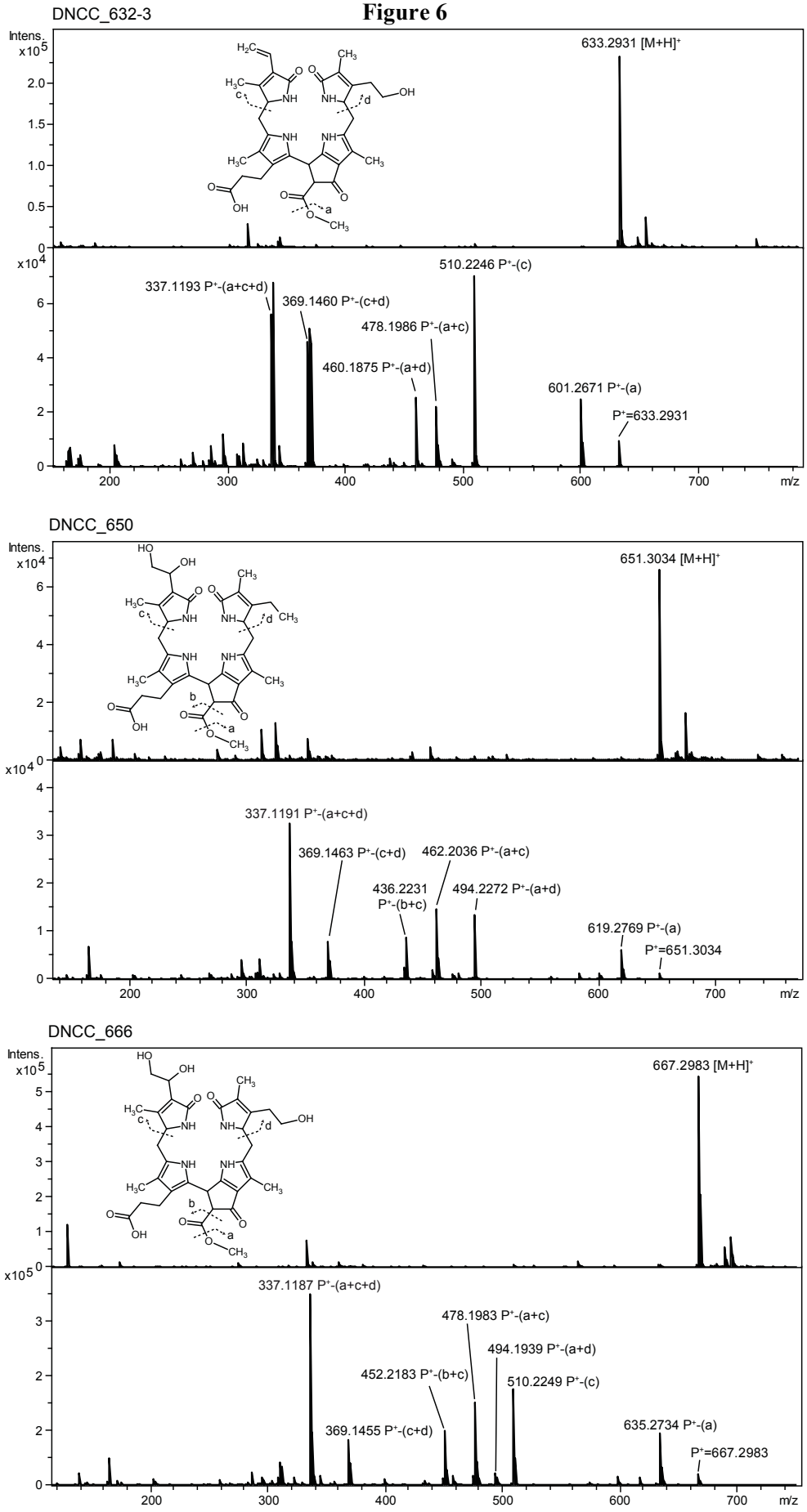
DNCC_632-3
Intens.
633.2931 [M+H]+
510.2246 P+-(c)
337.1193 P+-(a+c+d)
369.1460 P+-(c+d)
478.1986 P+-(a+c)
460.1875 P+-(a+d)
601.2671 P+-(a)
P+=633.2931
m/z
DNCC_650
651.3034 [M+H]+
337.1191 P+-(a+c+d)
369.1463 P+-(c+d)
462.2036 P+-(a+c)
436.2231 P+-(b+c)
494.2272 P+-(a+d)
619.2769 P+-(a)
P+=651.3034
DNCC_666
667.2983 [M+H]+
337.1187 P+-(a+c+d)
478.1983 P+-(a+c)
494.1939 P+-(a+d)
452.2183 P+-(b+c)
510.2249 P+-(c)
369.1455 P+-(c+d)
635.2734 P+-(a)
P+=667.2983

Figure 6 (continued)

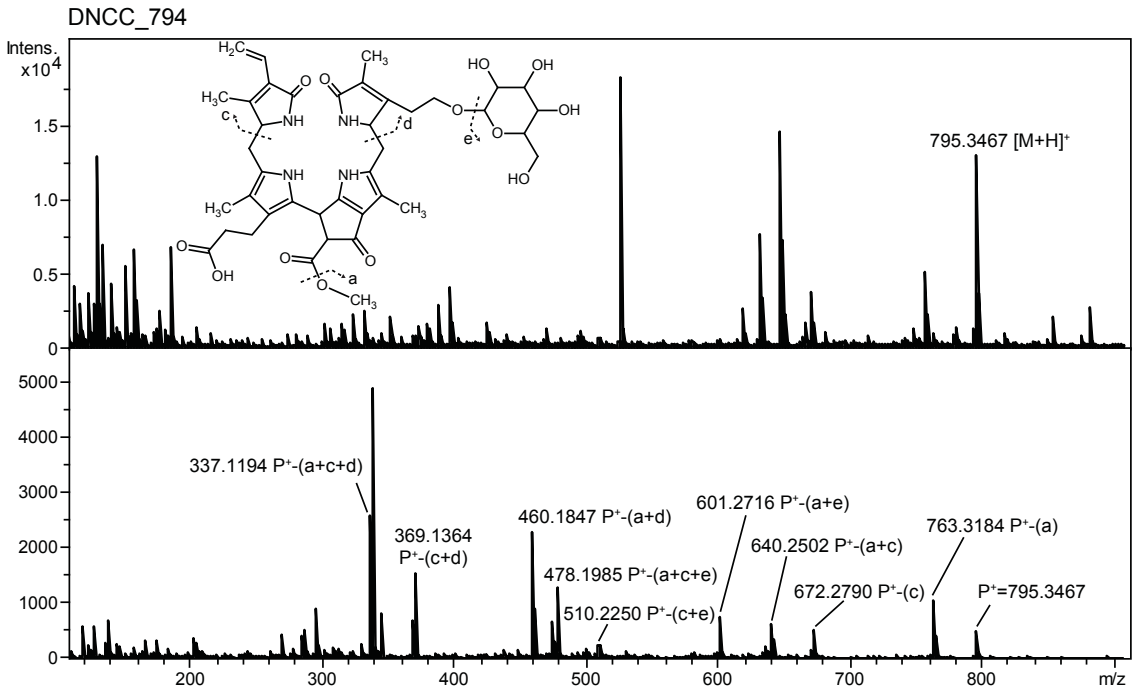

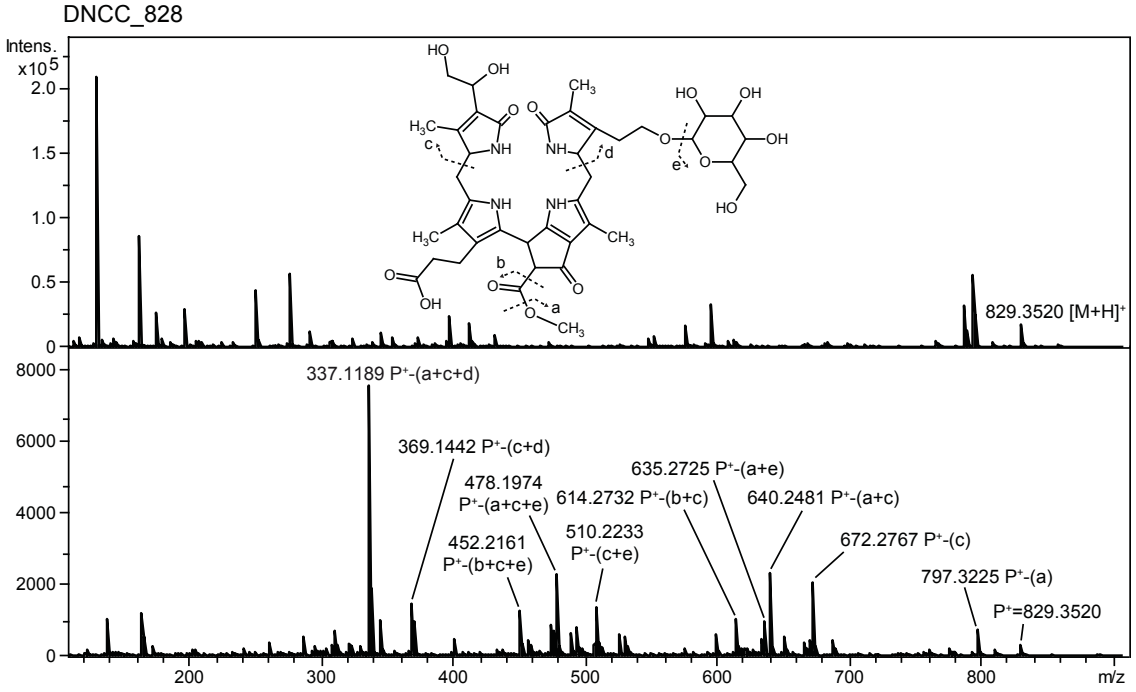

Figure 6 (continued)

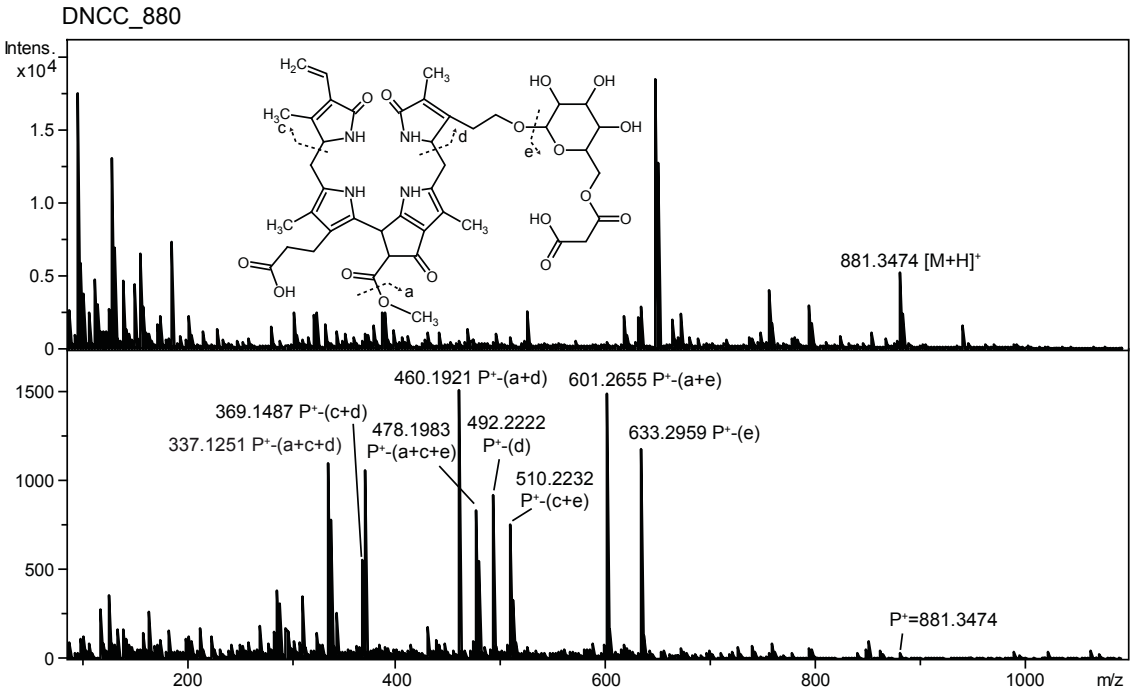

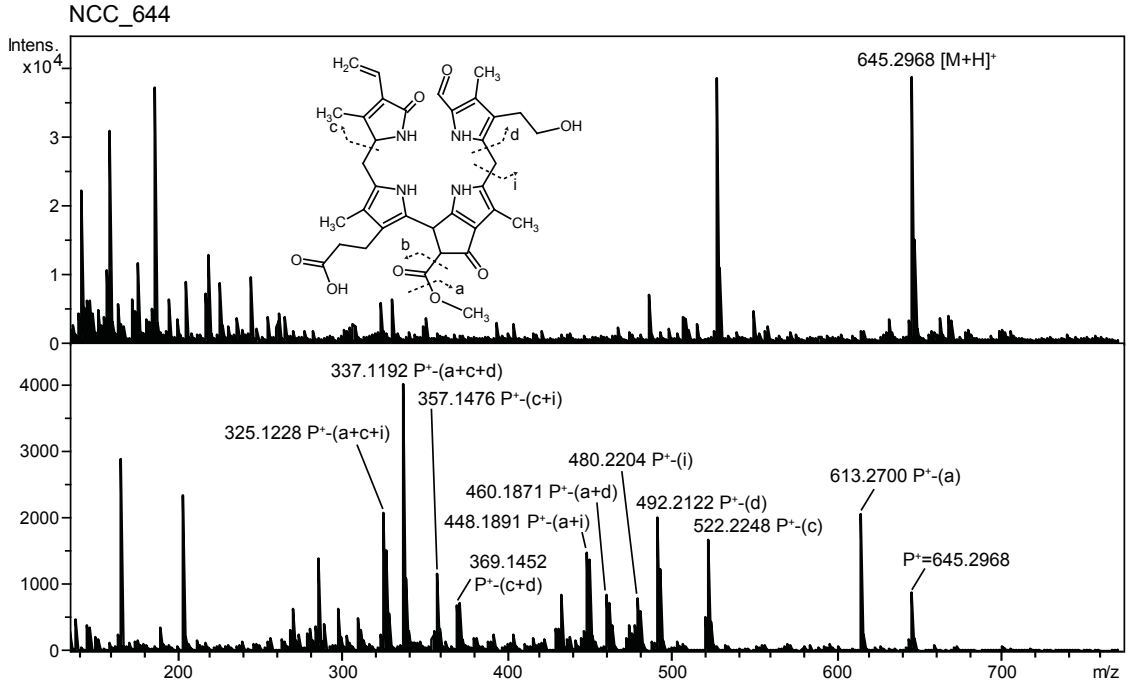

Figure 6 (continued)

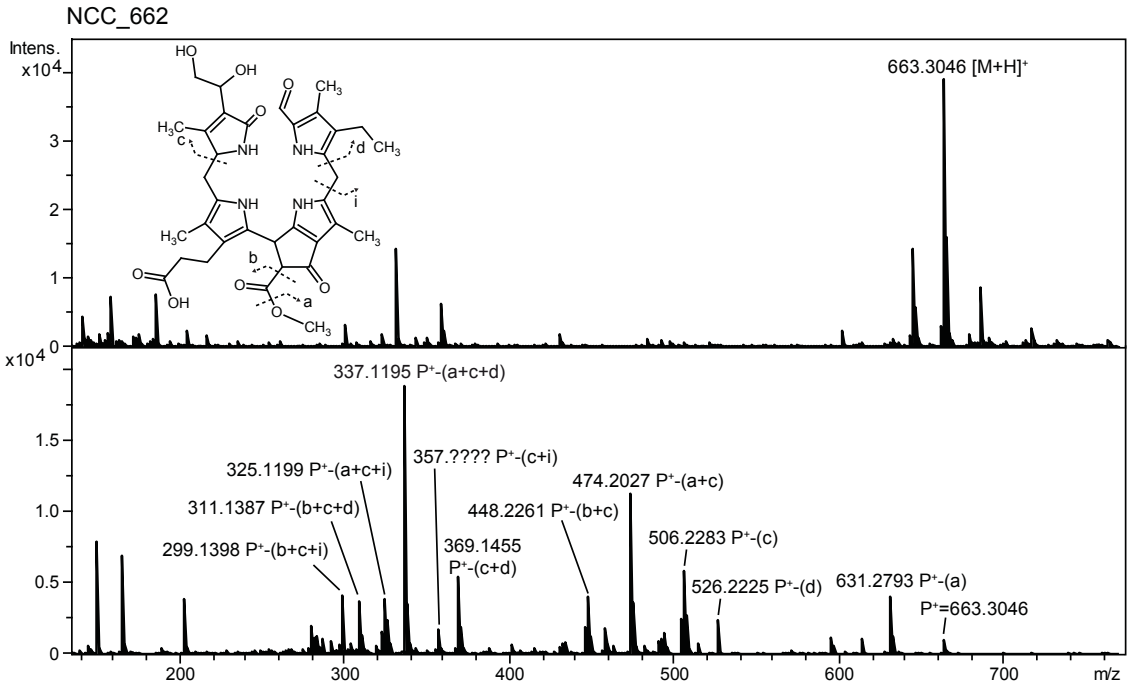

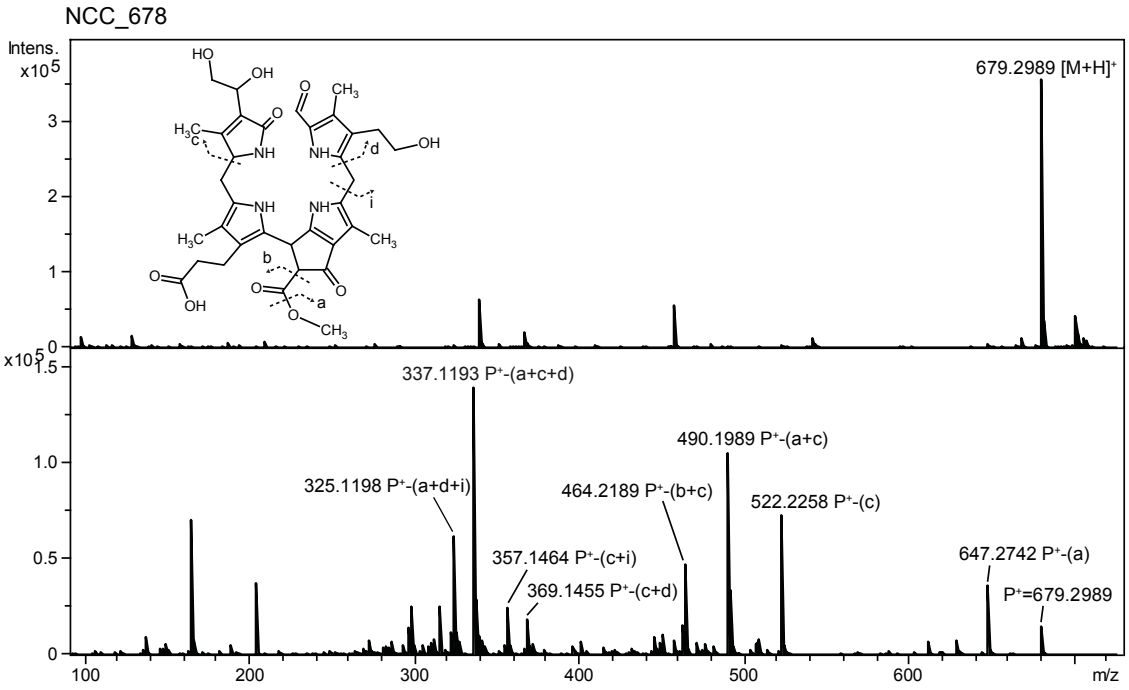

Figure 6 (continued)

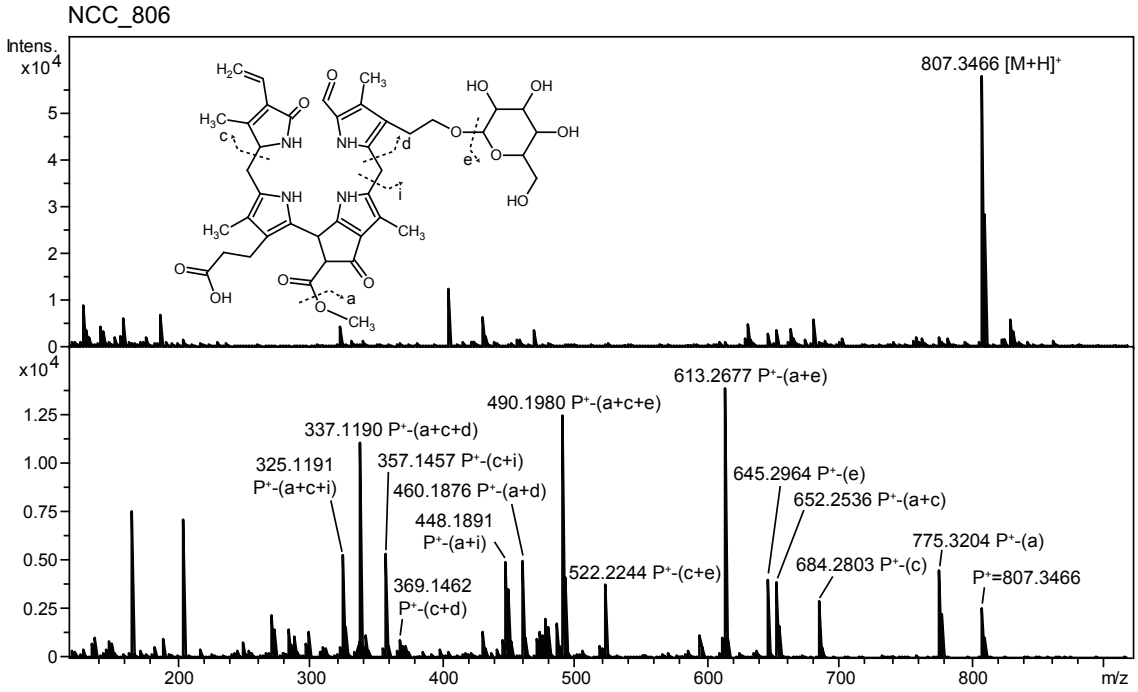

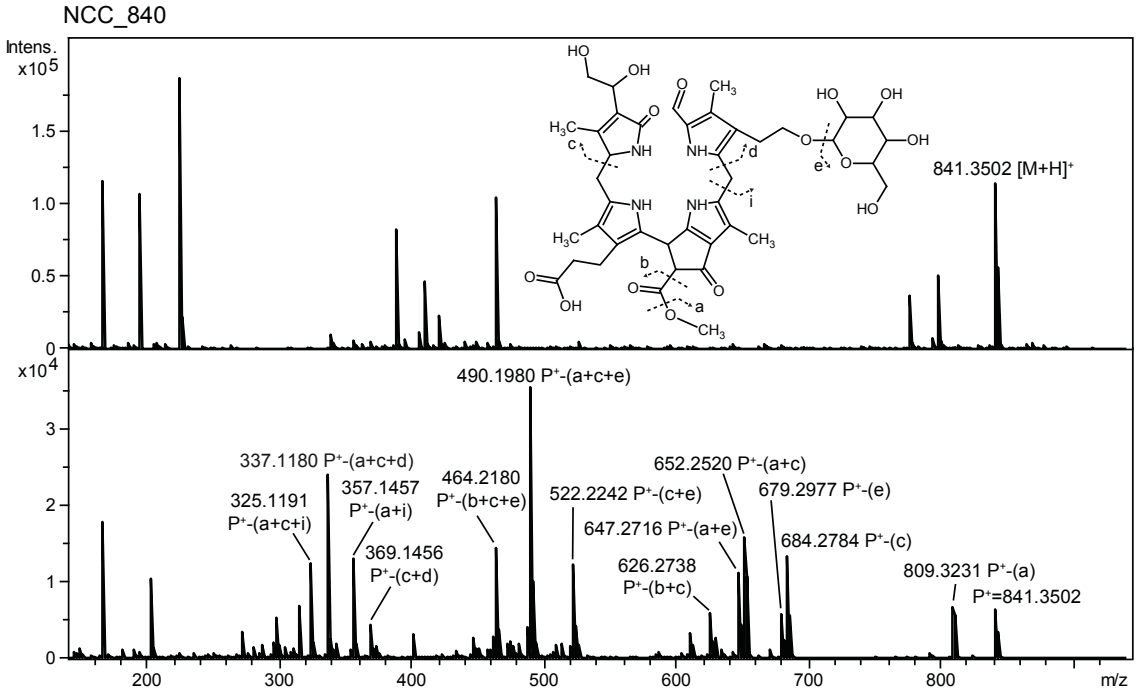

Figure 6 (continued)

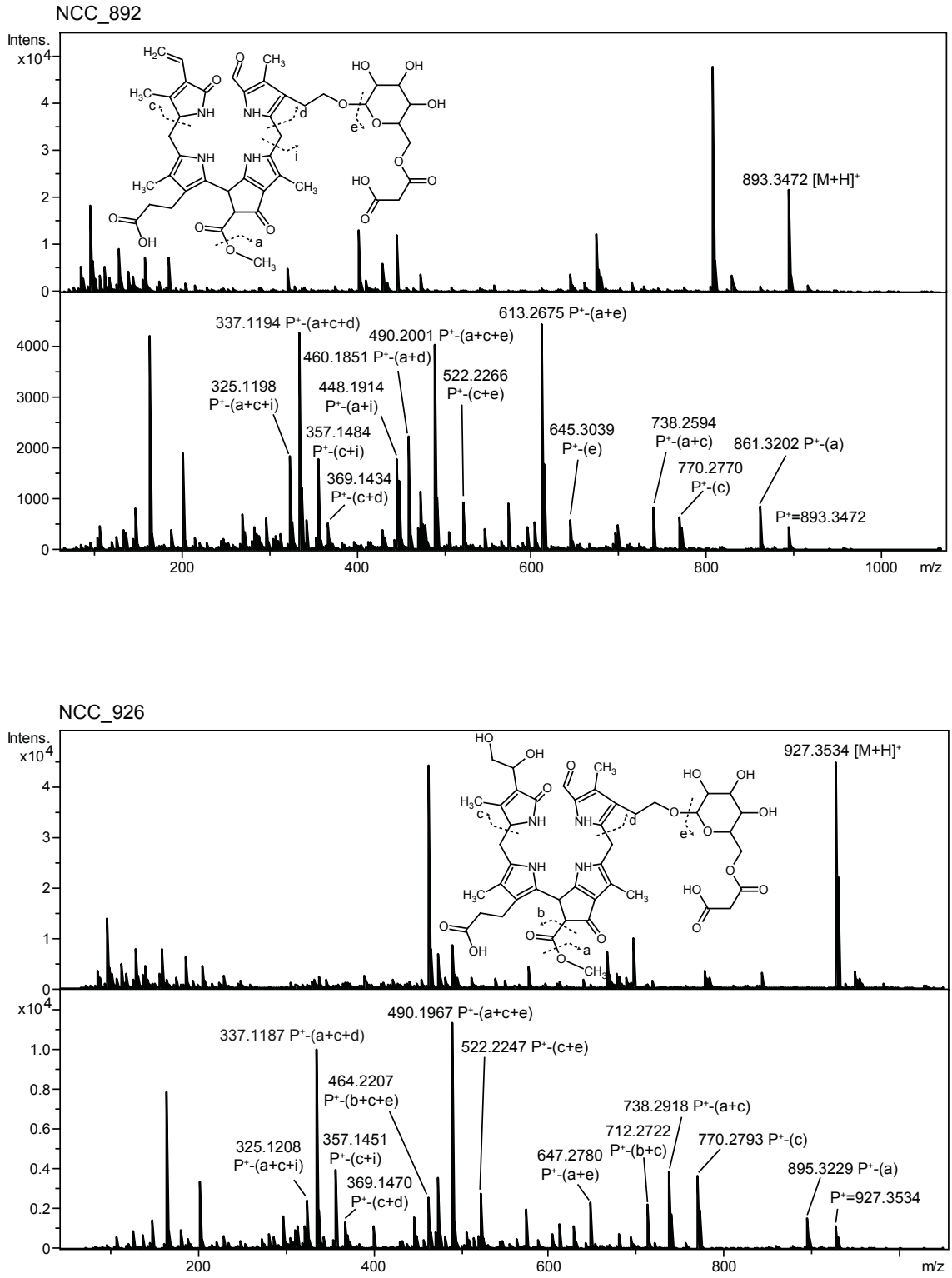

Figure 6: MS (top) and MS/MS (bottom) spectra of the grass phyllobilins detected in this work. Constitutional formulae and MS/MS fragmentation sites are shown. P^+, protonated precursor ion.

1.2. Relative abundance of phyllobilins in grass varieties

The senescent leaf extracts of various species were compared to corresponding green leaf extracts using LC-ESI-MS in the positive ion-mode. Base peak chromatogram (BPC) and extracted ion chromatogram (EIC) analyses of senescent samples, as shown in **Figures 7, 8** and 9, represent the pseudo-molecular ions $[M+H]^+$ for all the catabolites found in each variety. Respective peaks were not present in the extracts from green tissue (not shown) which was a positive indicator of the senescent-specific occurrence of phyllobilins that produced rather intense MS-ions using our experimental set-up.

The most abundant phyllobilins across various varieties in all analyzed species are consistently represented in both BPCs and EICs. From **Figure 7**, showing data of two barley varieties, it is evident that NCC_678 and DNCC_666 are the most abundant phyllobilins in Baraka and Golden Promise, respectively. NCC_678 is consistently found at highest abundance in all four varieties of wheat used in this study (**Figure 8**). Among other DNCCs present in ryegrass, DNCC_632-3 is the most abundant one, while NCC_840 and DNCC_666 are the most abundant phyllobilins in sorghum and rice, respectively (**Figure 9**).

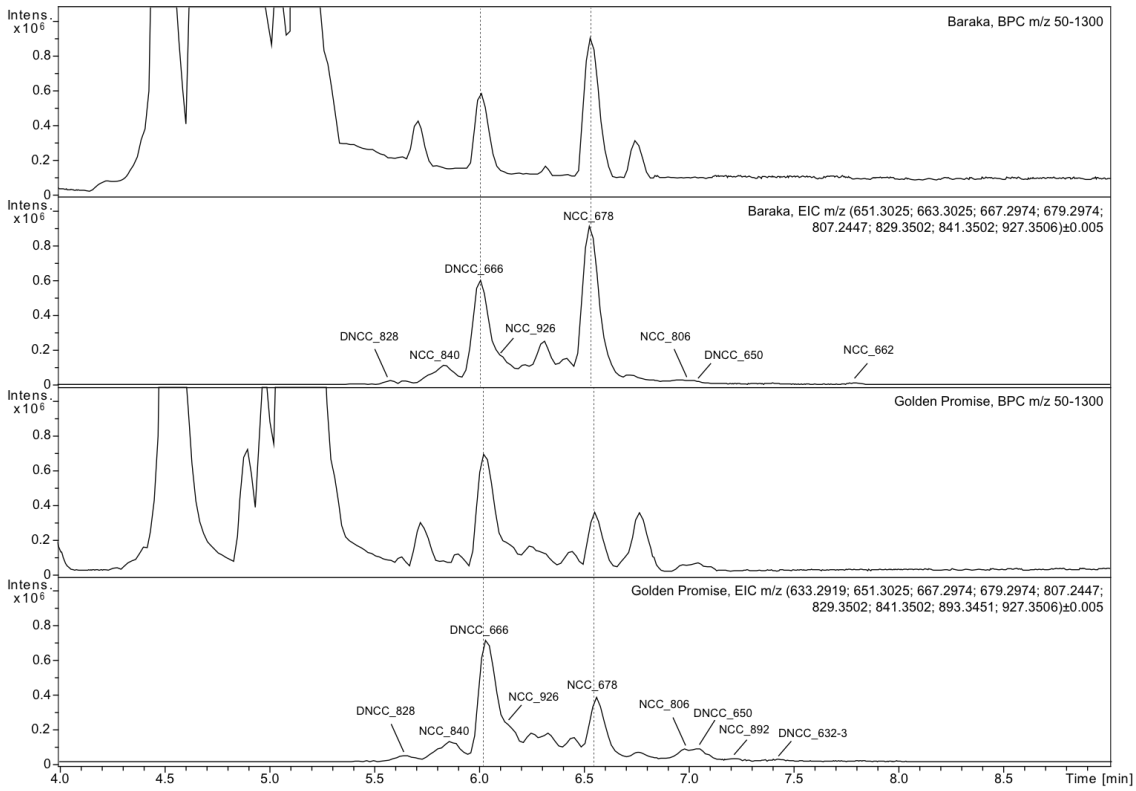

Figure 7: Base peak chromatograms (BPCs) and extracted ion chromatograms (EICs) of senescent leaf extracts from *Hordeum vulgare* var. Baraka and Golden Promise (barley) lines. For MS and MS/MS spectral details of the identified phyllobilins, see **Figure 6**.

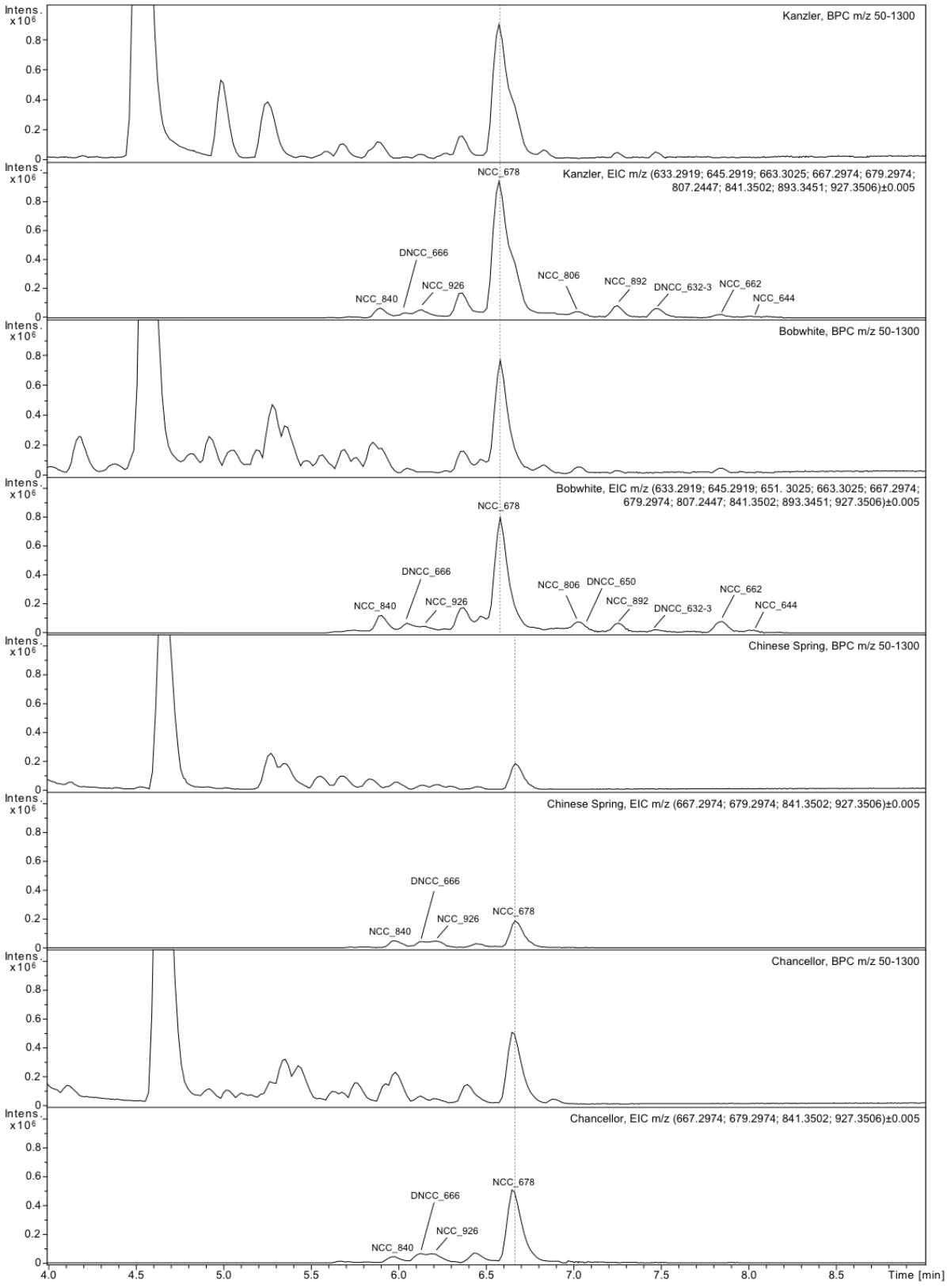

Figure 8: Base peak chromatograms (BPCs) and extracted ion chromatograms (EICs) of senescent leaf extracts from *Triticum aestivum* var. Kanzler, Bobwhite, Chinese Spring and Chancellor (wheat) lines. For MS and MS/MS spectral details of the identified phyllobilins, see **Figure 6**.

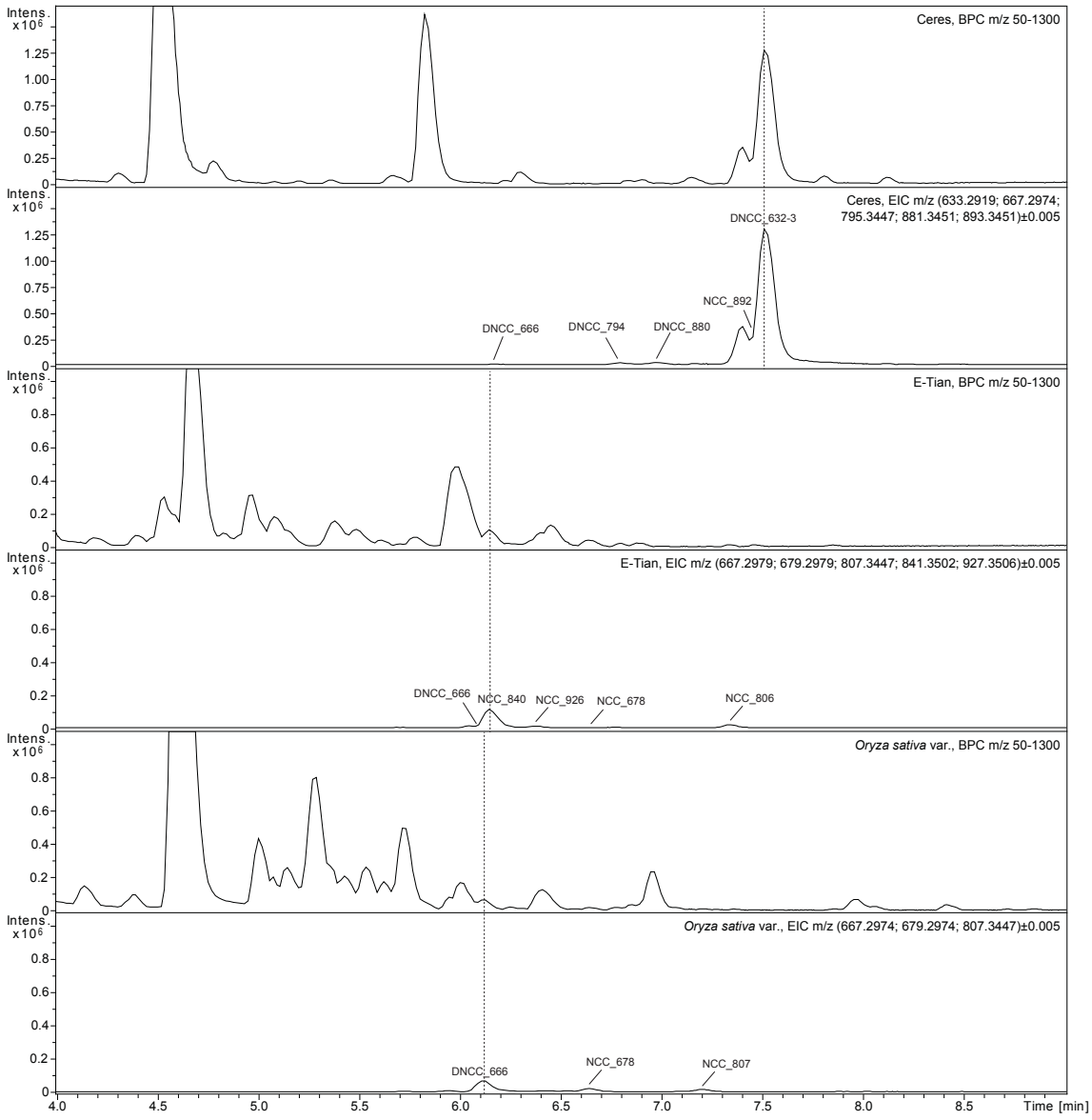

Figure 9: Base peak chromatograms (BPCs) and extracted ion chromatograms (EICs) of senescent leaf extracts from *Lolium perenne* var. Ceres (ryegrass), *Sorghum bicolor* var. E-Tian (sorghum) and *Oryza sativa* var. Nipponbare (rice) line. For MS and MS/MS spectral details of the identified phyllobilins, see **Figure 6**.

1.3. Comparison of phyllobilin composition in modern and ancestral varieties of grasses

As already mentioned above, both NCCs and DNCCs were detected in the modern varieties of barley with DNCCs being more abundant than NCCs (**Figure 10B**). This is opposite in the case of wheat, where modern varieties showed predominance of NCCs over DNCCs (**Figure 10A**). Among the tested species, the highest proportion of DNCC was found in ryegrass, in fact quantifiable amounts of NCCs were missing, while opposite to this, mostly

NCCs were present in sorghum, with trace amounts of DNCCs being detectable (**Figure 10C**). For this study additional ancestral varieties were chosen for wheat and barley. Under artificially induced senescence conditions, all the types of NCCs and DNCCs mentioned earlier **(Table 12)** were detected in the barley samples (**Figure 10B**). The proportion of NCCs and DNCCs found in the ancestral varieties of barley was more or less the same when compared to the modern varieties. Analysis of ancestral wheat varieties showed negligible amounts of DNCCs, while NCCs were found to be the predominant phyllobilins (**Figure 10A**).

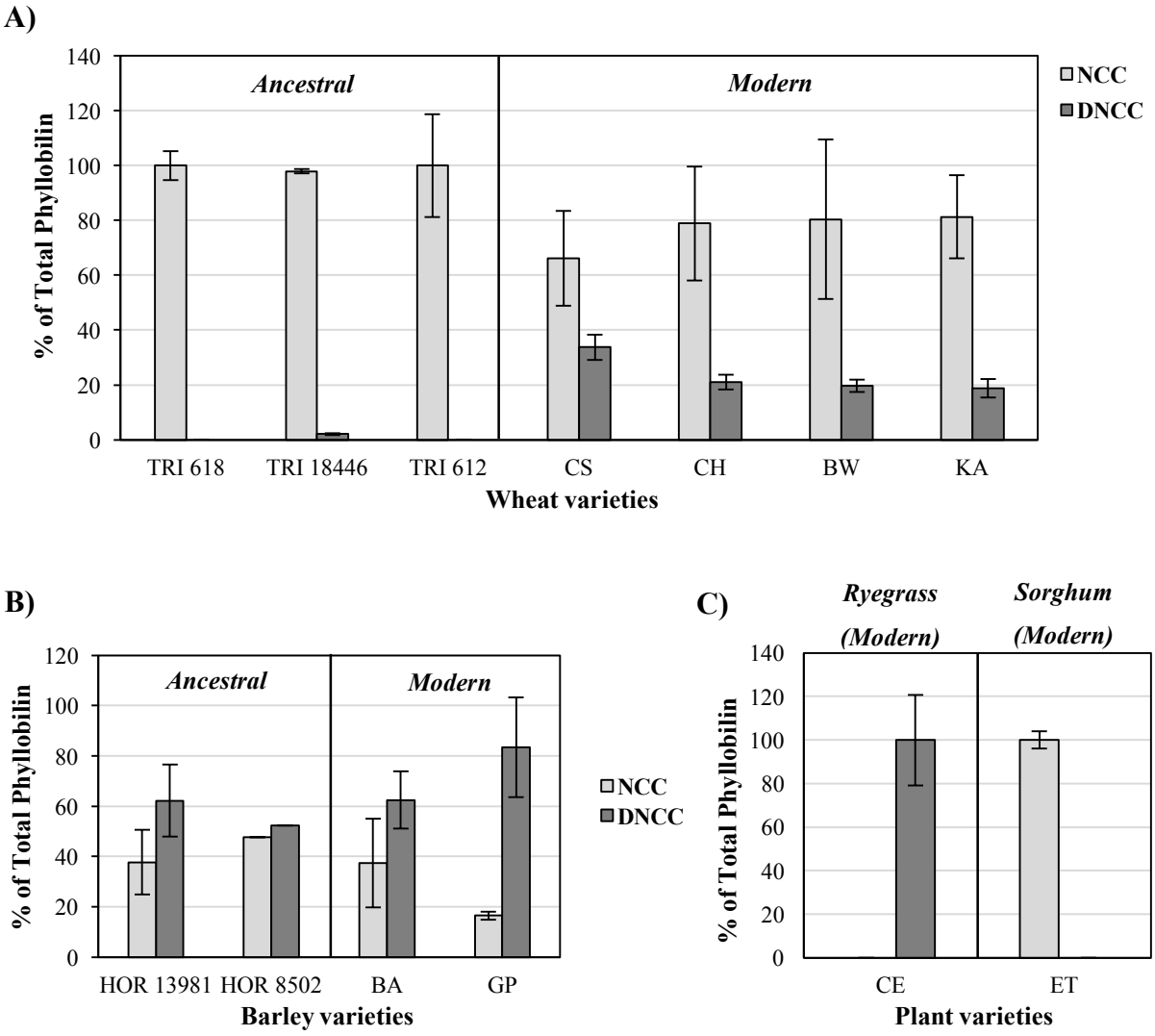

Figure 10: Phyllobilin distribution in modern and ancestral varieties of various plant species. Types of phyllobilins formed and their relative abundance in senescent primary leaves of: **A)** the ancestral varieties: TRI 618, TRI 18446 & TRI 612 and the modern varieties: Chinese Spring (CS), Chancellor (CH), Bobwhite (BW) & Kanzler (KA) of wheat; **B)** the ancestral varieties: HOR 13981 & HOR 8502 and the modern varieties: Baraka (BA) & Golden Promise (GP) of barley; and **C)** the modern varieties: Ceres wild-type (CE) of ryegrass and E-Tian (ET) of sorghum. Rice not shown because there are only traces of both DNCC and NCC type phyllobilins. Data are reported as mean ± s.d. of triplicates.

2. Impact of carbon monoxide and heavy oxygen on phyllobilin formation in grasses

It was reported for *Arabidopsis* that treatment of primary leaves with a 50% carbon monoxide (CO) atmosphere resulted in a decrease in DNCCs and an increase in NCC formation under artificially induced senescence conditions due to inhibition of CYP89A9, the cytochrome P450 monooxygenase that catalyzes DNCC formation in *Arabidopsis* (Christ et al., 2013). Similar experiments were carried out with barley (Golden Promise var.) and ryegrass to test the involvement of cytochrome P450s and to understand the underlying mechanism of phyllobilin formation in grasses. The results indicated no change in DNCC or NCC formation implying no involvement of any CYP450 activity in phyllobilin formation in grasses (**Figure 11A**). By contrast, in *Arabidopsis*, used as a positive control, abundance of DNCCs significantly diminished in the presence of CO.

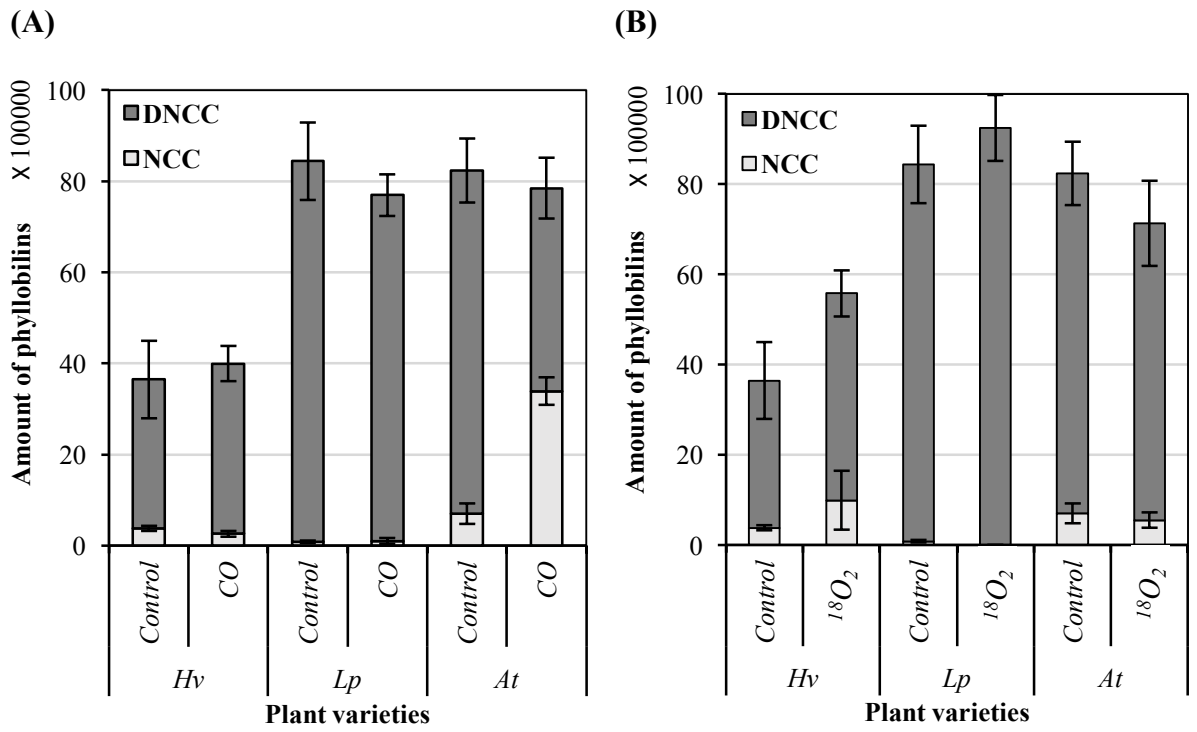

Figure 11: Effect of carbon monoxide and isotope-labeled dioxygen on the production of phyllobilins in grasses. The figure shows an HPLC analysis of the relative abundance of NCCs and DNCCs in barley (*Hv*), ryegrass (*Lp*) and *Arabidopsis* (*At*) during dark incubation in glass containers containing either 50% (v/v) CO mixed with ambient air **(A)** or 100% $^{18}O_2$ **(B)**. Control samples were incubated in 100% ambient air. Data are mean ± s.d. of triplicates.

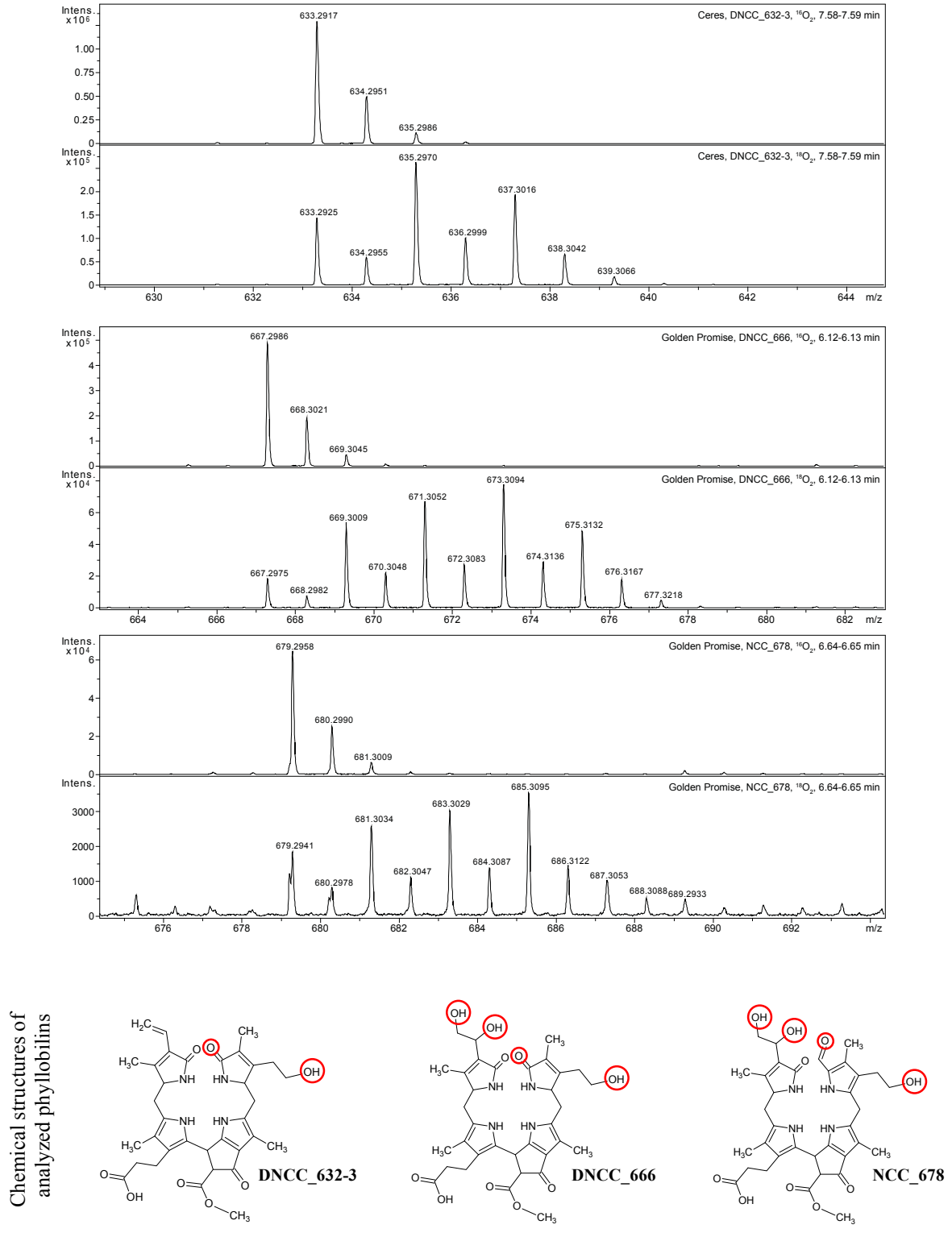

Figure 12: Mass spectra of selected phyllobilins from leaves of Ceres (top panel) or Golden Promise (middle and bottom panel) that were senesced under ambient atmosphere (top; $^{16}O_2$) or in heavy oxygen gas (bottom; $^{18}O_2$). Note that the incorporation of one ^{18}O atom increases the mass of the respective phyllobilin by two mass units. Thus, DNCC_632-3 contains up to two oxygens that are derived from molecular oxygen, while DNCC_666 and NCC_678 each contain up to four oxygen labels (red circles).

Similarly, $^{18}O_2$ labelling was used to determine if enzymes involved in the breakdown of chlorophyll used molecular oxygen. Previous studies have shown that several enzymes involved in the PAO/phyllobilin pathway such as PAO, CYP89A9 (Christ et al., 2013) and TIC55-IV (Hauenstein et al.; a manuscript submitted for publication, see **Chapter 5**) use molecular oxygen. Presence of $^{18}O_2$ did not largely alter overall phyllobilin abundance and composition (**Figure 11B**) and we observed labelled phyllobilins in barley (Golden Promise), ryegrass and *Arabidopsis*. This indicated that chlorophyll breakdown in crops also involves enzymes that are homologous to the ones that have been described previously in other species such as *Arabidopsis*. MS analysis of these samples demonstrated the presence of peaks representing the incorporation of ^{18}O atoms as shown in **Figure 12**. In detail, this analysis uncovered four reactions to be O_2 dependent, i.e. porphyrin ring cleavage (PAO leading to NCCs), $C3^2$ deformylating activity (responsible for DNCC formation), hydroxylating activity (TIC55 in *Arabidopsis*) and C18-dihydroxylating activity.

——— (Part 2) ———

Validation of the PAO / phyllobilin pathway in grasses

3. Investigating the PAO/phyllobilin pathway using barley as a model

3.1. Sequence identity and similarity of various Chl catabolite enzyme homologs

Multiple alignments of amino acid sequences of five Chl catabolic enzymes (CCEs) involved in the Chl degradation pathway were performed to obtain an understanding of identities and similarities between *Arabidopsis*, barley and rice CCE homologs (**Figure 13**). These CCEs include the chlorophyll(ide) *b* reductase non-yellow coloring 1 (NYC1), NYC1-like (NOL), pheophytin pheophorbide hydrolase (pheophytinase, PPH), pheophorbide *a* oxygenase (PAO) and stay-green protein (SGR). Proteins were identified using BLASTP at NCBI (http://blast.ncbi.nlm.nih.gov). While searching for PPH homologs, two closely similar sequences named *Hv*PPH_1 and *Hv*PPH_2 were found in barley and were included in the analysis (**Figure 13C**). The identity percentages of the aligned protein sequences of each CCE are summarized in **Table 13**. Recent studies have shown that PPH from *Arabidopsis* and many other species contain a conserved domain called PPH domain that harbors an active-site serine residue defining PPH as a serine esterase (Schelbert et al., 2009). This motif was present and highly conserved in both cases in barley and rice. Likewise, conserved motifs were identified in barley and rice PAO (**Figure 13D**).

A) NYC1: **Figure 13**

```
AtNYC1      --MTTLTKIQVYPQVLEHRL-FFRDPIRVGSRLTCRERSNRVYVHRCEKK 47
HvNYC1      -MAAAVVHLSVHARIRRSPEAVVSQACHRPSLLRCRAFKQEAGGDGENKP 49
OsNYC1      MAAAAVVHLSVHGRLRRSPE-LHARPYHRPSLLRCRAFKQEADNGGEEAS 49

AtNYC1      VERK---RKVEKFKGNGSWDSLKSGFLGFSKLGFLSKDEYN----QKVEN 90
HvNYC1      SSPP----NEPRKRRKGPLYTLKAAMQGLAGSRSAAAEVYGGQYELAVEK 95
OsNYC1      SSPPPPTTAEARRRRKGPLYKLKAAIQGLAGSRSAAAEAYGGEYQRAVEK 99
```

Figure 13 (continued)

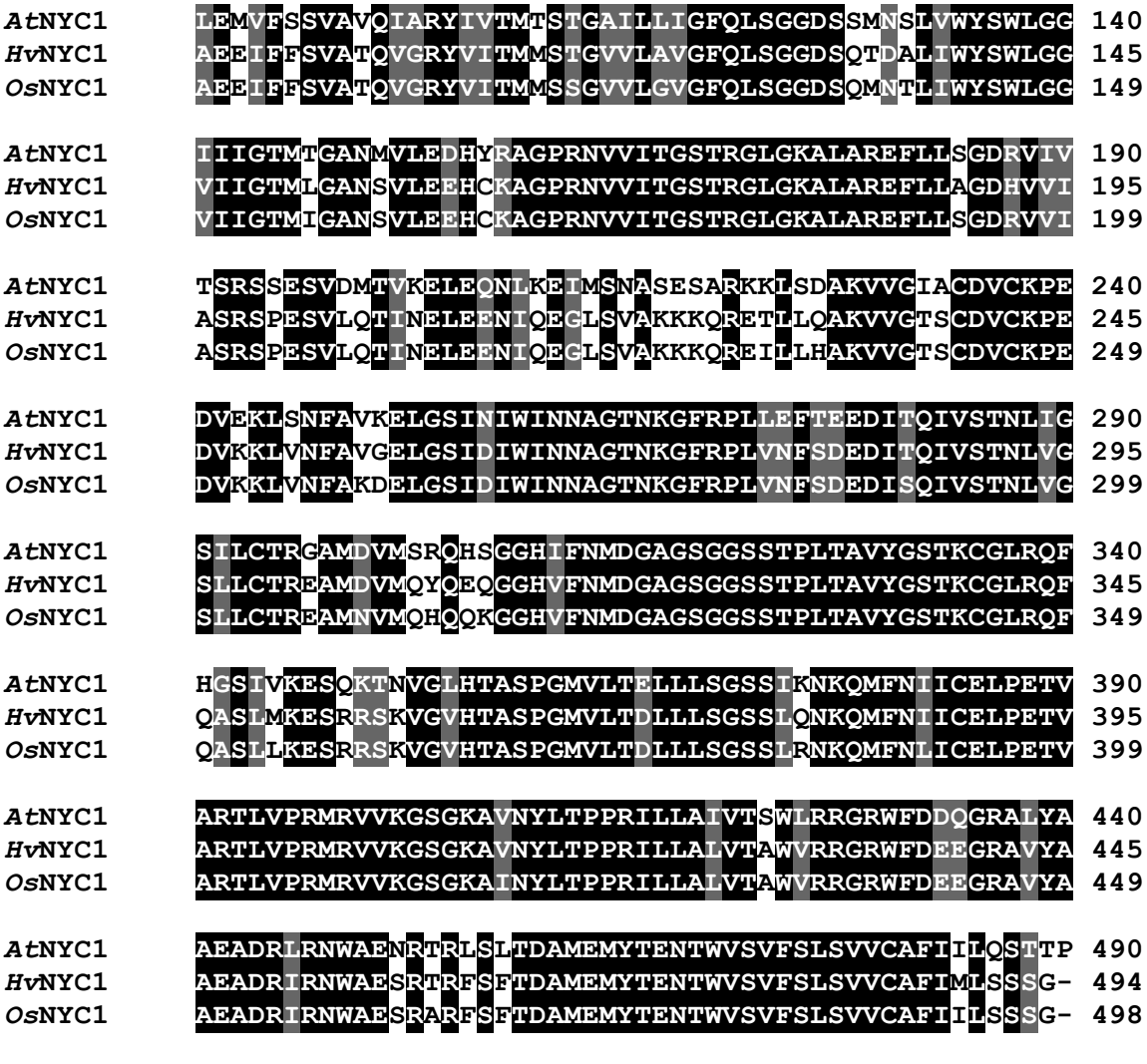

B) <u>NOL</u>:

Figure 13 (continued)

C) **PPH**:

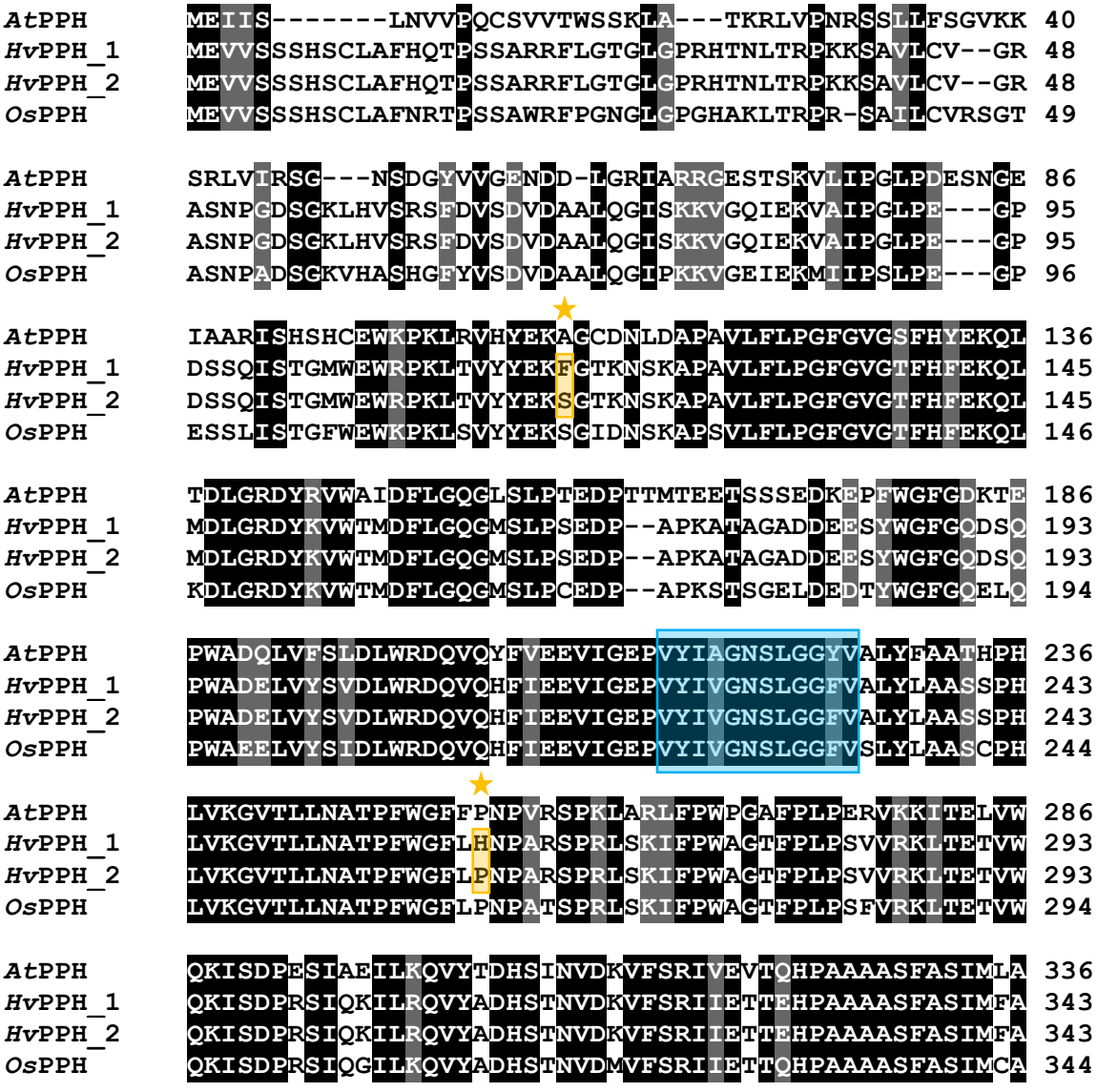

Figure 13 (continued)

```
AtPPH       PGGELSFSEALSRCKENNVQICLMYGREDPWVRPLWGKKIKKEIPNAPYY 386
HvPPH_1     PMGQISFQEALSRCQRQDIPISLMYGKEDPWVRPYWGIRVKQQVPEAPYY 393
HvPPH_2     PMGQISFQEALSRCQRQDIPISLMYGKEDPWVRPYWGIRVKQQVPEAPYY 393
OsPPH       PKGQISFEEALSRCQRQGIPISLMYGREDPWVRPIWGIKVKQQVPESPYY 394

AtPPH       EISPAGHCPHDEVPEVVNYLMRGWIKHLESGGFEALPLLEDTEEDWEESR 436
HvPPH_1     EISPAGHCPHDEVPEVINYLLRGWLKNVESEGTVDLPFLED--SSFEEHG 441
HvPPH_2     EISPAGHCPHDEVPEVT---------------------------------- 410
OsPPH       EISPAGHCPHDEVPEVINYLLRGWLKNVESEGSVAVPFLEE--PSYAENG 442

AtPPH       IGREIEFPRDGWKKAVNLWLYGSNYTYWRGVRESFR--SSFIRVFGGKSA 484
HvPPH_1     VSRELEFVRTGSKKSVSVRLFGSQISMWSQLSSFLKRHASNLRVVSR--- 488
HvPPH_2     --------------IVAVYKL------------------------------ 417
OsPPH       VSRELEFVRGGSKKSVHVRLFGSKISLWSQLRSLLK---SNTWVISR--- 486
```

D) PAO:

```
AtPAO       ------------------------------------------------- 0
HvPAO       ------------------------------------------------- 0
OsPAO       MRAPAAHLSPASSAVPSRNHGLLLHLRFLLSSSVSHLSARENSNPPSGCW 50

AtPAO       ------------------------------------------------- 0
HvPAO       ------------------------------------------------- 0
OsPAO       FSCQKQAILPVPVSSRLPPPPSCYYSVLLEEHWSPRLPQSPLTTPGASYK 100

AtPAO       ------------------MS------VVLLSSTSATITKSQSKKIPFLSP 26
HvPAO       ------------------MP------AVAMPTASLTLLSPRHRP-SLLLP 25
OsPAO       NRHAKNLQNHTETSDLRGFPSESTKMPVMAPTASL-LLSPRPLPASRRVP 149

AtPAO       TT-KFPLKVSISPSRSK--LFHNPLRVAAPPSVPTSDSTEEKRIEEEYGG 73
HvPAO       ASRPCSSGLRLRPRRGRGRVGSTRLRVAAPPSVPG-EAERAEDPSTSASA 74
OsPAO       SLPALSASGRLRLRRAR---ADTRLRVAAPPSVPG-EADQAPG-ETEPST 194

AtPAO       DKEEEGSEFKWRDHWYPVSLVEDLDPNVPTPFQLLGRDLVLWFDRNDQKW 123
HvPAO       SPGSPEERFVWRDHWYPVSLVEDLDPRVPTPFQLLNRDLVIWNDPNSGDW 124
OsPAO       S--SADEKFVWRDHWYPVSLVEDLDPSVPTPFQLLNRDLVIWKDPKSGEW 242

AtPAO       AAFDDLCPHRLAPLSEGRIDENGHLQCSYHGWSFGGCGSCTRIPQAATSG 173
HvPAO       VALDDRCPHRLAPLSEGRIDETGGLQCSYHGWSFDGSGACTRIPQAAAEG 174
OsPAO       VALDDRCPHRLAPLSEGRIDETGCLQCSYHGWSFDGSGACTRIPQAAPEG 292

AtPAO       PEARAVKSPRACAIKFPTMVSQGLLFVWPDENGWDRANSIEPPRLPDDFD 223
HvPAO       PEARAVRSPRACATKFPTLLSQGLLFVWPDENGWDKAKATKPPMLPKEFD 224
OsPAO       PEAKAVRSPKACAIKFPTLVSQGLLFVWPDENGWEKATATKPPMLPKEFE 342

AtPAO       KPEFSTVTIQRDLFYGYDTLMENVSDPSHIDFAHHKVTGRRDRAKPLPFK 273
HvPAO       DPAFSTVTIQRDLFYGYDTLMENVSDPSHIEFAHHKVTGRRDRAKPLPFK 274
OsPAO       DPAFSTVTIQRDLYYGYDTLMENVSDPSHIEFAHHKVTGRRDRARPLPFK 392

AtPAO       VESSGPWGFQGANDDSPRITAKFVAPCYSMNKIELDAKLPIVGNQKWVIW 323
HvPAO       MESSGAWGYSGANTGNPRITATFEAPCYALNKIEIDTKLPIVGDQKWVIW 324
OsPAO       MESSGAWGYSGSNSGNPRISATFVAPCYALNKIEIDTKLPIFGDQKWVIW 442
```

Figure 13 (continued)

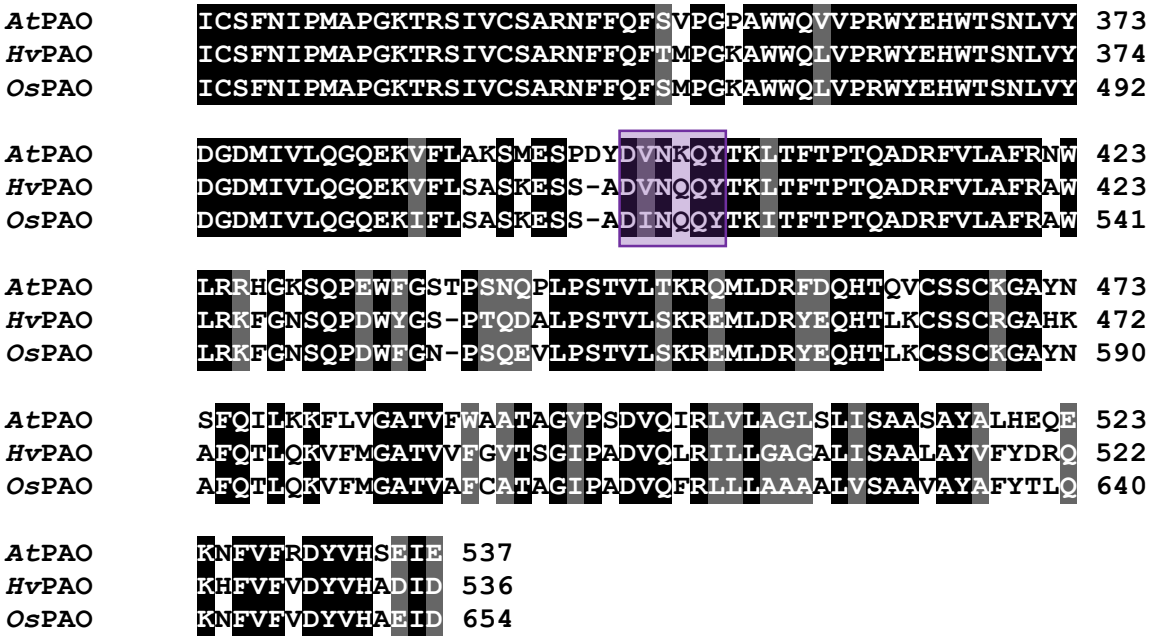

E) SGR:

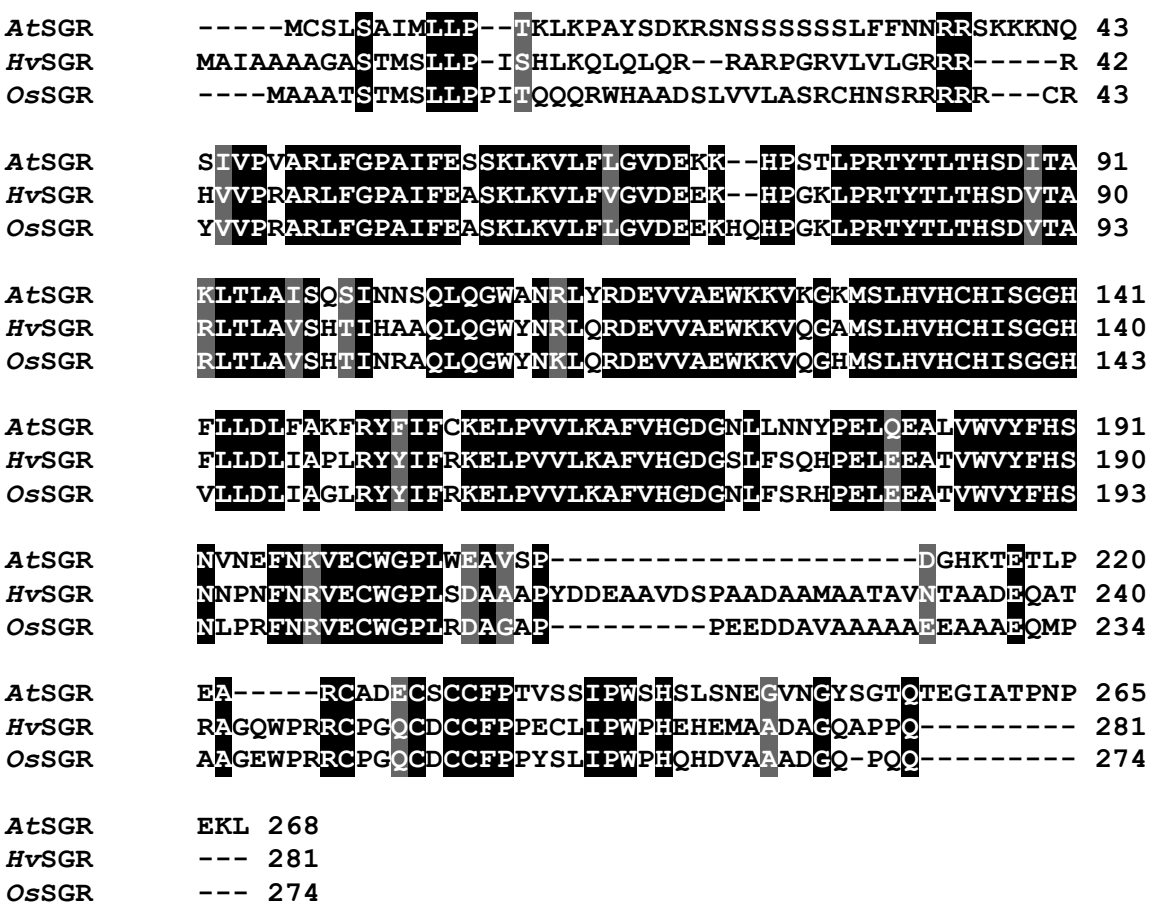

Figure 13: Protein sequence alignment of various Chl catabolic enzymes (CCEs) involved in Chl degradation. Comparison of amino acid sequences of: **A)** NYC1, **B)** NOL, **C)** PPH, **D)** PAO and **E)** SGR proteins, found in *Arabidopsis thaliana*, *Hordeum vulgare* and *Oryza sativa*. Shaded regions

denote evolutionarily conserved sequences (black) along with conservative or semi-conservative mutations (grey). The blue box represents the conserved PPH motif (containing the proposed active site serine residue) (Schelbert et al., 2009). Single amino acid substitutions in barley PPH sequences are highlighted by starred yellow boxes. The red, green and purple boxes represent the Rieske centre, the mononuclear iron-binding site and a proposed Ca^{2+}-dependent protein kinase (CDPK) binding site of PAO, respectively (Chung, 2006). Sequences were aligned using the Clustal Omega multiple sequence alignment tool (http://www.ebi.ac.uk/Tools/msa/clustalo).

Table 13: Pairwise sequence identity of various Chl catabolic enzymes (CCEs) involved in Chl degradation. Listed is the percentage identity of amino acid sequences of five investigated CCEs found in *A. thaliana, H. vulgare* and *O. sativa.*

Pair of species	***% Identity of various CCEs***				
	NYC1	**NOL**	**PPH (1/2)**	**PAO**	**SGR**
A. thaliana vs. H. vulgare	76	81	63/68	73	64
A. thaliana vs. O. sativa	75	81	60	68	61
H. vulgare vs. O. sativa	90	82	83/85	83	73

3.2. Determination of HvPPH activity

A closer look into the output sequences of the BLASTP search for *At*PPH homologs revealed two predicted protein sequences in barley i.e. *Hv*PPH_1 and *Hv*PPH_2 (named for convenience) with high similarities and sequence identities of 63% and 68%, respectively (**Figure 13C**). Besides differing C-termini, *Hv*PPH_1 contains a phenylalanine in place of a serine at position 118 and a histidine in place of a proline at position 261 when compared with *Hv*PPH_2. **Figure 11** shows the missense mutations responsible for the amino acid differences of *Hv*PPH_1 and *Hv*PPH_2 together with one representative expressed sequence tag (EST) sequence. Out of many ESTs present in the GenBank database (http://blast.ncbi.nlm.nih.gov, 11 exhibited the sequence version of *Hv*PPH_2, while the one of *Hv*PPH_1 was represented only one time. To test whether both proteins possess PPH activity, truncated versions of these proteins (devoid of the predicted chloroplast transit peptide) were fused to maltose binding protein (MBP) named MBP-Δ*Hv*PPH_1 and MBP-Δ*Hv*PPH_2, and expressed in *E. coli*. The recombinant proteins were found to be located in the soluble cell fraction as determined by SDS-PAGE and Western blot analysis (**Figure 15**). The activity of the enzymes was determined with pheophytin as substrate and by using HPLC to analyze for the presence of Pheide *a,* the product of PPH catalyzed conversion of pheophytin. Surprisingly, MBP-

Δ*Hv*PPH_1 was unable to produce Pheide *a,* while MBP-Δ*Hv*PPH_2 showed the presence of pheide *a* like MBP-Δ*At*PPH, which was used as a positive control (**Figure 16**). This indicates that the serine 118 and/or proline 261 residues play an important role for PPH activity, despite the fact that they lie outside the PPH motif (**Figure 13**) The *Hv*PPH_2 sequence was used in the following analyses.

Figure 14

```
HvPPH_1      ATGGAAGTGGTTTCTTCCAGCCACTCTTGCTTGGCATTTCATCAAACACCTAGCAGTGCTCGGAGGTTCC 70
HvPPH_2      ATGGAAGTGGTTTCTTCCAGCCACTCTTGCTTGGCATTTCATCAAACACCTAGCAGTGCTCGGAGGTTCC 70
HvPPH_EST    ------------------------------------------------------------------------ 0

HvPPH_1      TGGGCACTGGCCTTGGTCCGCGGCATACCAATCTTACCCGGCCAAAGAAAAGCGCAGTGCTCTGTGTTGG 140
HvPPH_2      TGGGCACTGGCCTTGGTCCGCGGCATACCAATCTTACCCGGCCAAAGAAAAGCGCAGTGCTCTGTGTTGG 140
HvPPH_EST    ------------------------------------------------------------------------ 0

HvPPH_1      GAGAGCTTCAAATCCAGGTGATTCAGGAAAGCTTCATGTCAGCCGCAGCTTCGATGTAAGCGATGTCGAT 210
HvPPH_2      GAGAGCTTCAAATCCAGGTGATTCAGGAAAGCTTCATGTCAGCCGCAGCTTCGATGTAAGCGATGTCGAT 210
HvPPH_EST    ------------------------------------------------------------------------ 0

HvPPH_1      GCTGCCCTCCAGGGCATCTCCAAGAAGGTAGGCCAGATCGAAAAAGTGGCGATTCCTGGTCTGCCAGAAG 280
HvPPH_2      GCTGCCCTCCAGGGCATCTCCAAGAAGGTAGGCCAGATCGAAAAAGTGGCGATTCCTGGTCTGCCAGAAG 280
HvPPH_EST    ------------------------------------------------------------------AAG 3

HvPPH_1      GGCCAGACAGTTCCCAAATCAGCACTGGTATGTGGGAGTGGAGGCCGAAGCTGACGGTATACTACGAGAA 350
HvPPH_2      GGCCAGACAGTTCCCAAATCAGCACTGGTATGTGGGAGTGGAGGCCGAAGCTGACGGTATACTACGAGAA 350
HvPPH_EST    GGCCAGACAGTTCCCAAATCAGCACTGGTATGTGGGAGTGGAGGCCGAAGCTGACGGTATACTACGAGAA 73

HvPPH_1      GTTTGGCACCAAGAATAGCAAGGCGCCAGCGGTGCTTTTTCTACCAGGTTTTGGAGTGGGCACCTTCCAT 420
HvPPH_2      GTCTGGCACCAAGAATAGCAAGGCGCCAGCGGTGCTTTTTCTACCAGGTTTTGGAGTGGGCACCTTCCAT 420
HvPPH_EST    GTCTGGCACCAAGAATAGCAAGGCGCCAGCGGTGCTTTTTCTACCAGGTTTTGGAGTGGGCACCTTCCAT 143

HvPPH_1      TTTGAGAAGCAATTGATGGATCTTGGACGTGATTACAAGGTGTGGACAATGGATTTTCTAGGACAGGGAA 490
HvPPH_2      TTTGAGAAGCAATTGATGGATCTTGGACGTGATTACAAGGTGTGGACAATGGATTTTCTAGGACAGGGAA 490
HvPPH_EST    TTTGAGAAGCAATTGATGGATCTTGGACGTGATTACAAGGTGTGGACAATGGATTTTCTAGGACAGGGAA 213

HvPPH_1      TGTCATTGCCGTCGGAAGACCCTGCTCCTAAGGCCACGGCAGGGGCGGATGATGAGGAATCGTATTGGGG 560
HvPPH_2      TGTCATTGCCGTCGGAAGACCCTGCTCCTAAGGCCACGGCAGGGGCGGATGATGAGGAATCGTATTGGGG 560
HvPPH_EST    TGTCATTGCCGTCGGAAGACCCTGCTCCTAAGGCCACGGCAGGGGCGGATGATGAGGAATCGTATTGGGG 283

HvPPH_1      TTTTGGACAAGATTCGCAACCATGGGCAGATGAATTGGTGTACTCTGTAGACTTGTGGCGTGACCAGGTC 630
HvPPH_2      TTTTGGACAAGATTCGCAACCATGGGCAGATGAATTGGTGTACTCTGTAGACTTGTGGCGTGACCAGGTC 630
HvPPH_EST    TTTTGGACAAGATTCGCAACCATGGGCAGATGAATTGGTGTACTCTGTAGACTTGTGGCGTGACCAGGTC 353

HvPPH_1      CAGCATTTCATTGAGGAGGTTATCGGTGAACCAGTTTATATTGTTGGAAACTCTCTTGGAGGTTTTGTTG 700
HvPPH_2      CAGCATTTCATTGAGGAGGTTATCGGTGAACCAGTTTATATTGTTGGAAACTCTCTTGGAGGTTTTGTTG 700
HvPPH_EST    CAGCATTTCATTGAGGAGGTTATCGGTGAACCAGTTTATATTGTTGGAAACTCTCTTGGAGGTTTTGTTG 423

HvPPH_1      CTCTGTATTTAGCTGCATCCAGTCCACACCTTGTAAAGGGGGTCACATTGCTTAATGCAACGCCATTTTG 770
HvPPH_2      CTCTGTATTTAGCTGCATCCAGTCCACACCTTGTAAAGGGGGTCACATTGCTTAATGCAACGCCATTTTG 770
HvPPH_EST    CTCTGTATTTAGCTGCATCCAGTCCACACCTTGTAAAGGGGGTCACATTGCTTAATGCAACGCCATTTTG 493

HvPPH_1      GGGTTTCCTTCATAATCCTGCAAGATCTCCTCGTTTGTCAAAGATTTTTCCATGGGCTGGGACATTTCCT 840
HvPPH_2      GGGTTTCCTTCCTAATCCTGCAAGATCTCCTCGTTTGTCAAAGATTTTTCCATGGGCTGGGACATTTCCT 840
HvPPH_EST    GGGTTTCCTTCCTAATCCTGCAAGATCTCCTCGTTTGTCAAAGAATTTTTACATGGGCTGGGACATNTCCT 563
```

Figure 14 (continued)

```
HvPPH_1      CTTCCATCAGTTGTGAGGAAACTTACTGAAACAGTGTGGCAGAAGATAAGCGACCCAAGAAGTATACAGA 910
HvPPH_2      CTTCCATCAGTTGTGAGGAAACTTACTGAAACAGTGTGGCAGAAGATAAGCGACCCAAGAAGTATACAGA 910
HvPPH_EST    CTTCCATCAGGTGGGAGGATACTTACTGANACAGTGTGGCAGAAGATAA-CGACCCAGGATGTCTACTGA 632

HvPPH_1      AGATACTCAGGCAAGTATATGCTGACCACTCAACAAATGTTGATAAGGTGTTCTCGCGTATTATAGAGAC 980
HvPPH_2      AGATACTCAGGCAAGTATATGCTGACCACTCAACAAATGTTGATAAGGTGTTCTCGCGTATTATAGAGAC 980
HvPPH_EST    AGATACTCAAGCGAGT---------------------------------------------------- 648

HvPPH_1      AACAGAACACCCGGCAGCTGCTGCATCATTTGCCTCCATTATGTTTGCTCCAATGGGCCAGATATCCTTT 1050
HvPPH_2      AACAGAACACCCGGCAGCTGCTGCATCATTTGCCTCCATTATGTTTGCTCCAATGGGCCAGATATCCTTT 1050
HvPPH_EST    ---------------------------------------------------------------------- 648

HvPPH_1      CAGGAGGCACTATCTAGGTGCCAAAGGCAGGACATTCCCATTTCCCTTATGTATGGGAAAGAAGATCCTT 1120
HvPPH_2      CAGGAGGCACTATCTAGGTGCCAAAGGCAGGACATTCCCATTTCCCTTATGTATGGGAAAGAAGATCCTT 1120
HvPPH_EST    ---------------------------------------------------------------------- 648

HvPPH_1      GGGTTAGACCTTATTGGGGTATCAGAGTCAAGCAGCAGGTCCCAGAAGCACCCTATTATGAAATCAGCCC 1190
HvPPH_2      GGGTTAGACCTTATTGGGGTATCAGAGTCAAGCAGCAGGTCCCAGAAGCACCCTATTATGAAATCAGCCC 1190
HvPPH_EST    ---------------------------------------------------------------------- 648

HvPPH_1      TGCCGGTCACTGTCCTCATGATGAGGTTCCTGAGGTTATAAACTATTTGCTCCGAGGATGGCTTAAGAAT 1260
HvPPH_2      TGCCGGTCACTGTCCTCATGATGAGGTTCCTGAGGT----AACTATTGTTGCCGTGTACAAATTATAG-- 1254
HvPPH_EST    ---------------------------------------------------------------------- 648

HvPPH_1      GTGGAGTCTGAGGGTACAGTTGACCTCCCATTTCTTGAAGATTCCAGCTTTGAAGAACATGGGGTATCGA 1330
HvPPH_2      ---------------------------------------------------------------------- 1254
HvPPH_EST    ---------------------------------------------------------------------- 648

HvPPH_1      CATGTGGAGCCAACTGAGCTCATTCTTGAAGCGACATGCCTCCAACCTACGGGTAGTGTCCAGATGA 1467
HvPPH_2      ---------------------------------------------------------------- 1254
HvPPH_EST    ---------------------------------------------------------------- 648
```

Figure 14: Nucleotide sequence alignment of various PPH CDSs and EST in *H. vulgare*. Comparison of various pheophytin pheophorbide hydrolase (PPH) coding sequences (*Hv*PPH_1 and *Hv*PPH_2) found in *Hordeum vulgare* with an expressed sequence tag (*Hv*PPH_EST; EST name: HV_CEa0008D10f and GenBank gi: 13261186). The key differences between the sequences are highlighted by starred red boxes. Sequences were globally aligned using the Clustal Omega multiple sequence alignment tool (http://www.ebi.ac.uk/Tools/msa/clustalo).

A)

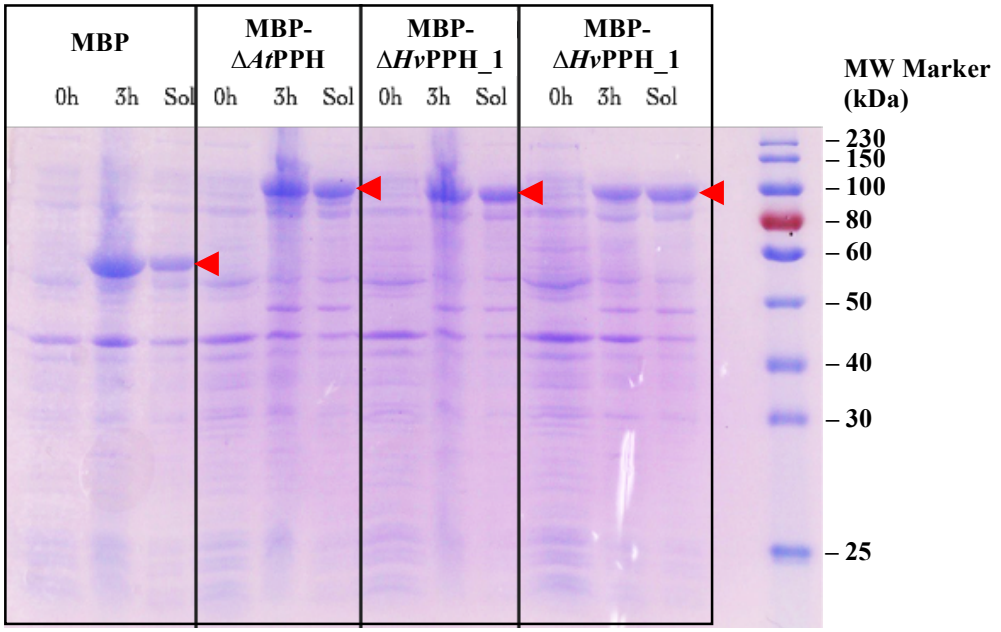

B)

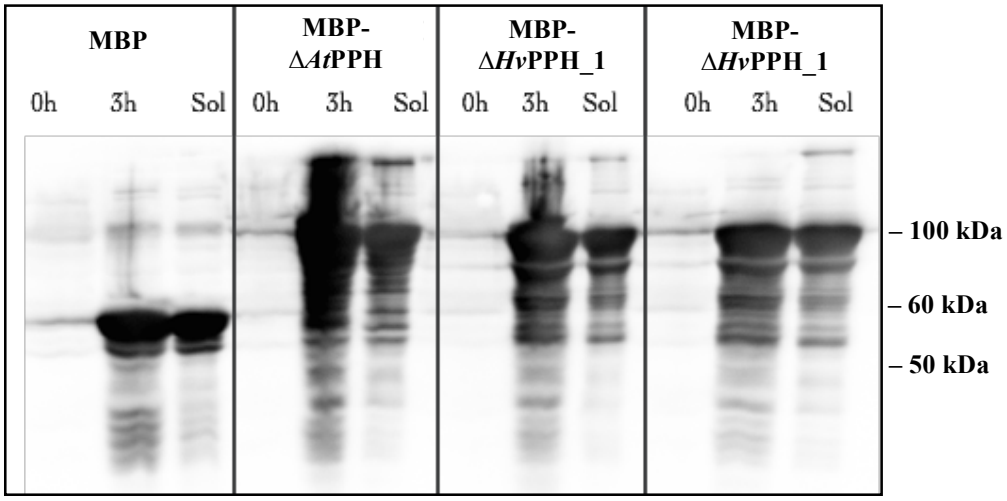

Figure 15: Biochemical analyses of recombinant *Hv*PPH_1 and *Hv*PPH_2 proteins. **A)** Coomassie blue stained SDS-PAGE image of *E. coli* cells (BL21-DE3) expressing N-terminal truncated versions of *Hv*PPH fused to MBP (MBP-Δ*Hv*PPH). Strains expressing free MBP and MBP-Δ*At*PPH were used as control. Samples analyzed include whole cell lysates before induction with IPTG (0h), 3 hours after induction (3h) and soluble protein fractions (Sol). Gel loadings are based on equal amounts of cell cultures at OD_{600} = 1.5. Arrowheads indicate positions of recombinant proteins. Molecular weight markers (kDa) are indicated on the right side of the image. **B)** Immunoblot detection of MBP using a mouse anti-MBP monoclonal antibody (dil. 1:10,000).

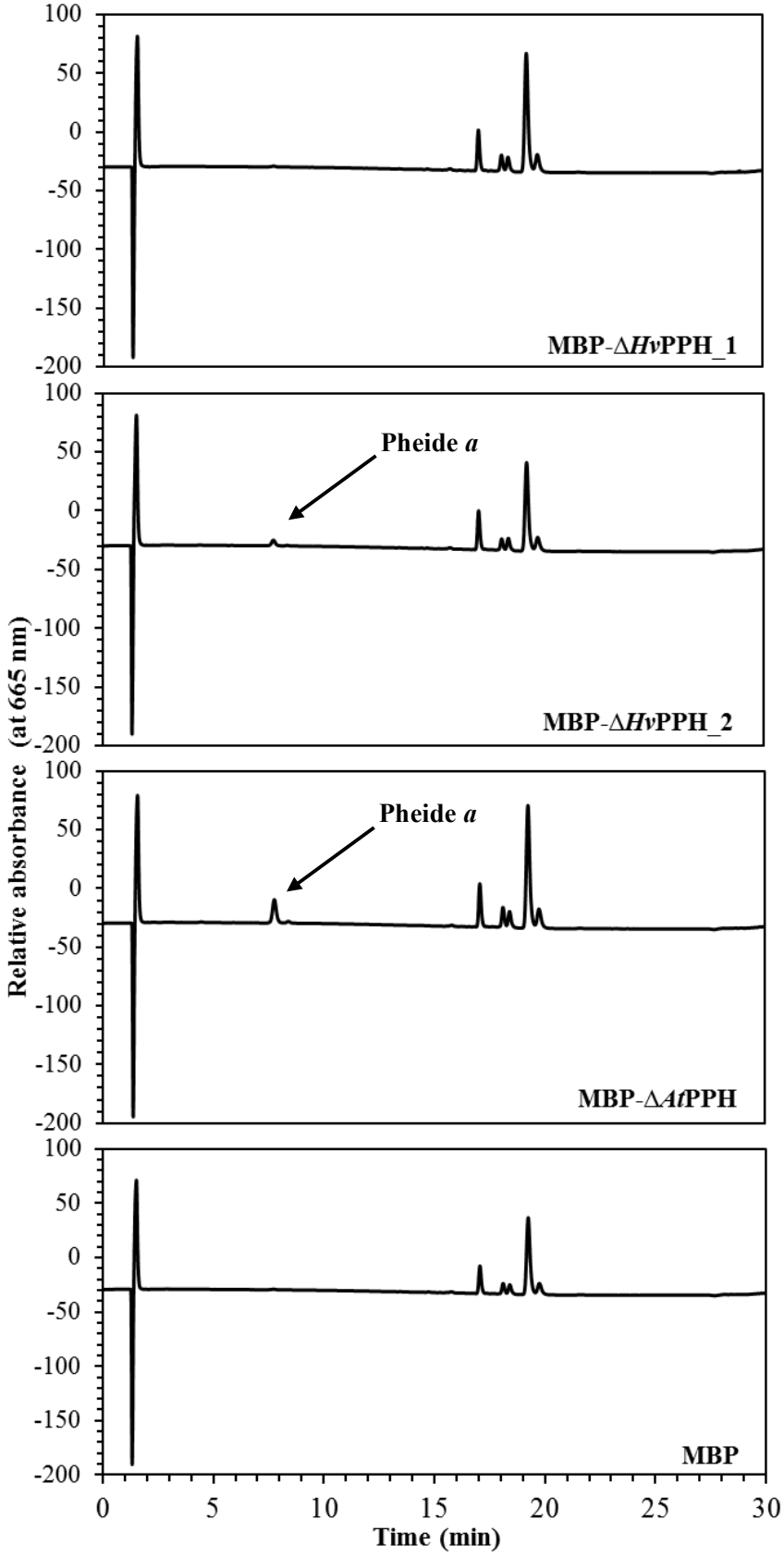

Figure 16: HPLC analysis of recombinant *Hv*PPH_1 and *Hv*PPH_2 proteins. HPLC analysis of assays employing soluble *E. coli* lysates expressing MBP-Δ*Hv*PPH. HPLC traces recorded at 665 nm are shown for assays that were incubated for 30 min at 34°C.

3.3. HvCCEs are localized to chloroplasts in barley

In order to investigate the sub-cellular localization of *Hv*CCEs in barley, C-terminal GFP fusions were created and analyzed in the protoplasts of the wild-type barley var. Golden Promise (GP).

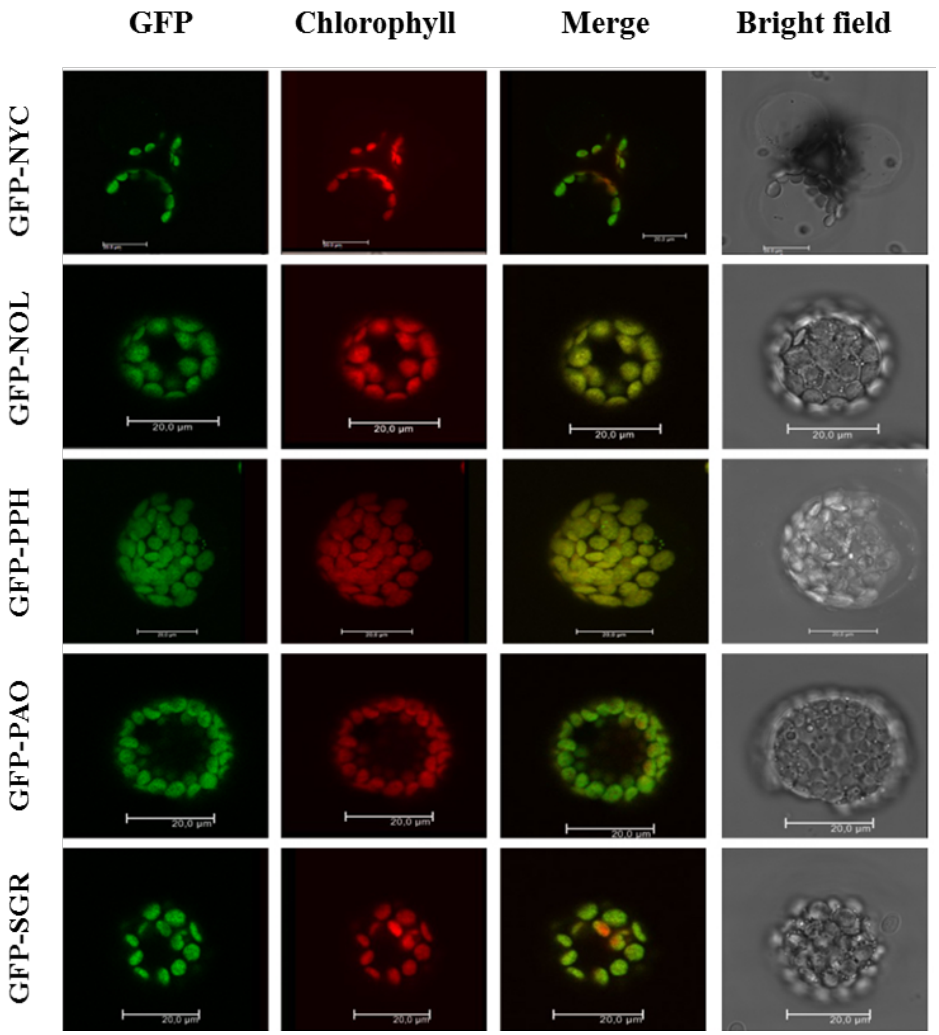

Figure 17: *In vivo* localization studies of GFP constructs in barley mesophyll protoplasts. The microscopic images show sub-cellular localization of *Hv*CCEs by transient transformation in barley protoplasts. GFP fluorescence (GFP) and chlorophyll autofluorescence (chlorophyll) were examined by confocal laser scanning microscopy. The merge panels show overlays of GFP and autofluorescence. Bars = 20 µm.

The transient expression of NYC-GFP, NOL-GFP, PPH-GFP, PAO-GFP and SGR-GFP was analyzed based on GFP fluorescence using confocal microscopy. All fusion proteins distinctly localized to chloroplasts, i.e. largely co-localized with chlorophyll autofluorescence

(**Figure 17**). This analysis revealed that like in *Arabidopsis* (Sakuraba et al., 2012) all investigated CCE are targeted to either the thylakoid membrane or the stroma.

3.4. Genes encoding HvCCEs are upregulated during leaf senescence

Detached primary leaves of GP were incubated in the dark for 8 days. RNA was extracted from 0ddi, 4ddi and 8ddi (**Figure 18A**). Expression of the genes involved in the chlorophyll breakdown pathway, was analyzed by real-time quantitative RT-PCR. In this study, *Hv*S40, a known SAG (Gregersen et al., 2008) was used as a positive control and expression was normalized to *ADP*, a housekeeping gene that encodes ADP-ribosylation factor 1-like protein (Vicente et al., 2015). All genes encoding *Hv*CCEs followed an increasing trend in gene expression with the progression of senescence.

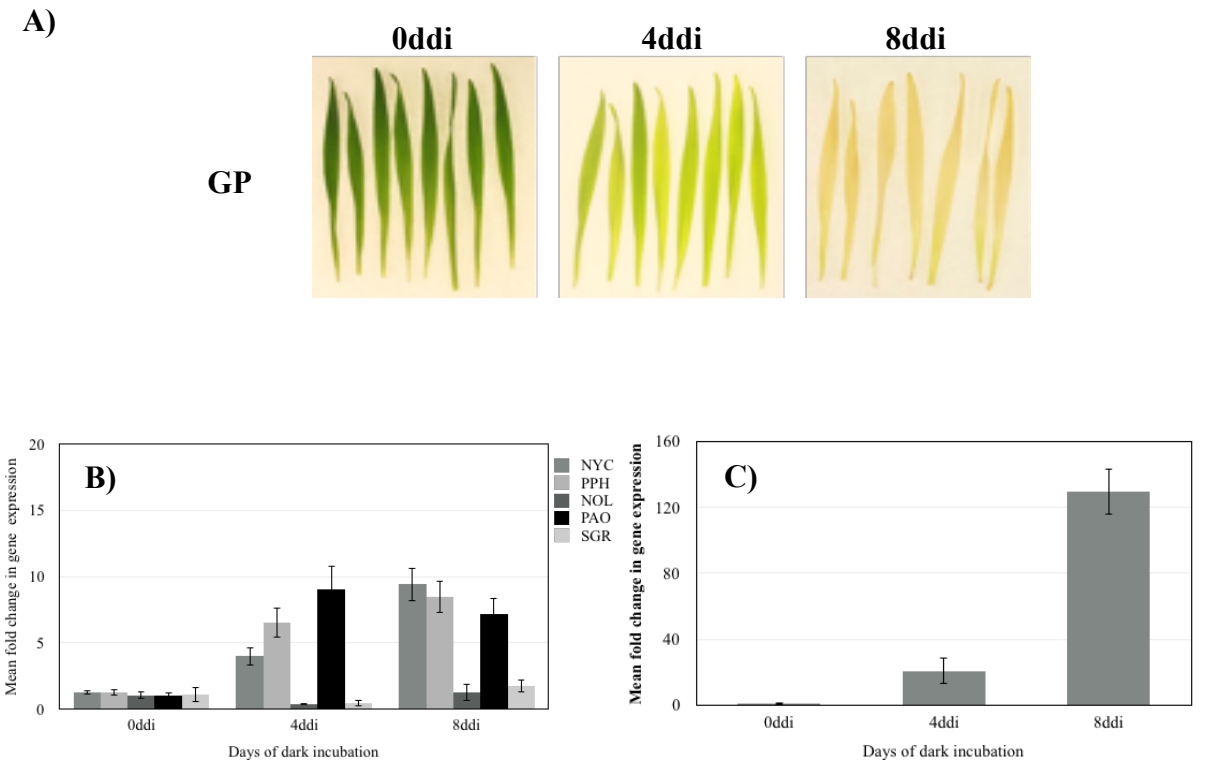

Figure 18: Quantitative analysis of gene expression in primary leaves of wild-type barley var. Golden Promise (GP). **A)** Photographs showing the visible loss of chlorophyll in barley leaves, 4 and 8 days after dark incubation. The graphs represent quantitative and comparative analyses of expression of: **B)** *Hv*CCE genes: *NYC, PPH, NOL, PAO* and *SGR* involved in Chl catabolism; and **C)** *HvS40* (control) during dark-induced senescence. Data are mean ± s.d. of triplicates.

Expression of *PAO* was highest after 4 days but slightly reduced by the 8th day of incubation whereas *NYC*, *NOL*, *PPH* and *SGR* showed maximum expression at the end of the experimental period (**Figure 18B**). *HvS40* showed an exceptional increase after 8 days of dark incubation which was expected for a SAG (**Figure 18C**). Thus, all investigated *Hv*CCEs are senescence-upregulated.

3.5. HvPAO protein abundance increases during senescence

*Hv*PAO was highly upregulated during senescence, as deduced from the gene expression data (**Figure 18**). Western blot analysis of leaf membrane protein fractions confirmed that the PAO protein abundance increased with senescence progression (**Figure 19**).

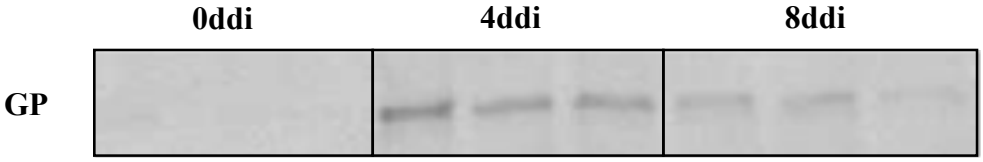

Figure 19: PAO protein abundance in barley var. GP. The Western blot image shows the upregulation of PAO protein after 4 days of dark incubation followed by slight reduction during the last stage of senescence. Three biological replicates are shown for each time point.

3.6. Confirmation of PAO activity in barley using the inhibitor bipyridyl

To investigate the *in vivo* involvement of PAO in the breakdown of chlorophyll in barley, senescence was induced in the presence of 2,2'-bipyridyl (Bpy), which earlier has been employed in canola (*Brassica napus*) for the interruption of the Chl breakdown pathway at the level of the oxygenolytic ring opening by PAO (Hörtensteiner et al., 1995). Thus, detached barley primary leaves were treated with 0.5 mM Bpy while control leaves were senesced on water-soaked filter paper. After 8 days of dark incubation, Bpy-treated leaves retained visibly more chlorophyll than the control (**Figure 20A**). HPLC analysis confirmed the retention of Chl in these samples. In addition, it showed that the treated samples accumulated considerable amounts of Pheide *a,* whereas Pheide *a* was not detected in control samples (**Figure 20B**). The

metal-chelating action of Bpy was able to block PAO causing a delay or interruption of Chl degradation. Thus, it becomes evident that the Chl breakdown process in barley also employs PAO which has been shown in *Arabidopsis* to be the key regulatory enzyme in the pathway (Pruzinska et al., 2005).

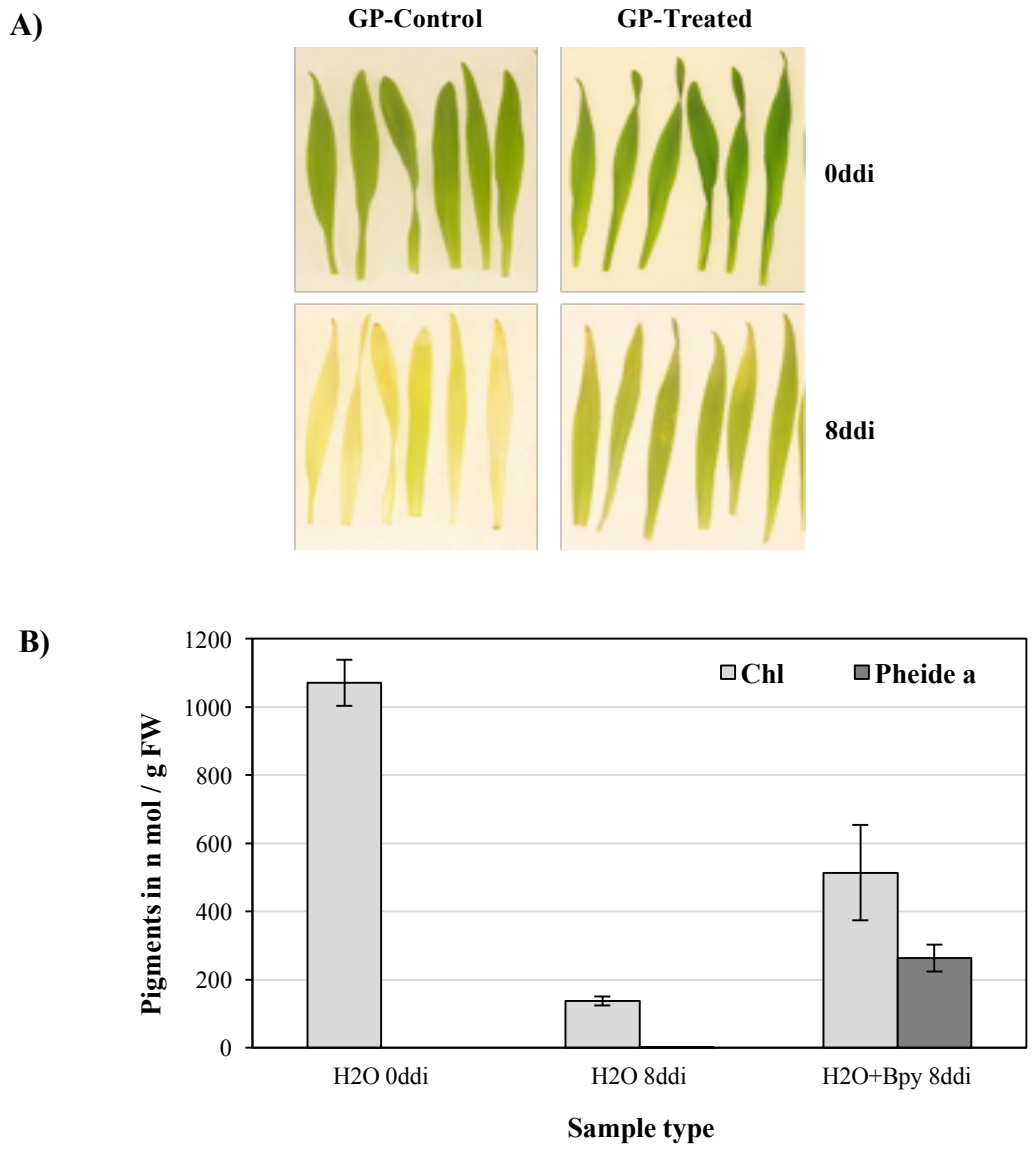

Figure 20: Investigation of PAO activity in barley var. Golden Promise using 2,2'-bipyridyl (Bpy). **A)** Photographs of barley primary leaves showing greater retention of chlorophyll after 8 days of dark incubation when treated with 0.5 mM Bpy compared to H_2O (control). **B)** The graphs show the loss of chlorophyll content after 8 days in control samples when compared to the 0 day samples. It also shows the accumulation of Pheide *a* in the treated samples indicating the interruption of PAO activity caused by Bpy. This shows that the pathway is actively followed to degrade chlorophyll in barley like in *Arabidopsis*. Data are mean ± s.d. of triplicates.

3.7. HvPAO complements the Arabidopsis pao1 knockout mutant

In *Arabidopsis*, *pao1* knockout mutant leaves have been reported to show an age- and light- dependent cell death phenotype. In dark, the mutant shows a stay-green phenotype, which is accompanied by the accumulation of photoreactive Pheide *a*. *Hv*PAO cDNA was expressed in *pao1* under the control of the 35S promoter. 11 primary transformants were obtained and 8 lines were further investigated in the T2 generation. Homozygosity of the original *pao1* T-DNA was confirmed by PCR (**Table 14**). Homozygosity of the 35S:*Hv*PAO construct was confirmed by kanamycin resistance tests in the T3 generation. Finally, one transformant (# 9) was selected for complementation tests in T2. Detached leaves from *pao1*/35S:*Hv*PAO plants exhibited loss of chlorophyll under dark-induced senescence. Thus, the stay-green phenotype was complemented.

In addition, HPLC analysis showed absence of Pheide *a* in the complementing line when compared to *pao1* (**Figure 21B and 21C**). In summary, *Hv*PAO fully complemented the absence of *At*PAO in *pao1* confirming that the former plays the same role in Chl breakdown in barley as the latter does in *Arabidopsis*.

Table 14: Table showing the overview of genotyping data used for confirmation of *pao1* and transgene.

Primers	**Col-0**	***pao1***	***pao1*/35S:*Hv*PAO lines**							
			# 1	**# 2**	**# 4**	**# 5**	**# 7**	**# 9**	**# 10**	**# 11**
LP/RP (N14)	+	-	Faint	Faint	-	-	-	-	-	-
LBb 3.1/ RP	-	+	+	+	+	+	+	+	+	+
***Hv*PAO**	-	-	-	+	+	+	Faint	+	+	-

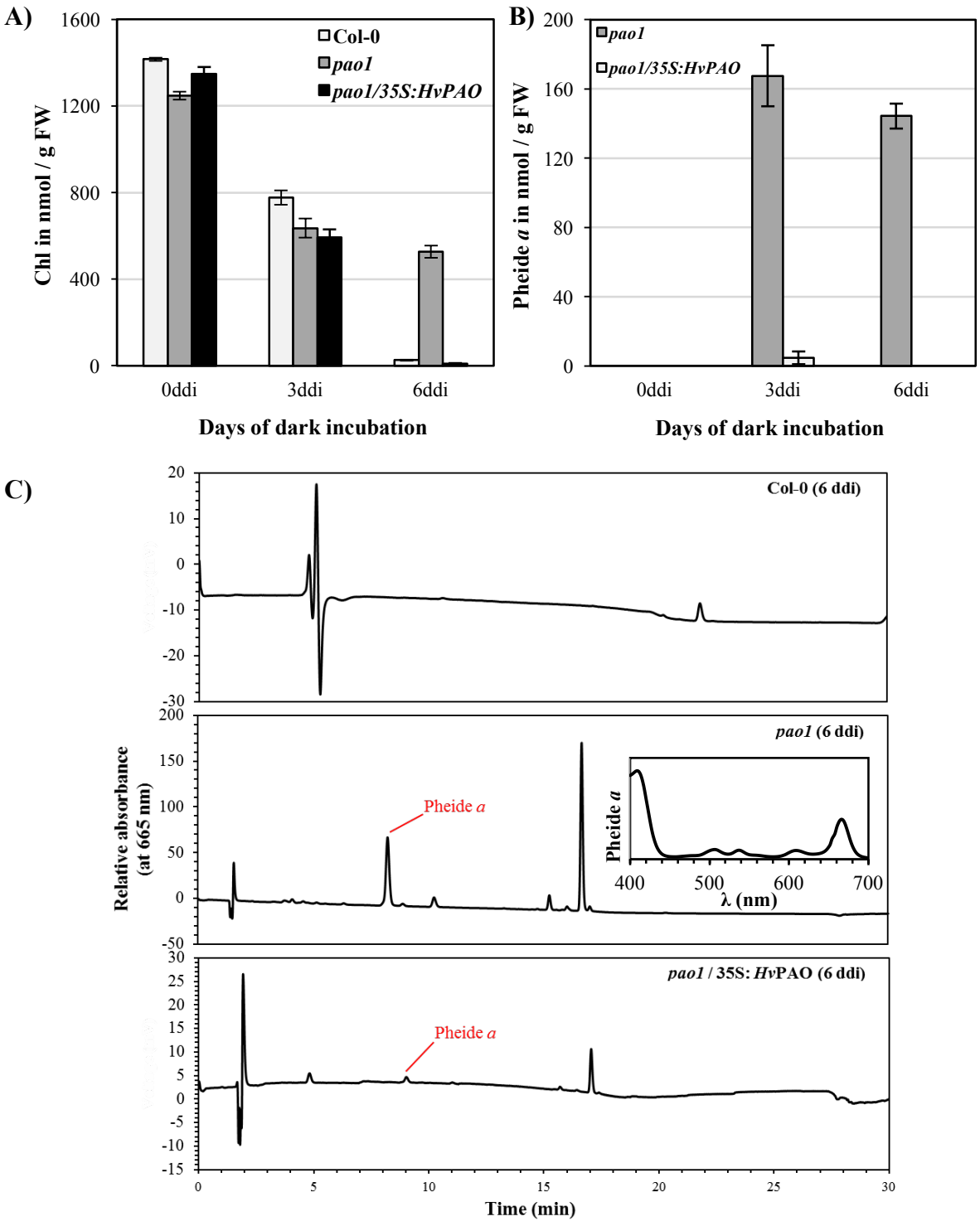

Figure 21: Complementation of the stay-green phenotype of *pao1* with a 35S:*Hv*PAO cDNA construct. **A)** The graph shows decrease in chlorophyll content in Col-0 (positive control) and the complemented line after 6 days of dark incubation whereas *pao1* (negative control) still held sufficient amounts of chlorophyll to exhibit a stay-green phenotype. **B)** The graph shows accumulation of Pheide *a* in *pao1* mutant plants after 3 and 6 days of dark incubation whereas the complemented plants showed negligible amounts of Pheide *a* after 3 days and nothing at all after 6 days of dark incubation. Pheide *a* accumulation was absent in the control plants (data not shown). **C)** The chromatogram shows a clear Pheide *a* peak (spectrum of the peak shown on the right) only in case of the *pao1* mutant. It was a clear indication that in the complemented lines, *Hv*PAO could complement the absence of *At*PAO and lead to senescence progression.

3.8. HvPPH complements AtPPH in pph-1 knockout mutants

Deficiency of PPH in *Arabidopsis PPH* mutants (*pph-1*), leads to accumulation of Phein *a* (during dark-induced senescence) and results in a cosmetic stay-green phenotype. Similar to *Hv*PAO, *Hv*PPH cDNA was also introduced into *pph-1* under the control of the 35S promoter. In the T1 generation, 8 positively transformed lines were obtained and 4 lines were further investigated in the T2 generation. Genotyping results confirmed the homozygosity of the original *pph-1* T-DNA in these lines (**Table 15**). To further confirm the homozygosity of the 35S:*Hv*PPH construct, kanamycin resistant tests were carried out in the T3 generation. This led to the selection of one transformant (# 7) that was used for complementation tests in the T2 generation. Upon dark-induced senescence, *pph-1*/35S:*Hv*PPH plants degraded chlorophyll like the wild-type. Thus, the stay-green phenotype was complemented.

In addition, HPLC analysis showed no accumulation of Phein *a* in the complementing line when compared to *pph-1* (**Figure 22B and 22C**). Therefore, stay-green phenotype was complemented in *pph-1*/35S:*Hv*PPH plants indicating that PPH plays the same role in Chl degradation in barley and in *Arabidopsis*.

Table 15: Table showing the overview of genotyping data used for confirmation of *pph-1* and transgene.

Primers	**Col-0**	***pph-1***	***pph-1*/35S:*Hv*PPH lines**			
			# 2	**# 3**	**# 6**	**# 7**
LP/RP (95)	+	Faint	Faint	Faint	Faint	Faint
LBb 3.1/ RP	-	+	+	+	+	+
***Hv*PPH**	-	-	+	Faint	+	+

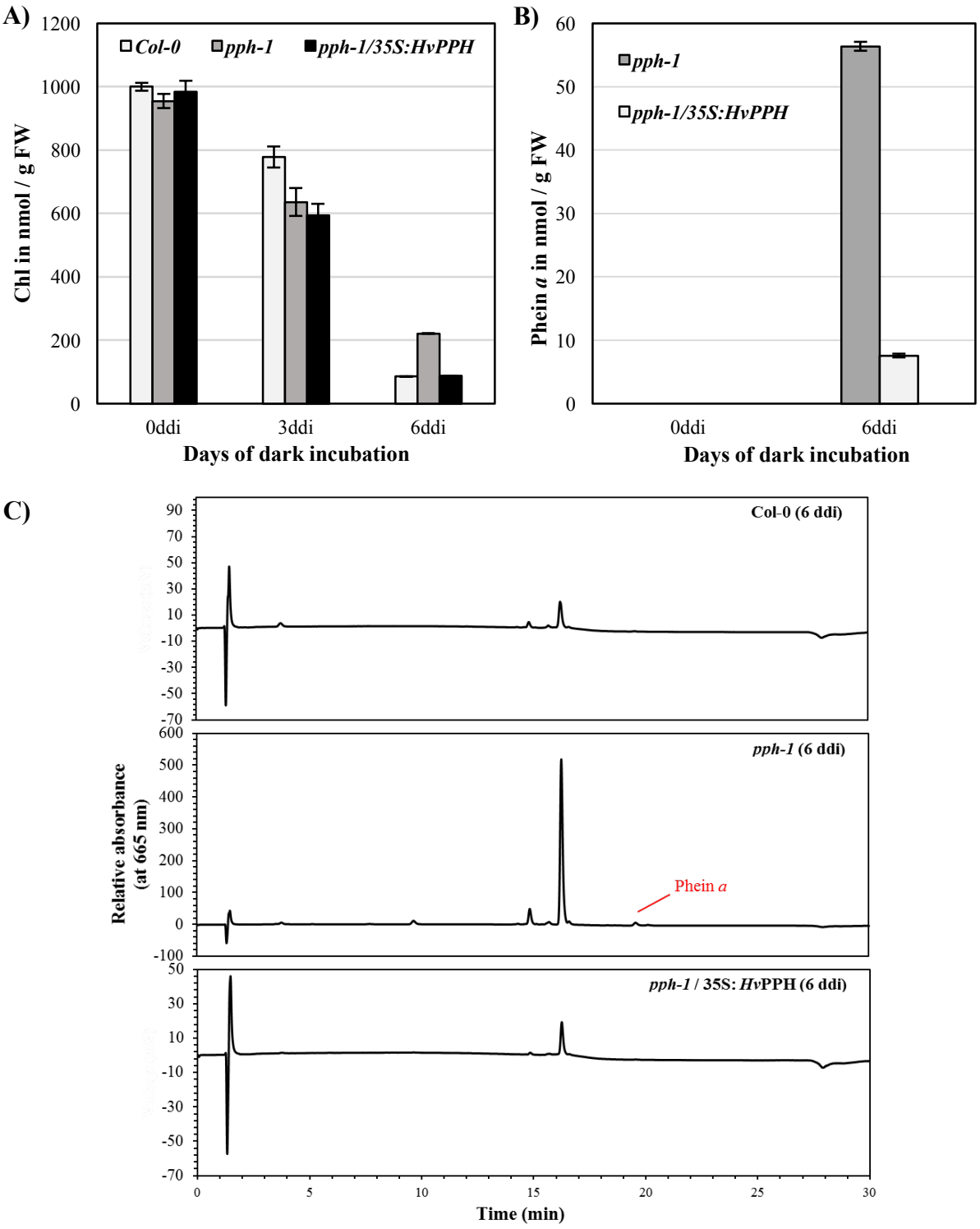

Figure 22: Complementation of the stay-green phenotype of *pph-1* with a 35S:*Hv*PPH cDNA construct. **A)** The graph shows gradual decrease in the amount of chlorophyll in Col-0 (positive control) and *pph-1*/35S:*Hv*PPH plants after 6 days of dark-induced senescence whereas *pph-1* (negative control) displayed comparatively higher chlorophyll content. **B)** The graph shows a considerable amount of Phein *a* accumulated in *pph-1* mutant plants whereas the complemented plants showed much less amounts of Phein *a* after 6 days of dark incubation. **C)** The chromatogram shows a prominent Phein *a* peak only in *pph-1* mutant. It was a clear indication that in the complemented lines, *Hv*PPH could complement the absence of *At*PPH and lead to senescence progression.

4. Abundance of phyllobilins in grasses

4.1. Abundance of phyllobilins in modern grass varieties

It was shown for *Arabidopsis* that the abundance of phyllobilins that accumulate in senescent leaves roughly matches the amount of degraded chlorophyll (Christ et al., 2013). To investigate this in grasses, we used LC-MS (Christ et al., 2016) for phyllobilin quantification and correlated the obtained amounts to the Chl values determined spectrophotometrically from the same plant material.

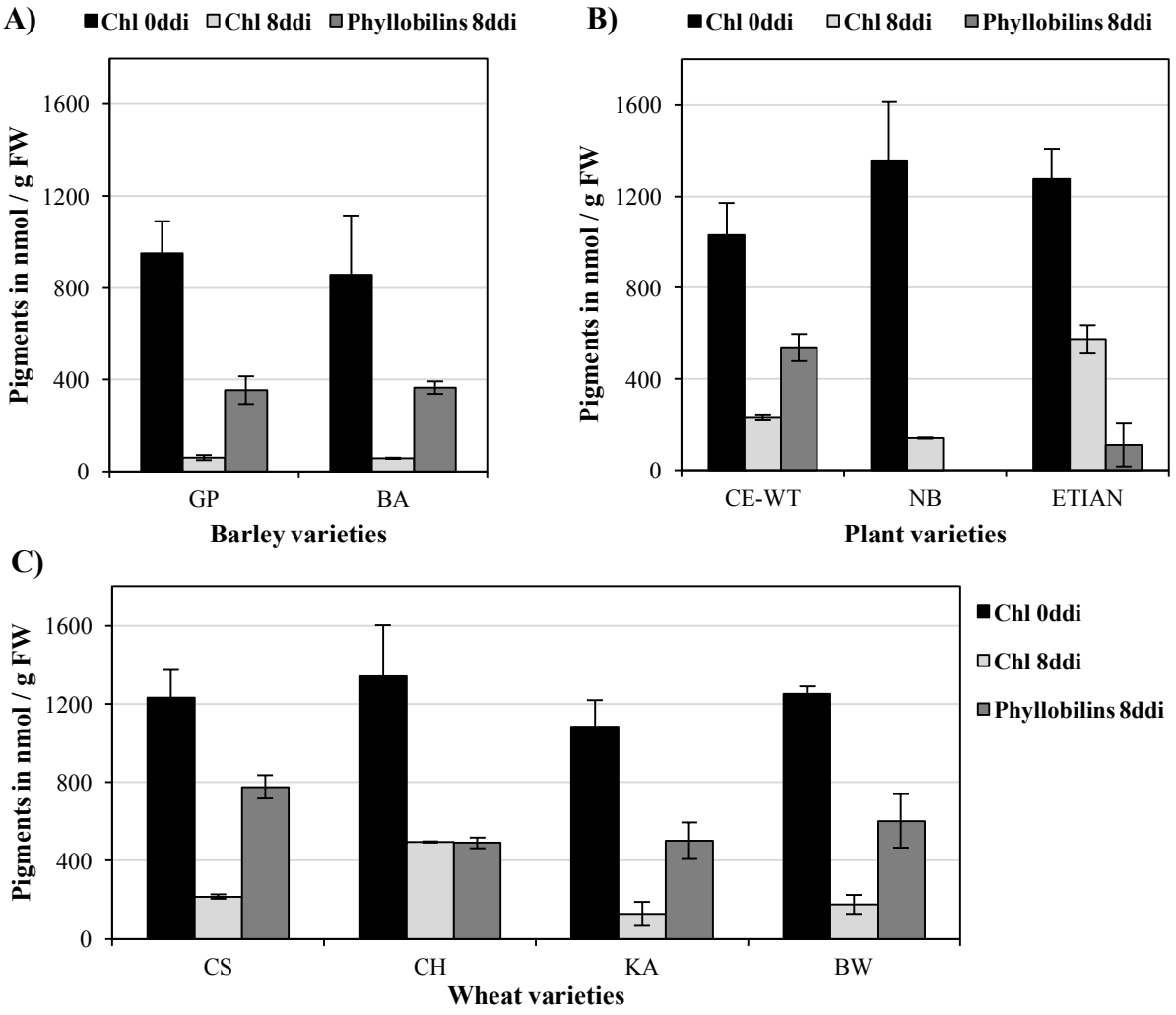

Figure 23: Chl and phyllobilin quantification in different modern grass varieties. The graph shows the amounts of phyllobilins produced and Chl degraded in the primary leaves of various varieties of: **A)** wheat – Chinese Spring (CS), Chancellor (CH), Kanzler (KA) and Bobwhite (BW); **B)** barley – Baraka (BA) and Golden Promise (GP); and **C)** ryegrass – Ceres wild-type (CE), rice – Nippon Bare (NB) and sorghum – E-Tian (ET), after 8 days of dark-induced senescence (8ddi). No phyllobilins were detected at the beginning of the incubation (0ddi). Data are mean ± s.d. of three biological replicates.

Chl and phyllobilins were quantified in a number of modern, cultivated varieties of various species, i.e. barley, wheat, ryegrass, rice and sorghum, under artificially induced senescence conditions. After 8 days of dark incubation, every tested species showed a significant decrease in the chlorophyll content as indicated in **Figure 23**. Except for rice, where only traces of a few phyllobilins were detected (see **Table 12**) phyllobilin quantity increased during senescence. However, the increase was not proportional to the magnitude of Chl breakdown. Taking into consideration all the varieties of a given species, Chl to phyllobilins conversion ratios were approximately 42% in barley, 60% in wheat, 67% in ryegrass, 15% in sorghum and less than 1% in rice.

The analyses discussed above came from greenhouse plant samples grown under artificially induced senescence. In order to correlate the obtained data of barley (**Figure 23B**) with natural conditions, plant material was collected from barley var. Golden Promise (GP) grown in the field. The field samples were selected based on leaf coloration and were grouped into three distinct stages of senescence: early (green), mid (pale-green) and late (yellow). A significant decrease in the chlorophyll content was evident during the late phase as shown in **Figure 24**. However, despite the obvious drop in Chl content, no phyllobilins were detected by HPLC and UV/Vis spectroscopic analyses.

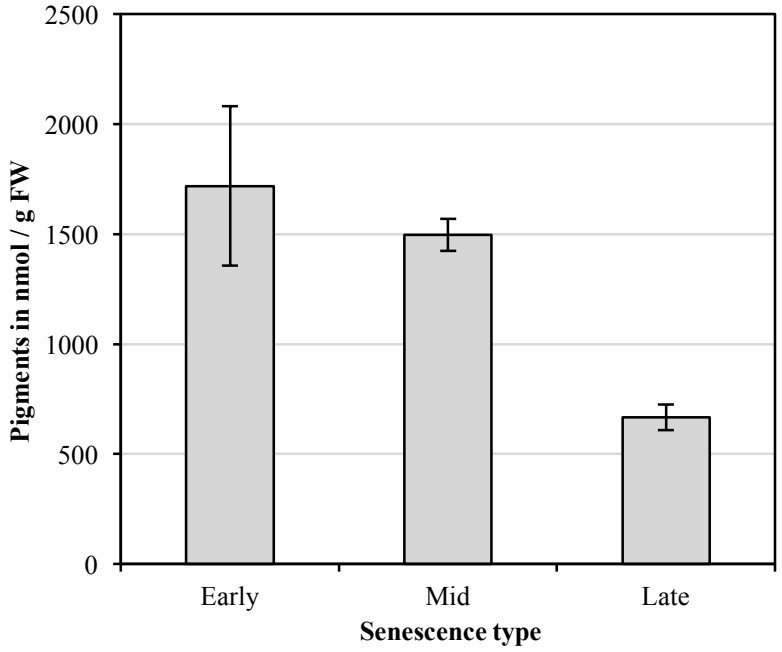

Figure 24: Chl quantification in field-grown barley. The graph shows the amount of Chl present in the primary leaves of field-grown barley var. Golden Promise (GP) at different stages of natural senescence. Data are mean ± s.d. of three biological replicates.

4.2. Abundance of phyllobilins in ancestral varieties

Chl and phyllobilin quantification was also performed in ancestral varieties of barley and wheat. After inducing senescence by incubating the plants in dark for 8 days, varieties of both species showed a significant decrease in the chlorophyll content (**Figure 25A** and **25B).** Like in the modern varieties, an increase in phyllobilin quantity was also observed at the end of the experimental period for the ancestral varieties, which again was disproportional to the magnitude of Chl breakdown (**Figure 25C**).

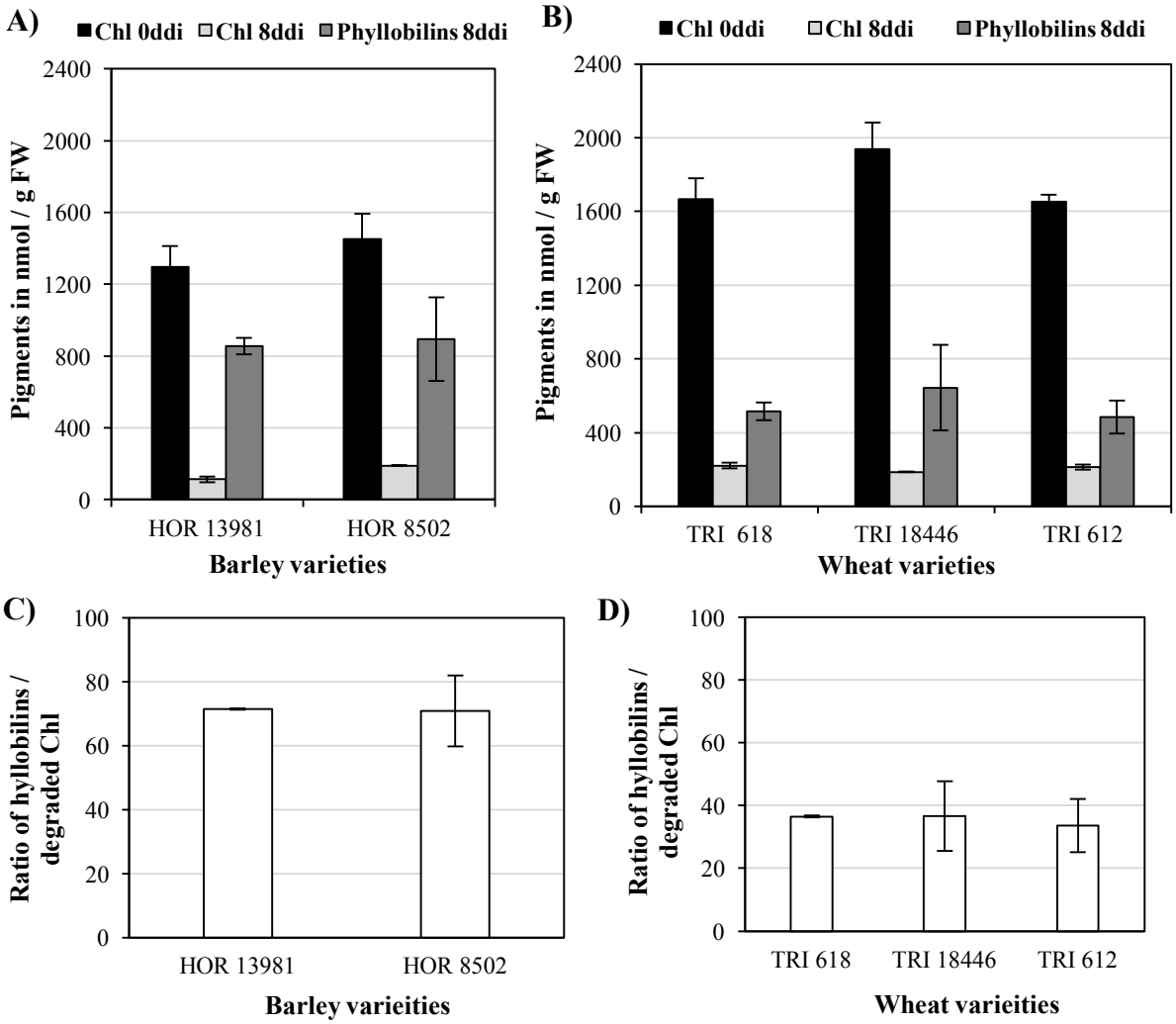

Figure 25: Chl and phyllobilin quantification in different ancestral varieties. The graph shows the amount of phyllobilins produced and Chl degraded in the primary leaves of various ancestral varieties of: **A)** barley (HOR 13981 and 8502) and **B)** wheat (TRI 618, 18446 and 612), after 8 days of dark-induced senescence. No phyllobilins were detected at the beginning of incubation (0ddi). Data are mean ± s.d. of three biological replicates. Ratio of formed phyllobilins to amounts of degraded Chl in primary leaves of various varieties of: **C)** barley (HOR 13981 and 8502) and **D)** wheat (TRI 618, 18446 and 612) after 8 days of dark-induced senescence are also shown. Data are mean ± s.d. of triplicates.

DISCUSSION AND OUTLOOK

The central focus of my PhD thesis was the investigation of the chlorophyll degradation pathway in grasses which include economically valuable crop plants like rice, wheat, barley, sorghum and ryegrass. The phenotypic loss of chlorophyll is an integral aspect of leaf senescence, which in addition is characterized by the breakdown and remobilization of chloroplast components to vegetative parts and sink organs like seeds (i.e. grains in crops). Thus, studying monocarpic senescence in crop plants is crucial as modulating senescence processes may enhance crop yield. Its known that in *Arabidopsis* chlorophyll is broken down via the PAO/phyllobilin pathway leading to the formation of phyllobilins that are finally stored in the vacuole (Hörtensteiner, 2013). Based on this information, I began my investigations with two main questions: i) is chlorophyll broken down through the same known pathway in grasses? and ii) what is the phyllobilin profile in grasses?

To answer the first query, experiments were performed mostly in barley. The early phase of the PAO/phyllobilin pathway comprises of CCEs which are known to be highly conserved among higher plant species, including barley and rice as evident from my sequence homology search that resulted in the identification for both grass species of sequence homologs of CCEs including NYC1, NOL, PPH, PAO and SGR. Previous studies in *Arabidopsis* have shown that NYC1 and PAO are located in thylakoid membranes, while SGR, NOL and PPH localize in the stroma. Although I have not studied the sub-chloroplast localization of the *Hv*CCEs in detail, I found that all *Hv*CCEs are localized in the chloroplast as well. Previous studies have shown that rice NYC1 and NOL localize in the chloroplast and encode chlorophyll *b* reductases. The *nyc1* and *nol* mutants show a stay-green phenotype by inhibiting Chl *b* degradation and thereby retaining light-harvesting complex during senescence. In addition to this, the rice NYC1 and NOL were shown to act together as a protein complex (Kusaba et al., 2007; Sato et al., 2009). Similar stay-green phenotypes have been observed in *Arabidopsis* or rice mutants that are impaired in PPH (Morita et al., 2009; Schelbert et al., 2009). In contrast to it, *pao* mutants in different plant species show cell death phenotypes due to Pheide *a* accumulation (Pruzinská et al., 2003; Tang et al., 2011) . These mutants act as tools to understand the underlying molecular mechanism of the PAO/phyllobilin pathway. I have exploited such mutants to investigate the functionality of the identified *Hv*PPH and *Hv*PAO

genes. Indeed, both barley genes were able to complement respective *Arabidopsis pph1* and *pao1* mutants. This confirmed that the identified genes are the orthologs of pheophytinase and pheophorbide *a* oxygenase in barley. In addition to this I could also show that wild-type barley leaves accumulate Pheide *a*, the substrate of PAO, when treated with 2,2'-bipyridyl, which validates the need of PAO to degrade chlorophyll via the known PAO/phyllobilin pathway in barley. This confirms previous studies in rice, where *acd1*/*pao* silencing lines have been shown to accumulate the photo-reactive intermediate leading to a leaf-death phenotype (Tang et al., 2011). Furthermore, I could confirm the transcriptional upregulation of the genes encoding *Hv*CCEs during dark-induced senescence similar as observed earlier in rice and *Arabidopsis* (Hörtensteiner, 2013). All these findings suggest that chlorophyll is commonly degraded via the PAO/phyllobilin pathway in grasses as well and that the CCEs are indeed sequentially and functionally similar across dicots and monocots. In the future, RNA interference knockdown of *Hv*PAO could be performed in order to obtain additional *in vivo* confirmation of the involvement of the PAO/phyllobilin pathway as the sole mechanism of chlorophyll degradation. The strategy would be an improvement over my current transient study using 2,2'-bipyridyl which also blocks many other biochemical pathways due to its rather non-specific chelation activity of metals required by various enzymes (Hörtensteiner et al., 1995; Fang and Kao, 2001).

Apart from mutations in NYC and PPH, mutations in SGR, which helps to recruit all the CCEs to the thylakoid membrane (Sakuraba et al., 2012), also produce the cosmetic stay-green phenotype. SGR-deficient stay-green mutants have already been documented in various plants like *Arabidopsis*, bell pepper, soybean, tomato, meadow fescue, pea and rice, and were supposed to be present in other cereals like wheat and sorghum (Hörtensteiner, 2009). However, a barley SGR mutant has not been identified so far. The employment of functional stay-green phenotypes in crop species has often been associated with improved yield and is highly desirable because this trait enables plants to postpone the onset of senescence by retaining their photosynthetic rate, even under stress conditions. This is expected to give additional yield to the crop plants (Bell et al., 2015; Johnson et al., 2015; Luche and Oliveira, 2015). In case of sorghum, maize and soybean, yields have been shown to be positively correlated to the stay-green trait. However, in wheat, it is associated with an increase in leaf area, duration of grain filling and photosynthetic competence (better protection of photosynthetic apparatus, maintenance of PS II and controlled content of ROS) (Fu et al., 2009; Reynolds-Henne et al., 2010). The stay-green trait also aids plants such as sorghum, pearl millet

and maize to be heat-tolerant by its ability to maintain lower canopy temperatures (due to the green color) under high atmospheric temperatures. In addition to these benefits, the stay-green trait is also associated with reduction of lodging in crops and production of more fertile tillers (Spano et al., 2003; Jiang et al., 2007; Rong et al., 2013; Luche and Oliveira, 2015). Due to its numerous benefits, producing stay-green barley lines based on the *Hv*SGR identified in this study would be a highly desirable objective.

The PAO/phyllobilin pathway is the key mechanistic pathway through which degradation of chlorophyll is carried out by plants as elucidated in the dicot model *Arabidopsis* (Süssenbacher et al., 2015). In *Arabidopsis*, 90% of the total phyllobilins are comprised of DNCCs while NCCs account for only 10% (Christ et al., 2013). These phyllobilins have been discovered to be formed through various side chain modifications of *p*FCCs and ultimate transport to vacuoles. Therefore, various plant species accumulate phyllobilins differently based on their respective side chain modifications. Among grasses, for instance, the modern and ancestral varieties of barley have slightly more DNCCs than NCCs whereas in modern and ancestral varieties of wheat, NCCs are more prevalent than DNCCs. A striking difference exists between ryegrass and sorghum where DNCCs are predominant in the former whereas the latter favors the formation of NCCs. From recent studies, it is known that in *Arabidopsis*, DNCCs are formed by oxidative deformylation of C1 by CYP89A9, a cytochrome P450 monooxygenase. This reaction is carried out prior to demethylation of the C8^2-carboxymethyl group by MES16 occurring basically in 100% of all phyllobilins (Christ et al., 2012; Christ et al., 2013). Taking this into consideration, it looks as if the process of oxidative deformylation is more active in ryegrass and barley compared to wheat and sorghum while grasses do not contain an enzyme (no MES16 homology) responsible for demethylation, because all phyllobilins identified in this study carry an intact C8^2-carboxymethyl group. Strikingly, however, also a clear CYP89-homologs is not present in barley. Likely, deformylation is not carried out by another cytochrome P450 enzyme because no difference in DNCC or NCC amounts was found after exposure to CO, a potent inhibitor of CYPs. In contrast to barley, CO inhibition experiments in *Arabidopsis* show a change in relative amounts of DNCCs and NCCs when exposed to CO (**Figure 11 A**) (Christ et al., 2013). Thus, the nature of enzymes responsible for DNCC and NCC formation in grasses remains unknown and provides a very intriguing topic to investigate in the future in light of the evolution of Chl breakdown to better understand species-specific phyllobilin formation.

Among the DNCCs identified, DNCC_666 (*Hv*-UCC-1) was most commonly found and was present in all varieties of grass species studied here. Another recently characterized DNCC of *Arabidopsis,* DNCC_632_3 (also named *At-mes16*-DNCC-38), was detected in barley, wheat and ryegrass but was absent in sorghum and rice. Two of the four DNCCs newly identified in this study, i.e. DNCC_794 and DNCC_880, were only present in ryegrass. Together with the fact that the only NCC found in ryegrass, NCC_892, has a C18-vinyl group, this points to a rather weak C18-dihydroxylation activity to be present in this species. I could show that dihydroxylation involves incorporation of molecular oxygen however the molecular nature of the activity remains elusive. CO treatment did not change the proportion of dihydroxylated phyllobilins (data not shown), questioning the involvement of CYP enzyme.

The first ever characterized NCC, i.e. NCC_678 (*Hv*-NCC-1), was found in all the grasses except in ryegrass. Ryegrass possessed only NCC_892 (*Nr*-NCC-1) which was also identified in barley and wheat. NCC_644 (*Cj*-NCC-1) was detected only in wheat. Like sorghum, rice was observed to contain NCC_806 (*Nr*-NCC-2) along with NCC_678. However, sorghum also contained two newly identified NCCs, namely NCC_840 and 926, which were also abundant in barley and wheat. An additional NCC_662 was also found in barley and wheat.

In light of the fact that phyllobilins exist in diverse forms with subtle changes in chemical structures, it is obvious to ask the question about the purpose they serve in plants undergoing senescence. Until date, no physiological significance of Chl catabolites has been elucidated. It seems fairly possible that the existence of different structural variants of NCCs and DNCCs is a direct consequence of the diversity in geographic and climatic conditions that favor the growth and yield of the crop plants researched in this study. For example, (see Table 6), while a tropical climate with temperatures ranging from 24°C to 28°C, high rainfall (100 cm to 200 cm) and over 70% humidity are ideal for rice growth, barley and wheat are more adapted to temperate conditions such as 16°C to 22°C temperature, lower rainfall (50 cm to 100 cm) with cold moisture rich climate during cultivation and hot dryer climate during harvest. In case of ryegrass, significantly lower light intensity (~ 60-120 mol photons $m^{-2}s^{-1}$) favors growth when compared to other crops while sorghum requires lower humidity. Upon comparison of the growth conditions of various crops, one can deduce that the enzymes present in these plants have evolved to function optimally under specific temperature and pH ranges. Because of this reason, certain enzymes may operate at higher efficiency in some plants, while their counterparts fail to display similar level of activity in the biochemical pathways of other

species. The same may hold true for the enzymes that participate in the PAO/phyllobilin pathway of chlorophyll breakdown. This observation, albeit fail to verify evidentially, definitely hints towards the existence of various structural variants of phyllobilins in different crops undergoing senescence.

Onset and duration of various stages of senescence in crop plants have critical importance in determining their susceptibility to pests and insects. While most cereals are at risk of direct feeding damage from grain aphids, some, such as winter barley, are known to be less affected due to the occurrence of early senescence in these species (Ellis et al., 2010). Some crops suffer greater injury from infestation due to lower reserves of soluble stem carbohydrates. The chlorophyll catabolites that are glucosylated and/or malonylated at the $C3^2$ position indicate that these forms of phyllobilins are possibly prevalent in plants with higher levels of soluble carbohydrates in leaves (or stem) and therefore at lower risk of incurring damages associated with diseases and drought. If this notion is proven true, then the existence of non-glycosylated forms of DNCCs and NCCs in crops can serve as a marker for their propensity to develop pest-inflicted diseases. Knowledge of such predisposition can help researchers develop disease-resistant crops by manipulation of genes involved in carbohydrate metabolism as well as Chl breakdown pathways.

From the results presented here, it is evident that in contrast to *Arabidopsis* the total amounts of phyllobilins produced during dark-induced senescence do not correlate with the total amounts of chlorophyll degraded in the various species of crop plants. This was most obvious in sorghum and rice, but also seen in naturally senescing barley samples. At the same time, and as discussed above, the core PAO/phyllobilin pathway is active in barley and rice, as seen from the fact that all investigated varieties accumulated phyllobilins. Thus, the question remains whether there is an additional, PAO-independent, pathway of Chl breakdown, that is differently active in different species, or whether phyllobilins are further degraded, for example, to monopyrrolic products, and thus escape their identification in the analytical set up. To address this, experiments were designed to track isotope-labeled chlorophyll and its catabolites through various biosynthetic and degradative phases (**Figure 26**). For this purpose, ^{13}C-labeling of Chl was to be performed using C4 labeled 4-aminolevulinic acid (ALA). Synthesized from glutamate via a three-step reaction, ALA is the universal and sole building block of the porphyrin/chlorin ring of chlorophyll, heme (and phytochromobilin) and siroheme. The branching of the biosynthetic pathway for the production of the first two tetrapyrrole

species is directly preceded by conversion of ALA to protoporphyrin IX (Kannangara and Schouboe, 1985; Rissler et al., 2002).

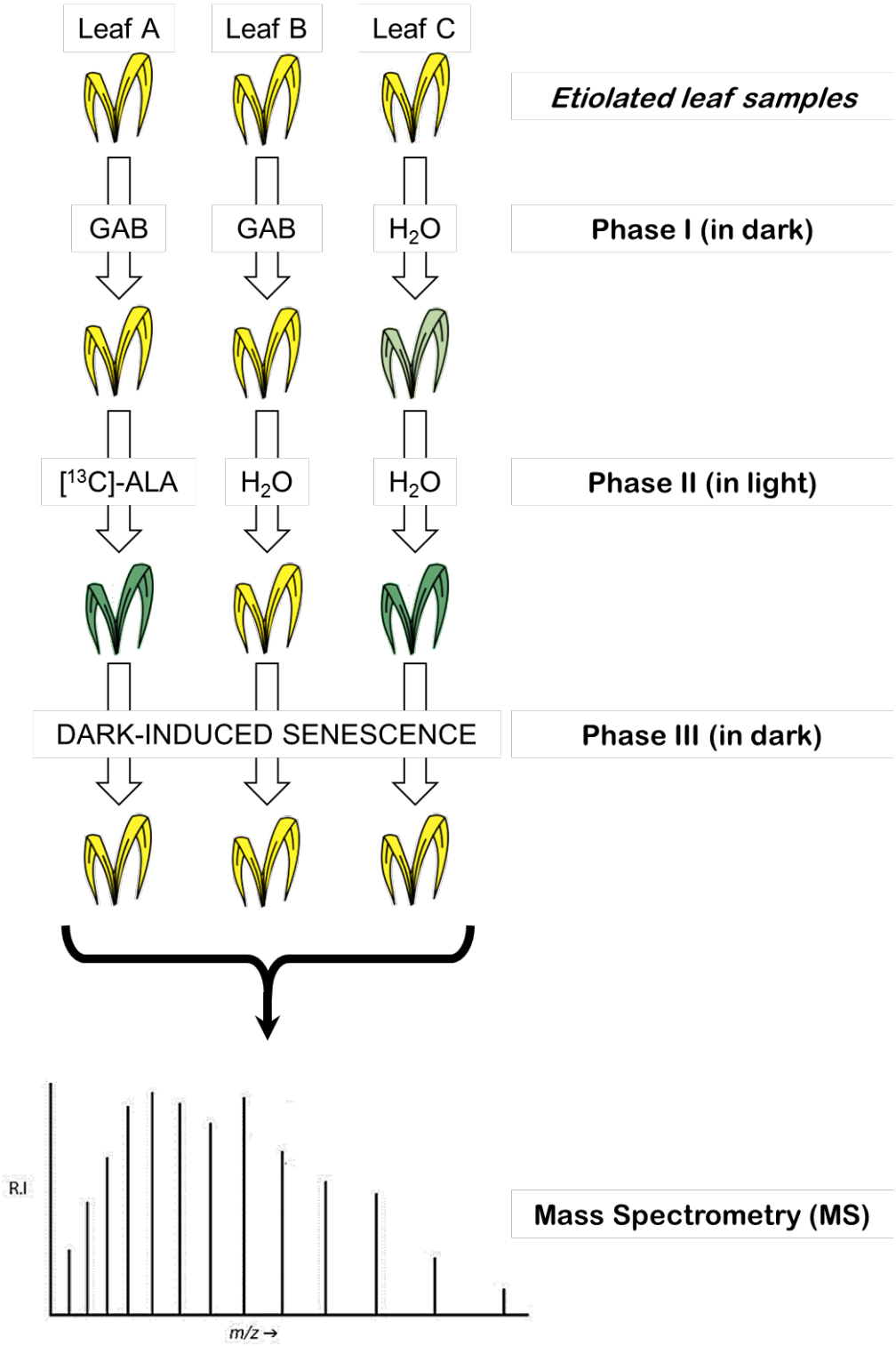

Figure 26: Isotope labelling assay. Schematic representation of an experiment of isotope-based tracking of chlorophyll and its catabolites in etiolated leaf samples incubated with 4-[^{13}C]-ALA with endogenous ALA synthesis inhibition by gabaculine (GAB).

In the isotope-labeling study, etiolated leaf samples (**Figure 26A–C**) are subjected to three different treatments. During the first phase, leaves A and B are treated with gabaculine (GAB), a specific inhibitor of endogenous ALA synthesis, while sample C is incubated in water as a control. GAB-treated leaves are expected to have no endogenous levels of ALA while normal ALA production is expected in the control leaf. During the second phase in the light, samples A are incubated in the presence of 4-[^{13}C]-ALA while leaves B and C are incubated in water. Thus, it is expected that samples A synthesize isotope-labeled chlorophyll. Same color change can be expected in control, while samples C produce unlabeled Chl and samples B remain pale. The third phase of the experiment involves artificial induction of senescence of all three samples with the expectation of yellowing of leaves A and C due to chlorophyll breakdown during senescence. Subsequently, LC-MS analysis of Chl breakdown products in the leaves obtained from the isotope-labeling experiment will allow identification of ^{13}C-labeled masses that can be attributed to Chl catabolites and aid in the identification of novel phyllobilins in various crop plants, including tetra- as well as speculated monopyrrolic end products.

Although the experiment explained above was designed as an isotope-labeling assay, preliminary tests were executed with barley and rice using non-labeled ALA to test whether the system is principally working. However, the findings from these studies were too inconclusive (data not shown) and further effort is therefore required in the future to elucidate the ultimate fate of Chl in grasses in particular in those species that accumulate only trace amounts of phyllobilins such as rice.

MANUSCRIPT 1

A novel role for TIC55 as a hydroxylase of phyllobilins, the products of chlorophyll breakdown during plant senescence.

Mareike Hauenstein, Bastien Christ[1], Aditi Das, Sylvain Aubry and Stefan Hörtensteiner[2]

Institute of Plant Biology, University of Zurich, Zollikerstrasse 107, CH-8008 Zurich, Switzerland; and

[1]Present address: Whitehead Institute, Massachusetts Institute of Technology, Cambridge, MA 02139-4307

[2]Address correspondence to shorten@botinst.uzh.ch

Submitted to The Plant Cell

A novel role for TIC55 as a hydroxylase of phyllobilins, the products of chlorophyll breakdown during plant senescence.

Mareike Hauenstein, Bastien Christ[1], Aditi Das, Sylvain Aubry and Stefan Hörtensteiner[2]

Institute of Plant Biology, University of Zurich, Zollikerstrasse 107, CH-8008 Zurich, Switzerland; and

[1]Present address: Whitehead Institute, Massachusetts Institute of Technology, Cambridge, MA 02139-4307

[2]Address correspondence to shorten@botinst.uzh.ch

Running title: TIC55 involved in chlorophyll breakdown

The author responsible for distribution of materials integral to the findings presented in this article in accordance with the policy described in the Instructions for Authors (www.plantcell.org) is: Stefan Hörtensteiner (shorten@botinst.uzh.ch)

Estimated manuscript length: ?? pages

Synopsis:

This work identifies TIC55, a Rieske-type oxygenase previously described as component of the chloroplast protein import machinery, as chlorophyll catabolite hydroxylase. The site-specific hydroxylation catalyzed by TIC55 is a prerequisite for subsequent catabolite glucosylation in *Arabidopsis*. Our findings identify the molecular basis of an important reaction during chlorophyll breakdown, which ubiquitously occurs in higher plants.

ABSTRACT

Chlorophyll degradation is the most obvious hallmark of leaf senescence. Phyllobilins, linear tetrapyrroles that are derived from opening of the chlorin macrocycle by the Rieske-type oxygenase PHEOPHORBIDE *a* OXYGENASE (PAO), are the end products of chlorophyll degradation. Phyllobilins carry defined modifications at several peripheral positions within the tetrapyrrole backbone. While most of these modifications are species-specific, hydroxylation at the $C3^2$ position is commonly found in all species analyzed to date. We demonstrate this hydroxylation to occur in senescent chloroplasts of *Arabidopsis thaliana.* Using bell pepper chromoplasts, we establish phyllobilin hydroxylation to be catalyzed by a membrane-bound, molecular oxygen- and ferredoxin-dependent activity. As these features resemble the requirements of PAO, we considered membrane-bound Rieske-type oxygenases as potential candidates. Analysis of mutants of the two Rieske-type oxygenases that besides PAO exist in Arabidopsis, uncovered that phyllobilin hydroxylation depends on TRANSLOCON AT THE INNER CHLOROPLAST ENVELOPE 55 (TIC55). Our work demonstrates a first catalytic activity for TIC55, which in the past has been considered as a redox sensor of protein import into plastids. Given the wide evolutionary distribution of both PAO and TIC55, we consider that chlorophyll degradation likely appeared with the evolution of land plants.

INTRODUCTION

Chlorophyll is the main pigment of the photosynthetic apparatus of plants and is responsible for the absorption of the energy of sunlight. In the process of photosynthesis, this energy is converted to chemical energy used for carbon fixation. During leaf senescence, however, when the photosynthetic machinery is dismantled in order to retrieve nutrients, in particular nitrogen, to sink organs such as seeds (Hörtensteiner and Feller, 2002), the photodynamic properties of chlorophyll become potentially cell toxic. As a consequence, the pigment is detoxified to uncolored and photodynamically inactive products that are termed phyllobilins (Kräutler, 2014). Chlorophyll degradation to phyllobilins is catalyzed by a multistep process, named "PAO/phyllobilin" pathway (Hörtensteiner and Kräutler, 2011; Kräutler and Hörtensteiner, 2014), to acknowledge PAO (pheophorbide *a* oxygenase), a Rieske-type oxygenase that is the key component of this pathway (Pružinská et al., 2003). PAO, in concert with red chlorophyll catabolite reductase (RCCR), catalyzes the ring opening reaction of pheophorbide *a*, the phytol- and Mg-free intermediate of the early part of chlorophyll breakdown, to a *primary* fluorescent chlorophyll catabolite (*p*FCC) that is the precursor of all subsequently formed phyllobilins. The direct product of the PAO reaction, red chlorophyll catabolite (RCC), does not accumulate, but is immediately reduced at the C15/C16-double bond by RCCR in an intriguing stereospecific manner (Wüthrich et al., 2000; Pružinská et al., 2007) (for atom and pyrrole numbering of phyllobilins, see the structure of pFCC in Figure 1B) . Thus, depending on the source of the enzyme, two C16-stereoisomers, *p*FCC or *epi-p*FCC, may occur (Mühlecker et al., 1997; Mühlecker et al., 2000). For example, the RCCR of *Arabidopsis thaliana* (*Arabidopsis*) (*At*-RCCR) produces *p*FCC, while in *Capsicum annuum* (bell pepper) or *Solanum lycopersicum* (tomato) *epi-p*FCC is formed (Hörtensteiner et al., 2000). It was shown *in vitro* that the stereospecificity of *Arabidopsis* RCCR is defined by a single amino acid residue, Phe_{219}, which when mutated to Val changes the specificity (Pružinská et al., 2007). Likewise, complementation of the *accelerated cell death2* (*acd2*) mutant of Arabidopsis that is deficient in RCCR with an RCCR version 'X', where six amino acids of the wildtype sequence including Phe_{219} were replaced by the respective residues of the tomato RCCR (*acd2-2+At*-RCCR-X), caused the exclusive accumulation during senescence of C16-isomerized phyllobilins (Pružinská et al., 2007).

Phyllobilins are categorized into two types (Kräutler, 2014): (C1-) formyl-(C19-) oxobilins, also termed nonfluorescent chlorophyll catabolites (NCCs), are the ultimate products of PAO

activity, while the activity of a cytochrome P450 monooxygenase, as shown for *Arabidopsis* (Christ et al., 2013), gives rise to (C1,19-) dioxobilins, also named dioxobilin-type nonfluorescent chlorophyll catabolites (DNCCs). NCCs and DNCCs are found in the vacuoles of senescent cells (Matile et al., 1988; Christ et al., 2012) and have been shown to be derived from respective fluorescent precursors (FCCs and DFCCs) as the result of non-enzymatic isomerization inside the acidic vacuolar sap (Oberhuber et al., 2003; Christ et al., 2013). Since the first identification of an NCC in senescent leaves of *Hordeum vulgare* (barley) in 1991 (Kräutler et al., 1991), phyllobilins were found in senescent leaves from more than 20 different angiosperm species (Kräutler, 2016), but are also formed during fruit ripening (Müller et al., 2007; Moser et al., 2009). Although the principle linear tetrapyrrole backbone of all phyllobilins is identical, they exhibit rather great structural diversity among the investigated species. Thus, for example, 90% of the phyllobilins that accumulate in senescent *Arabidopsis* leaves are DNCCs (Christ et al., 2013), while *Cercidiphyllum japonicum* exclusively produces NCCs (Oberhuber et al., 2003). Furthermore, some species, like *Arabidopsis*, accumulate an array of up to eight different phyllobilins simultaneously (Christ et al., 2016), while others, like *C. japonicum*, produce only two (Oberhuber et al., 2003). The molecular basis for these differences are enzyme activities that modify *p*FCC in a species-specific manner at different peripheral positions of the tetrapyrrole backbone structure. Best investigated in this respect is *Arabidopsis* where, besides CYP89A9, the already mentioned cytochrome P450 monooxygenase that is responsible for DNCC formation (Christ et al., 2013), methylesterase 16 (MES16) has been identified (Christ et al., 2012). This enzyme demethylates the $C8^2$ carboxymethyl ester present in chlorophyll with high efficiency. Again, other species, such as *C. japonicum*, exclusively produce phyllobilins that carry the intact carboxymethyl group, indicating that they lack a MES16 ortholog. Interestingly, these modifying reactions are localized in the cytosol (MES16) (Christ et al., 2012) and at the endoplasmic reticulum (CYP89A9) (Christ et al., 2013), while all enzymes identified to date that are required for the conversion of chlorophyll to *p*FCC are located within the plastid (Sakuraba et al., 2012). This led to the concept that reactions that commonly occur during chlorophyll breakdown take place in senescing chloroplasts, while species-specific modifications occur outside. Consequently, *p*FCC is believed to be exported from plastids, but the nature of *p*FCC transport at the plastid envelope is unknown (Christ and Hörtensteiner, 2014). An intriguing common modification of phyllobilins found in all species that have been analyzed so far is the specific hydroxylation at the $C3^2$ ethyl side chain (Christ and Hörtensteiner, 2014; Kräutler, 2014). This indicates that, distinct to other species-specific modifications, phyllobilin hydroxylation may be a

reaction commonly occurring in angiosperms and that the activity may be localized in the plastid.

The aim of this work was to identify the molecular nature of the hydroxylating activity. We could show that, indeed, senescent chloroplasts (gerontoplasts) contained both *p*FCC and hydroxylated *p*FCC (hydroxy-*p*FCC), indicating the respective activity to be a chloroplast protein. Using bell pepper chromoplasts as starting material, we successfully established an *in vitro* enzyme assay that allowed us to biochemically characterize the properties of the enzyme in question. Based on these analyses and on $^{18}O_2$ labeling and CO inhibition studies we could narrow down the number of likely candidates to two Rieske-type oxygenases: translocon at the inner chloroplast envelope55 (TIC55) and protochlorophyllide-dependent translocon at the inner chloroplast envelope52 (PTC52) that both have been thought to be implicated in chloroplast protein import. Analysis of respective T-DNA insertion mutants verified that *tic55* mutants are unable to produce hydroxylated phyllobilins, while in a *ptc52* mutant hydroxylation was unaffected. Thus, TIC55 is responsible for phyllobilin hydroxylation during chlorophyll breakdown. TIC55 orthologs are widely distributed in higher plants, but are phylogenetically distinct to PAO orthologs. This indicates that phyllobilin hydroxylation likely appeared with the evolution of land plants.

RESULTS

Hydroxy-*p*FCC is Present in Gerontoplasts of *Arabidopsis*.

The steps of chlorophyll to *p*FCC conversion have been shown to take place in gerontoplasts (Sakuraba et al., 2012). In agreement with this, fluorescent HPLC fractions corresponding to *p*FCC and to *epi*-*p*FCC have been identified in extracts of gerontoplasts of *Brassica napus* (oilseed rape) and barley (Schellenberg et al., 1993; Ginsburg et al., 1994; Moser and Matile, 1997). However, these early analyses indicated additional, more polar fluorescent fractions to be present in plastids. To investigate which, if any, chlorophyll catabolites are found in *Arabidopsis* plastids, isolated gerontoplasts were analyzed by liquid-chromatography (LC) – tandem mass spectrometry (MS/MS). Indeed, besides *p*FCC that produced a pseudomolecular ion of $[M+H]^+ = C_{35}H_{41}N_4O_7$ (m/z 629.2977) in positive ionization mode, we identified a second, more polar fraction with a mass of m/z 645.2929 ($[M+H]^+ = C_{35}H_{41}N_4O_8$), i.e. containing one additional oxygen atom (Figure 1A). In tandem MS experiments (Figure 1B

and C), both ions fragmented in an identical manner that earlier had been shown to be characteristic for *p*FCC fragmentation (Mühlecker et al., 1997; Mühlecker et al., 2000). Thus, pyrrole ring A (cleavage 'd' shown in Figure 1B and C) and/or the $C8^3$ methoxy group (cleavage 'a' shown in Figure 1B and C; loss as methanol) were lost with high efficiency, while pyrrole ring D was stable in both ions. To confirm this experimentally, we performed isomerization experiments using *epi*-*p*FCC that we produced from pheophorbide *a* in a well-established *in vitro* system using bell pepper chromoplasts (Christ et al., 2012). On reversed-phase HPLC, *epi*-*p*FCC has a longer retention time than *p*FCC (see Figure 2C) (Rodoni et al., 1997), but the fragmentation behavior in tandem MS experiments with a stable ring D was identical to the one of *p*FCC (Supplemental Figure 1A online). When incubating at pH 5, *epi*-*p*FCC isomerized to a more polar compound (Supplemental Figure 1B online), which when analyzed by tandem MS fragmented as a typical NCC, i.e. with high probability of ring D loss (Supplemental Figure 1A online), confirming the identity of the catabolites isolated from senescent *Arabidopsis* chloroplasts as FCCs, specifically as *p*FCC and hydroxy-*p*FCC, which solely differ by the attachment in the latter of an additional oxygen atom at ring A, likely at the $C3^2$ ethyl side chain.

To verify that hydroxy-*p*FCC was present – and thus also likely formed – inside the intact plastids and to exclude the possibility that the identified FCCs were derived from extraplastidial contaminations of our chloroplast preparations, we took advantage of the fact that MES16 demethylates FCCs (Christ et al., 2012). Thus, we incubated plastid preparations before and after mechanical rupture with MES16 and analyzed the formation of the respective demethylated forms of *p*FCC and hydroxy-*p*FCC by LC-MS/MS (Figure 1A). Only after chloroplast rupture, pseudomolecular ions ($[M+H]^+$) corresponding to desmethyl-*p*FCC (m/z 615.282; $C_{34}H_{39}N_4O_7$) and desmethyl-hydroxy-*p*FCC (m/z 631.277; $C_{34}H_{39}N_4O_8$) were produced, indicating that indeed, hydroxy-*p*FCC formation from *p*FCC takes place within intact senescent plastids.

***p*FCC Hydroxylation Localizes in Plastid Membranes and Requires Molecular Oxygen and Ferredoxin.**

The above-mentioned *in vitro* assay that uses bell pepper chromoplasts as the source of PAO and RCCR for the production of *epi*-*p*FCC from pheophorbide *a* yielded, as a by-product, a second, more polar, fluorescing fraction (Figure 2A) that exhibited a typical FCC absorption

spectrum (Supplemental Figure 2A), which we reckoned could be hydroxy-*epi*-*p*FCC, indicating that the chromoplast extracts used for *epi*-*p*FCC synthesis may also contain the activities required for catabolite hydroxylation. Indeed, in an identical assay, but using *epi*-*p*FCC instead of pheophorbide *a* as substrate, the polar FCC fraction increased in a time-dependent manner (Figure 2B). To confirm identity of this compound as hydroxy-*epi*-*p*FCC, we compared its retention time in HPLC with the retention times of the FCCs accumulating in gerontoplasts of Col-0 plants and of *acd-22*+*At*-RCCR-X plants (Pružinská et al., 2007) that were complemented with the *epi*-*p*FCC-producing 'X' version of *Arabidopsis* RCCR (see Introduction). Co-injection experiments indeed confirmed that the product of *in vitro* hydroxylation of *epi*-*p*FCC is identical to the polar FCC fraction from *acd2-2*+*At*-RCCR-X chloroplasts (Figure 2C). In addition, the product of *in vitro* hydroxylation was analyzed by LC-MS/MS (Supplemental Figure 2B and C), demonstrating it to be hydroxy-*epi*-*p*FCC with an identical mass and fragmentation pattern as shown for hydroxy-*p*FCC (Figure 1B).

The $C3^2$ hydroxylation reaction introduces one oxygen atom into respective phyllobilins. To analyze whether this oxygen was derived from molecular oxygen, we dark-incubated *Arabidopsis* wild-type leaves in the presence of $^{18}O_2$ and analyzed phyllobilin labelling by LC-MS. Several phyllobilins known to be $C3^2$ hydroxylated, such as DNCC_618 and NCC_630 (Christ et al., 2016) carried up to two labelled oxygen atoms, while only one ^{18}O-label was found in non-hydroxylated phyllobilins, such as DNCC_602 and NCC_614 (Figure 3). In all cases the labelled oxygen atoms were exclusively bound to pyrrole ring A. In the case of NCCs, one label was derived from PAO activity (Hörtensteiner et al., 1998), while CYP89A9 activity, ultimately leading to DNCCs, replaced the PAO-derived label by another labelled oxygen (Christ et al., 2013). This explained the presence of one ^{18}O-label in non-hydroxylated phyllobilins, implying that the second label that was present in hydroxylated ones was derived by the activity of the hydroxylase, which introduced the oxygen atom at $C3^2$ from molecular oxygen.

These data indicated that the hydroxylating activity could be a cytochrome P450 monooxygenase. Although most of these enzymes reside in the endoplasmic reticulum, the *Arabidopsis* genome encodes several P450 monooxygenases that likely are directed to the chloroplast (Schuler et al., 2006). P450 monooxygenases are highly sensitive to CO (Schuler, 1996), which we used in a mixture with 50% (v/v) ambient air to test for inhibition in the hydroxylation assay. However, CO did not inhibit hydroxy-*epi*-*p*FCC formation as compared to an atmosphere containing a 1:1 (v/v) mixture of ambient air and nitrogen gas, while

incubation in 100% nitrogen atmosphere largely inhibited the activity (Figure 4A). Thus, the responsible enzyme was unlikely a P450 monooxygenase.

The bell pepper chromoplast-based *in vitro* assay for *epi-p*FCC production from pheophorbide *a* was shown to require both chromoplast membranes, as the source of PAO, and a soluble chromoplast fraction, as the source of RCCR. To further dissect the requirements for *in vitro epi-p*FCC hydroxylation, we fractionated total chromoplasts into soluble and membrane fractions. After two washing steps using ultracentrifugation (UC), the activity remained in the membrane fraction, indicating that the responsible enzyme(s) are tightly associated with chloroplast membranes (Figure 4B). Similarly, the *in vitro epi-p*FCC hydroxylation assay was analyzed for the requirement for the additional cofactors present in the original PAO/RCCR assay, i.e. ferredoxin (Fd) and a Fd-reducing system, consisting of NADPH, Fd-NADPH oxidoreductase (FNR), glucose-6-phosphate (G-6-P) and G-6-P dehydrogenase (GDH). Using 2xUC washed membranes to reduce carry over of potential cofactors, respective assays for the production of hydroxy *epi-p*FCC demonstrated the requirement of both Fd and the Fd-regenerating system (Figure 4C). Some activity was obtained without the addition of Fd, which likely was caused by some residual Fd remaining attached to the chromoplast membranes during the washing procedure.

Phyllobilin Hydroxylation is catalyzed by TIC55, a Rieske-Type Monooxygenase.

Taking together, the properties for the *in vitro epi-p*FCC hydroxylating activity determined above, were similar to the requirements of PAO, a Rieske-type monooxygenase (Schellenberg et al., 1993; Hörtensteiner et al., 1995; Hörtensteiner et al., 1998), i.e. activity was attached to plastid membranes, was dependent on Fd, was not inhibited by CO, and the incorporated oxygen atom was derived from molecular oxygen. The *Arabidopsis* genome encodes five Rieske-type oxygenases (Gray et al., 2004), all of which have been shown to localize to chloroplasts (Rathinasabapathi et al., 1997; Tanaka et al., 1998; Bartsch et al., 2008). In addition, three of them, PAO (At3g44880), TIC55 (At2g24820) and PTC52 (At4g25650) possess predicted C-terminally located transmembrane domains (Figure 5A) that likely anchor these proteins to plastid membranes, while the other two Rieske-type oxygenases in Arabidopsis, chlorophyll *a* oxygenase (At1g44446) and choline monooxygenase (CMO)-like (At4g29890) are predicted to be soluble proteins (Tusnády and Simon, 2001). TIC55 and PTC52 have, respectively, been considered to be involved in protein import into the chloroplast (Küchler et al., 2002) and to putatively catalyze protochlorophyllide *a* to protochlorophyllide

b oxidation during chlorophyll biosynthesis as a prerequisite for protochlorophyllide oxidoreductase import into the plastid (Reinbothe et al., 2004). Nevertheless, we considered both proteins as likely candidates for FCC hydroxylation. First, we re-analyzed their predicted localization in the envelope (Bartsch et al., 2008) by transiently expressing GFP fusion proteins in mesophyll protoplasts isolated from senescent *Arabidopsis* wild-type leaves (Figure 5B). Indeed, GFP signals for both TIC55 and PTC52 surrounded the chloroplasts, i.e. indicating envelope localization like the envelope positive control, TIC110, while PAO co-localized with chlorophyll autofluorescence, i.e. confirming thylakoid localization (Sakuraba et al., 2012).

To investigate whether one (or both) of these candidates catalyze FCC hydroxylation *in vivo*, we analyzed respective T-DNA insertion lines for both genes. None of the lines showed growth differences compared to wild-type nor a visible phenotype during senescence. However, LC-MS analysis of senescent leaf extracts uncovered major phyllobilin differences between the three analyzed *tic55* alleles and *ptc52*, which looked like wild-type (Supplemental Figure 3 online). Although the relative abundance of DNCCs and NCCs was unaltered in all investigated lines (Figure 6A), two of the three *tic55* mutants, *tic55-2* and *tic55-3*, lacked hydroxylated phyllobilins (Figure 6B). *tic55-1* had a largely reduced proportion of hydroxylated phyllobilins, implying some residual activity to be present in this allele. By contrast, *ptc52* was comparable to Col-0 with about 60% of all phyllobilins being hydroxylated. As expected and because phyllobilin glucosylation depends on prior $C3^2$ hydroxylation, glucosylated phyllobilins were absent from *tic55* mutants (Figure 6C). These results demonstrated that phyllobilin hydroxylation is catalyzed by TIC55, but not by PTC52. To our surprise, *tic55* mutants accumulated a smaller proportion of $O8^4$ demethylated phyllobilins (Figure 6D), indicating that MES16, catalyzing demethylation in *Arabidopsis* (Christ et al., 2012), might preferentially accept hydroxylated catabolites as substrate. Furthermore, the proportion of hydroxymethylated phyllobilins was higher in *tic55* mutants (Figure 6E), which was in agreement with the suggestion that C2 or C4 hydroxymethylation and $C3^2$ hydroxylation exclude each other (Süssenbacher et al., 2015).

We additionally confirmed the absence of *p*FCC hydroxylation in *tic55-3* by analyzing the FCC pattern of isolated plastids. As expected, hydroxy-*p*FCC was absent from gerontoplasts, which contained relatively more *p*FCC (Supplemental Figure 4 online).

TIC32 and TIC62 are Not Involved in the Redox-Cycle of TIC55.

TIC55 had been considered to exhibit a redox regulatory role of protein import together with TIC32 and TIC62, two further proposed components of the protein import machinery at the inner chloroplast envelope (Küchler et al., 2002; Hörmann et al., 2004). Both proteins were shown to possess NADPH binding domains and, in addition, TIC62 is able to interact with FNR (Bölter et al., 2015). This implies that one or both of these additional TIC components could be involved in delivering electrons to the Rieske and/or the mononuclear iron center of TIC55 and, thus, drive the redox cycle required for TIC55 activity. To test this possibility, we analyzed phyllobilin accumulation in *tic32* and *tic62* T-DNA insertion mutants during leaf senescence. As seen in Figure 6F, mutations in these genes did not affect phyllobilin hydroxylation, indicating that electron supply towards TIC55 is independent from TIC62 or TIC32.

DISCUSSION

Phyllobilin Hydroxylation by TIC55

Most of the phyllobilins that have been identified to date as degradation products of chlorophyll in higher plants carry a hydroxyl group at the $C3^2$ position (Christ and Hörtensteiner, 2014; Kräutler, 2014, 2016; Scherl et al., 2016). Furthermore, hydroxylated phyllobilins have been found in each single species analyzed so far (Figure 7A), and in many cases have been shown to represent the major phyllobilin fraction (Oberhuber et al., 2003; Christ et al., 2013). This implies that chlorophyll catabolite hydroxylation is a common and important reaction, which, together with the upstream reactions that lead to the formation of *p*FCC, forms the core part of the PAO/phyllobilin pathway of chlorophyll breakdown in higher plants. Here we identified TIC55, an envelope-localized member of the Rieske-type oxygenases, as the phyllobilin hydroxylase in Arabidopsis. Our biochemical characterization and subsequent analysis of mutants defective in likely candidates unequivocally demonstrates that TIC55 is solely responsible for the formation of hydroxylated phyllobilins during leaf senescence-related chlorophyll breakdown.

This finding is rather surprising, because TIC55 was originally identified as a potential component of the protein import machinery at the chloroplast inner envelope (Calibe et al.,

1997). Specifically, it was proposed that TIC55 together with TIC62 and TIC32 functions as redox sensor that links protein import to the redox state of the chloroplast (Balsera et al., 2010). As such, TIC55, TIC62 and TIC32 would play a regulatory role rather than being core components of the inner envelope import machinery itself, the exact composition of which is still under debate (Bölter et al., 2015). The rationale behind this proposed function is the presence in TIC55 of redox-active cysteine residues at the C-terminus that have been shown to be regulated by the thioredoxin system (Bartsch et al., 2008). Furthermore, the other two components of the so-called redox regulon (Stengel et al., 2007), i.e. TIC62 and TIC32, possess NADPH-binding sites and could exert their regulatory role depending on changes of the $NADP^+$/NADPH ratio, a well-known read-out of the redox state of the chloroplast. Indeed, TIC62 was shown to shuttle between thylakoids and the inner envelope in a $NADP^+$/NADPH ratio-dependent manner (Stengel et al., 2008), which together with its additional ability to bind FNR (Benz et al., 2009), could allow electron fluxes at these membranes to be highly dynamically regulated (Bölter et al., 2015). Metabolic $NADP^+$/NADPH ratios directly influenced import efficiency of a subset of preproteins in *Pisum sativum* (Stengel et al., 2009). In addition, inhibition of protein import by ionomycin and ophiobolin A, two drugs that disrupt calcium signaling, has been attributed to inhibition of TIC32, which possesses a calmodulin binding site (Chigri et al., 2006). However, mutant analysis of redox regulon components did not show clear phenotypes, implying that under standard conditions this redox control may be not essential for plant viability and/or chloroplast protein import (Benz et al., 2009; Boij et al., 2009; Balsera et al., 2010).

Here we show that TIC55 exhibits a defined role as phyllobilin hydroxylase; however, ferredoxin-derived electrons that are required to drive the redox cycle of this Rieske-type oxygenase (Ferraro et al., 2005) unlikely involve TIC62 and/or TIC62-bound FNR, because respective mutants did not exhibit phyllobilin hydroxylation deficiency.

Rieske-type Oxygenases Play a Dominant Role in Chlorophyll Metabolism

As stated above, the role of TIC55 in protein import has not firmly been established. The Rieske-type iron-sulfur cluster and the mononuclear iron site present in this protein were considered as parts of a hypothetical electron transport chain at the inner envelope with potential final transfer of electrons to oxygen, thus integrating protein import to the redox regulatory network of chloroplasts (Bölter et al., 2015). However, potential substrates for TIC55 that, as a genuine Rieske-type oxygenase (Ferraro et al., 2005), catalyzes activation and incorporation of molecular oxygen have neither been considered nor identified. Our $^{18}O_2$

labeling experiments of senescent leaves combined with *in vitro* activity assays demonstrate that TIC55 is a monooxygenase that incorporates one oxygen atom derived from molecular oxygen into *p*FCC.

The Arabidopsis genome encodes five Rieske-type oxygenases (Gray et al., 2002). With the identification of TIC55 as a phyllobilin hydroxylase reported here, four out of these five have been attributed to chlorophyll metabolism. Two of them are involved in chlorophyll biosynthesis, i.e. CAO that catalyzes the oxidation of chlorophyll(ide) *a* to chlorophyll(ide) *b* (Tanaka et al., 1998), and PTC52 that has been proposed to carry out the same oxidation, but using protochlorophyllide *a* as substrate (Reinbothe et al., 2004). However, an *in vivo* role of protochlorophyllide *b* has been questioned (Scheumann et al., 1999; Armstrong et al., 2000). The other two Rieske-type oxygenases are involved in chlorophyll degradation, i.e. PAO responsible for porphyrin ring opening of pheophorbide *a* (Pružinská et al., 2005), and TIC55. The fifth Rieske-type oxygenase, CMO-like, is highly homologous to CMO of *Spinacia oleracea* (spinach) that catalyzes the first step of glycine betaine biosynthesis (Rathinasabapathi et al., 1997). However, Arabidopsis does not produce glycine betaine and Arabidopsis CMO-like was unable to promote glycine betaine formation (Hibino et al., 2002). Phylogenetic analyses had revealed that for all five Rieske-type oxygenases highly homologous proteins are present in higher plants (Gray et al., 2004). Re-evaluation of the homologies of PAO, PTC52 and TIC55 incorporating sequences from *Klebsormidium flaccidum* (Hori et al., 2014) and from the Phytozome database (https://phytozome.jgi.doe.gov/pz/portal.html) that currently includes 52 sequenced Viridiplantae species uncovered clustering of these three Rieske-type oxygenase into three distinct clades (Figure 7B). TIC55 and PAO orthologs are present in all land plants, including *Selaginella moellendorffii*, a member of the Lycopodiopsida, the oldest lineage of vascular plants, and the bryophyte *Physcomitrella patens*. The wide distribution of all three homologs within land plant species, but apparent absence from chlorophyte green algae for which genomes are available, such as *Chlamydomonas reinhardtii*, *Micromonas pusilla*, *Volvox carteri* and *Ostreococcus lucimarinus*, suggests that TIC55 in higher plants most likely originated from a recent gene duplication and subsequent neofunctionalisation to play a potential role in the adaptation to a terrestrial growth habit and/or high light adaptation. Interestingly, the genome of the early charophyte species *Klebsormidium flaccidum*, which is considered to be a close ancestor of land plants (Hori et al.) also encodes TIC55- and PAO-like proteins that exhibit rather high sequence homologies to the respective land plant proteins. This is in support of the idea that chlorophyll degradation co-evolved with the colonization of land plants.

Spatial Distribution of Chlorophyll Catabolic Enzymes within the Plastid

The common reactions of the PAO/phyllobilin pathway leading to *p*FCC localize to the chloroplast. This has been substantiated by numerous investigations using different approaches, among them GFP-fusion protein analysis, subcellular fragmentation studies and enzyme activity measurements on isolated chloroplast fractions (for recent reviews on the biochemistry of chlorophyll breakdown, see (Hörtensteiner, 2013a, b). However, the sub-chloroplast location of respective reactions remained largely unclear until recently; in particular, because of the inconsistency with regard to the presence or absence of transmembrane domains in these proteins. Thus, for example, PAO is an integral membrane protein with two predicted transmembrane domains (Figure 5A) (Sakuraba et al., 2012), while RCCR, with which it physically interacts during catalysis (Rodoni et al., 1997; Pružinská et al., 2007), is a soluble protein (Wüthrich et al., 2000). Recently, based on protein interaction studies, we proposed the model that all chloroplast-located chlorophyll catabolic enzymes form a highly dynamic multiprotein complex at the thylakoid membrane with interaction with light harvesting complex II proteins (Sakuraba et al., 2012).

The identification of the envelope-bound TIC55 as the phyllobilin hydroxylase is intriguing in this respect (see Figure 8 for a topographical model of the PAO/phyllobilin pathway integrating TIC55). Nevertheless, one can speculate that there is no requirement of including TIC55 in the above-mentioned thylakoid membrane-bound degradative complex, because the proposed rationale behind this complex, i.e. metabolic channeling of degradation intermediates to prevent potential phototoxicity (Sakuraba et al., 2012), is reached with the formation of *p*FCC. A *p*FCC-derivative was recently shown to be able to efficiently produce singlet oxygen *in vitro* when excited with UV light (Jockusch et al., 2014). Nevertheless, when compared with pheophorbide that absorbs a much wider spectral range and is known as being highly cell phototoxic (Xodo et al., 2012), the *in vivo* capacity of *p*FCC to produce reactive oxygen species and, thus, to act as a phototoxin is most likely rather limited. Envelope-localization of TIC55 implies the requirement for *p*FCC movement from the thylakoid to the envelope, but it remains unclear whether this is achieved by simple diffusion or is protein-guided. Rather than being important for intermediate detoxification, like the upstream reactions, the localization of TIC55 at the envelope rather implies a link to catabolite export from the plastid. The molecular nature of the chloroplast exporter(s) for chlorophyll catabolites is unknown to date, but it has been speculated to be driven by an active transport mechanism (Matile et al., 1992). The former link of TIC55 with protein import at the inner envelope (Küchler et al., 2002) implies the intriguing

possibility for phyllobilin export through the same protein complex; however, this is highly speculative and export through the TIC/TOC system has never been described. Whether TIC55 may directly interact with potential catabolite exporters remains unclear, because phyllobilin export does not absolutely require previous reaction by TIC55, as demonstrated by the presence of a substantial proportion of non-hydroxylated phyllobilins in senescent wild-type leaves (Figure 6B) (Christ et al., 2016)

What is the Biological Role of Phyllobilin Modification?

None of the Arabidopsis mutants that are deficient in one of the so far known phyllobilin modifying reactions, i.e. CYP89A9, MES16 or TIC55, show an obvious visible phenotype or are compromised in chlorophyll breakdown during senescence (Christ et al., 2012; Christ et al., 2013). Furthermore, deformylation (through CYP89A9 in Arabidopsis) and demethylation (through MES16 in Arabidopsis), but also C18-dihydroxylation and $C3^2$-OH group conjugation are species-specific reactions (Hörtensteiner and Kräutler, 2011; Kräutler, 2014). This implies them to be non-essential reactions in chlorophyll degradation. Nevertheless, the fact that all three, i.e. TIC55, CYP89A9 and MES16, are members of protein subfamilies with 3, 7 and 3 members, respectively, in Arabidopsis (Gray et al., 2004; Bak et al., 2011; Christ et al., 2012), suggests that they have been specifically recruited during evolution to function in chlorophyll breakdown. The identification of TIC55 in this work offers the tool of producing a *cyp89a9mes16tic55* triple mutant in the future, for a more indebt analysis about the role of phyllobilin modification during chlorophyll breakdown.

METHODS

Plant Material and Senescence Induction

Arabidopsis ecotype Columbia-0 (Col-0) was used as the wild-type. T-DNA insertion lines for the following genes were used: *TIC55* (AT2G24820), *PTC52* (AT4G25650), *TIC32* (At4g23430) and *TIC62* (At3g18890). They were from the following collections: SALK lines (Alonso et al., 2003): *tic55-1*, SALK_137948; *tic55-2*, SALK_086048C; *ptc52*, SALK_006984; GABI-KAT lines (Rosso et al., 2003): *tic32*, GK_117H08; *tic62*, GK_439H04; SAIL lines (Sessions et al., 2002): *tic55-3*, SAIL_167_G08. These lines were obtained from the European *Arabidopsis* Center, Nottingham, UK. Homozygous plants were

identified by PCR using T-DNA- and gene-specific primers as listed in Supplemental Table 1 online. Two Arabidopsis *acd2-2* complementation lines that express RCCR with either stereospecificity (*acd2-2+At*-RCCR, producing *p*FCC; and *acd2-2+At*-RCCR-X, producing *epi-p*FCC) (Pružinská et al., 2007) were used as reference for HPLC analysis.

For biochemical and physiological experiments, plants were either grown under short-day conditions (16 h dark/8 h light) or under long-day conditions (16 h light/8 h dark) under fluorescent light of 60 to 120 µmol photons m^{-2} s^{-1} at 22°C. Plants for seed production and DNA isolation were grown in a greenhouse with rates of 100 to 200 µmol photons m^{-2} s^{-1} at 22°C. Leaf senescence was inducted by incubating detached leaves on wet filter paper for up to 8 d in permanent darkness. For dark incubation under $^{18}O_2$ atmosphere, leaves from short-day-grown Col-0 plants were excised and placed on wet filter paper in a glass desiccator. After evacuation with a vacuum pump, the desiccator was aerated with $^{18}O_2$ (97.1%, Campro Scientific GmbH, Germany) and leaves senesced in the dark for 5 d. Red bell pepper fruits used for chromoplast isolation were bought from a local market.

Biocomputational Methods

Orthologs of TIC55, PAO and PTC52 were identified using BLASTP searches (Altschul et al., 1997) at the Phytozome database of the Joint Genome Institute (https://phytozome.jgi.doe.gov). Kle*bsormidium flaccidum* sequences were likewise obtained from the National Center for Biotechnology Information (http://ncbi.nlm.nih.gov). For phylogenetic analysis, a multiple sequence alignment was generated with the neighborhood joining method using MEGA7 (Kumar et al., 2016). Bootstrap analysis was performed with 1000 replicates.

GFP Fusion Protein Production and Confocal Microscopy

TIC55 (BX819909) and *PTC52* (pda06002) full-length cDNAs were, respectively, obtained from the Centre National de Ressources Génomiques Végétales, France, and the RIKEN Tsukuba Institute BioResourceCenter, Japan. *TIC55* was amplified by PCR with KAPA HiFi HotStart ReadyMix (Kapa Biosystems) using the primers listed in Supplemental Table 1 online. The resulting PCR fragment was cut with *Xma*I and *Spe*I and ligated to *Xma*I/*Spe*I-digested pUC18-spGFP6 (Meyer et al., 2006) to create a fusion between TIC55 and GFP at the C-terminus. Likewise, *PTC52* was amplified by PCR using the primers listed in Supplemental

Table 1 online and cloned into pUC18-spGFP6 via *Bam*HI. Correctness of cDNA sequences and orientation was verified by sequencing. As references for localization, GFP fusion proteins of TIC110 (chloroplast inner envelope membrane) and PAO (thylakoid membrane) (Sakuraba et al., 2012) were used. The constructs were used to transform Arabidopsis protoplasts isolated from 6-week-old plants grown in short-day conditions. Isolation of protoplasts was performed according to a published protocol (Christ et al., 2012 and references therein). GFP fluorescence was imaged with a laser scanning confocal microscope (TCS SP5; Leica Microsystems) at an excitation wavelength of 488 nm and signals were detected between 495 nm and 530 nm. Chlorophyll autofluorescence was recorded at 643-730 nm.

Arabidopsis Chloroplast Isolation and MES16 Incubation

4-6-week-old plants grown in short-day conditions were used for chloroplast isolation in a two-step purification procedure. A published protocol (Schelbert et al., 2009) was adapted to optimize isolation of senescent protoplasts and chloroplasts. Leaves were detached and dark incubated for 4 d. After isolation, mesophyll protoplasts were lysed by the addition of breakage buffer [containing 300 mM sorbitol, 20 mM Tricine-KOH pH 8.4, 5 mM EDTA, 5 mM EGTA, 10 mM $NaHCO_3$ and 0.1% (w/v) BSA] and gerontoplasts purified on a discontinuous [85% and 40% (v/v)] gradient of Percoll containing the same salts as the breakage buffer. After washing the chloroplasts obtained from the 85%/40% interphase twice with HEPES-sorbitol buffer (330 mM sorbitol and 50 mM Hepes-KOH pH 8) they were analyzed for colorless catabolites by HPLC or by LC-MS/MS (see below). For this, chloroplast fractions were supplemented with one volume of methanol (v/v), mixed by vortexing and twice centrifuged (16,000*g*; 2 min). Alternatively, isolated chloroplasts were incubated for 10 min with heterologously expressed MES16 (Christ et al., 2012). MES16 was either added directly to intact chloroplasts or to chloroplasts that were broken-up by a freezing in liquid N_2 prior to the addition of the enzyme. Reactions were stopped by the addition of one volume of methanol (v/v) and vortexing. After twice centrifugation (16,000*g*; 2 min) the formation of demethylated hydroxy-*p*FCC was analyzed by LC-MS/MS (see below).

*epi-p*FCC Preparation

In order to produce *epi-p*FCC as substrate for the hydroxylation assay, PAO and RCCR were extracted from red bell pepper chromoplasts according to a published protocol (Christ et al.,

2012). The extracted enzymes were then used to convert pheophorbide *a* (Hörtensteiner et al., 1995) to *epi-p*FCC according to an established assay (Pružinská et al., 2007). *epi-p*FCC was concentrated on C18-SepPak columns (Waters, Baden-Dättwil, Switzerland) and purified by HPLC (see below) for later use in hydroxylation assays.

Isolation of the Hydroxylating Activity From Bell Pepper Chromoplasts and Activity Determination

Total chromoplasts isolated from red bell pepper fruits were also used as source of the hydroxylating enzyme. Essentially the same protocol as for the extraction of PAO and RCCR (Christ et al., 2012) was used, but with some modifications. Briefly, red bell pepper exocarp was blended with a fruit juicer in chromoplast isolation buffer (1.33 mL g^{-1} tissue; Christ et al., 2012), filtered through Miracloth and then centrifuged for 10 min at 12,000*g*. The pellet was carefully resuspended in chromoplast isolation buffer (0.33 mL g^{-1} tissue; Christ et al., 2012) and re-centrifuged. The pellet was finally resuspended in 8 ml of 25 mM Tris-MES pH 8 (25 µL g^{-1} tissue) and chromoplasts were broken by pressing them 10 times through a 0.6 mm syringe needle. The resulting *Total Chromoplast Protein* fraction was either frozen in liquid nitrogen and stored at -80°C for later use or centrifuged (15,000*g*, 10 min) to separate *Supernatant* and *Pellet*. The supernatant was further fractionated by ultra-centrifugation (UC) at 150,000*g* for 60 min into *1xUC-Membrane* and *1xUC-Stroma*. The obtained pellet was resuspended in the start volume of 25 mM Tris-MES pH 8 and 10 times pushed through a needle as above. The UC step was repeated, yielding *2xUC-Membrane* and *2xUC-Stroma* fractions, respectively.

The standard hydroxylation assays (total volume 50 µL) consisted of 28 µL of respective chromoplast fractions, 15 µM of *epi-p*FCC, 10 µg of Fd (SigmaAldrich), and a Fd-reducing system consisting of 10 mM G-6-P, 2.5 mM NADPH, 50 milliunits GDH, and 5 milliunits of FNR (SigmaAldrich). After incubation at 25°C in darkness for up to 40 min, the reactions were terminated by adding methanol to a final concentration of 50% (v/v). After centrifugation for 2 min at 16,000*g*, samples were analyzed by HPLC or by LC-MS/MS as described below. For reactions under defined atmospheric conditions, assays were set up on ice in glass bulbs. After removal of the ambient air by vacuum suction, bulbs were flushed with the desired gas mixtures, and assays performed as described above.

Colorless Chlorophyll Catabolites.

Chlorophyll catabolites were either analyzed by HPLC or by LC-MS/MS.

HPLC

For HPLC analysis, plant material was ground in liquid nitrogen and colorless catabolites were extracted with 3 volumes (w/v) of 50 mM phosphate buffer pH 7/methanol (1:3, v/v). Plant extracts or hydroxylation assay reactions were analyzed on a revered-phase HPLC system as described (Christ et al., 2012). The column was developed with a gradient (flow rate 1 mL min^{-1}) of solvent A (25 mM potassium phosphate pH 7.0), solvent B (methanol) and solvent C (H_2O) as follows [%A/%B/%C (v/v/v)]: from 80/20/0 to 40/60/0 in 35 min, to 0/60/40 in 12 min, to 0/100/0 in 2 min, back to 0/60/40 in 7 min, and finally back to 80/20/0 in 2 min. Peak detection was performed with sequential monitoring using a PDA-100 photodiode array detector (200–700 nm; ThermoFisher Scientific) and a RF2000 fluorescence detector (excitation at 320 nm, emission at 450 nm; Shimadzu). Chlorophyll catabolites were identified by their absorption (FCCs, NCCs and DNCCs) and fluorescence (FCCs) properties. Relative amounts of hydroxy-*epi*-*p*FCC obtained in hydroxylation assays were determined by peak areas at 320 nm.

LC-MS/MS

For LC-MS/MS analysis, plant material was collected in 2-mL Eppendorf tubes containing 500 µL of 1.25-1.65 mm glass beads. The tissue was ground in liquid nitrogen using a MM300 Mixer Mill (Retsch, Germany) at 30 Hz for 5 min. Chlorophyll catabolites were extracted with 5 volumes (w/v) of ice-cold 80% methanol, 20% H_2O and 0.1% formic acid (v/v/v) containing 1 µg mL^{-1} ampicillin as internal standard, sonicated for 2 min and twice centrifuged at 16,000*g* for 2 min. Total plant extracts, chloroplast extracts or reactions of hydroxylation assays were analyzed by LC-MS/MS (UltiMate 3000 RSLC system Thermo Fisher Scientific, coupled to a Compact Q-TOF mass spectrometer with electron spay ionization (ESI), Bruker Daltonics) as described (Christ et al., 2016). Two different LC programs were employed. In the short program (Christ et al., 2016) the column was developed with a gradient (flow rate of 0.3 mL min^{-1}) of solvent B [acetonitrile with 0.1% (v/v) formic acid] in solvent A [water with 0.1% (v/v) formic acid] as follows (all v/v): 30% for 0.5 min, 30% to 70% in 7.5 min, 70% to 100% in 0.1 min and 100% for 3.9 min. In the long program, identical solvents were used, but the column was developed as follows (all v/v): 5% B for 0.5 min, 30% B to 100% B in 11 min and

100% B for 4 min. Phyllobilins were identified and quantified using an *in-house-built* spectrum library (Christ et al., 2016).

Accession Numbers

Sequence data from *Klebsormidium flaccidum* can be found in GenBank/EMBL database (http://www.ncbi.nlm.nih.gov) under the following accession numbers: Kfla_1 (GAQ77973.1), Kfla_2 (GAQ78701.1), Kfla_3 (GAQ92150.1).

All other sequences can be found in the Phytozome database (https://phytozome.jgi.doe.gov) under the following accession numbers: *Aquilegia coerulea*: Acor_1, 22029521; Acor_2, 22030025; Acor_3, 22030648; Acor_4, 22035222; Acor_5, 22062530; *Arabidopsis lyrata*: Alyr_1, 16058352; Alyr_2, 16049304; Alyr_3, 16052333; *Arabidopsis thaliana*: Atha_PAO (At3g44880), 19664072; Atha_PTC52 (At4g25650), 19646489; Atha_TIC55, 19643456 (At2g24820); *Amborella trichopoda*: Atri_1, 31571943; Atri_2, 31573466; Atri_3, 31569219; *Brachypodium distachon*: Bdis_1, 32798942; Bdis_2, 32805471; Bdis_3, 32814680; *Brassica rapa*: Brap_1, 30640093; Brap_2, 30639463; Brap_3, 30615756; *Brachypodium stacei*: Bsta_1, 32873310; Bsta_2, 32877401; Bsta_3, 32863896; *Boechera stricta*: Bstr_1, 30657466; Bstr_2, 30657466**;** Bstr_3, 30677801; *Citrus clementina*: Ccle_1, 20794617; Ccle_2, 20794921; Ccle_3, 20814974; Ccle_4, 20817945; Ccle_5, 20814172; *Capsella grandiflora*: Cgra_1, 28896530; Cgra_2., 28912086; Cgra_3., 28914744; *Carica papaya*: Cpap_1, 16406577; Cpap_2, 16406579; Cpap_3, 16409268; Cpap_4, 16420643; *Capsella rubella*: Crub_1, 20894180; Crub_2, 20886114; Crub_3, 20902616; *Cucumis sativus*: Csat_1, 16963640; Csat_2, 16963642; Csat_3, 16968781; Csat_4, 16973514; *Citrus sinensis*: Csin_1, 18104396; Csin_2, 18110147; Csin_3, 18110062; Csin_4, 18109308; Csin_5, 18109304; *Eucalyptus grandis*: Egra_1, 32059933; Egra_2, 32036721; Egra_3, 32033828; *Eutrema salsugineum*: Esal_1, 20208666; Esal_2, 20196368; Esal_3, 20194144; *Fragaria vesca*: Fves_1, 27274244; Fves_2, 27249443; Fves_3, 27248027; Fves_4, 27263237; Fves_5, 27276459; Fves_6, 27275924; *Glycine max*: Gmax_1, 30490036; Gmax_2, 30523624; Gmax_3, 30553241; Gmax_4, 30540276; Gmax_5, 30528498; Gmax_6, 30548653; *Gossypium raimondii*: Grai_1, 26820373; Grai_2, 26773144; Grai_3, 26773258; Grai_4, 26773690; Grai_5, 26765361; *Kalanchoe marnieriana*: Kmar_1, 32592111; Kmar_2, 32568622; Kmar_3, 32585756; Kmar_4, 32565330; Kmar_5, 32587661; Kmar_6, 32537639; *Linum usitatissimum*: Lusi_1, 23170108; Lusi_10, 23152413; Lusi_11, 23179897; Lusi_12,

23153476; Lusi_2, 23178747; Lusi_3, 23178807; Lusi_4, 23178789; Lusi_5, 23178765; Lusi_6, 23150802; Lusi_7, 23150844; Lusi_8, 23150790; Lusi_9, 23156438; *Musa acuminata*: Macu_1, 32305345; Macu_2, 32298593; Macu_3, 32299412; Macu_4, 32301167; *Malus domestica*: Mdom_1, 22648216; Mdom_2, 22680745; Mdom_3, 22673860; Mdom_4, 22657421; Mdom_5, 22669270; Mdom_6, 22681531; Mdom_7, 22646192; Mdom_8, 22657424; *Manihot esculenta*: Mesc_1, 32328964; Mesc_2, 32352206; Mesc_3, 32352768; Mesc_4, 32351848; Mesc_5, 32351381; Mesc_6, 32343636; *Mimulus guttatus*: Mgut_1, 28939106; Mgut_2, 28929299; Mgut_3, 28927831; Mgut_4, 28928063; *Medicago truncatula*: Mtru_1, 31054512; Mtru_2, 31108864; Mtru_3, 31076177; Mtru_4, 31075891; Mtru_5, 31071508; *Oryza sativa*: Osat_1, 33136036; Osat_2, 33129257; Osat_3, 33130101; Osat_4, 33126987; Osat_5, 33128763; *Panicum hallii*: Phal_1, 32526147; Phal_2, 32510109; *Physcomitrella patens*: Ppat_1, 32958411; Ppat_2, 32971600; Ppat_3, 32943162; Ppat_4, 32923430; Ppat_5, 32934884; *Prunus persica*: Pper_1, 32111912; Pper_2, 32118911; Pper_3, 32087889; Pper_4, 32086408; *Populus trichocarpa*: Ptri_1, 27044612; Ptri_2, 27044125; Ptri_3, 26998722; Ptri_4, 26997353; Ptri_5, 26997432; Ptri_6, 26992599; Ptri_7, 27007363; Ptri_8, 27010289; *Panicum virgatum*: Pvir_1, 30249395; Pvir_2, 30232924; Pvir_3, 30210200; Pvir_4, 30208474; Pvir_5, 30224983; *Phaseolus vulgaris*: Pvul_1, 27170687; Pvul_2, 27168327; Pvul_3, 27147757; Pvul_4, 27151382; *Ricinus communis*: Rcom_1, 16802948; Rcom_2, 16802951; Rcom_3, 16803313; Rcom_4, 16811159; *Sorghum bicolor*: Sbic_1, 32753731; Sbic_2, 32754631; Sbic_3, 32744056; *Sphagnum fallax*: Sfal_1, 32628626; Sfal_2, 32612026; Sfal_3, 32611292; Sfal_4, 32631199; Sfal_5, 32631202; Sfal_6, 32631211; Sfal_7, 32615809; *Setaria italica*: Sita_1, 32697922; Sita_2, 32693755; Sita_3, 32689656; *Solanum lycopersicum*: Slyc_1, 27278224; Slyc_2, 27297008; Slyc_3, 27308810; *Selaginella moellendorffii*: Smoe_1, 15421380; Smoe_2, 15420984; *Spirodela polyrhiza*: Spol_1, 31503412; Spol_2, 31521506; Spol_3, 31512183; Spol_4, 31510559; *Salix purpurea*: Spur_1, 31446831; Spur_2, 31444937; Spur_3, 31408599; Spur_4, 31425200; Spur_5, 31434385; Spur_6, 31420119; Spur_7, 31420805; Spur_8, 31420645; *Solanum tuberosum*: Stub_1, 24409796; Stub_2, 24385728; Stub_3, 24377864; *Setaria viridis*: Svir_1, 32663617; Svir_2, 32653526; Svir_3, 32653709; *Theobroma cacao*: Tcac_1, 27426931; Tcac_2, 27427235; Tcac_3, 27426954; *Vitis vinifera*: Vvin_1, 17833437; Vvin_2, 17833438; Vvin_3, 17837646; Vvin_4, 17841070; *Zea mays*: Zmay_1, 30990042; Zmay_2, 31009998; Zmay_3, 31016834.

Supplemental Data

The following materials are available in the online version of this article.

Supplemental Figure 1. Confirmation of ***epi-p*FCC and *p*FCC Identity and *epi-p*FCC-to-*epi-p*NCC Isomerization.**

Supplemental Figure 2. LC-MS Confirmation of Hydroxy-***epi-p*FCC**.

Supplemental Figure 3. LC-MS Analysis of Phyllobilins from Col-0 and Rieske-type Oxygenase Mutants.

Supplemental Figure 4. Hydroxy-*p*FCC is absent from *tic55-3* Gerontoplasts.

Supplemental Table 1. List of Primers Used in This Study.

ACKNOWLEDGMENTS

This work was supported by the Swiss National Science Foundation (grant no. 31003A_149389) and CropLife (to S.H.).

AUTHOR CONTRIBUTIONS

S.H. designed research; M.H., B.C., and A.D. performed research; M.H., B.C., S.A. and S.H. analyzed data; and M.H., and S.H. wrote the paper.

REFERENCES

Alonso, J.M., Stepanova, A.N., Leisse, T.J., Kim, C.J., Chen, H., Shinn, P., Stevenson, D.K., Zimmermann, J., Barajas, P., Cheuk, R., Gadrinab, C., Heller, C., Jeske, A., Koesema, E., Meyers, C.C., Parker, H., Prednis, L., Ansari, Y., Chory, N., Deen, H., Geralt, M., Hazari, N., Hom, E., Karnes, M., Mulholland, C., Ndubaku, R., Schmidt, I., Guzman, P., Aguilar-Henonin, L., Schmid, M., Weigel, D., Carter, D.E., Marchand, T., Risseeuw, E., Brogden, D., Zeko, A., Crosby, W.L., Berry, C.C., and Ecker, J.R. (2003). Genome-wide insertional mutagenesis of *Arabidopsis thaliana*. Science **301,** 653-657.

Altschul, S.F., Madden, T.L., Schaffer, A.A., Zhang, J.H., Zhang, Z., Miller, W., and Lipman, D.J. (1997). Gapped BLAST and PSI-BLAST: a new generation of protein database search programs. Nucl. Acids Res. **25,** 3389-3402.

Armstrong, G.A., Apel, K., and Rüdiger, W. (2000). Does a light-harvesting protochlorophyllide *a*/*b*-binding protein complex exist? Trends Plant Sci. **5,** 40-44.

Bak, S., Beisson, F., Bishop, G., Hamberger, B., Höfer, R., Paquette, S., and Werck-Reichhart, D. (2011). Cytochromes P450. BioOne: The Arabidopsis Book **9,** e0144.

Balsera, M., Soll, J., and Buchanan, B.B. (2010). Redox extends its regulatory reach to chloroplast protein import. Trends Plant Sci. **15,** 515-521.

Bartsch, S., Monnet, J., Selbach, K., Quigley, F., Gray, J., von Wettstein, D., Reinbothe, S., and Reinbothe, C. (2008). Three thioredoxin targets in the inner envelope membrane of chloroplasts function in protein import and chlorophyll metabolism. Proc. Natl. Acad. Sci. USA **105,** 4933-4938.

Benz, J.P., Stengel, A., Lintala, M., Lee, Y.H., Weber, A., Philippar, K., Gügel, I.L., Kaieda, S., Ikegami, T., Mulo, P., Soll, J., and Bölter, B. (2009). *Arabidopsis* Tic62 and ferredoxin-NADP(H) oxidoreductase form light-regulated complexes that are integrated into the chloroplast redox poise. Plant Cell **21,** 3965-3983.

Boij, P., Patel, R., Garcia, C., Jarvis, P., and Aronsson, H. (2009). *In vivo* studies on the roles of Tic55-related proteins in chloroplast protein import in *Arabidopsis thaliana*. Mol. Plant **2,** 1397-1409.

Bölter, B., Soll, J., and Schwenkert, S. (2015). Redox meets protein trafficking. Biochim. Biophys. Acta **1847,** 949-956.

Calibe, A., Grimm, R., Kaiser, G., Lübeck, J., Soll, J., and Heins, L. (1997). The chloroplastic protein import machinery contains a Rieske-type iron-sulfur cluster and a mononuclear iron-binding protein. EMBO J. **16,** 7342-7350.

Chigri, F., Hörmann, F., Stamp, A., Stammers, D.K., Bölter, B., Soll, J., and Vothknecht, U.C. (2006). Calcium regulation of chloroplast protein translocation is mediated by calmodulin binding to Tic32. Proc. Natl. Acad. Sci. USA **103,** 16051-16056.

Christ, B., and Hörtensteiner, S. (2014). Mechanism and significance of chlorophyll breakdown. J. Plant Growth Regul. **33,** 4-20.

Christ, B., Hauenstein, M., and Hörtensteiner, S. (2016). A liquid chromatography-mass spectrometry platform for the analysis of phyllobilins, the major degradation products of chlorophyll in *Arabidopsis thaliana*. Plant J.**,** , in press.

Christ, B., Schelbert, S., Aubry, S., Süssenbacher, I., Müller, T., Kräutler, B., and Hörtensteiner, S. (2012). MES16, a member of the methylesterase protein family, specifically demethylates fluorescent chlorophyll catabolites during chlorophyll breakdown in Arabidopsis. Plant Physiol. **158,** 628-641.

Christ, B., Süssenbacher, I., Moser, S., Bichsel, N., Egert, A., Müller, T., Kräutler, B., and Hörtensteiner, S. (2013). Cytochrome P450 CYP89A9 is involved in the formation of major chlorophyll catabolites during leaf senescence in *Arabidopsis*. Plant Cell **25,** 1868-1880.

Ferraro, D.J., Gakhar, L., and Ramaswamy, S. (2005). Rieske business: Structure-function of Rieske non-heme oxygenases. Biochem. Biophys. Res. Comm. **338,** 175-190.

Ginsburg, S., Schellenberg, M., and Matile, P. (1994). Cleavage of chlorophyll-porphyrin. Requirement for reduced ferredoxin and oxygen. Plant Physiol. **105,** 545-554.

Gray, J., Janick-Bruckner, D., Bruckner, B., Close, P.S., and Johal, G.S. (2002). Light-dependent death of maize *lls1* cells is mediated by mature chloroplasts. Plant Physiol. **130,** 1894-1907.

Gray, J., Wardzala, E., Yang, M., Reinbothe, S., Haller, S., and Pauli, F. (2004). A small family of LLS1-related non-heme oxygenases in plants with an origin amongst oxygenic photosynthesizers. Plant Mol. Biol. **54,** 39-54.

Hibino, T., Waditee, R., Araki, E., Ishikawa, H., Aoki, K., Tanaka, Y., and Takabe, T. (2002). Functional characterization of choline monooxygenase, an enzyme for betaine synthesis in plants. J. Biol. Chem. **277,** 41352-41360.

Hori, K., Maruyama, F., Fujisawa, T., Togashi, T., Yamamoto, N., Seo, M., Sato, S., Yamada, T., Mori, H., Tajima, N., Moriyama, T., Ikeuchi, M., Watanabe, M.,

Wada, H., Kobayashi, K., Saito, M., Masuda, T., Sasaki-Sekimoto, Y., Mashiguchi, K., Awai, K., Shimojima, M., Masuda, S., Iwai, M., Nobusawa, T., Narise, T., Kondo, S., Saito, H., Sato, R., Murakawa, M., Ihara, Y., Oshima-Yamada, Y., Ohtaka, K., Satoh, M., Sonobe, K., Ishii, M., Ohtani, R., Kanamori-Sato, M., Honoki, R., Miyazaki, D., Mochizuki, H., Umetsu, J., Higashi, K., Shibata, D., Kamiya, Y., Sato, N., Nakamura, Y., Tabata, S., Ida, S., Kurokawa, K., and Ohta, H. (2014). *Klebsormidium flaccidum* genome reveals primary factors for plant terrestrial adaptation. Nat. Commun. **5,** 3978.

Hörmann, F., Küchler, M., Sveshnikov, D., Oppermann, U., Li, Y., and Soll, J. (2004). Tic32, an essential component in chloroplast biogenesis. J. Biol. Chem. **279,** 34756-34762.

Hörtensteiner, S. (2013a). The pathway of chlorophyll degradation: catabolites, enzymes and pathway regulation. In Plastid Development in Leaves during Growth and Senescence, B. Biswal and K. Krupinska, eds (Dordrecht, The Netherlands: Springer), pp. 363-392.

Hörtensteiner, S. (2013b). Update on the biochemistry of chlorophyll breakdown. Plant Mol. Biol. **82,** 505-517.

Hörtensteiner, S., and Feller, U. (2002). Nitrogen metabolism and remobilization during senescence. J. Exp. Bot. **53,** 927-937.

Hörtensteiner, S., and Kräutler, B. (2011). Chlorophyll breakdown in higher plants. Biochim. Biophys. Acta **1807,** 977-988.

Hörtensteiner, S., Vicentini, F., and Matile, P. (1995). Chlorophyll breakdown in senescent cotyledons of rape, *Brassica napus* L.: enzymatic cleavage of phaeophorbide *a in vitro*. New Phytol. **129,** 237-246.

Hörtensteiner, S., Wüthrich, K.L., Matile, P., Ongania, K.-H., and Kräutler, B. (1998). The key step in chlorophyll breakdown in higher plants. Cleavage of pheophorbide *a* macrocycle by a monooxygenase. J. Biol. Chem. **273,** 15335-15339.

Hörtensteiner, S., Rodoni, S., Schellenberg, M., Vicentini, F., Nandi, O.I., Qiu, Y.-L., and Matile, P. (2000). Evolution of chlorophyll degradation: the significance of RCC reductase. Plant Biol. **2,** 63-67.

Jockusch, S., Turro, N.J., Banala, S., and Kräutler, B. (2014). Photochemical studies of a fluorescent chlorophyll catabolite - source of bright blue fluorescence in plant tissue and efficient sensitizer of singlet oxygen. Photochem. Photobiol. Sci. **13,** 407-411.

Kräutler, B. (2014). Phyllobilins - the abundant bilin-type tetrapyrrolic catabolites of the green plant pigment chlorophyll. Chem. Soc. Rev. **43,** 6227-6238.

Kräutler, B. (2016). Breakdown of chlorophyll in higher plants - Phyllobilins as abundant, yet hardly visible signs of ripening, senescence, and cell death. Angew. Chem. Int. Ed. **55,** 4882-4907.

Kräutler, B., and Hörtensteiner, S. (2014). Chlorophyll breakdown: chemistry, biochemistry and biology. In Handbook of Porphyrin Science - Chlorophyll, Photosynthesis and Bio-inspired Energy, G.C. Ferreira, K.M. Kadish, K.M. Smith, and R. Guilard, eds (Singapore: World Scientific Publishing), pp. 117-185.

Kräutler, B., Jaun, B., Bortlik, K.-H., Schellenberg, M., and Matile, P. (1991). On the enigma of chlorophyll degradation: the constitution of a secoporphinoid catabolite. Angew. Chem. Int. Ed. Engl. **30,** 1315-1318.

Küchler, M., Decker, S., Hörmann, F., Soll, J., and Heins, L. (2002). Protein import into chloroplasts involves redox-regulated proteins. EMBO J. **21,** 6136-6145.

Kumar, S., Stecher, G., and Tamura, K. (2016). MEGA7: Molecular Evolutionary Genetics Analysis version 7.0 for bigger datasets. Mol Biol Evol **33,** 1870-1874.

Matile, P., Schellenberg, M., and Peisker, C. (1992). Production and release of a chlorophyll catabolite in isolated senescent chloroplasts. Planta **187,** 230-235.

Matile, P., Ginsburg, S., Schellenberg, M., and Thomas, H. (1988). Catabolites of chlorophyll in senescing barley leaves are localized in the vacuoles of mesophyll cells. Proc. Natl. Acad. Sci. USA **85,** 9529-9532.

Meyer, A., Eskandari, S., Grallath, S., and Rentsch, D. (2006). AtGAT1, a high affinity transporter for g-aminobutyric acid in *Arabidopsis thaliana*. J. Biol. Chem. **281,** 7197-7204.

Moser, D., and Matile, P. (1997). Chlorophyll breakdown in ripening fruits of *Capsicum annuum*. J. Plant Physiol. **150,** 759-761.

Moser, S., Müller, T., Holzinger, A., Lutz, C., Jockusch, S., Turro, N.J., and Kräutler, B. (2009). Fluorescent chlorophyll catabolites in bananas light up blue halos of cell death. Proc. Natl. Acad. Sci. USA **106,** 15538-15543.

Mühlecker, W., Ongania, K.-H., Kräutler, B., Matile, P., and Hörtensteiner, S. (1997). Tracking down chlorophyll breakdown in plants: elucidation of the constitution of a 'fluorescent' chlorophyll catabolite. Angew. Chem. Int. Ed. Engl. **36,** 401-404.

Mühlecker, W., Kräutler, B., Moser, D., Matile, P., and Hörtensteiner, S. (2000). Breakdown of chlorophyll: a fluorescent chlorophyll catabolite from sweet pepper (*Capsicum annuum*). Helv. Chim. Acta **83,** 278-286.

Müller, T., Ulrich, M., Ongania, K.H., and Kräutler, B. (2007). Colorless tetrapyrrolic chlorophyll catabolites found in ripening fruit are effective antioxidants. Angew. Chem. Int. Ed. **46,** 8699-8702.

Oberhuber, M., Berghold, J., Breuker, K., Hörtensteiner, S., and Kräutler, B. (2003). Breakdown of chlorophyll: a nonenzymatic reaction accounts for the formation of the colorless "nonfluorescent" chlorophyll catabolites. Proc. Natl. Acad. Sci. USA **100,** 6910-6915.

Pružinská, A., Anders, I., Tanner, G., Roca, M., and Hörtensteiner, S. (2003). Chlorophyll breakdown: pheophorbide *a* oxygenase is a Rieske-type iron-sulfur protein, encoded by the *accelerated cell death 1* gene. Proc. Natl. Acad. Sci. USA **100,** 15259-15264.

Pružinská, A., Anders, I., Aubry, S., Schenk, N., Tapernoux-Lüthi, E., Müller, T., Kräutler, B., and Hörtensteiner, S. (2007). *In vivo* participation of red chlorophyll catabolite reductase in chlorophyll breakdown. Plant Cell **19,** 369-387.

Pružinská, A., Tanner, G., Aubry, S., Anders, I., Moser, S., Müller, T., Ongania, K.-H., Kräutler, B., Youn, J.-Y., Liljegren, S.J., and Hörtensteiner, S. (2005). Chlorophyll breakdown in senescent Arabidopsis leaves: characterization of chlorophyll catabolites and of chlorophyll catabolic enzymes involved in the degreening reaction. Plant Physiol. **139,** 52-63.

Rathinasabapathi, B., Burnet, M., Russell, B.L., Gage, D.A., Liao, P.C., Nye, G.J., Scott, P., Golbeck, J.H., and Hanson, A.D. (1997). Choline monooxygenase, an unusual iron-sulfur enzyme catalyzing the first step of glycine betaine synthesis in plants: prosthetic group characterization and cDNA cloning. Proc. Natl. Acad. Sci. USA **94,** 3454-3458.

Reinbothe, S., Quigley, F., Gray, J., Schemenewitz, A., and Reinbothe, C. (2004). Identification of plastid envelope proteins required for import of protochlorophyllide oxidoreductase A into the chloroplast of barley. Proc. Natl. Acad. Sci. USA **101,** 2197-2202.

Rodoni, S., Mühlecker, W., Anderl, M., Kräutler, B., Moser, D., Thomas, H., Matile, P., and Hörtensteiner, S. (1997). Chlorophyll breakdown in senescent chloroplasts. Cleavage of pheophorbide *a* in two enzymic steps. Plant Physiol. **115,** 669-676.

Rosso, M.G., Li, Y., Strizhov, N., Reiss, B., Dekker, K., and Weisshaar, B. (2003). An *Arabidopsis thaliana* T-DNA mutagenized population (GABI-Kat) for flanking sequence tag-based reverse genetics. Plant Mol. Biol. **53,** 247-259.

Sakuraba, Y., Schelbert, S., Park, S.-Y., Han, S.-H., Lee, B.-D., Besagni Andrès, C., Kessler, F., Hörtensteiner, S., and Paek, N.-C. (2012). STAY-GREEN and chlorophyll catabolic enzymes interact at light-harvesting complex II for chlorophyll detoxification during leaf senescence in *Arabidopsis*. Plant Cell **24,** 507-518.

Schelbert, S., Aubry, S., Burla, B., Agne, B., Kessler, F., Krupinska, K., and Hörtensteiner, S. (2009). Pheophytin pheophorbide hydrolase (pheophytinase) is involved in chlorophyll breakdown during leaf senescence in Arabidopsis. Plant Cell **21,** 767-785.

Schellenberg, M., Matile, P., and Thomas, H. (1993). Production of a presumptive chlorophyll catabolite *in vitro*: requirement for reduced ferredoxin. Planta **191,** 417-420.

Scherl, M., Müller, T., Kreutz, C.R., Huber, R.G., Zass, E., Liedl, K.R., and Kräutler, B. (2016). Chlorophyll catabolites in fall leaves of the wych elm tree present a novel glyosylation motif. Chem-Eur J **22,** 9498-9503.

Scheumann, V., Klement, H., Helfrich, M., Öster, U., Schoch, S., and Rüdiger, W. (1999). Protochlorophyllide *b* does not occur in barley etioplasts. FEBS Lett. **445,** 445-448.

Schuler, M.A. (1996). Plant cytochrome P450 monooxygenases. Critical Rev. Plant Sci. **15,** 235-284.

Schuler, M.A., Duan, H., Bilgin, M., and Ali, S. (2006). *Arabidopsis* cytochrome P450s through the looking glass: a window on plant biochemistry. Phytochem. Rev. **5,** 205-237.

Sessions, A., Burke, E., Presting, G., Aux, G., McElver, J., Patton, D., Dietrich, B., Ho, P., Bacwaden, J., Ko, C., Clarke, J.D., Cotton, D., Bullis, D., Snell, J., Miguel, T., Hutchison, D., Kimmerly, B., Mitzel, T., Katagiri, F., Glazebrook, J., Law, M., and Goff, S.A. (2002). A high-throughput Arabidopsis reverse genetics system. Plant Cell **14,** 2985-2994.

Stengel, A., Soll, J., and Bölter, B. (2007). Protein import into chloroplasts: new aspects of a well-known topic. Biol. Chem. **388,** 765-772.

Stengel, A., Benz, P., Balsera, M., Soll, J., and Bölter, B. (2008). TIC62 redox-regulated translocon composition and dynamics. J. Biol. Chem. **283,** 6656-6667.

Stengel, A., Benz, J.P., Buchanan, B.B., Soll, J., and Bölter, B. (2009). Preprotein import into chloroplasts via the Toc and Tic complexes is regulated by redox signals in *Pisum sativum*. Mol. Plant **2,** 1181-1197.

Süssenbacher, I., Christ, B., Hörtensteiner, S., and Kräutler, B. (2015). Hydroxymethylated phyllobilins in senescent *Arabidopsis thaliana* leaves - sign of a puzzling intermezzo of chlorophyll breakdown. Chem.-Eur. J. **21,** 11664-11670.

Tanaka, A., Ito, H., Tanaka, R., Tanaka, N.K., Yoshida, K., and Okada, K. (1998). Chlorophyll *a* oxygenase (*CAO*) is involved in chlorophyll *b* formation from chlorophyll *a*. Proc. Natl. Acad. Sci. USA **95,** 12719-12723.

Tusnády, G.E., and Simon, I. (2001). The HMMTOP transmembrane topology prediction server. Bioinformatics **17,** 849-850.

Wüthrich, K.L., Bovet, L., Hunziker, P.E., Donnison, I.S., and Hörtensteiner, S. (2000). Molecular cloning, functional expression and characterisation of RCC reductase involved in chlorophyll catabolism. Plant J. **21,** 189-198.

Xodo, L.E., Rapozzi, V., Zacchigna, M., Drioli, S., and Zorzet, S. (2012). The chlorophyll catabolite pheophorbide *a* as a photosensitizer for the photodynamic therapy. Curr Med Chem **19,** 799-807.

FIGURE LEGENDS

Figure 1. *p*FCC and Hydroxy-*p*FCC Accumulate in Gerontoplasts of Arabidopsis.

(A) Extracted ion chromatograms (EICs) of intact and broken gerontoplasts incubated with MES16. In intact gerontoplasts, *p*FCC (EIC 629.2977±0.01) and hydroxy-*p*FCC (EIC 645.2929±0.01) are not demethylated by the added MES16. However, in broken gerontoplasts, MES16 can access both as substrate, leading to the formation of demethylated products (EIC 615.2827 and EIC 631.2777, respectively). Thus, *p*FCC hydroxylation occurs inside the chloroplast.
(B) and (**C**) MS (top panel) and MS/MS spectra (bottom panel) of *epi*-*p*FCC [EIC 629.2980±0.01 (**B**)] and hydroxy-*epi*-*p*FCC [EIC 645.2929±0.01 (**C**)]. Constitutional formulae and MS/MS fragmentation sites are shown. $[M+H]^+$ indicates the precursor ion.

Figure 2. *In vitro* Formation of Hydroxy-*epi*-*p*FCC from *epi*-*p*FCC in Bell Pepper Chromoplast Extracts.

(A) *In vitro* assay for the production of *epi*-*p*FCC from pheophorbide *a* using a bell pepper chromoplast extract. Besides *epi*-*p*FCC, the HPLC chromatogram shows a small, polar peak that was identified as hydroxy-*epi*-*p*FCC.
(B) Time-dependent synthesis of hydroxy-*epi*-*p*FCC from *epi*-*p*FCC in an assay that is identical to the one used in (**A**) for the production of *epi*-*p*FCC from pheophorbide *a*.
(C). HPLC-based confirmation of the product of the *in vitro* hydroxylation assay as hydroxy-*epi*-*p*FCC. Chromatograms from top: gerontoplast extracts from *acd2-2*+*At*-RCCR (Pružinská et al., 2007) that produces *p*FCC and hydroxy-*p*FCC; gerontoplast extracts from *acd2-2*+*At*-RCCR-X (Pružinská et al., 2007) that produces *epi*-*p*FCC and hydroxy-*epi*-*p*FCC; *in vitro* assay after 40 min of incubation; co-injection of *acd2-2*+*At*-RCCR-X and the assay, yielding a single polar peak that corresponds to hydroxy-*epi*-*p*FCC.

Figure 3. $^{18}O_2$-Labelling of Phyllobilins during Col-0 Leaf Senescence.

MS spectra of selected DNCCs (**A**) and NCCs (**B**) produced in the presence of ambient air ($^{16}O_2$; top spectra) or in an $^{18}O_2$ atmosphere (bottom spectra). Note that in the presence of $^{18}O_2$ $C3^2$-hydroxylated phyllobilins (e.g. DNCC_618 and NCC_630) carry two labeled oxygens, while non-hydroxylated phyllobilins (e.g. DNCC_602 and NCC_614) only carry one. This confirms that the $C3^2$ hydroxyl group-oxygen is derived from molecular oxygen.

Figure 4. Biochemical Characterization of *epi-p*FCC Hydroxylation.

(A). *In vitro* hydroxylation assays with *epi-p*FCC as substrate were performed in different atmospheric conditions as indicated. Note that absence of oxygen largely inhibits *epi-p*FCC formation, thus confirming the molecular oxygen incorporation shown in Figure 3. Note also that CO treatment does not affect *epi-p*FCC formation, likely excluding the respective enzyme to be a cytochrome P450 monooxygenase.
(B) Fractionation of the *epi-p*FCC hydroxylating activity in bell pepper extracts. Fractionation at low centrifugation speed (15'000*g*) into a soluble (*Supernatant*) and membrane (*Pellet*) fraction was unable to clearly separate the activity; however, subsequent twofold ultracentrifugation (UC) (150'000*g*) of the *Supernatant* fraction uncovered the activity to reside in chromoplast membranes (*1xUC*- and *2xUC-Membrane*), while no activity was found in respective supernatants (*1xUC*- and *2xUC-Stroma*).
(C) *epi-p*FCC hydroxylation depends on ferredoxin. Co-factor requirement was analyzed in assays using the *2xUC-Membrane* fraction of (**B**) and added factors as indicated. *All cofactors* are ferredoxin (Fd), NADPH, glucose-6-phosphate (G-6-P) and G-6-P dehydrogenase (GDH). Note that in the absence of Fd little activity was retained, likely because of the presence of residual amounts of Fd in the *2xUC-Membrane* fraction. Data are the mean of three replicates. Error bars indicate SD.

Figure 5. Protein Alignment, and Analysis of Subcellular Localization of the Arabidopsis Rieske-type Oxygenases TIC55, PTC52 and PAO.

(A) Sequence alignment of Arabidopsis TIC55, PTC52 and PAO. Sequences were aligned using the program DIALIGN. Dark gray shading highlights residues identical between all three proteins, light gray shading highlights residues identical between two proteins, with Blosum62

similarity groups enabled. The following colored domains are boxed: green, Rieske center; blue, mononuclear iron site; purple, predicted transmembrane domains. The predicted cleavage sites of chloroplast transit peptides are indicated with red lines.
(B) Localization of Rieske-type oxygenase-green fluorescent protein (GFP) fusion proteins in protoplasts isolated from senescent Arabidopsis wild-type leaves. GFP fluorescence (column 1) and chlorophyll autofluorescence (column 2) were examined by confocal laser scanning microscopy. Column 3, merge of GFP and chlorophyll fluorescence; column 4, bright field image. Bars = 20 μm.

Figure 6. Phyllobilin Analysis of *tic* and *ptc52* Mutants.

Abundances of phyllobilins were determined by LC-MS/MS analysis according to a published method (Christ et al., 2016) and are shown as relative values. Data are the mean of four biological replicates. Error bars indicate SD.
(**A**)-(**E**) Phyllobilin abundance in short-day-grown *tic55* and *ptc52* mutants after senescence induction for 5 d. Note the different scale used in (**C**) and (**D**) because of the low abundance of glucosylated and demethylated phyllobilins.
(**F**) Abundance of hydroxylated phyllobilins in a *tic32* and *tic62* mutant.

Figure 7. Phyllobilin Distribution and Phylogenetic Analysis of Rieske-type Oxygenases in Plants.

(A) Phyllobilin hydroxylation (R^1) is a common modification, which is found in DNCCs (red square) and NCCs (green square) of all 20 species analyzed so far for structures of phyllobilins. By contrast, other modifications (R^2-R^4; see DNCC and NCC structures for the position of these modifications) occur in a species-specific manner.
(B) Phylogenetic analysis of Arabidopsis TIC55 (yellow asterisk), PAO (blue asterisk) and PTC52 (red asterisk) homologs in plants. Note that except a few (black lines), most of the 204 protein sequences compared in this analysis cluster in one of three distinct clades. Also note that for each species at least one Rieske-type oxygenase protein is located within each clade. The tree was generated with the neighborhood joining method using MEGA7 (Kumar et al., 2016). Important nodes separating the three clades are labeled with bootstrap values (% of

1,000 replicates). Acor, *Aquilegia coerulea;* Alyr, *Arabidopsis lyrata;* Atha, *Arabidopsis thaliana;* Atri, *Amborella trichopoda;* Bdis, *Brachypodium distachon;* Brap, *Brassica rapa;* Bsta, *Brachypodium stacei;* Bstr, *Boechera stricta;* Ccle, *Citrus clementina;* Cgra, *Capsella grandiflora;* Cpap, *Carica papaya;* Crub, *Capsella rubella;* Csat, *Cucumis sativus;* Csin, *Citrus sinensis;* Egra, *Eucalyptus grandis;* Esal, *Eutrema salsugineum;* Fves, *Fragaria vesca;* Gmax, *Glycine max;* Grai, *Gossypium raimondii;* Kfla, *Klebsormidium flaccidum;* Kmar, *Kalanchoe marnieriana;* Lusi, *Linum usitatissimum;* Macu, *Musa acuminata;* Mdom, *Malus domstica;* Mesc, *Manihot esculenta;* Mgut, *Mimulus guttatus;* Mtru, *Medicago truncatula;* Osat, *Oryza sativa;* Phal, *Panicum hallii;* Ppat, *Physcomitrella patens;* Pper, *Prunus persica;* Ptri, *Populus trichocarpa;* Pvir, *Panicum virgatum;* Pvul, *Phaseolus vulgaris;* Rcom, *Ricinus communis;* Sbic, *Sorghum bicolor;* Sfal, *Sphagnum fallax;* Sita, *Setaria italica;* Slyc, *Solanum lycopersicum;* Some, *Selaginella moellendorffii;* Spol, *Spirodela polyrhiza;* Spur, *Salix purpurea;* Stub, *Solanum tuberosum;* Svir, *Setaria viridis;* Tcac, *Theobroma cacao;* Vvin, *Vitis vinifera;* Zmay, *Zea mays*.

Figure 8. Topographical Model of the Chlorophyll Breakdown Pathway Integrating the Findings of This Work.

The model shows the subcellular localization of *p*FCC-modifying activities, i.e. CYP89A9 (deformylation), MES16 (demethylation) and TIC55 (hydroxylation). Note, that all the reactions involved in converting chlorophyll to *p*FCC, including pheophorbide *a* oxygenase (PAO) the name-giving key enzyme of the PAO/phyllobilin pathway are not shown, but have been considered to form a highly dynamic complex at the thylakoid membrane to prevent release into the stroma of potentially phototoxic breakdown intermediates upstream of *p*FCC (Sakuraba et al., 2012). Note also that due to the fact that non-hydroxylated phyllobilin occur in wild-type *Arabidopsis*, a fraction of *p*FCC likely leaves the chloroplast without hydroxylation. As indicated by question marks, the molecular identity of phyllobilin transporters at the chloroplast envelope and the tonoplast is unknown. DFCC, dioxobilin-type fluorescent chlorophyll catabolites; DNCC, dioxobilin-type nonfluorescent chlorophyll catabolites; ER, endoplasmic reticulum; FCC, formyloxobilin-type fluorescent chlorophyll catabolites; NCC, formyloxobilin-type nonfluorescent chlorophyll catabolites; *p*FCC, *primary* fluorescent chlorophyll catabolite.

Figure 1

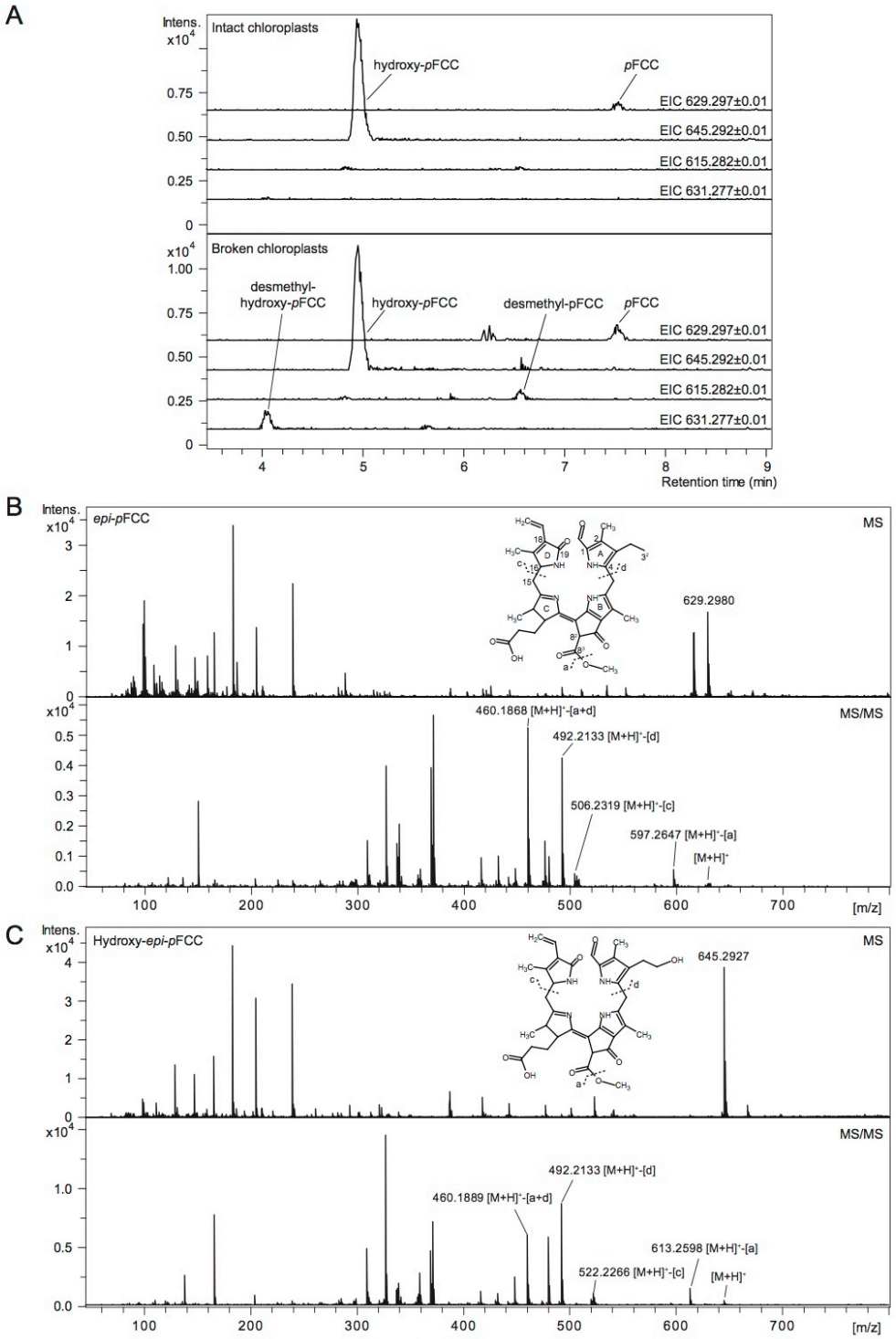

Figure 1. *p*FCC and Hydroxy-*p*FCC Accumulate in Gerontoplasts of Arabidopsis.

(A) Extracted ion chromatograms (EICs) of intact and broken gerontoplasts incubated with MES16. In intact gerontoplasts, *p*FCC (EIC 629.2977±0.01) and hydroxy-*p*FCC (EIC 645.2929±0.01) are not demethylated by the added MES16. However, in broken gerontoplasts, MES16 can access both as substrate, leading to the formation of demethylated products (EIC 615.2827 and EIC 631.2777, respectively). Thus, *p*FCC hydroxylation occurs inside the chloroplast.
(B) and **(C)** MS (top panel) and MS/MS spectra (bottom panel) of *p*FCC [EIC 629.2980±0.01 **(B)**] and hydroxy-*p*FCC [EIC 645.2929±0.01 **(C)**]. Constitutional formulae and MS/MS fragmentation sites are shown. $[M+H]^+$ indicates the precursor ion.

Figure 2

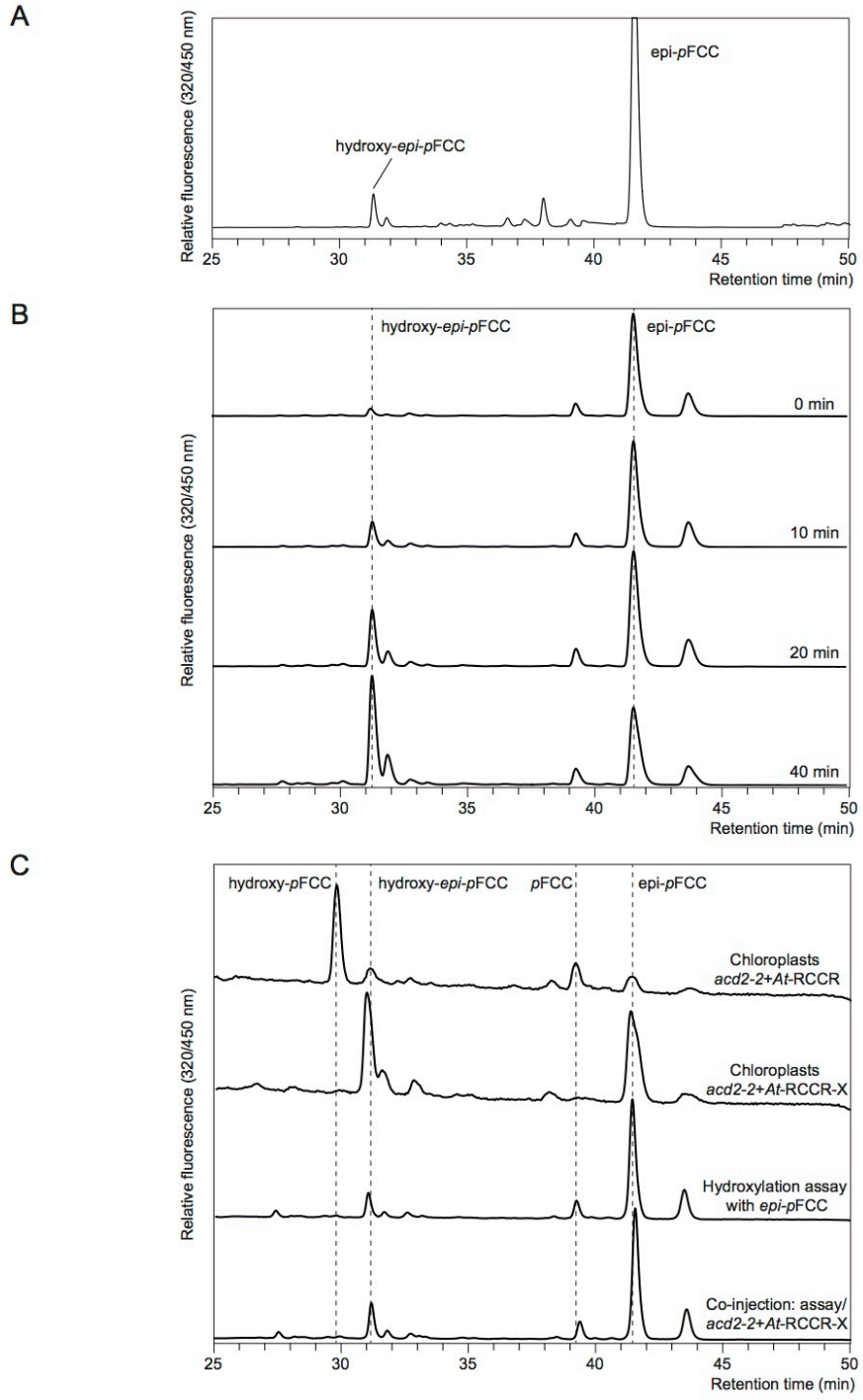

Figure 2. *In Vitro* Formation of Hydroxy-*epi*-*p*FCC from *epi*-*p*FCC in Bell Pepper Chromoplast Extracts.

(A) *In vitro* assay for the production of *epi*-*p*FCC from pheophorbide *a* using a bell pepper chromoplast extract. Besides *epi*-*p*FCC, the HPLC chromatogram shows a small, polar peak that was identified as hydroxy-*epi*-*p*FCC.
(B) Time-dependent synthesis of hydroxy-*epi*-*p*FCC from *epi*-*p*FCC in an assay that is identical to the one used in **(A)** for the production of *epi*-*p*FCC from pheophorbide *a*.
(C) HPLC-based confirmation of the product of the *in vitro* hydroxylation assay as hydroxy-*epi*-*p*FCC. Chromatograms from top: gerontoplast extracts from *acd2-2+At*-RCCR (Pružinská et al., 2007) that produces *p*FCC and hydroxy-*p*FCC; gerontoplast extracts from *acd2-2+At*-RCCR-X (Pružinská et al., 2007) that produces *epi*-*p*FCC and hydroxy-*epi*-*p*FCC; *in vitro* assay after 40 min of incubation; co-injection of *acd2-2+At*-RCCR-X and the assay, yielding a single polar peak that corresponds to hydroxy-*epi*-*p*FCC.

Figure 3

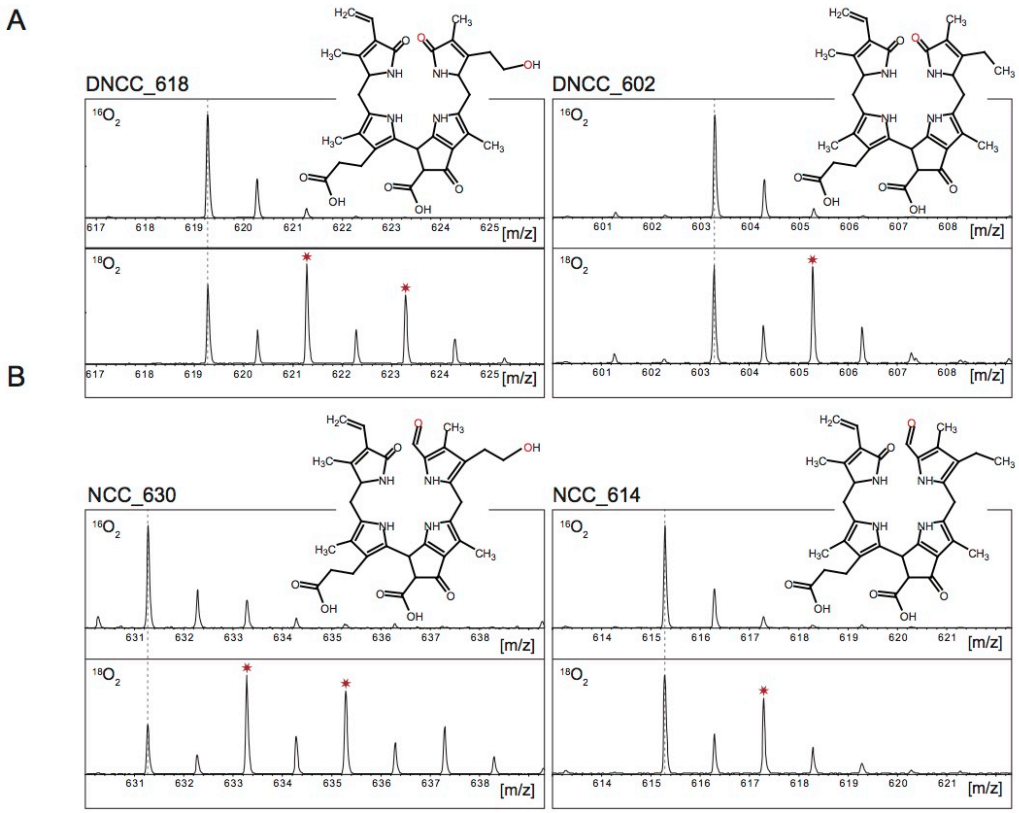

Figure 3. $^{18}O_2$-Labelling of Phyllobilins during Col-0 Leaf Senescence.

MS spectra of selected DNCCs **(A)** and NCCs **(B)** produced in the presence of ambient air ($^{16}O_2$; top spectra) or in an $^{18}O_2$ atmosphere (bottom spectra). Note that in the presence of $^{18}O_2$ $C3^2$-hydroxylated phyllobilins (e.g. DNCC_618 and NCC_630) carry two labeled oxygens, while non-hydroxylated phyllobilins (e.g. DNCC_602 and NCC_614) only carry one. This confirms that the $C3^2$ hydroxyl group-oxygen is derived from molecular oxygen.

Figure 4

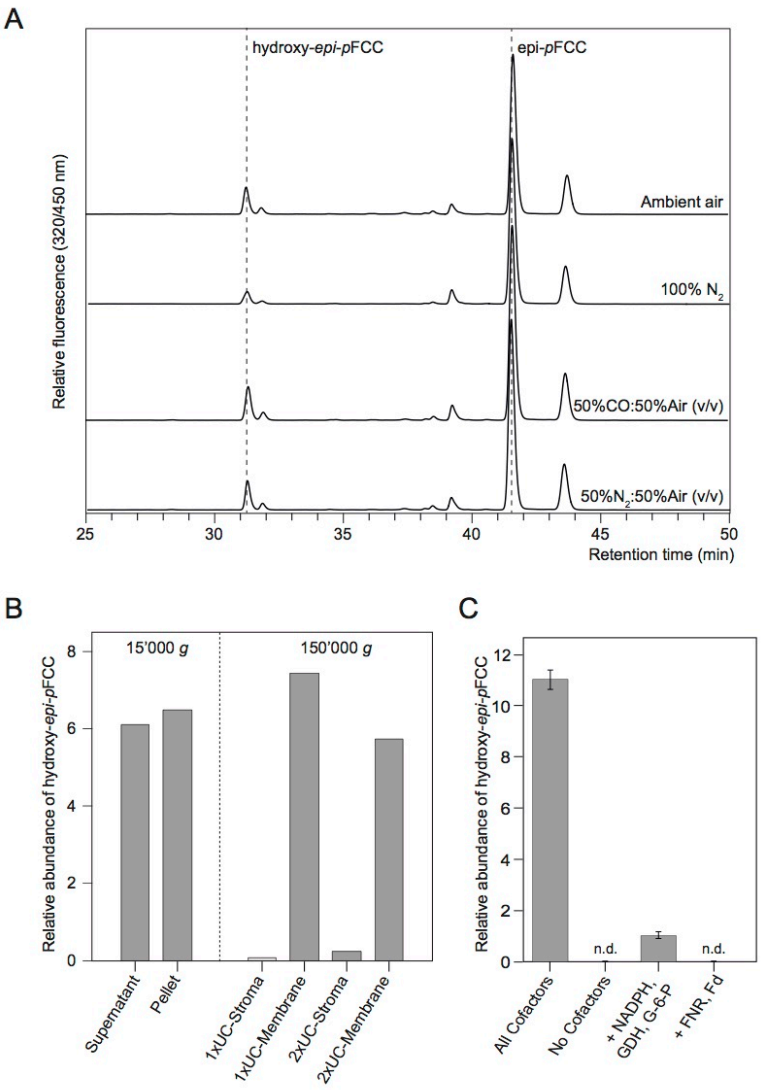

Figure 4. Biochemical Characterization of *epi-p*FCC Hydroxylation.

(A) *In vitro* hydroxylation assays with *epi-p*FCC as substrate were performed in different atmospheric conditions as indicated. Note that absence of oxygen largely inhibits *epi-p*FCC formation, thus confirming the molecular oxygen incorporation shown in Figure 3. Note also that CO treatment does not affect *epi-p*FCC formation, likely excluding the respective enzyme to be a cytochrome P450 monooxygenase.
(B) Fractionation of the *epi-p*FCC hydroxylating activity in bell pepper extracts. Fractionation at low centrifugation speed (15'000*g*) into a soluble (*Supernatant*) and membrane (*Pellet*) fraction was unable to clearly separate the activity; however, subsequent twofold ultracentrifugation (UC) (150'000*g*) of the *Supernatant* fraction uncovered the activity to reside in chromoplast membranes (*1xUC-* and *2xUC-Membrane*), while no activity was found in respective supernatants (*1xUC-* and *2xUC-Stroma*).
(C) *epi-p*FCC hydroxylation depends on ferredoxin. Co-factor requirement was analyzed in assays using the *2xUC-Membrane* fraction of **(B)** and added factors as indicated. All cofactors are ferredoxin (Fd), NADPH, glucose-6-phosphate (G-6-P) and G-6-P dehydrogenase (GDH). Note that in the absence of Fd little activity was retained, likely because of the presence of residual amounts of Fd in the *2xUC-Membrane* fraction. Data are the mean of three replicates. Error bars indicate SD.

Figure 5

A

B

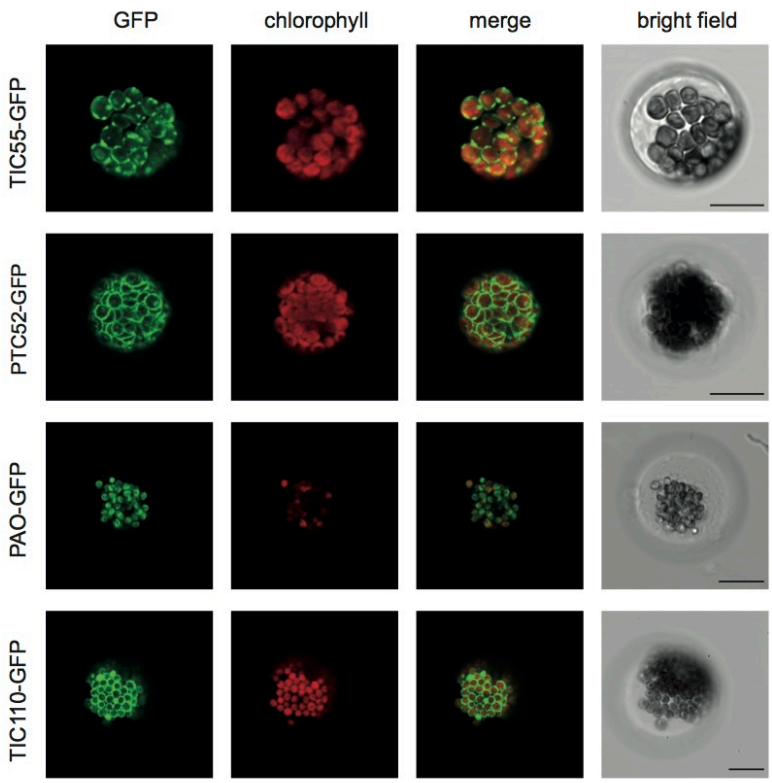

Figure 5. Protein Alignment, and Analysis of Subcellular Localization of the Arabidopsis Rieske-type Oxygenases TIC55, PTC52 and PAO.

(A) Sequence alignment of Arabidopsis TIC55, PTC52 and PAO. Sequences were aligned using the program DIALIGN. Dark gray shading highlights residues identical between all three proteins, light gray shading highlights residues identical between two proteins, with Blosum62 similarity groups enabled. The following colored domains are boxed: green, Rieske center; blue, mononuclear iron site; purple, predicted transmembrane domains. The predicted cleavage sites of chloroplast transit peptides are indicated with red lines.
(B) Localization of Rieske-type oxygenase-green fluorescent protein (GFP) fusion proteins in protoplasts isolated from senescent Arabidopsis wild type leaves. GFP fluorescence (column 1) and chlorophyll autofluorescence (column 2) were examined by confocal laser scanning microscopy. Column 3, merge of GFP and chlorophyll fluorescence; column 4, bright field image. Bars = 20 µm.

Figure 6

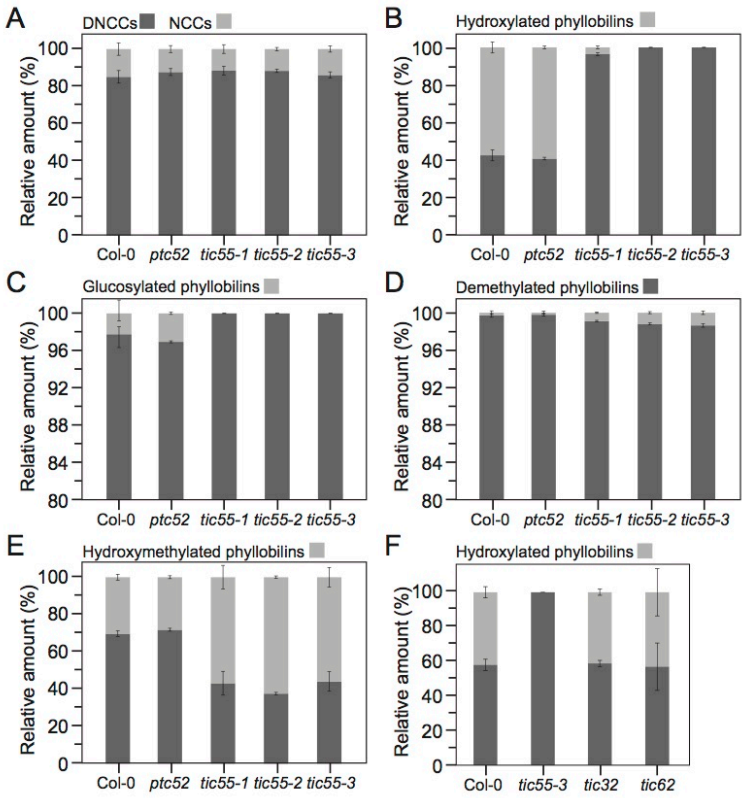

Figure 6. Phyllobilin Analysis of *tic* and *ptc52* Mutants.

Abundances of phyllobilins were determined by LC-MS/MS analysis according to a published method (Christ et al., 2016) and are shown as relative values. Data are the mean of four biological replicates. Error bars indicate SD.
(A)-**(E)** Phyllobilin abundance in short-day-grown *tic55* and *ptc52* mutants after senescence induction for 5 d. Note the different scale used in **(C)** and **(D)** because of the low abundance of glucosylated and demethylated phyllobilins.
(F) Abundance of hydroxylated phyllobilins in a *tic32* and *tic62* mutant.

Figure 7

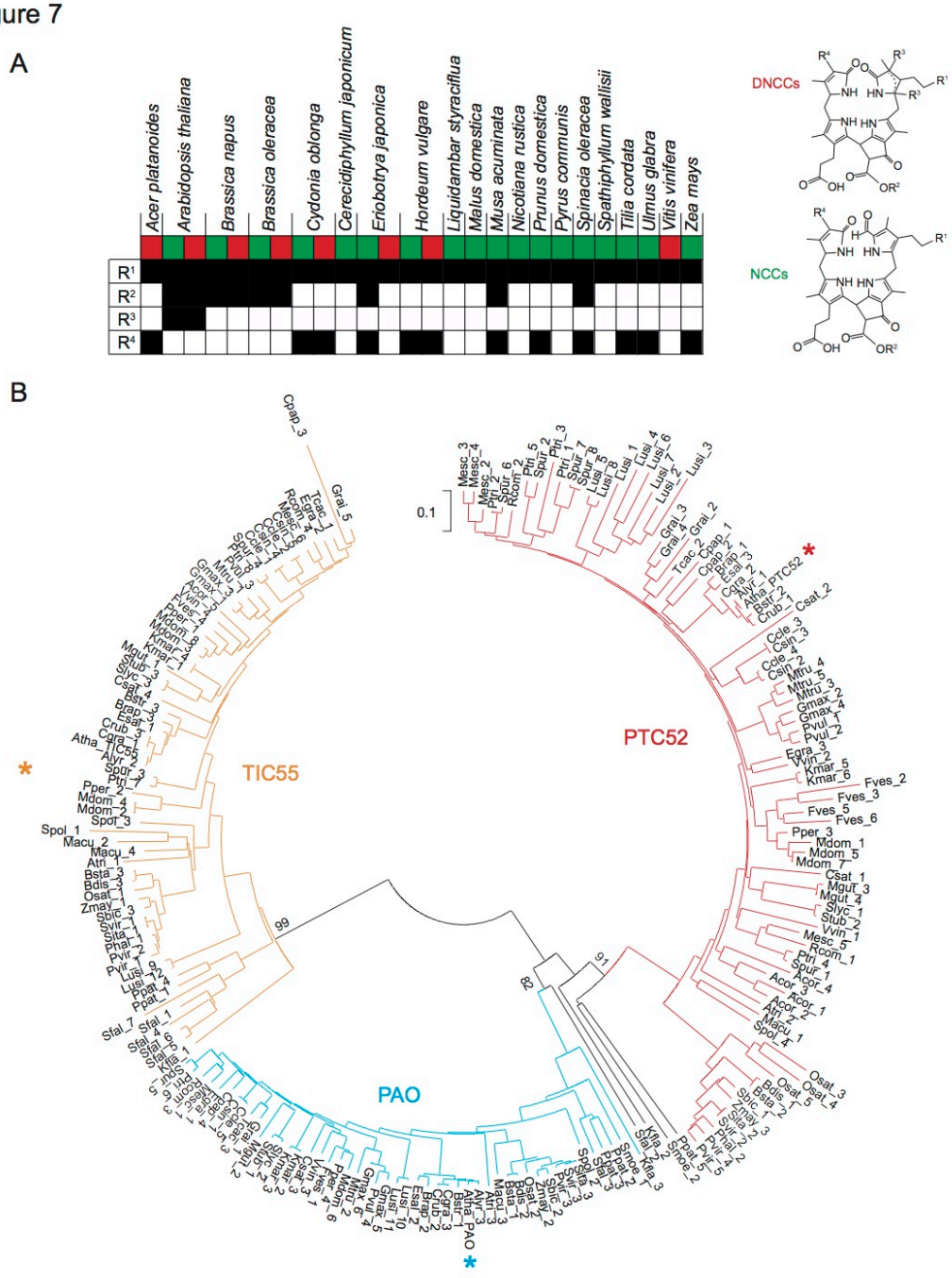

Figure 7. Phyllobilin Distribution and Phylogenetic Analysis of Rieske-type Oxygenases in Plants.

(A) Phyllobilin hydroxylation (R^1) is a common modification, which is found in DNCCs (red square) and NCCs (green square) of all 20 species analyzed so far for structures of phyllobilins. By contrast, other modifications (R^2-R^4; see DNCC and NCC structures for the position of these modifications) occur in a species-specific manner.
(B) Phylogenetic analysis of Arabidopsis TIC55 (yellow asterisk), PAO (blue asterisk) and PTC52 (red asterisk) homologs in plants. Note that except a few (black lines), most of the 204 protein sequences compared in this analysis cluster in one of three distinct clades. Also note that for each species at least one Rieske-type oxygenase protein is located within each clade. The tree was generated with the neighborhood joining method using MEGA7 (Kumar et al., 2016). Important nodes separating the three clades are labeled with bootstrap values (% of 1,000 replicates). Acor, *Aquilegia coerulea*; Alyr, *Arabidopsis lyrata*; Atha, *Arabidopsis thaliana*; Atri, *Amborella trichopoda*; Bdis, *Brachypodium distachon*; Brap, *Brassica rapa*; Bsta, *Brachypodium stacei*; Bstr, *Boechera stricta*; Ccle, *Citrus clementina*; Cgra, *Capsella grandiflora*; Cpap, *Carica papaya*; Crub, *Capsella rubella*; Csat, *Cucumis sativus*; Csin, *Citrus sinensis*; Egra, *Eucalyptus grandis*; Esal, *Eutrema salsugineum*; Fves, *Fragaria vesca*; Gmax, *Glycine max*; Grai, *Gossypium raimondii*; Kfla, *Klebsormidium flaccidum*; Kmar, *Kalanchoe marnieriana*; Lusi, *Linum usitatissimum*; Macu, *Musa acuminata*; Mdom, *Malus domstica*; Mesc, *Manihot esculenta*; Mgut, *Mimulus guttatus*; Mtru, *Medicago truncatula*; Osat, *Oryza sativa*; Phal, *Panicum hallii*; Ppat, *Physcomitrella patens*; Pper, *Prunus persica*; Ptri, *Populus trichocarpa*; Pvir, *Panicum virgatum*; Pvul, *Phaseolus vulgaris*; Rcom, *Ricinus communis*; Sbic, *Sorghum bicolor*; Sfal, *Sphagnum fallax*; Sita, *Setaria italica*; Slyc, *Solanum lycopersicum*; Some, *Selaginella moellendorffii*; Spol, *Spirodela polyrhiza*; Spur, *Salix purpurea*; Stub, *Solanum tuberosum*; Svir, *Setaria viridis*; Tcac, *Theobroma cacao*; Vvin, *Vitis vinifera*; Zmay, *Zea mays*.

Figure 8

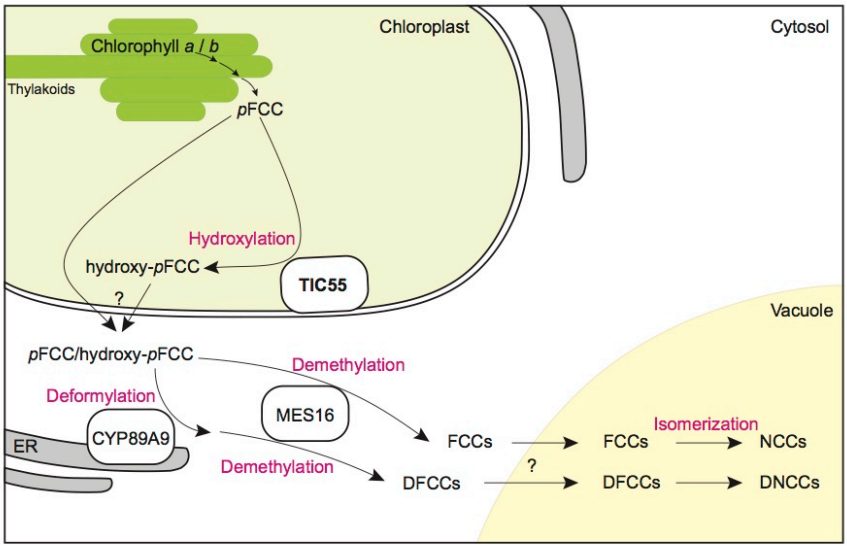

Figure 8. Topographical Model of the Chlorophyll Breakdown Pathway Integrating the Findings of this Work.

The model shows the subcellular localization of *p*FCC-modifying activities, i.e. CYP89A9 (deformylation), MES16 (demethylation) and TIC55 (hydroxylation). Note, that all the reactions involved in converting chlorophyll to *p*FCC, including pheophorbide *a* oxygenase (PAO) the name-giving key enzyme of the PAO/phyllobilin pathway are not shown, but have been considered to form a highly dynamic complex at the thylakoid membrane to prevent release into the stroma of potentially phototoxic breakdown intermediates upstream of *p*FCC (Sakuraba et al., 2012). Note also that due to the fact that non-hydroxylated phyllobilin occur in wild type Arabidopsis, a fraction of *p*FCC likely leaves the chloroplast without hydroxylation. As indicated by question marks, the molecular identity of phyllobilin transporters at the chloroplast envelope and the tonoplast is unknown. DFCC, dioxobilin-type fluorescent chlorophyll catabolites; DNCC, dioxobilin-type nonfluorescent chlorophyll catabolites; ER, endoplasmic reticulum; FCC, formyloxobilin-type fluorescent chlorophyll catabolites; NCC, formyloxobilin-type nonfluorescent chlorophyll catabolites; *p*FCC, primary fluorescent chlorophyll catabolite.

Supplemental Figure 1

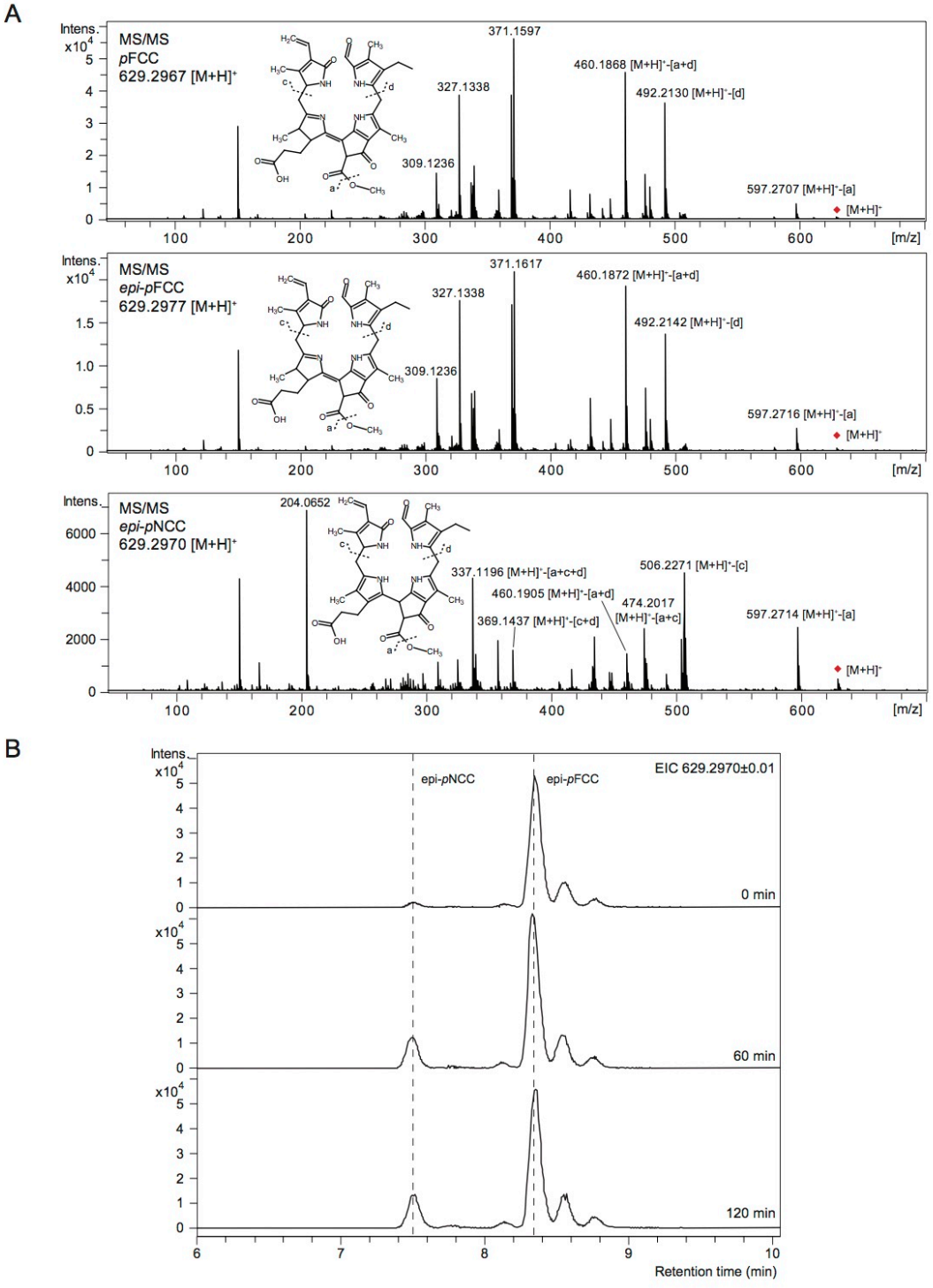

Supplemental Figure 1. Confirmation of *epi*-*p*FCC and *p*FCC Identity and *epi*-*p*FCC-to-*epi*-*p*NCC Isomerization.

(A) MS/MS fragmentation spectra of *p*FCC (top panel; obtained from extracts of *acd2-2+At*-RCCR chloroplasts; see Figure 2C) and *epi*-*p*FCC [middle panel; used for acid-catalyzed isomerization; see panel **(B)** 0 min] are identical, but distinct from *epi*-*p*NCC [bottom panel; product of acid-catalyzed isomerization; see panel **(B)** 120 min]. Constitutional formulae and MS/MS fragmentation sites are shown. $[M+H]^+$ indicates the precursor ion.
(B) *epi*-*p*FCC-to- *epi*-*p*NCC isomerization assay. Purified *epi*-*p*FCC obtained from PAO/RCCR assays was incubated at pH 5 for up to 120 min and analyzed by LC-MS. Extracted ion chromatograms at 629.2977±0.01 are shown.

Supplemental Figure 2

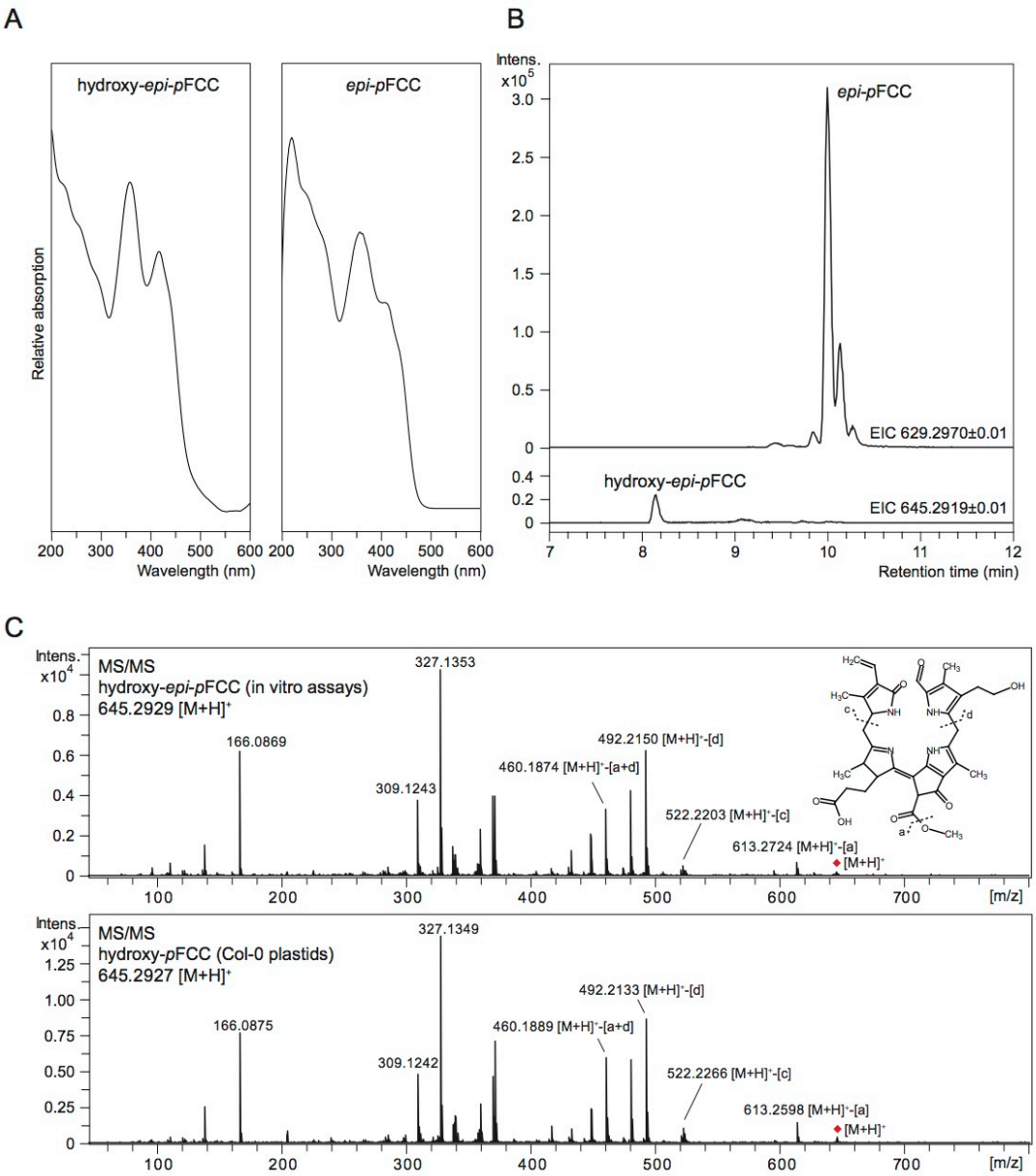

Supplemental Figure 2. LC-MS Confirmation of Hydroxy-*epi*-*p*FCC.

(A) Absorption spectra of hydroxy-*epi*-*p*FCC (left) and *epi*-*p*FCC (right) obtained from PAO/RCCR assays (see Figure 2A).
(B) A hydroxylation assay after 40 min incubation (see Figure 2B) was analyzed by LC-MS/MS. Extracted ion chromatograms (EIC) for *epi*-*p*FCC (629.2977±0.01) and hydroxy-*epi*-*p*FCC (645.2929±0.01) are shown.
(C) MS/MS spectra of hydroxy-*epi*-*p*FCC [obtained from the in vitro assay shown in panel **(B)**] and hydroxy-**p**FCC (obtained from wild type Arabidopsis gerontoplasts; see Figure 1A) are shown. Note that the MS/MS spectra are highly similar.

Supplemental Figure 3

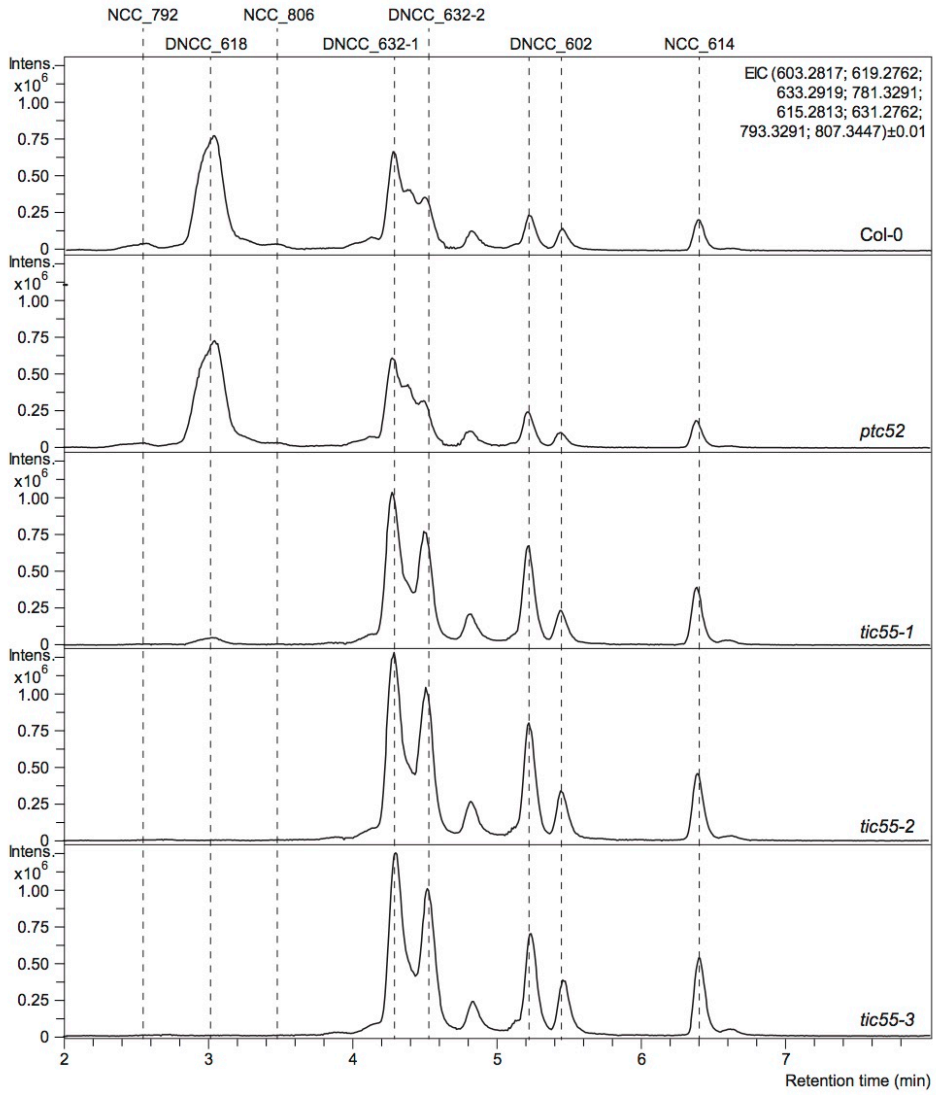

Supplemental Figure 3.LC-MS Analysis of Phyllobilins from Col-0 and Rieske-type Oxygenase Mutants.

Leaves of short-day-grown plants after 5 d of dark-induced senescence were extracted and analyzed by LC-MS. Extracted ion chromatograms (EICs) for masses of phyllobilins known to occur in Col-0 (Christ et al., 2016) are shown. Note that the phyllobilin patterns are highly similar between wild type and *ptc52*, but distinct in all three *tic55* mutants. Thus, the most abundant hydroxylated phyllobilin (DNCC_618) is absent in *tic55-2* and *tic55-3*, and highly reduced in *tic55-1*.

Supplemental Figure 4

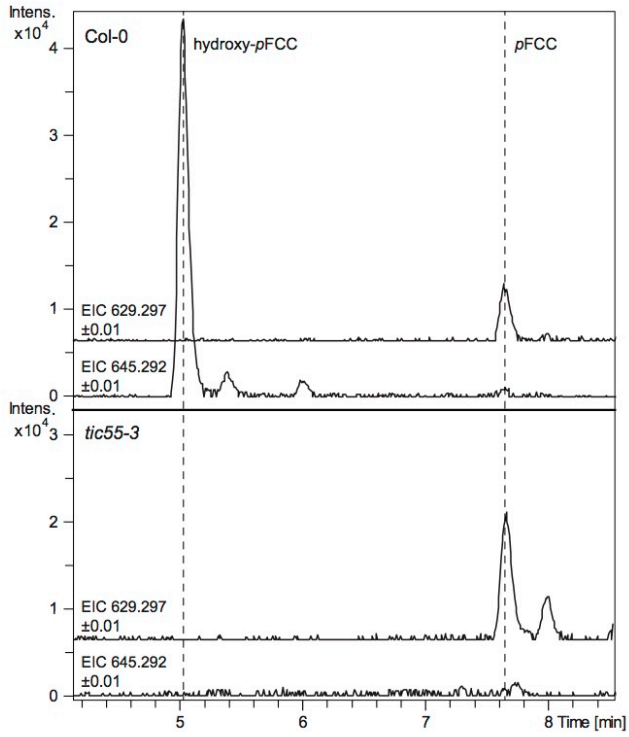

Supplemental Figure 4. Hydroxy-*p*FCC is absent from *tic55-3* Gerontoplasts.

Extracted ion chromatograms (EICs) of *p*FCC (EIC 629.2977±0.01) and hydroxy-*p*FCC (EIC 645.2929±0.01) of gerontoplasts of wild type (Col-0) and *tic55-3* are shown. Note the absence of hydroxy-*p*FCC from the mutant.

MANUSCRIPT 2

Chlorophyll and chlorophyll catabolite analysis by HPLC

Aditi Das[1], Luzia Guyer[1] and Stefan Hörtensteiner*

Institute of Plant Biology, University of Zurich, Zollikerstrasse 107, CH-8008 Zurich, Switzerland

[1] these authors contributed equally to this work

*corresponding author: shorten@botinst.uzh.ch +41 44 634 82 82

Submitted to Methods in Molecular Biology

Chlorophyll and chlorophyll catabolite analysis by HPLC

Aditi Das[1], Luzia Guyer[1] and Stefan Hörtensteiner*

Institute of Plant Biology, University of Zurich, Zollikerstrasse 107, CH-8008 Zurich, Switzerland

[1] these authors contributed equally to this work

*corresponding author:

shorten@botinst.uzh.ch

+41 44 634 82 82

Running title: Chlorophyll catabolite analysis

Abstract

The most obvious event of leaf senescence is the loss of chlorophyll. Chlorophyll degradation proceeds in a well-characterized pathway that, although being common to higher plants, yields a species-specific set of chlorophyll catabolites, termed phyllobilins. Analysis of chlorophyll degradation and phyllobilin accumulation by high performance liquid chromatography (HPLC) is a valuable tool to investigate senescence processes in plants. In this chapter, methods for the extraction, separation and quantification of chlorophyll and its degradation products are described. Because of their different physicochemical properties, chlorin-type pigments (chlorophylls and magnesium-free pheo-pigments) and phyllobilins (linear tetrapyrroles) are analyzed separately. Specific spectral properties and polarity differences allow the identification of the different classes of known chlorins and phyllobilins. The methods provided facilitate the analysis of chlorophyll degradation and the identification of chlorophyll catabolites in a wide range of plant species, in different tissues, and under a variety of physiological conditions that involve loss of chlorophyll.

Key words

Chlorophyll, pheophytin, pheophorbide, phyllobilin, leaf senescence, fruit ripening, HPLC, chlorophyll catabolite

1. Introduction

Chlorophyll, the most abundant plant pigment, absorbs sun light as a key factor for the conversion of solar energy to chemical energy during photosynthesis. At the same time, however, chlorophyll is a potentially phototoxic molecule, whose biosynthesis and degradation has to be tightly regulated. During leaf senescence, when photosynthetic activity diminishes and photosystem protein components are degraded for nitrogen remobilization to other parts of

the plant, chlorophyll is metabolized for its detoxification. Breakdown of chlorophyll has been used as a diagnostic tool for induction and progression of leaf senescence, but also for monitoring other processes of plant development, such as fruit ripening and seed maturation, and as plants' responses to biotic and abiotic stress challenge.

In recent years, a pathway of chlorophyll breakdown has been elucidated that converts chlorophylls, green-colored tetrapyrroles with a chlorin ring structure, to colorless, linear tetrapyrroles termed phyllobilins [1]. This pathway consists of several enzymatic steps that produce different short-lived catabolite intermediates and a plant species-specific set of phyllobilins that ultimately accumulate in the vacuole of senescing cells [2,3]. The series of intermediary and final catabolites is depicted in Fig. 1. The pathway is structured into two parts: (i) reactions from chlorophyll to a *primary* fluorescent chlorophyll catabolite (*p*FCC) that are localized in the chloroplast and commonly occur in all plant species investigated so far [4], and (ii) species-specific, largely cytosolic, reactions that site-specifically modify peripheral positions of *p*FCC and that give rise to the more or less complex pattern of phyllobilins detectable in a given species [5-7]. The majority of phyllobilins that accumulate are nonfluorescent, because fluorescent precursors rather quickly isomerize to their nonfluorescent equivalents within the vacuole due the low pH of the vacuolar sap [8,6]. Exceptions are so-called *hypermodified* FCCs found in a few species, in which modification of the propionyl side chain (Fig. 1) prevents efficient isomerization to their respective nonfluorescent equivalents [9,10]. Two major classes of phyllobilins are distinguished, that are, formyloxobilin-type (FCCs and NCCs) and dioxobilin-type tetrapyrroles (DFCCs and DNCCs) (Fig. 1) [7], the latter of which are (formally) derived from the former ones through an oxidative deformylation [6]. In some cases, NCCs were shown to be oxidized to yellow chlorophyll catabolites [11].

Along the pathway of degradation, polarity of chlorophyll catabolites increases together with a general shift of absorption towards shorter wavelengths [3,7]. These features allow (i) the

separation of chlorophyll catabolites by reversed-phase HPLC, (ii) the identification of different groups of catabolites based on their characteristic UV/Vis absorption spectra (Fig. 1) and (iii) the quantification of several groups of compounds for which standards are available or can relatively easy been produced.

In this chapter, two methods for the separation, identification and quantification of either chlorin- or phyllobilin-structured chlorophyll catabolites are described.

2. Materials

2.1. Solvents and chemicals

1. Analytical grade chemicals used for pigment extraction and/or HPLC analysis are Tris-HCl, KH_2PO_4, K_2HPO_4 and ammonium acetate. Solvents used for pigment extraction and HPLC are acetone and methanol (MeOH) of HPLC grade and milli-Q water (18 MΩ).
2. Phyllobilin standards are not commercially available. *Cj*-NCC-1 is the major nonfluorescent chlorophyll catabolite from senescent leaves of *Cercidiphyllum japonicum*, a deciduous tree grown in many gardens and parks. *Cj*-NCC-1 can rather easily be isolated and purified by HPLC according to published methods [12] and can be used for NCC quantifications.
3. Several chlorin standards can be purchased from certified suppliers or are isolated from leaf extracts and purified by analytical HPLC as described here or according to published methods (see, for example [13,14]).

2.2. Chlorophyll/phyllobilin extraction

1. *Chlorin extraction buffer*: 0.2 M Tris-HCl pH 8:acetone, 10:90 (v/v) (*see* **Note 1**).

2. *Phyllobilin extraction buffer*: 50 mM potassium phosphate (KPi) buffer pH 7.0:methanol, 25:75 (v/v) (*see* **Note 2**).
3. Liquid nitrogen.
4. Mortars and pestles (*see* **Note 3**).
5. Microcentrifuge tubes (1.5 and 2 mL).
6. Holders for microcentrifuge tubes.
7. Spatula and thumb forceps.
8. Analytical balance.
9. Microcentrifuge.
10. Vortex mixer.
11. Ice.
12. Pipettes and pipette tips.
13. Conical HPLC vials (200-300 µL) and caps.

2.3. HPLC analysis

1. Solvent system for chlorins (*see* **Note 4**).

   Solvent A: 1 M ammonium acetate:MeOH, 20:80 (v/v) (*see* **Notes 5** and **6**).

   Solvent B: acetone:MeOH, 20:80 (v/v).
2. Solvent system for phyllobilins.

   Solvent A: 50 mM KPi, pH 7.0 (*see* **Note 7**).

   Solvent B: MeOH.

   Solvent C: milli-Q water.
3. A remote-controlled HPLC system interfaced with a photodiode array detector with an absorption range between 200 and 700 nm is required (*see* **Note 8**). The HPLC system should contain a pump able to produce a gradient of at least two solvents (*see* **Note 9**)

and a thermostatted column compartment set to 28° C (*see* **Note 10**). To avoid gas formation caused by mixing of solvents, an efficient degasser should be installed with the pump system (*see* **Note 11**).

4. C18 Hypersil ODS columns should be used (for chlorins: 125 x 4.0 mm, 5 µm; for phyllobilins: 250 x 4.6 mm, 5 µm) (*see* **Note 12**)
5. Manual syringe injector with a 50 µL loop and a 50 µL syringe for injection of chlorin extracts (*see* **Note 13**); a coolable autosampler for injection of phyllobilin extracts (*see* **Note 14**).

2.4. Quantification

1. Calibration solutions for chlorins.

   Pure solutions of respective chlorins, prepared at defined concentrations (~ 2 mM) in acetone are used for calibrating HPLC peak absorptions (*see* **Note 15**).

2. Calibration solution for *Cj*-NCC-1 (*see* **Note 16**)

   Cj-NCC-1 (see section 2.1.2.) dissolved in H_2O is quantified spectrophotometrically at 314 nm (log ε_{314} = 4.23; [12]) (*see* **Note 17**). Defined concentrations are used to calibrate HPLC peak absorptions and can be used for quantification of NCCs.

3. Methods

3.1. Extraction of chlorins (*see* **Notes 18** and **19**)

1. Harvest green or senescent plant material (*see* **Note 20**) and immediately flash-freeze in liquid nitrogen. Store at -80° C until use.
2. Grind plant material with mortar and pestle in liquid nitrogen to a fine powder (*see* **Note 21**).

3. Weigh 50-100 mg of plant material into a microcentrifuge tube (pre-cooled in liquid nitrogen) and keep the samples in liquid nitrogen until extraction (*see* **Note 22**).
4. For pigment extraction work on ice at 4° C (*see* **Note 23**). To the frozen plant material add 5-10 volumes of *chlorin extraction buffer* (v/w) and vortex vigorously for around 10 sec until plant material is thawed (*see* **Note 24**).
5. Incubate in the dark (*see* **Note 25**) at -20° C for 2-16 h until all pigments are extracted into the buffer (*see* **Note 26**).
6. Pellet plant extracts by centrifugation for 2 min at 16,000 x *g* and 4° C. Transfer the supernatant into a new microcentrifuge tube and immediately flash-freeze and store in liquid nitrogen until HPLC analysis (*see* **Notes 27** and **28**).

3.2. Extraction of phyllobilins (*see* **Note 18**)

1. Harvest green or senescent plant material (*see* **Note 20**) and immediately flash-freeze in liquid nitrogen. Store at -80° C until use.
2. Grind plant material with mortar and pestle in liquid nitrogen to a fine powder (*see* **Note 21**).
3. Weigh 100-200 mg of plant material into a microcentrifuge tube (pre-cooled in liquid nitrogen) and keep the samples in liquid nitrogen until extraction (*see* **Note 22**).
4. For phyllobilin extraction, add 3 volumes of *phyllobilin extraction buffer* (v/w) and vortex vigorously for about 10-15 seconds until the plant material is thawed and uniformly mixed with the buffer.
5. Sonicate for 10 min in an ice-cooled sonication bath.
6. Centrifuge the mixture at 16,000 x *g* for 5 min and then transfer the supernatant to a new 1.5 mL microcentrifuge tube.

7. Re-centrifuge the supernatant at 16,000 x *g* for 5 min (*see* **Note 29**) and transfer 100-200 µL of the supernatant to a HPLC vial (*see* **Note 30**).

3.3. HPLC analysis and quantification of chlorins (*see* **Note 31**)

1. Remove a sample just prior to injection from liquid nitrogen and thaw it (*see* **Notes 13** and **32**). Inject a defined volume (e.g. 50 µL) into the HPLC system and run the following HPLC program.
2. HPLC program used for chlorin analysis (flow rate 1 ml min^{-1}):

Time [min]	**Solvent A**	**Solvent B**
0	100%	0%
15	0%	100%
25	0%	100%
28	100%	0%
32	100%	0%

3. Calibration: Inject standard solutions of respective chlorins and determine the retention times and absorption spectra. Fig. 1 shows the spectra for different chlorins, and in Table 1, the retention times are listed (*see* **Note 33**). Integrate peak areas of standard solutions with known concentrations (*see* **Note 15**) at 665 nm (*see* **Note 34**) and determine the relation between absorption and amount/concentration.
4. In order to identify the chlorins present in your sample, compare the absorption spectra and retention times of peaks with standard solutions.
5. Integrate the peak areas at 665 nm and convert into amounts/concentrations using the factors calculated with standard solutions.

3.4. HPLC analysis of phyllobilins

1. Place samples in the precooled (7-10° C) autosampler of the HPLC system (*see* **Note 35**). Run the batch of samples by injecting defined volumes (e.g. 50 µL) with the following HPLC program.
2. HPLC program used for phyllobilin analysis (flow rate 1 ml min^{-1}):

Time [min]	**Solvent A**	**Solvent B**	**Solvent C**
0	80%	20%	0%
5	80%	20%	0%
35	40%	60%	0%
45	40%	60%	0%
47	40%	60%	0%
49	0%	100%	0%
54	0%	100%	0%
56	0%	60%	40%
58	80%	20%	0%
60	80%	20%	0%

3. Calibration: Inject defined amounts of *Cj*-NCC-1 standard solutions (see section 2.1.2.) into the HPLC. Integrate peak areas at 315 nm (*see* **Note 36**) and determine the relation between absorption and amount/concentration.
4. To identify the phyllobilins that are present in your sample, screen chromatograms at 254 nm (*see* **Note 36**) and search for peaks that exhibit UV/Vis absorption spectra typical for the different known types of phyllobilins (Fig. 1) (*see* **Note 37**).
5. For quantification of NCCs, integrate the peak areas at 320 nm and convert into amounts/concentrations using the factors calculated with the *Cj*-NCC-1 standard.

6. Retention times of the major phyllobilins from senescent leaves of *Arabidopsis* [15,6] are listed in Table 2 (*see* **Note 38**).

4. Notes

1. Chlorophyll is sensitive to acidic pH causing artefactual pheophytin formation [16].
2. A stock of 10x concentrated (0.5 M) KPi buffer pH 7 is prepared by mixing solutions of 0.5 M K_2HPO_4 and 0.5 M KH_2PO_4, until reaching a pH of 7 (per 100 mL of 0.5 M KPi buffer this requires approximately 42 mL of 0.5 M K_2HPO_4 and 58 mL of 0.5 M KH_2PO_4). Filter through a 0.45 µm nylon filter. For preparing solvent A, dilute the stock solution 10-fold in milli-Q H_2O. Aqueous KPi buffers are prone to bacterial contaminations. Store aliquots of the 10x stock solution at -20° C. Once prepared, use solvent A rather quickly.
3. For small sample amounts (100 mg or less), grinding is best done in a mixer mill (e.g. Retsch MM200, Haan, Germany). For this, place the plant tissue in 1.5 mL centrifuge tubes, add 5-10 glass beads (3 mm diameter) and freeze in liquid nitrogen. Place tubes in the Teflon holders provided with the mill (precooled in liquid nitrogen) and run at a frequency of 30 Hz for 3 x 30 sec with re-cooling in liquid nitrogen in-between.
4. Before use, degas solvents by sonication in a sonication bath for 5 min to prevent gas formation within the HPLC system.
5. Filter the 1 M ammonium acetate solution through a 0.45 µm nylon filter, store as a stock at 4° C.
6. To avoid the effect of end volume changes when mixing an aqueous solution with an organic solvent, measure MeOH and the 1 M ammonium acetate solution in separate measuring cylinders and subsequently combine them.

7. Maintaining a pH of 7.0 is critical to avoid undesired FCC/DFCC to NCC/DNCC conversion during the HPLC run that may occur at low pH [17,8].
8. Availability of a fluorescence detector is advantageous for the detection of FCCs/DFCCs, which emit blue fluorescence at 450 nm when exited at 360 nm [7].
9. If only two solvent channels are available, reduce the concentration of the KPi buffer to 10 mM for phyllobilin analysis. This is necessary, because high MeOH concentrations used during the HPLC run could cause precipitation of phosphate salts.
10. A temperature-controlled column is recommended for phyllobilin separation to guarantee uniform retention times; however, this is less critical for separation of chlorins.
11. Gas formation is particularly critical during phyllobilin analysis when mixing the KPi buffer (solvent A) with MeOH (solvent B). If no degasser is available, premix the KPi buffer with MeOH to the start conditions (i.e. 20% MeOH, when using the gradient provided in section 3.4.2.), desgas by sonication and adjust the HPLC gradient accordingly.
12. HPLC columns should be stored in MeOH:H_2O, 50:50 (v/v) to prevent precipitation of salts on the column.
13. Autosamplers should not be employed for chlorin analysis, because of the instability of phytylated pigments even at 4° C, which is caused by chlorophyllases potentially still active in the extracts [18]. Instead, it is crucial for chlorin extracts to be kept in liquid nitrogen until injection into the HPLC.
14. Although an autosampler is not abolutely necessary, it allows running a batch of multiple samples without the need of manual injection. Consider, however, that phyllobilins are rather thermo-labile and light-sensitive, so they should be cooled in the autosampler and be protected from light.

15. If the concentrations of chlorin standards is unknown, e.g. because of manual extraction and preparation of pigments (see section 2.1.3.), the concentration can be determined spectrophotometrically prior to HPLC injection. For calculating concentrations use the following equations valid for pigments in 80 % acetone [19,20] (A = absorption at indicated wavelength):

    chlorophyll *a* or chlorophyllide *a* [µg ml^{-1}] = 11.63 A_{665} – 2.39 A_{649}

    chlorophyll *b* or chlorophyllide *b* [µg ml^{-1}] = 20.11 A_{649} – 5.18 A_{665}

    pheophytin *a* or pheophorbide *a* [µg ml^{-1}] = 22.42 A_{665} – 6.81 A_{653}

    pheophytin *a* or pheophorbide *a* [µg ml^{-1}] = 40.17 A_{653} – 18.58 A_{665}

16. Due to the commercial unavailability of phyllobilin standards and the limited spectral data available for the different classes of phyllobilins, relatively accurate quantification is so far only possible for NCCs.
17. Rather similar log ε values have been determined for NCCs from different plant species (see, for example [21-23]), allowing the approximate quantification of (unknown) NCCs from any plant sample using *Cj*-NCC-1 as standard.
18. With the method presented, chlorins or phyllobilins have been analyzed in leaves and fruits of different plant species such as *Arabidopsis* and tomato [24,25]. If other organs or plant species are analyzed, the method might require adaptations, in particular concerning the ratio of tissue amount to extraction buffer volume and the time of extraction.
19. An extensive comparison of different methods for chlorophyll extraction, including a sub-zero temperature method using acetone similar to the one described here, has recently been published [18].
20. Senescence induction in leaves (e.g. from *Arabidopsis*) can be performed by incubating detached leaves in the dark. Leaves are cut and incubated on wet filter paper in a closed

container at room temperature in the dark. Induction of senescence can be detected after 3-5 days. Alternatively, leaves can be covered with aluminum foil while being attached to the plant. If induction of leaf senescence is applied to other plant species, the procedure might require adaptations.

21. Work fast and make sure that the plant material does not thaw during the procedure.
22. To avoid thawing of the tissue during transferring to the microcentrifuge tube, dip the microcentrifuge tube in liquid nitrogen and use it as a shuffle to transfer the desired amount of tissue. Immediately, weigh the sampled tissue using a fine balance that has been tared with an empty microcentrifuge tube. Record the weight and use for extraction (see section 3.2.4.).
23. Chlorophyllases are ubiquitously present in plant tissue and might get activated during the process of pigment extraction. Therefore it is very important to work quickly and in a cold environment, in order to prevent artefactual chlorophyllide and/or pheophorbide formation [24,18].
24. The required amount of buffer depends on chlorophyll concentration. Five volumes of buffer are generally sufficient for leaves of *Arabidopsis*. For tomato or other species that contain high amounts of chlorophyll, the buffer volume may need to be increased.
25. Make sure samples are not exposed to light to prevent bleaching of the pigments.
26. Extraction time depends on the plant sample. For green or senescent *Arabidopsis* leaves, 2 h of incubation is normally sufficient. For other plant tissues that are more fibrous and/or contain high chlorophyll levels (such as tomato or barley leaves), extraction can be done overnight. Alternatively, 2-3 rounds of extraction each followed by a centrifugation step can be done with subsequent pooling of extracted fractions or extracts may be sonicated for a few minutes in an ice-cooled sonication bath.
27. Transfer as much supernatant as possible, but ensure that no solids are transferred.

28. Only when pellets are colorless, all chlorins have been extracted into the acetone phase. If the pellet still appears green, multiple rounds of extraction can be performed (*see* also **Note 26**).
29. Twice centrifugation ensures that samples are free of solid particles. This may particularly be necessary with leaf samples from e.g. Poaceae species, like barley, which are rather fibrous.
30. If HPLC analysis will be performed at a later time point, prepared HPLC vials can be frozen in liquid nitrogen.
31. The extraction of chlorins described in section 3.1. simultaneously extracts carotenoids from plant tissues. Thus, HPLC analysis of these extracts allows the simultaneous analysis of carotenoids. Methods for carotenoid analysis and quantification have been published (see, for example [26]).
32. Frozen acetone develops high pressure while thawing. To avoid possible explosion of the microcentrifuge tube, release pressure by opening the microcentrifuge lid.
33. These values were obtained with the following HPLC system: column: C18 Hypersil ODS column (125 x 4.0 mm, 5 µm) (MZ Analysentechnik), pump: Gynkotek High Precision Pump Model 480 (Thermo Fisher Scientific); photodiode array detector: 206 PHD (365-700 nm; Linear); software: ChromQuest version 2.51 (Thermo Fisher Scientific). For other HPLC system, retention times may vary.
34. Although peak maxima differ between different chlorins (see Fig. 1), 665 nm is an ideal wavelength for simultaneous quantification of all chlorins.
35. If sample-containing HPLC vials had been stored in liquid nitrogen, make sure no air bubbles are trapped in the conical tip of the HPLC vials.
36. 254 nm is best suited for detection of all types of phyllobilin, while e.g. DNCCs do only weakly absorb at 315 nm [6], the wavelength suitable for quantification of NCCs.

37. Peak resolution and baseline settings are important parameters for accurately quantifying NCC peaks. Senescent leaves of different plant species tend to accumulate phyllobilin-unrelated compounds that absorb in the UV range and may co-elute with phyllobilins, and, thus, may interfere with phyllobilin identification and quantification.
38. These values were obtained with the following Dionex HPLC system (Thermo Fisher Scientific): column: C18 Hypersil ODS column (250 x 4.6 mm, 5 µm); autosampler: AS-100; column compartment: TCC-100 (set to 28°C); detectors: PA-100 photodiode array detector (200-700 nm) and RF2000 fluorescence detector (excitation at 360 nm, emission at 450 nm); software: Chromeleon 6.8 chromatography data system. For other HPLC system, retention times may vary.

Acknowledgements

This work was supported by grants from the Swiss National Science Foundation and by *CropLife*, an EU Marie-Curie Initial Training Network.

References

1. Kräutler B, Hörtensteiner S (2013) Chlorophyll breakdown: chemistry, biochemistry and biology. In: Ferreira GC, Kadish KM, Smith KM, Guilard R (eds) Handbook of Porphyrin Science, vol 28. World Scientific Publishing, Hackensack, NJ, USA, pp 117-185

2. Hörtensteiner S, Kräutler B (2011) Chlorophyll breakdown in higher plants. Biochim Biophys Acta 1807:977-988

3. Christ B, Hörtensteiner S (2014) Mechanism and significance of chlorophyll breakdown. J Plant Growth Regul 33:4-20

4. Sakuraba Y, Schelbert S, Park S-Y et al (2012) STAY-GREEN and chlorophyll catabolic enzymes interact at light-harvesting complex II for chlorophyll detoxification during leaf senescence in *Arabidopsis*. Plant Cell 24:507-518

5. Christ B, Schelbert S, Aubry S et al (2012) MES16, a member of the methylesterase protein family, specifically demethylates fluorescent chlorophyll catabolites during chlorophyll breakdown in Arabidopsis. Plant Physiol 158:628-641

6. Christ B, Süssenbacher I, Moser S et al (2013) Cytochrome P450 CYP89A9 is involved in the formation of major chlorophyll catabolites during leaf senescence in *Arabidopsis*. Plant Cell 25:1868-1880

7. Kräutler B (2014) Phyllobilins - the abundant bilin-type tetrapyrrolic catabolites of the green plant pigment chlorophyll. Chem Soc Rev doi:10.1039/c4cs00079j

8. Oberhuber M, Berghold J, Breuker K et al (2003) Breakdown of chlorophyll: a nonenzymatic reaction accounts for the formation of the colorless "nonfluorescent" chlorophyll catabolites. Proc Natl Acad Sci USA 100:6910-6915

9. Moser S, Müller T, Ebert MO et al (2008) Blue luminescence of ripening bananas. Angew Chem Int Ed 47:8954-8957

10. Kräutler B, Banala S, Moser S et al (2010) A novel blue fluorescent chlorophyll catabolite accumulates in senescent leaves of the peace lily and indicates a divergent path of chlorophyll breakdown. FEBS Lett 584:4215-4221

11. Ulrich M, Moser S, Müller T et al (2011) How the colourless 'nonfluorescent' chlorophyll catabolites rust. Chem-Eur J 17:2330-2334

12. Curty C, Engel N (1996) Detection, isolation and structure elucidation of a chlorophyll *a* catabolite from autumnal senescent leaves of *Cercidiphyllum japonicum*. Phytochemistry 42:1531-1536

13. Shioi Y, Fukae R, Sasa T (1983) Chlorophyll analysis by high-performance liquid chromatography. Biochim Biophys Acta 722:72-79

14. Perkins HJ, Roberts DWA (1962) Purification of chlorophylls, pheophytins and pheophorbides for specific activity determinations. Biochem Biophys Acta 58:486-498

15. Pružinská A, Tanner G, Aubry S et al (2005) Chlorophyll breakdown in senescent Arabidopsis leaves: characterization of chlorophyll catabolites and of chlorophyll catabolic enzymes involved in the degreening reaction. Plant Physiol 139:52-63

16. Mazaki H, Watanabe T, Takahashi T et al (1992) Pheophytination of eight chlorophyll derivatives in aqueous acetone. Bull Chem Soc Jpn 65:3212-3214

17. Oberhuber M, Berghold J, Kräutler B (2008) Chlorophyll breakdown by a biomimetic route. Angew Chem Int Ed 47:3057-3061

18. Hu XY, Tanaka A, Tanaka R (2013) Simple extraction methods that prevent the artifactual conversion of chlorophyll to chlorophyllide during pigment isolation from leaf samples. Plant Methods 9:19

19. Lichtenthaler HK (1987) Chlorophylls and carotenoids: pigments of photosynthetic biomembranes. Meth Enzymol 148:350-382

20. Strain HH, Cope BT, Svec WA (1971) Analytical procedures for the isolation, identification, estimation and investigation of the chlorophylls. Methods Enzymol 23:452-476

21. Kräutler B, Jaun B, Bortlik K-H et al (1991) On the enigma of chlorophyll degradation: the constitution of a secoporphinoid catabolite. Angew Chem Int Ed Engl 30:1315-1318

22. Berghold J, Eichmüller C, Hörtensteiner S et al (2004) Chlorophyll breakdown in tobacco: on the structure of two nonfluorescent chlorophyll catabolites. Chem Biodivers 1:657-668

23. Scherl M, Müller T, Kräutler B (2012) Chlorophyll catabolites in senescent leaves of the lime tree (*Tilia cordata*). Chem Biodivers 9:2605-2617

24. Schenk N, Schelbert S, Kanwischer M et al (2007) The chlorophyllases AtCLH1 and AtCLH2 are not essential for senescence-related chlorophyll breakdown in *Arabidopsis thaliana*. FEBS Lett 581:5517-5525

25. Guyer L, Schelbert Hofstetter S, Christ B et al (2014) Different mechanisms are responsible for chlorophyll dephytylation during fruit ripening and leaf senescence in tomato. Plant Physiol doi:10.1104/pp.114.239541

26. Guzman I, Yousef GG, Brown AF (2012) Simultaneous extraction and quantitation of carotenoids, chlorophylls, and tocopherols in Brassica vegetables. J Agric Food Chem 60:7238-7244

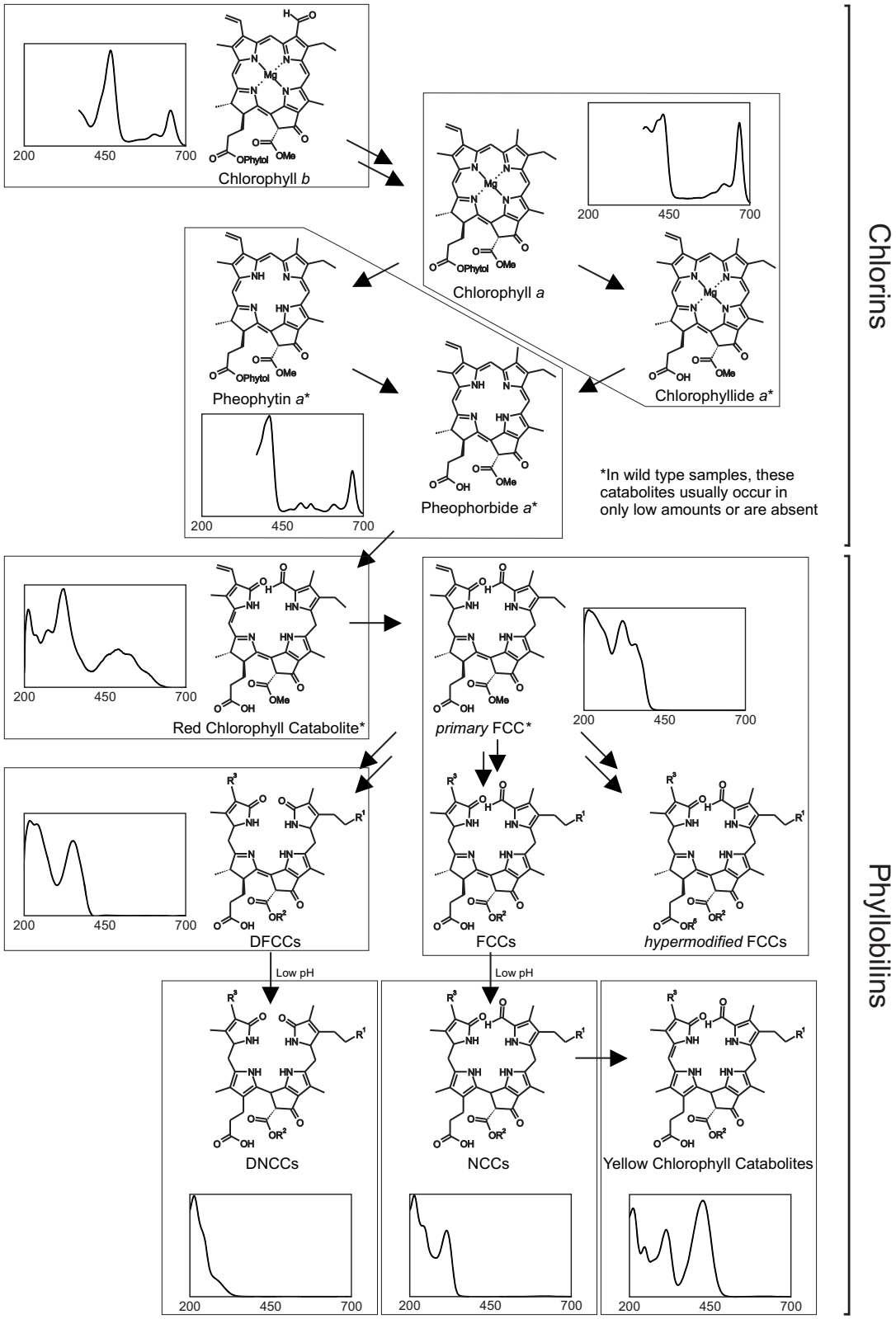

Fig. 1. Constitutional formulas and UV/Vis absorption spectra of chlorophyll-derived chlorins and phyllobilins occurring during chlorophyll breakdown.

Table 1. Approximate retention times of chlorins using the HPLC system outlined in Note 33.

Pigment	Retention time [min]
Chlorophyllide *b*	1.5
Chlorophyllide *a*	3
Pheophorbide *b*	7
Pheophorbide *a*	9
Chlorophyll *b*	16
Chlorophyll *a*	18
Pheophytin *b*	21
Pheophytin *a*	23

Table 2. Approximate retention times of the major *Arabidopsis* phyllobilins using the HPLC system outlined in Note 38.

Phyllobilin	Retention time [min]
At-DNCC-1	21.5
At-NCC-1	23.7
At-DNCC-2	24.7
At-NCC-2	26.4
At-DNCC-3	27.3
At-NCC-3	27.8
At-NCC-4	29.1
At-DNCC-4	29.2
At-DNCC-5	30.5
At-NCC-5	36.2

REFERENCES

Abreu ME, Munné-Bosch S (2008) Salicylic acid may be involved in the regulation of drought-induced leaf senescence in perennials: A case study in field-grown *Salvia officinalis L.* plants. Environ Exp Bot **64**: 105–112

Bell A, Moreau C, Chinoy C, Spanner R, Dalmais M, Le Signor C, Bendahmane A, Klenell M, Domoney C (2015) SGRL can regulate chlorophyll metabolism and contributes to normal plant growth and development in *Pisum sativum L*. Plant Mol Biol **89**: 539–558

Biswas A, Choudhuri M (1980) Mechanism of monocarpic senescence in rice. Plant Physiol **65**: 340–345

Boote KJ, Jones JW, Pickering NB (1996) Potential uses and limitations of crop models. Agron J **716**: 704–716

Bradford KJ, Hsiao TC, Yang SF (1982) Inhibition of ethylene synthesis in tomato plants subjected to anaerobic root stress. Plant Physiol **70**: 1503–1507

Breeze E, Harrison E, McHattie S, Hughes L, Hickman R, Hill C, Kiddle S, Kim YS, Penfold CA, Jenkins D, et al (2011) High-resolution temporal profiling of transcripts during Arabidopsis leaf senescence reveals a distinct chronology of processes and regulation. Plant Cell **23**: 873–894

Buchanan-Wollaston V (1997) The molecular biology of leaf senescence. J Exp Bot **48**: 181–199

Buchanan-Wollaston V, Page T, Harrison E, Breeze E, Lim PO, Nam HG, Lin JF, Wu SH, Swidzinski J, Ishizaki K, et al (2005) Comparative transcriptome analysis reveals significant differences in gene expression and signalling pathways between developmental and dark/starvation-induced senescence in Arabidopsis. Plant J **42**: 567–585

Burger JC, Chapman MA, Burke JM (2008) Molecular insights into the evolution of crop plants. Am J Bot **95**: 113–122

Christ B, Hauenstein M, Hörtensteiner S (2016) A liquid chromatography-mass spectrometry platform for the analysis of phyllobilins, the major degradation products of chlorophyll in *Arabidopsis thaliana*. Plant J (In press)

Christ B, Hörtensteiner S (2014) Mechanism and significance of chlorophyll breakdown. J Plant Growth Regul **33**: 4–20

Christ B, Schelbert S, Aubry S, Süssenbacher I, Müller T, Kräutler B, Hörtensteiner S (2012) MES16, a Member of the methylesterase protein family, specifically demethylates fluorescent chlorophyll catabolites during chlorophyll breakdown in Arabidopsis. Plant Physiol **158**: 628–641

Christ B, Süssenbacher I, Moser S, Bichsel N, Egert A, Müller T, Kräutler B, Hörtensteiner S (2013) Cytochrome P450 CYP89A9 is involved in the formation of major chlorophyll catabolites during leaf senescence in Arabidopsis. Plant Cell **25**: 1868–1880

Christiansen MW, Gregersen PL (2014) Members of the barley NAC transcription factor gene family show differential co-regulation with senescence-associated genes during senescence of flag leaves. J Exp Bot **65**: 4009–4022

Chung DW (2006) The Role of Pheophorbide *a* Oxygenase Expression and Activity in the Canola Green Seed Problem. Plant Physiol **142**: 88–97

Costa ML, Civello PM, Chaves AR, Martinez GA (2002) Characterization of Mg-dechelatase activity obtained from *Fragaria x ananassa* fruit. Plant Physiol Biochem **40**:

111–118

de Souza Luche H, da Silva JAG, da Maia LC, de Oliveira AC (2015) Stay-green: a potentiality in plant breeding. Cienc Rural **45**: 1755–1760

Ellis CM, Nagpal P, Young JC, Hagen G, Guilfoyle TJ, Reed JW (2005) AUXIN RESPONSE FACTOR1 and AUXIN RESPONSE FACTOR2 regulate senescence and floral organ abscission in *Arabidopsis thaliana*. Development **132**: 4563–4574

Ellis S, White S, Holland J, Smith B, Collier R, Jukes A (2014) Encyclopaedia of pests and natural enemies in field crops. AHDB (Cereals & Oilseeds, Horticulture and Potatoes), Warwickshire

Fang W, Kao CH (2001) Inhibition of methyl jasmonate-promoted senescence in rice leaves by a metal chelator , 2,2′-bipyridine. Plant Growth Regul **33**: 87–93

Finkelstein R (2013) Abscisic acid synthesis and response. Arabidopsis Book **11**: e0166

Forest NC (1995) Barley growth and development 1-72

Fu J-D, Yan Y-F, Lee B-W (2009) Physiological characteristics of a functional stay-green rice "SNU-SG1" during grain-filling period. J Crop Sci Biotechnol **12**: 47–52

Gan S (2007) Mitotic Senescence in Plants. Senescence Process Plants **26**: 1–11

Gan S (2014) Leaf senescence as an important target for improving crop production. Adv Crop Sci Technol **2**: 10–11

Gan S, Amasino RM (1997) Making sense of senescence: molecular genetic regulation and manipulation of leaf senescence. Plant Physiol **113**: 313–319

Gan S, Amasino RM (1995) Inhibition of leaf senescence by autoregulated production of cytokinin. Science **270**: 1986–1987

Gepstein S, Sabehi G, Carp MJ, Hajouj T, Nesher MFO, Yariv I, Dor C, Bassani M (2003) Large-scale identification of leaf senescence-associated genes. Plant J **36**: 629–642

Gray J, Close PS, Briggs SP, Johal GS (1997) A novel suppressor of cell death in plants encoded by the Lls1 gene of maize. Cell **89**: 25–31

Greenberg JT, Guo A, Klessig DF, Ausubel FM (1994) Programmed cell death in plants: A pathogen-triggered response activated coordinately with multiple defense functions. Cell **77**: 551–563

Gregersen PL, Culetic A, Boschian L, Krupinska K (2013) Plant senescence and crop productivity. Plant Mol Biol **82**: 603–622

Gregersen PL, Holm PB, Krupinska K (2008) Leaf senescence and nutrient remobilisation in barley and wheat. Plant Biol (Stuttg) **10 Suppl 1**: 37–49

Guo Y, Gan SS (2014) Translational researches on leaf senescence for enhancing plant productivity and quality. J Exp Bot **65**: 3901–3913

Guyer L, Hofstetter SS, Christ B, Lira BS, Rossi M, Hörtensteiner S (2014) Different mechanisms are responsible for chlorophyll dephytylation during fruit ripening and leaf senescence in tomato. Plant Physiol **166**: 44–56

Hamilton AJ, Lycett GW, Grierson D (1990) Antisense gene that inhibits synthesis of the hormone ethylene in transgenic plants. Nature **346**: 284–287

Han M, Kim C, Lee J, Lee S, Jeon J (2014) *Os*WRKY42 represses *Os*MT1d and induces reactive oxygen species and leaf senescence in rice. Mol Cells **37**: 532–539

Hauenstein M, Christ B, Das A, Aubry S, Hörtensteiner S A novel role for TIC55 as a hydroxylase of phyllobilins, the products of chlorophyll breakdown during plant senescence. (Manuscript submitted for publication)

Hennig L (2004) Transcriptional Programs of Early Reproductive Stages in Arabidopsis. Plant Physiol **135**: 1765–1775

Hensel LL, Grbic V, Baumgarten DA, Bleecker AB (1993) Developmental and age-related processes that influence the longevity and senescence of photosynthetic tissues in Arabidoposis. Plant Cell **5**: 553–564

Hirai Y, Tamiaki H, Kashimura S, Saga Y (2009) Demetalation kinetics of natural chlorophylls purified from oxygenic photosynthetic organisms: effect of the formyl groups conjugated directly to the chlorin pi-macrocycle. Photochem Photobiol Sci **8**: 1701–1707

Hörtensteiner S (2006) Chlorophyll degradation during senescence. Annu Rev Plant Biol **57**: 55–77

Hörtensteiner S (2012) Update on the biochemistry of chlorophyll breakdown. Plant Mol Biol 1-13

Hörtensteiner S (2013) Update on the biochemistry of chlorophyll breakdown. Plant Mol Biol **82**: 505–517

Hörtensteiner S (2009) Stay-green regulates chlorophyll and chlorophyll-binding protein degradation during senescence. Trends Plant Sci **14**: 155–62

Hörtensteiner S, Feller U (2002) Nitrogen metabolism and remobilization during senescence. J Exp Bot **53**: 927–937

Hörtensteiner S, Kräutler B (2000) Chlorophyll breakdown in oilseed rape. Photosynth Res **64**: 137–146

Hörtensteiner S, Rodoni S, Schellenberg M, Vicentini F, Nandi OI, Qiu Y-L, Matile P (2000) Evolution of chlorophyll degradation: the significance of RCC reductase. Plant Biol **2**: 63–67

Hörtensteiner S, Vicentini F, Matile P (1995) Chlorophyll breakdown in senescent cotyledons of rape, *Brassica napus L.*: enzymatic cleavage of phaeophorbide an *in vitro*. New Phytol **129**: 237–246

Hoth S, Morgante M, Sanchez J-P, Hanafey MK, Tingey S V, Chua N-H (2002) Genome-wide gene expression profiling in *Arabidopsis thaliana* reveals new targets of abscisic acid and largely impaired gene regulation in the *abi1-1* mutant. J Cell Sci **115**: 4891–4900

Ito H, Ohysuka T, Tanaka A (1996) Conversion of chlorophyll *b* to chlorophyll *a* via 7-hydroxymethyl chlorophyll. J Biol Chem **271**: 1475–1479

Jayakannan M, Bose J, Babourina O, Shabala S, Massart A, Poschenrieder C, Rengel Z (2015) The NPR1-dependent salicylic acid signalling pathway is pivotal for enhanced salt and oxidative stress tolerance in Arabidopsis. J Exp Bot **66**: 1865–1875

Ji Q, Xu X, Wang K (2013) Genetic transformation of major cereal crops. Int J Dev Biol **57**: 495–508

Jiang H, Li M, Liang N, Yan H, Wei Y, Xu X, Liu J, Xu Z, Chen F, Wu G (2007) Molecular cloning and function analysis of the stay green gene in rice. Plant J **52**: 197–209

Jirage D, Tootle TL, Reuber TL, Frost LN, Feys BJ, Parker JE, Ausubel FM, Glazebrook J (1999) *Arabidopsis thaliana* PAD4 encodes a lipase-like gene that is important for salicylic acid signaling. Proc Natl Acad Sci U S A **96**: 13583–13588

John I, Drake R, Farrell A, Cooper W, Lee P, Horton P, Grierson D (1995) Delayed leaf senescence in ethylene-deficient ACC-oxidase antisense tomato plants - molecular and physiological analysis. Plant J **7**: 483–490

Johnson SM, Cummins I, Lim FL, Slabas AR, Knight MR (2015) Transcriptomic analysis comparing stay-green and senescent *Sorghum bicolor* lines identifies a role for proline biosynthesis in the stay-green trait. J Exp Bot **66**: 7061–7063

Kannangara CG, Schouboe A (1985) Biosynthesis of Δ-aminolevulinate in greening barley leaves. VII. Glutamate 1-semialdehyde accumulation in gabaculine treated leaves. Carlsberg Res Commun **50**: 179–191

Kao CH, Yang SF (1983) Role of ethylene in the senescence of detached rice leaves. Plant Physiol **73**: 881–885

Kong Z, Li M, Yang W, Xue W, Yongbiao X (2006) A novel nuclear-localized CCCH-type zinc finger protein, *Os*DOS, is involved in delaying leaf. Plant Physiol **141**: 1376–1388

Koornneef M, Meinke D (2010) The development of Arabidopsis as a model plant. Plant J **61**: 909–921

Kräutler B, Matile P (1999) Solving the riddle of chlorophyll breakdown. Acc Chem Res **32**: 35–43

Kusaba M, Ito H, Morita R, Iida S, Sato Y, Fujimoto M, Kawasaki S, Tanaka R, Hirochika H, Nishimura M, et al (2007) Rice NON-YELLOW COLORING1 is involved in light-harvesting complex II and grana degradation during leaf senescence. Plant Cell **19**: 1362–1375

Lee IC, Hong SW, Whang SS, Lim PO, Nam HG, Koo JC (2011) Age-dependent action of an ABA-inducible receptor kinase, RPK1, as a positive regulator of senescence in Arabidopsis leaves. Plant Cell Physiol **52**: 651–662

Lim PO, Kim HJ, Nam HG (2007) Leaf senescence. Annu Rev Plant Biol **58**: 115–136

Lim PO, Woo HR, Nam HG (2003) Molecular genetics of leaf senescence in Arabidopsis. Trends Plant Sci **8**: 272–278

Lin JF, Wu SH (2004) Molecular events in senescing Arabidopsis leaves. Plant J **39**: 612–628

Liu L, Zhou Y, Zhou G, Ye RJ, Zhao L, Li XH, Lin YJ (2008) Identification of early senescence-associated genes in rice flag leaves. Plant Mol Biol **67**: 37–55

Lopes MS, Reynolds MP (2012) Stay-green in spring wheat can be determined by spectral reflectance measurements (normalized difference vegetation index) independently from phenology. J Exp Bot **63**: 3789–3798

Luo Z, Zhang J, Li J, Yang C, Wang T, Ouyang B, Li H, Giovannoni J, Ye Z (2013) A STAY-GREEN protein SlSGR1 regulates lycopene and β-carotene accumulation by interacting directly with SlPSY1 during ripening processes in tomato. New Phytol **198**: 442–452

Mach JM, Castillo AR, Hoogstraten R, Greenberg JT (2001) The Arabidopsis-accelerated cell death gene *ACD2* encodes red chlorophyll catabolite reductase and suppresses the spread of disease symptoms. Proc Natl Acad Sci U S A **98**: 771–776

Matile P, Ginsburg S, Schellenberg M, Thomas H (1988) Catabolites of chlorophyll in senescing barley leaves are localized in the vacuoles of mesophyll cells. Proc Natl Acad Sci U S A **85**: 9529–32

Matile P, Schellenberg M, Peisker C (1992) Production and release of a chlorophyll catabolite in isolated senescent chloroplasts. Planta **187**: 230–235

Matile P, Stefan H, Thomas H (1999) Chlorophyll degradation. Annu Rev Plant Physiol Plant Mol Biol **50**: 67–95

Meinke DW (1998) *Arabidopsis thaliana*: A model plant for genome analysis. Science **282**: 662–682

Meng C, Cai C, Zhang T, Guo W (2009) Characterization of six novel NAC genes and their responses to abiotic stresses in *Gossypium hirsutum L.* Plant Sci **176**: 352–359

Miao Y, Laun T, Zimmermann P, Zentgraf U (2004) Targets of the WRKY53 transcription factor and its role during leaf senescence in Arabidopsis. Plant Mol Biol **55**: 853–867

Michael TP, Jackson S (2013) The First 50 Plant Genomes. Plant Genome **6**: 1–7

Morita R, Sato Y, Masuda Y, Nishimura M, Kusaba M (2009) Defect in non-yellow coloring 3, an *a/b* hydrolase-fold family protein, causes a stay-green phenotype during leaf senescence in rice. Plant J **59**: 940–952

Morris K, MacKerness SA, Page T, John CF, Murphy AM, Carr JP, Buchanan-Wollaston V (2000) Salicylic acid has a role in regulating gene expression during leaf senescence. Plant J **23**: 677–685

Müller T, Moser S, Ongania K-H, Pruzinska A, Hörtensteiner S, Kräutler B (2006) A divergent path of chlorophyll breakdown in the model plant *Arabidopsis thaliana.* Chembiochem **7**: 40–42

Müller T, Ulrich M, Ongania KH, Kräutler B (2007) Colorless tetrapyrrolic chlorophyll catabolites found in ripening fruit are effective antioxidants. Angew Chem Int Ed **46**: 8699–8702

Noodén LD, Penney JP (2001) Correlative controls of senescence and plant death in *Arabidopsis thaliana* (Brassicaceae). J Exp Bot **52**: 2151–2159

Noodén LD, Singh S, Letham DS (1990) Correlation of xylem sap cytokinin levels with monocarpic senescence in soybean. Plant Physiol **93**: 33–39

Okushima Y, Mitina I, Quach HL, Theologis A (2005) AUXIN RESPONSE FACTOR 2 (ARF2): A pleiotropic developmental regulator. Plant J **43**: 29–46

Olsen AN, Ernst H a, Leggio L Lo, Skriver K (2005) NAC transcription factors: structurally distinct, functionally diverse. Trends Plant Sci **10**: 79–87

Park KY, Drory A, Woodson WR (1992) Molecular-cloning of an 1-aminocyclopropane-1-carboxylate synthase from senescing carnation flower petals. Plant Mol Biol **18**: 377–386

Parrott D, Yang L, Shama L, Fischer AM (2005) Senescence is accelerated, and several proteases are induced by carbon "feast" conditions in barley (*Hordeum vulgare L.*) leaves. Planta **222**: 989–1000

Parrott DL, McInnerney K, Feller U, Fischer AM (2007) Steam-girdling of barley (*Hordeum vulgare*) leaves leads to carbohydrate accumulation and accelerated leaf senescence, facilitating transcriptomic analysis of senescence-associated genes. New Phytol **176**: 56–69

Parthier B (1983) Jasmonates: Hormonal regulators or stress factors in leaf senescence? J Plant Growth Regul **9**: 57–63

Picton S, Barton SL, Bouzayen M, Hamilton AJ, Grierson D (1993) Altered fruit ripening and leaf senescence in tomatoes expressing an antisense ethylene-forming enzyme transgene. Plant J **3**: 469–481

Podzimska-Sroka D, O'Shea C, Gregersen P, Skriver K (2015) NAC transcription factors in senescence: from molecular structure to function in crops. Plants **4**: 412–448

Potschin M, Schlienger S, Bieker S, Zentgraf U (2014) Senescence networking: WRKY18 is an upstream regulator, a downstream target gene, and a protein interaction partner of WRKY53. J Plant Growth Regul **33**: 106–118

Pruzinská A, Tanner G, Anders I, Roca M, Hörtensteiner S (2003) Chlorophyll breakdown: pheophorbide *a* oxygenase is a Rieske-type iron-sulfur protein, encoded by the accelerated cell death 1 gene. Proc Natl Acad Sci U S A **100**: 15259–15264

Pruzinska A, Tanner G, Aubry S, Anders I, Moser S, Mu T, Pruz A, Youn J, Liljegren SJ, Ho S, et al (2005) Chlorophyll breakdown in senescent Arabidopsis leaves . characterization of chlorophyll catabolites and of chlorophyll catabolic enzymes involved in the degreening reaction 1. Plant Physiol **139**: 52–63

Quiles MJ, Garcia C, Cuello J (1995) Differential effects of abscisic acid and methyl jasmonate on endoproteinases in senescing barley leaves. Plant Growth Regul **16**: 197–204

Rabbani MA, Maruyama K, Abe H, Khan MA, Katsura K, Ito Y, Yoshiwara K, Seki M, Shinozaki K, Shinozaki KY (2003) Monitoring expression profiles of rice genes under cold, drought, and high-salinity stresses and abscisicacid application using cDNA microarray and RNAgel-blot analyses. Plant Physiol **133**: 1755–1767

Reinhard A. Weidhase, Heide-Mari Kramell, Jörg Lehmann, Hans-Werner Liebisch, Werner Lerbs BP (1987) Methyl jasmonate-induced changes in the polypeptide pattern of senescing barley leaf segments. Plant Sci **51**: 177–186

Reynolds-Henne CE, Langenegger A, Mani J, Schenk N, Zumsteg A, Feller U (2010) Interactions between temperature, drought and stomatal opening in legumes. Environ Exp Bot **68**: 37–43

Richmond AE, Lang A (1956) Effect of kinetin on protein content and survival of detached Xanthium leaves. Science **125**: 650–651

Rinerson CI, Scully ED, Palmer NA, Donze-Reiner T, Rabara RC, Tripathi P, Shen QJ, Sattler SE, Rohila JS, Sarath G, et al (2015) The WRKY transcription factor family and senescence in switchgrass. BMC Genomics **16**: 912

Rissler HM, Collakova E, DellaPenna D, Whelan J, Pogson BJ (2002) Chlorophyll biosynthesis. Expression of a second chl I gene of magnesium chelatase in Arabidopsis supports only limited chlorophyll synthesis. Plant Physiol **128**: 770–779

Robatzek S, Somssich IE (2001) A new member of the Arabidopsis WRKY transcription factor family, AtWRKY6, is associated with both senescence- and defence-related processes. Plant J **28**: 123–133

Robatzek S, Somssich IE (2002) Targets of AtWRKY6 regulation during plant senescence and pathogen defense. Genes Dev **16**: 1139–1149

Rodoni S, Vicentini F, Schellenberg M, Matile P, Hortensteiner S (1997) Partial purification and characterization of red chlorophyll catabolite reductase, a stroma protein lnvolved in chlorophyll breakdown. Plant Physiol **115**: 677–682

Rong H, Tang Y, Zhang H, Wu P, Chen Y, Li M, Wu G, Jiang H (2013) The Stay-Green Rice like (SGRL) gene regulates chlorophyll degradation in rice. J Plant Physiol **170**: 1367–1373

Rudell DR, Mattheis JP, Fan X, Fellman JK (2002) Methyl jasmonate enhances anthocyanin accumulation and modifies production of phenolics and pigments in "Fuji" apples. J Am Soc Hortic Sci **127**: 435–441

Saga Y, Tamiaki H (2012) Demetalation of chlorophyll pigments. Chem Biodivers **9**: 1659–1683

Sakuraba Y, Schelbert S, Park SY, Han SH, Lee BD, Andres CB, Kessler F, Hortensteiner S, Paek NC (2012) STAY-GREEN and chlorophyll catabolic enzymes interact at light-harvesting complex II for chlorophyll detoxification during leaf senescence in Arabidopsis. Plant Cell **24**: 507–518

Sato Y, Moria R, Katsuma S, Nishimura M, Tanaka A, Kusaba M (2009) Two short-chain dehydrogenase/reductases, NON-YELLOW COLORING 1 and NYC1-LIKE, are required for chlorophyll *b* and light-harvesting complex II degradation during senescence in rice. Plant J **57**: 120–131

Sato Y, Morita R, Nishimura M, Yamaguchi H, Kusaba M (2007) Mendel's green cotyledon gene encodes a positive regulator of the chlorophyll-degrading pathway. Proc Natl Acad Sci U S A **104**: 14169–14174

Schelbert S, Aubry S, Burla B, Agne B, Kessler F, Krupinska K, Hörtensteiner S (2009) Pheophytin pheophorbide hydrolase (pheophytinase) is involved in chlorophyll breakdown during leaf senescence in Arabidopsis. Plant Cell **21**: 767–85

Schenk N, Schelbert S, Kanwischer M, Goldschmidt EE, Dörmann P, Hörtensteiner S (2007) The chlorophyllases AtCLH1 and AtCLH2 are not essential for senescence-related chlorophyll breakdown in *Arabidopsis thaliana*. FEBS Lett **581**: 5517–5525

Seki M, Narusaka M, Ishida J, Nanjo T, Fujita M, Oono Y, Kamiya A, Nakajima M, Enju A, Sakurai T, et al (2002) Monitoring the expression profiles of 7000 Arabidopsis genes under drought, cold and high-salinity stresses using a full-length cDNA microarray. Plant J **31**: 279–292

Shimamoto K, Kyozuka J (2002) Rice as a model for comparative genomics of plants. Annu Rev Plant Biol **53**: 399–419

Shioi Y, Watanabe K, Takamiya K (1996) Enzymatic conversion of pheophorbide *a* to a precursor of pyropheophorbide a in leaves of *Chenopodium album*. Plant Cell Physiol **37**: 1143–1149

Smart CM (1994) Gene expression during leaf senescence. New Phytol **126**: 419–448

Spano G, Di Fonzo N, Perrotta C, Platani C, Ronga G, Lawlor DW, Napier JA, Shewry PR (2003) Physiological characterization of "stay green" mutants in durum wheat. J Exp Bot **54**: 1415–1420

Spassieva S, Hille J (2002) A lesion mimic phenotype in tomato obtained by isolating and silencing an *Lls1* homologue. Plant Sci **162**: 543–549

Strable J, Scanlon MJ (2009) Maize (*Zea mays*): A Model Organism for Basic and Applied Research in Plant Biology. Cold Spring Harb Protoc **2009**: pdb.emo132

Süssenbacher I, Christ B, Hörtensteiner S, Kräutler B (2014) Hydroxymethylated phyllobilins: A puzzling new feature of the dioxobilin branch of chlorophyll breakdown. Chem-Eur J **20**: 87–92

Süssenbacher I, Hörtensteiner S, Kräutler B (2015) A Dioxobilin-type fluorescent chlorophyll catabolite as a transient early intermediate of the dioxobilin-branch of chlorophyll breakdown in *Arabidopsis thaliana*. Angew Chemie Int Ed **54**: 13777–13781

Suzuki T, Kunieda T, Murai F, Morioka S, Shioi Y (2005) Mg-dechelation activity in radish cotyledons with artificial and native substrates, Mg-chlorophyllin *a* and chlorophyllide *a*. Plant Physiol Biochem **43**: 459–464

Suzuki T, Shioi Y (2002) Re-examination of Mg-dechelation reaction in the degradation of chlorophylls using chlorophyllin *a* as substrate. Photosynth Res **74**: 217–223

Suzuki Y, Amano T, Shioi Y (2006) Characterization and cloning of the chlorophyll-degrading enzyme pheophorbidase from cotyledons of radish. Plant Physiol **140**: 716–725

Tan BC, Joseph LM, Deng WT, Liu L, Li QB, Cline K, McCarty DR (2003) Molecular characterization of the Arabidopsis 9-cis epoxycarotenoid dioxygenase gene family. Plant J **35**: 44–56

Tanaka R, Hirashima M, Satoh S, Tanaka A (2003) The Arabidopsis-accelerated cell death gene *ACD1* is involved in oxygenation of pheophorbide *a*: inhibition of pheophorbide *a* oxygenase activity does not lead to the "stay-green" phenotype in Arabidopsis. Plant Cell Physiol **44**: 1266–1274

Tanaka R, Tanaka A (2011) Chlorophyll cycle regulates the construction and destruction of the light-harvesting complexes. Biochim Biophys Acta - Bioenerg **1807**: 968–976

Tang YY, Li MR, Chen YP, Wu PZ, Wu GJ, Jiang HW (2011) Knockdown of OsPAO and OsRCCR1 cause different plant death phenotypes in rice. J Plant Physiol **168**: 1952–1959

Theologis A (1992) One rotten apple spoils the whole bushel: The role of ethylene in fruit ripening. Cell **70**: 181–184

Thomas H, Howarth CJ (2000) Five ways to stay green. J Exp Bot **51**: 329–337

Uauy C, Distelfeld A, Fahima T, Blechl A, Dubcovsky J (2006) A NAC gene regulating senescecnce improves grain protein, zinc and iron content in wheat. Science **314**: 1298–1330

Vicente R, Perez P, Martinez-Carrasco R, Usadel B, Kostadinova S, Morcuende R (2015) Quantitative RT-PCR platform to measure transcript levels of C and N metabolism-related genes in durum wheat: transcript profiles in elevated [CO_2] and high temperature at different levels of N supply. Plant Cell Physiol **56**: 1556–1573

van Doorn WG (2008) Is the onset of senescence in leaf cells of intact plants due to low or high sugar levels? J Exp Bot **59**: 1963–1972

Wingler A, Roitsch T (2008) Metabolic regulation of leaf senescence: interactions of sugar signalling with biotic and abiotic stress responses. Plant Biol **10**: 50–62

Woo HR, Kim HJ, Nam HG, Lim PO (2013) Plant leaf senescence and death - regulation by multiple layers of control and implications for aging in general. J Cell Sci **126**: 4823–4833

Wu X-Y, Kuai B-K, Jia J-Z, Jing H-C (2012) Regulation of leaf senescence and crop genetic improvement. J Integr Plant Biol **54**: 936–952

Wüthrich KL, Bovet L, Hunziker PE, Donnison IS, Hörtensteiner S (2000) Molecular cloning, functional expression and characterisation of RCC reductase involved in chlorophyll catabolism. Plant J **21**: 189–198

Yamburenko M V., Zubo YO, Vankova R, Kusnetsov V V., Kulaeva ON, Borner T (2013) Abscisic acid represses the transcription of chloroplast genes. J Exp Bot **64**: 4491–4502

Zarembinski TI, Theologis A (1994) Ethylene biosynthesis and action: a case of conservation. Plant Mol Biol **26**: 1579–1597

Zhang K, Halitschke R, Yin C, Liu C-J, Gan S-S (2013) Salicylic acid 3-hydroxylase regulates Arabidopsis leaf longevity by mediating salicylic acid catabolism. Proc Natl Acad Sci U S A **110**: 14807–14812

Zhao Y, Chan Z, Gao J, Xing L, Cao M, Yu C, Hu Y, You J, Shi H, Zhu Y, et al (2016) ABA receptor PYL9 promotes drought resistance and leaf senescence. Proc Natl Acad Sci U S A **113**: 1949–1954

Zhou C, Han L, Pislariu C, Nakashima J, Fu C, Jiang Q, Quan L, Blancaflor EB, Tang Y, Bouton JH, et al (2011a) From model to crop: functional analysis of a STAY-GREEN gene in the model legume Medicago truncatula and effective use of the gene for alfalfa improvement. Plant Physiol **157**: 1483–1496

Zhou X, Jiang Y, Yu D (2011b) WRKY22 transcription factor mediates dark-induced leaf senescence in Arabidopsis. Mol Cells **31**: 303–313

Zwack PJ, Rashotte AM (2013) Cytokinin inhibition of leaf senescence. Plant Signal Behav **8**: e24737-1-e24737-7

CURRICULUM VITAE

Name: DAS

First name: ADITI

Birthdate: 15.01.1989

Nationality: INDIAN

Education:

- **2002-2004:**
  Secondary school at Ramanath Secondary School, Visakhapatnam, INDIA
- **2004-2006:**
  Higher secondary school at Sri Chaitanya Junior College, Visakhapatnam, INDIA
- **2006-2009**:
  BSc. in Biotechnology at Manipal University, Manipal, INDIA
  Thesis title: *"Genotypic analysis of Prader Willi Syndrome using PCR".*
- **2009-2010:**
  MSc. in Plant genetics and crop improvement at University of East Anglia, Norwich, UNITED KINGDOM
  Thesis title: *"Staying Green: Investigating candidate genes for seed color stability in pea."*
- **2011-2016:**
  PhD in Plant physiology at the Institute of Plant and Microbial Biology, University of Zurich, SWITZERLAND
  Thesis title: *"Characterization of the PAO/phyllobilin pathway of chlorophyll breakdown in grasses."*

Teaching:

- 240 hours of scientific assistance involving laboratory experiment design and execution with theoretical sessions.
- 60 hours of scientific assistance involving experimental preparations.

Publications:

- **Hauenstein M, Christ B, Das A, Aubry S, Hörtensteiner S** (2016) A novel role for TIC55 as a hydroxylase of phyllobilins, the products of chlorophyll breakdown during plant senescence. *Manuscript submitted for publication*.
- **Das A, Guyer L, Hörtensteiner S** (2016) Chlorophyll and chlorophyll catabolite analysis by HPLC. *Manuscript submitted for publication*.